A DIAGNOSTIC STUDY OF THE LIFE CYCLES OF PERSISTENT FLOW ANOMALIES

by

Robert Xavier Black

B.S., Meteorology, McGill University
(1984)

Submitted to the Department of
Earth, Atmospheric and Planetary Sciences
in partial fulfillment of the requirements for the degree of

DOCTOR OF PHILOSOPHY
IN METEOROLOGY

at the

MASSACHUSETTS INSTITUTE OF TECHNOLOGY

September 1990

Signature of Author _____
Center for Meteorology and Physical Oceanography
24 August 1990

Certified by _____
Randall M. Dole, Thesis Supervisor

Accepted by _____
Thomas H. Jordan, Department Chairman

A DIAGNOSTIC STUDY OF THE LIFE CYCLES OF PERSISTENT FLOW ANOMALIES

by

ROBERT XAVIER BLACK

Submitted to the Department of Earth, Atmospheric and Planetary Sciences
on September 7, 1990 in partial fulfillment of the requirements for the Degree of
Doctor of Philosophy in Meteorology

ABSTRACT

The main objective of the thesis is to identify the primary mechanism(s) responsible for the formation of large-scale persistent flow anomalies. Towards this goal, we perform detailed synoptic and diagnostic analyses of the composite life cycles of persistent flow anomalies, focusing particularly on persistent flow anomaly (PA) development over the North Pacific and Atlantic Oceans during wintertime. The reproducibility of the results is demonstrated using an independent dataset, and a case study is presented in order to further illustrate the representativeness of the composite results.

We first construct ensemble averages centered on PA onset and breakdown times to obtain a thorough observational description of the typical three-dimensional flow structures associated with PA life cycles. Negative PA's over the North Atlantic and Pacific are preceded by intensification of the upstream climatological-mean subtropical jet stream and by positive anomalies in upper-tropospheric potential vorticity over the upstream continent. The early portion of both Pacific negative (PN) and Atlantic negative (AN) development is characterized by synoptic-scale cyclogenesis and enhanced geostrophic frontogenesis over the western ocean. Analogous baroclinic ridge development occurs over the western North Pacific during Pacific positive (PP) formation. AN and Atlantic positive (AP) developments are both initially characterized by the westward retrogression of a large-scale flow anomaly towards the key region. During large-scale development, all four types exhibit zonally elongated and westward tilting perturbation structures in the jet exit regions, with associated fluxes of zonal momentum and heat directed down their respective time-mean gradients. The PN and AN cases also exhibit strong upward heat fluxes in the troposphere during large-scale growth, with weaker vertical heat fluxes for the positive cases.

Specific diagnostic analyses are then applied in order to test particular hypotheses for PA development. Wave activity flux diagnostics indicate that the primary sources for PA development are local to mid-latitudes. Little evidence is found of anomalous tropical forcing. Except during PP developments, sources for development are also primarily local to the key regions. During PP developments, there is an anomalous wave activity flux from an upstream trough and a weak poleward flux emanating from the subtropical North Pacific. Nevertheless, budgets of energy and enstrophy suggest that, for all four PA types, local conversions associated with the composite perturbations are sufficient to account for eddy growth. The ratio of conversion to enstrophy change is largest during Pacific developments. Nonconservative processes and incoherent eddy forcing, calculated as a residual, oppose PA development. This effective dissipation is strongest during the Pacific developments. Potential vorticity analyses suggest that PN and AN

developments are related to upper-tropospheric extrusions of high potential vorticity air from the upstream continent eastward towards the key region.

The results provide strong evidence that PA development is primarily due to a large-scale instability of (or growth upon) the three-dimensional time-mean flow. Sources for development are predominantly local and enstrophy conversions from the time-mean flow into the large-scale eddies are sufficient to account for the observed eddy enstrophy increases. The main contributions to these conversions are associated with westward tilting and zonally elongated eddy structures located in the jet exit regions. Both baroclinic and barotropic conversions from the time-mean flow appear to contribute significantly to the developments. The results suggest that successful extended-range forecasts of PA development will depend significantly upon proper simulation of the climatological-mean stationary wave pattern.

Thesis supervisor: Dr. Randall M. Dole
Title: Associate Professor of Meteorology

TABLE OF CONTENTS

ACKNOWLEDGEMENTS

First of all, I would like to thank my advisor, Randy Dole, for his dedication and careful guidance during the course of my study. He allowed considerable flexibility in my research, while always encouraging me to do my best. I believe that he has prepared me well for my future in scientific research. Also, I have benefited considerably from discussions with my other thesis committee members; Drs. Alan Plumb, Brian Farrell and Paola Malanotte-Rizzoli.

Graduate student life would be incomplete without the daily academic (and social) interactions among fellow students. My officemates, Chris Davis and Brad Lyon were sources of continual intellectual stimulation. CMPO's weather "weenies" (including Chris, Brad, Josh Wurman, Peter Sousounis, Peter Neilley, Michael Morgan and others) helped to maintain the excitement of meteorology. I would also like to acknowledge my friendships with Keith Groves, Randy Mackie, Dave Genereux, Mike Bergman, Jeff Meredith, Neil Donahue, Ron Miller and Susane Lee. I was lucky enough to have two of my sisters, Lisa and Kathy, residing near Boston during my stay at MIT.

On a professional level, Peter Neilley constructed the primary datasets for the observational analyses of this thesis and Chris Davis developed the pseudopotential vorticity inversion routine used in Chapter V. Considerable assistance was also provided by Diana Spiegel, Jane McNabb, Tracey Stanelun and Joel Sloman, all of the Center.

A special thanks goes out to my friend, Dana Hartley, who gave me tremendous support during the final, and most difficult, stages of completing my thesis.

The thesis is dedicated to my housemates at 15 Sumner Ave. Their companionship and goodheartedness during the past five years were essential and will always be fondly remembered.

I. Introduction

The midlatitude troposphere exhibits variability on a variety of time scales. This spectrum is largely dominated by the power associated with the annual cycle that results from seasonal variations in incident solar radiation. However, significant temporal variability also exists within each season.

The most obvious temporal fluctuations are the day-to-day changes in surface weather observed with the passage of storms, high pressure systems and fronts. Since the early studies of Charney (1947) and Eady (1949), the understanding of these synoptic-scale disturbances has become deeply rooted in baroclinic instability theory. Although there is currently considerable debate as to the appropriateness (or relevance) of the normal mode approach (Farrell, 1982, 1984, 1985; Valdes and Hoskins, 1988), baroclinic instability theory successfully predicts typical structures and propagation characteristics of synoptic- scale eddies (Simmons and Hoskins, 1977; Frederiksen, 1978). Also, more recent instability analyses of zonally varying time-mean flows (Niehaus, 1980; Frederiksen, 1983b) account for some of the regional variations in synoptic-scale eddy activity.

Synopticians have long recognized, however, that the "regular" sequence of synoptic time-scale disturbances is often modified by persistent large-scale diversions of the upper-level jet stream (Berggren et al., 1949; Rex, 1950a). These upper-level flow anomalies often lead to prolonged abnormal weather conditions (Rex, 1951; Green, 1977) as well as to modifications of shorter time-scale variations. During the last decade, there has been a renewed interest in understanding the characteristics and sources of this low frequency, intraseasonal variability.

Early studies by Sawyer (1970) and Blackmon (1976) demonstrate that the majority of midlatitude intraseasonal variance in the tropospheric height field occurs at time scales *greater than* 10 days. During Northern Hemisphere wintertime, intraseasonal

low frequency variability (hereafter, LFV) exhibits local maxima over three regions: the North Pacific Ocean to the southwest of the Aleutian Islands, the North Atlantic Ocean to the southeast of Greenland, and the Northern Soviet Union (Blackmon, 1976). Further analyses indicate that much of the LFV in these regions is associated with the occurrence of particular persistent flow anomaly patterns (Wallace and Gutzler, 1981; Dole, 1986a). These persistent anomaly (PA) patterns are often associated with long-lived extremes in surface weather conditions (Namias, 1978; Edmon, 1980; Dole, 1986a) and as such, their occurrence is of considerable practical importance.

Several mechanisms have been proposed for the generation of LFV. These include *large-scale transient development* (Farrell 1989b) *or instability* (Simmons et al., 1983; Frederiksen, 1983b); *anomalous topographic or diabatic forcing* (Hoskins and Karoly, 1981; Navarra, 1990) *or mean flow variations* (DaSilva and Lindzen, 1987; Nigam and Lindzen, 1989); and *through anomalous potential vorticity tranports by synoptic-scale eddies* (Shutts, 1986; Tsou and Smith, 1990; Neilley, 1990). At the present time, the relative importance of the various mechanisms in generating LFV is highly uncertain.

In this thesis, we present detailed synoptic and diagnostic observational analyses of the time evolution of PA's. Our main goal is to identify the primary mechanisms responsible for PA development. This goal is approached in two parts. The first part is essentially descriptive in nature and documents the structures and eddy fluxes associated with PA development. In the second part, we perform additional diagnostic analyses that are aimed at identifying the primary mechanisms leading to PA development. Among the specific questions to be addressed are:

- What are the typical flow structures associated with PA time evolution?
- What is the relationship between eddy fluxes and the time-mean flow during the large-scale developments?

- Are the sources for PA's primarily local or remote to the development region? In particular, is there any evidence for anomalous tropical forcing?
- What are the potential roles of large-scale growth/instability and local non-conservative forcing in the developments?

The thesis is organized as follows. Chapter II provides the observational and theoretical background for our study. The primary datasets and methods are described in Chapter III. The main results of the thesis are contained in the subsequent two chapters.

Chapter IV presents detailed synoptic analyses which focus on PA developments. Ensemble averages are used to identify systematic flow anomalies accompanying both PA development and decay. In particular, Dole's (1989) 500 mb study is extended considerably by examining the vertical and thermal structures associated with composite PA time evolution. Diagnostic analyses are also presented of eddy heat and momentum fluxes during the developments. The analyses of Chapter IV provide an initial basis for evaluating theories of PA generation.

Chapter V then presents additional diagnostic analyses aimed at identifying the sources for PA development. Regional sources and sinks of wave activity are identified. Energy and enstrophy budgets are obtained to examine the roles of eddy/time-mean flow interactions and local non-conservative processes in the developments. Potential vorticity analyses are also presented to further interpret dynamical aspects of the large-scale developments.

In Chapter VI, the reproducibility of the results is demonstrated on an independent dataset, and a case study is presented to further illustrate the representativeness of the composite results. Finally, Chapter VII summarizes the primary results and principal conclusions of the thesis.

II. Background

We start by reviewing the observations and theories of persistent anomalies and other related phenomena. This chapter provides a foundation for the remainder of the thesis. Readers familiar with the literature on PA's and low frequency variability may choose to proceed directly to Chapter III.

A. Observations

Persistent anomalies are defined as long-lived local deviations in the upper-tropospheric flow field from climatological values. To be specific, in the initial study of Dole and Gordon (1983) searched for extended non-zero values of:

$$Z_\theta' = Z' [\sin(45^o)/\sin(\theta)]$$

where θ is latitude and Z' is the departure of the 500 mb geopotential height from its local seasonal trend value. This latitude scaling of Z' results in an anomaly pattern which is more indicative of *flow* anomalies and therefore provides a better indication than Z' of meridional energy dispersion (Hoskins et al., 1977). By choosing an amplitude threshold $\pm M$ and a minimum duration T, one can identify persistent anomalies by examining time series of Z_θ', as depicted in fig. 2.1. Note that this methodology differs from that used in other studies where cases are chosen on the basis of characteristics of the *total* (anomaly plus mean) flow field (e.g., Shutts, 1986; Mullen, 1987; Holopainen and Fortelius, 1987a; Tsou and Smith, 1990). To the extent that the climatological mean flow itself exhibits strong zonal variations, the PA (or similar) method provides a more objective means for identifying robust and typical low frequency flow *anomalies*.

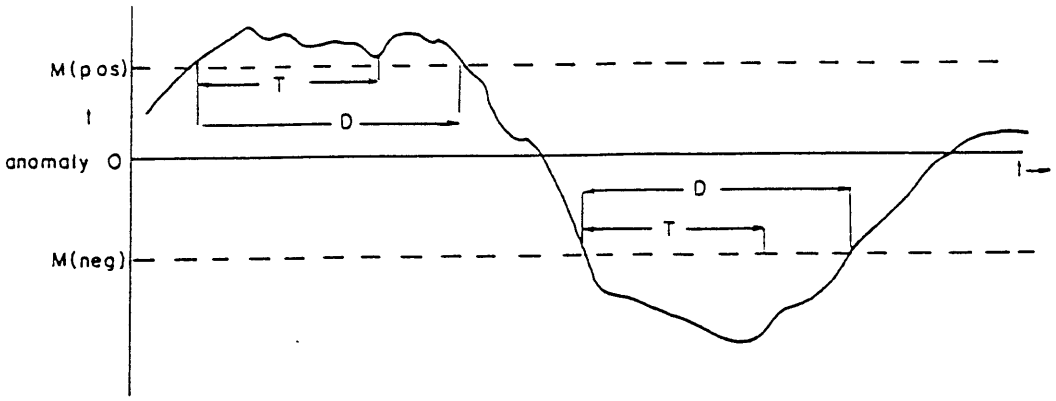

Fig. 2.1. Method for defining persistent anomalies. A case is identified if a positive (negative) height anomaly exceeds (is less than) the threshold M for at least T days. D is the duration of the case. From Dole and Gordon (1982).

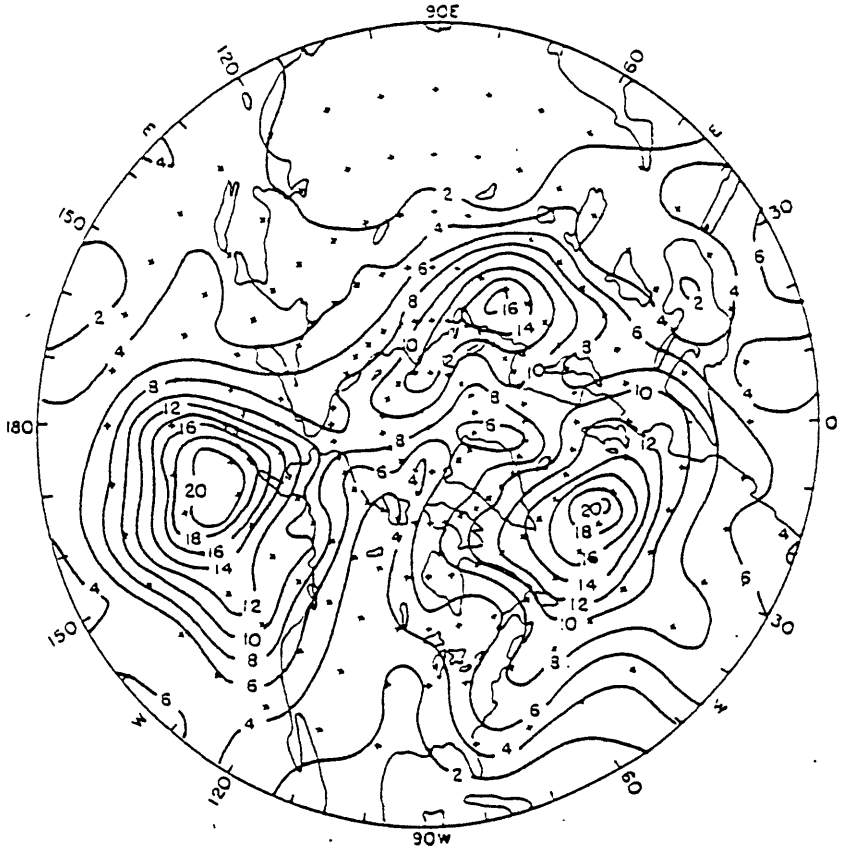

Fig. 2.2. Hemispheric distribution of positive and negative persistent anomalies occuring during the 14 winters seasons 1963-64 through 1976-77. The events are identified from low-pass time series using the anomaly criteria (100 m, 10 days). From Dole and Gordon (1982).

Using this approach, Dole and Gordon (hereafter DG) investigated the geographical distribution and regional statistics of PA's. They found that there were three local maxima in occurence (fig. 2.2), located over (1) the North Pacific Ocean (PAC), (2) the North Atlantic Ocean (ATL) and (3) the northern Soviet Union (NSU). (Hereafter, these maxima will often be referred to as "key points" and the surrounding regions as "key regions".) In each region, the number of positive and negative PA's were approximately the same. Typical durations (for M=100 m, T=10 days) were ~12-13 days but there were no strongly *preferred* durations. At large values of M, positive PAC and ATL PA's were generally more persistent than their respective negative counterparts.

Dole (1986a, hereafter D86a) studied the time-mean structures of PA's. He used compositing and EOF analysis techniques to identify typical structures for cases occuring in the three key regions. Dole found that in each region, certain large-scale upper tropospheric flow anomaly patterns tended to recur. The patterns are typically large-scale but regional in nature. Horizontal anomaly structures associated with the negative and positive phases in each region are quite similar. Using EOF analyses, the basic anomaly structures were identified as the primary regional patterns of LFV. The PAC and ATL composites resemble the PNA and EA teleconnection patterns, respectively, observed by Wallace and Gutzler (1981).

Near each key region, Dole found that the composite exhibits a large-scale upper level height anomaly (~zonal wavenumber 3-4). Weaker anomalies of alternating sign are found downstream and to the south of the primary anomaly. Vertical structure analyses show tropospheric thermal anomalies nearly in phase with the upper height anomalies. The mean anomaly patterns were approximately equivalent barotropic with maximum amplitudes (in geopotential height) near 300 mb.

Near the key regions, the *total* flow field associated with positive PA's exhibits relatively weak zonal flow, while negative PA's are associated with intensified zonal

flows. For PAC and ATL, respectively, negative PA's are associated with intensified Aleutian and Icelandic surface lows. As an example, fig. 2.3 displays the full field composite mean structure for PAC PA's. Note the upper level split flow of the positive phase (fig. 2.3a) and the strong Aleutian surface low of the negative phase (fig. 2.3d). Dole also demonstrated that PA's are associated with significant changes in synoptic scale eddy activity, as one might anticipate from the observed upper level flow variations.

In two subsequent studies, Dole (1986b, 1989) extended his analyses to look in detail at (primarily) the 500 mb *time evolution* of PA's. He focused on the typical characteristics of PA development and breakdown in each of the three regions. Ensemble averages were performed relative to the onset or termination time of each case. Dole found that in each of the three regions the development of the primary 500 mb height anomaly occurred rapidly (over several days) compared to typical duration time scales. Also, for each PA type no significant signature is observed near the key region until just prior to onset. After the development of the primary anomaly, anomalies of alternating sign developed in sequence downstream. The downstream centers remain quasi-stationary as they develop. PA breakdown also occurs relatively rapidly. At 500 mb, the horizontal anomaly patterns which precede breakdown appear broadly similar to the post-development structures. In each region, the time evolution of positive and negative cases show remarkable similarity.

There were, however, some distinct differences among the regional developments. The PAC developments are typically preceded by upstream variations in the East Asian subtropical jet. Prior to ATL developments, significant upper level flow perturbations are observed both to the southeast and southwest of the key region. Unfiltered analyses show that PAC developments follow the upstream intensification and eastward propagation of a synoptic-scale disturbance. The NSU cases are preceded by the formation of a well defined wavetrain upstream of the key region. During development, the primary anomaly centers in the PAC and ATL regions appear as zonally elongated

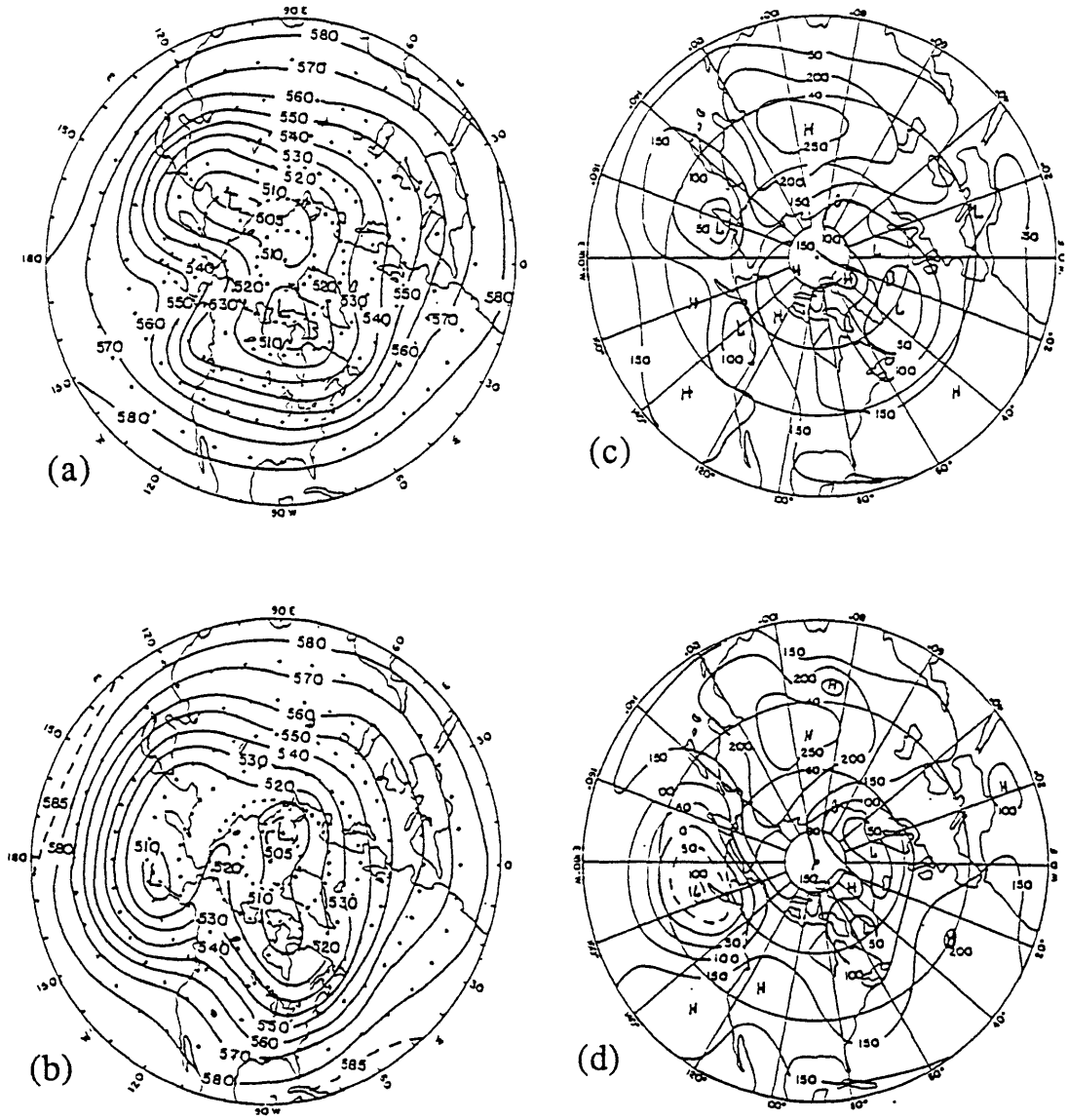

Fig. 2.3. Composite 500 mb heights (dam) for (a) 7 PAC positive cases and (b) 7 PAC negative cases. Composite 1000 mb heights (m) for the (c) positive cases and (d) negative cases. From Dole (1986a).

perturbations positioned in the exit regions of the climatological mean subtropical jet streams. Dole notes that the downstream evolutions resemble the behavior found in simple, time-dependent models of energy dispersion away from local sources on a sphere (Hoskins et al., 1977). Also, the zonally elongated patterns observed during PAC and ATL developments are similar to the structures found in the 2-D barotropic instability analyses of Simmons et al. (1983). They found unstable normal modes which extracted energy from predominantly the *zonal* variations of the mean flow kinetic energy.

An example of a composite evolution is displayed in fig. 2.4, which shows the composite unfiltered 500 mb height anomaly pattern observed during the development of PAC negative PA's. We note:

- anomalous cyclonic shear over southeast Asia at day -5
- an intensifying and eastward propating "synoptic" scale disturbance over the western North Pacific at days -3/-1
- the evolution towards a zonally elongated perturbation positioned near the date line at day +1
- quasi-stationary development of the primary anomaly after day +1
- subsequent downstream ridge and trough development over North America during days +3/+5

In Dole (1986b), preliminary vertical stucture analyses of PAC developments suggest that the growing disturbances exhibit marked westward tilts with height. In particular, PAC negative developments in many respects resemble an amplifying baroclinic wave. The strong thermal advections observed during PN (PAC negative) development appear consistent with (a) the strengthening and eastward extension of the East Asian subtropical jet and (b) the building of the ridge over western North America (Both features are found in the time-mean fields of fig 2.3c).

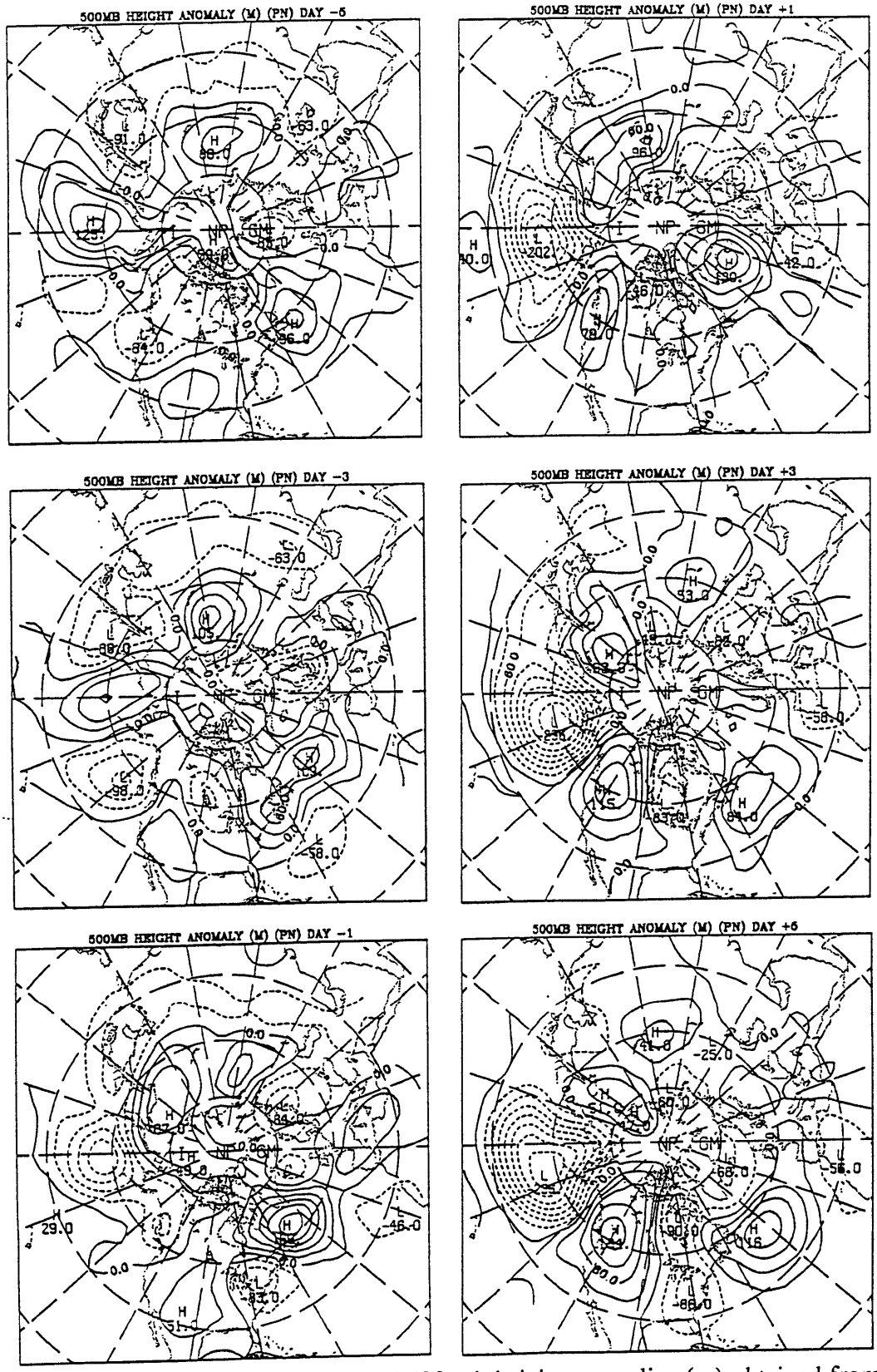

Fig. 2.4. Composite time evolution of 500 mb height anomalies (m) obtained from 14 PAC negative events. Evolution is displayed in two day intervals from day -5 to +5.

Independent studies have confirmed many aspects of Dole's observational analyses. The results of Shukla and Mo (1983) and Blackmon et al. (1986) reproduce the geographical distributions of DG. Correlation studies of Wallace and Gutzler (1981) and Blackmon et al. (1984a) and rotated principal component analyses of Horel (1981) and Barnston and Livezey (1987) find horizontal structures consistent with those of D86a. Recent observational analyses of the time variation of synoptic-scale variability confirm that two of the primary large-scale flow anomalies influencing the oceanic "storm tracks" closely resemble the fully developed PAC and ATL patterns (Lau, 1988; Anderson and Gyakum, 1989).

Few observational studies have examined the time evolution of mid latitude LFV. Blackmon et al. (1984b) used lag-correlation statistics to study the time variation of 500 mb geopotential height fluctuations at various intraseasonal frequencies. At "low" and "intermediate" frequencies their analyses bear some resemblance to the time evolution of particular PA's. Also, Schubert (1986) examined lag cross correlations between EOF's derived from fluctuations within particular frequency bands. The observational analyses of Dole (1989) suggest, however, that PA evolution involves a broad spectrum of temporal and spatial scales. Thus, it is possible that important components of the evolution will be masked if the data are arbitrarily separated into distinct spectral bands.

B. Theories of LFV

As mentioned in the introduction, the mechanisms proposed to explain PA development (or other large-scale flow anomaly growth) include the following, which are discussed in sequence:

i) Large-scale growth/instability

ii) Anomalous forced-wave response

iii) Response to anomalous synoptic-scale eddy forcing

i. Large-scale instabilities.

Linear instability analyses of zonally symmetric flows have proven successful in explaining many of the observed characteristics of midlatitude synoptic scale disturbances. Although analyses of realistic zonal flow profiles find peak growth rates near zonal wavenumber 8 (Simmons and Hoskins, 1977; Frederiksen, 1978), even normal mode analyses including Ekman damping allow some growth at planetary scales (Valdes and Hoskins, 1988). The growth rates associated with these planetary modes are quite small, however, with e-folding time scales much greater than one week.

More recent studies have examined linear instability characteristics of zonally varying flows on a sphere. The study of Simmons et al. (1983) includes a barotropic instability analysis where the basic state is the 300 mb climatological mean January flow. The normal modes evolve through a complex life cycle and do not have simple sinusoidal longitudinal variations. Their behavior is given by:

$$\psi' \sim e^{\sigma t} \{A(x,y) \sin(\omega t) + B(x,y) \cos(\omega t)\}$$

Where σ is growth rate, ω is frequency and A and B are spatially varying wave amplitudes. Consequently, the local "growth" rate may differ substantially from $(\sigma)^{-1}$ as the mode disperses nonuniformly on the sphere. The life cycle of their fastest growing normal mode contains phases which, locally, strongly resemble the primary anomaly evolution observed during composite PAC and ATL PA developments. As an example, compare fig. 2.5a (from Simmons et al.'s fig. 11) to the 500 mb composite height anomaly pattern at day +3 of the PAC negative development (fig. 2.5b). During the phase which resembles PAC development, Simmons et al. estimate local e-folding times for ψ' of ~3 days even though $(\sigma)^{-1}$ for the mode is ~7 days. More realistic damping reduces the "local" and global growth rates to ~4 and 22 days, respectively. For

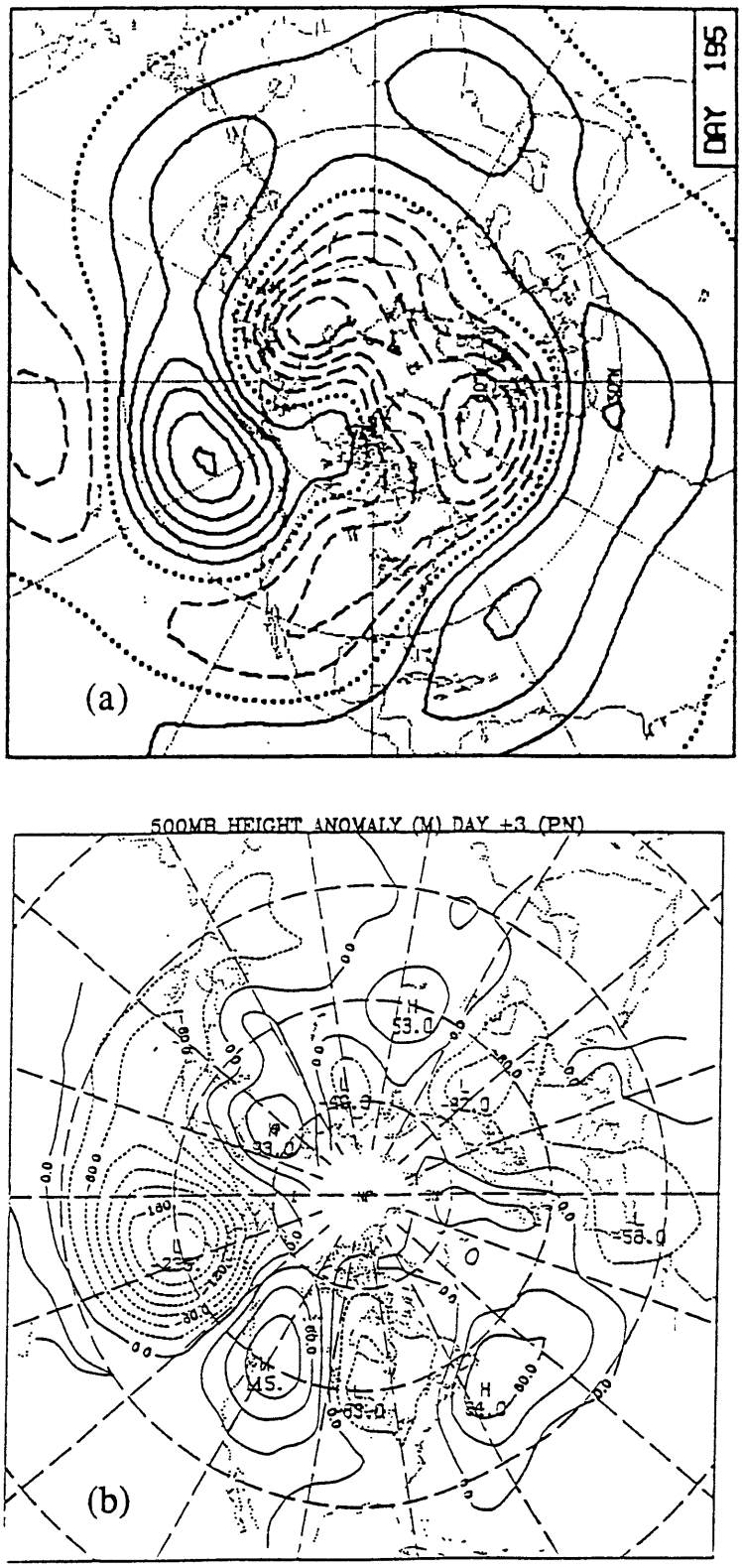

Fig. 2.5. (a) Streamfunction anomaly (arbitrary units) during one phase in the life cycle of the most unstable normal mode associated with the barotropic instability of the 300 mb climatological mean flow. From Simmons et al. (1983). (b) The composite 500 mb height anomalies (m) at day +3 of the PAC negative development.

comparison, during the strong growth phase of the PAC positive PA development, the 300 mb ψ' is observed to e-fold as quickly as 2-3.5 days. Certainly, barotropic instability of the zonally varying time-mean flow is one candidate for explaining some aspects of PAC (and perhaps ATL) developments. We note, however, to the extent that PA development is observed to be markedly baroclinic, the theory will be insufficient to simulate (or explain) important aspects of PA developments. In addition, the evolving modal structure of the barotropic model fails to adequately replicate the strong downstream anomaly development observed to occur over western North America during PAC developments.

The next step beyond Simmons et al.'s work is to extend their analyses to three-dimensional mean flows. Using a 2-layer quasi-geostrophic (hereafter QG) model on a sphere, Frederiksen (1982,1983b) analyzed the instability characteristics of an 8 winter average mean flow. In addition to finding westward tilting and eastward propagating modes as seen in localized synoptic-scale cyclogenesis, Frederiksen (1983b) identifies large scale, eastward propagating and baroclinic "onset-of-blocking" modes and quasi-stationary equivalent barotropic "mature anomaly" modes. He suggests that Pacific PA patterns may develop in a two-stage process. First, baroclinic development occurs during the growth and eastward propagation of an "onset-of-blocking" mode. Then, presumably through nonlinear processes (not contained in Frederiksen's model), the "onset-of-blocking" mode evolves into a quasi-stationary "mature anomaly" mode which grows approximately barotropically to form the mature PA pattern. Frederiksen's Pacific "mature anomaly" mode bears some resemblance to the mean PAC anomaly patterns. He compares his three-dimensional results with results obtained from a barotropic model. The Pacific "mature anomaly" pattern *locally* resembles the most unstable mode obtained from the barotropic model. Although the Pacific "mature anomaly" mode is roughly equivalent barotropic, Frederiksen notes an increase in growth rate in the baroclinic model over the analogous mode of the barotropic model. Also, the "mature anomaly"

mode of the baroclinic model exhibits a larger downstream response over western North America, a deficiency of the most unstable mode obtained in the barotropic model.

In later studies, Frederiksen extends his QG model to 5 vertical levels (Frederiksen, 1983a; Frederiksen and Puri, 1985; Frederiksen and Bell, 1987). These papers examine instability characteristics (1983a); nonlinear integrations (1985) and the possible effect of topographic instability (1987). Unfortunately, all of the Northern Hemisphere wintertime analyses use the time average flow of January 1978 as a climatology. As will be shown later, two strong PA events occurred during January 1978 (PAC negative and ATL positive). Consequently, the mean flow during that time is not representative of the long-term mean wintertime climatology. Indeed, the January 1978 mean flow may actually contain features that the analysis is attempting to explain, and may therefore be inappropriate. Also, Frederiksen studies modes whose structures resemble particular observed flow anomalies rather than carefully comparing the time evolution of the most unstable modes of his analysis. A more definitive study would examine in detail the *most unstable modes* in a spherical model having higher vertical resolution *and* a more representative mean flow. Despite these reservations, however, Frederiksen's initial 2-layer model results are encouraging.

Development in the atmophere is certainly not limited to normal mode instabilities. In a series of papers, Farrell (1982, 1984, 1985, 1989a, 1989b) has investigated initial value development in simple linear models of the atmosphere. In an examination of the initial value problem for the undamped Eady model, Farrell (1984) finds that, although exponentially growing normal modes eventually dominate the spectrum of model variability, non-modal growth of favorably configured initial perturbations can temporarily compare to (or exceed) modal growth. Farrell (1985) looks at the Eady and Charney models including boundary (Ekman) damping. He determines that, in both models, the inclusion of realistic damping leads to a virtual elimination of normal mode instability. Initial value growth, however, still provides robust development on time

scales compatible with observed cyclogenesis.

In his 1989b paper, Farrell studies transient growth in a barotropic model linearized about a basic state which includes streamwise variations. He analyzes the time evolution of idealized streamfunction perturbations located in the diffluent and confluent regions of a pure deformation flow (which does not support modal instabilities). One interesting result is that, in regions of diffluence, zonally elongated perturbations can experience explosive transient development. Using deformation values typical of the climatological jet exit regions, the streamfunction of an idealized zonally elongated perturbation e-folds in ~2-days. Even including the effects of divergence, ψ' growth occurs on a time scale of ~4 days.

In inviscid linear instability analyses, the most unstable normal mode is the structure which the theory predicts will eventually dominate the perturbation spectrum. In the theory of transient development, one looks for initial perturbations which either (1) optimally excite particular waveforms or (2) exhibit maximum growth rates over a fixed time. For example, Farrell (1989a) examines optimal excitation of baroclinic waves in the Charney model. Further study of optimal growth in realistic 3-D flows will provide additional insight into the potential role of transient development in PA formation.

Theories of large-scale growth/instability predict that there are favored perturbation structures which are able to grow at the expense of the mean flow in particular regions. The results of Simmons et al. (1983) and Farrell (1989b) suggest that zonally elongated eddies can experience significant local development in jet exit regions. Frederiksen's (1983b) study indicates that large-scale westward-tilting eddies can grow baroclinically in the jet exit regions, as well. To test these theories one needs to check if the eddy structures and fluxes observed during the time evolution of large-scale developments are consistent with the above studies. Sources for development will be primarily local and there should be a positive eddy/mean flow interaction sufficient to account for eddy growth.

ii. Anomalous forced waves

Anomalous forced waves can arise in the atmosphere in two general ways. The most obvious is simply to introduce anomalous forcing as studied by Hoskins and Karoly (1981), Branstator (1985), Sardeshmukh and Hoskins (1988) and Navarra (1990). Alternatively, anomalous forced waves can be produced by modifying the mean flow while keeping the forcing distribution fixed. This alters the refractive index of the atmosphere, changing the propagation characteristics of stationary waves. This mechanism has been investigated by Jacqmin and Lindzen (1985), DaSilva and Lindzen (1987), Nigam and Lindzen (1989) and DaSilva (1989).

Since the early work of Charney and Eliassen (1949) steady-state linear models have proved very useful in studying the forced waves of the atmosphere. During the past decade, many forced wave studies have used models linearized about zonally averaged flows (Hoskins and Karoly; Simmons, 1982; Jacqmin and Lindzen; Nigam et al., 1986). Such models have been used to study anomalous forced waves (Hoskins and Karoly, Simmons) as well as the time-mean stationary wave pattern (Held, 1983; Jacqmin and Lindzen; Nigam et al.; Valdes and Hoskins, 1989).

Hoskins and Karoly investigated the response to idealized thermal and orographic forcing in a 5-layer baroclinic model on a sphere. One of their key results is that the steady remote reponse to localized forcing consisted of an equivalent barotropic Rossby wavetrain emanating from the region of forcing. They determine that subtropical thermal forcing anomalies are much more effective in producing midlatitude flow anomalies than realistic thermal forcing anomalies at mid to high latitudes. At midlatitudes, Hoskins and Karoly find that the local response to anomalous diabatic heating consists of a westward tilting low with the surface center located to the east of the anomalous heating. The structure of the forced wave is quite sensitive to the vertical structure of the heating anomaly. Held (1983) examined the steady midlatitude response to orographic forcing in

a baroclinic QG model on a β-plane. He demonstrates that the vertical structure of the forced response depends strongly on the horizontal scale of the mountain (for a fixed zonal mean flow). At small scales, the forced waves are in phase with the topography and decay equivalent away from the boundary. Intermediate scales lead to equivalent barotropic forced waves with peak amplitudes near the tropopause. At longer scales the forced waves tilt westward with height and propagate significantly into the stratosphere.

Some recent studies of the response to anomalous forcing have employed models linearized about zonally varying time mean flows (Simmons et al., 1983; Branstator, 1985; Sardeshmukh and Hoskins, 1988; Navarra, 1990). The primary focus of many of these modeling studies was the extratropical response to idealized tropical diabatic heating anomalies (motivated primarily by a recent interest in the extratropical atmospheric response to tropical heating anomalies associated with ENSO). All of these studies show that the remote extratropical response is strongly affected by the presence of stationary waves in the basic state. In particular, many of the linear analyses indicate that particular midlatitude flow anomalies are effectively produced by placing anomalous forcing to the south of the climatological mean subtropical jet streams (Simmons et al., Branstator, Navarra). This behaviour has been confirmed in various nonlinear modeling studies (Simmons, 1982; Blackmon et al., 1983; Geisler et al., 1985; Palmer and Owen, 1986). The resulting midlatitude flow anomalies resemble certain prominent atmospheric teleconnection patterns (Simmons, Simmons et al., Branstator, Palmer and Owen). A number of the studies conclude, however, that a significant portion of the extratropical response is due to an interaction between the remotely forced anomaly and the zonally and meridionally varying basic state (Simmons et al., Blackmon et al., Branstator, Palmer and Owen). In Simmons et al.'s study, the excited midlatitude response is related to the most unstable mode of the barotropic instability of the zonally varying climatological mean 300 mb flow.

Thus it appears as if there are at least two ways in which remote forcing anomalies

may initiate large-scale midlatitude flow anomalies. The first is simply the development of an equivalent barotropic Rossby wavetrain extending from the region of anomalous forcing into the region of interest. Second, the forcing could indirectly force midlatitude flow anomalies by producing a remote wavetrain which excites (through instability or otherwise) preferred "modes" of midlatitude variability. In both cases, the remote forcing is clearly of great importance. Insofar as the remote midlatitude responses in the above studies resemble particular teleconnection patterns, anomalous remote forcing (tropical or extratropical) appears to be another possible mechanism for initiating PA's. Dole (1986b) notes, however, that the time scales for PA development are inconsistent with the long time scales associated with changes in atmospheric boundary conditions (e.g. sea surface temperature). Also, he finds no evidence of a Rossby wavetrain emanating from the tropical Pacific during PAC developments. An intriguing possibility, on the other hand, is the possible tropical influence upon the upstream fluctuations in the East Asian Jet observed prior to PAC developments (Dole, 1986b). The above modeling studies (Simmons, 1982; Simmons et al., 1983; Navarra, 1990) suggest that anomalous tropical forcing at this longitude can lead to a marked midlatitude response. More detailed observational analyses will be necessary to determine whether remote forcing plays a role in PA development and, if so, whether the role is direct or indirect. If the forcing is direct, one would expect equivalent barotropic Rossby wavetrains and horizontal wave activity flux anomalies emanating from the region of anomalous forcing to the region of development. Indirect tropical forcing would involve anomalous forcing of the midlatitude precursors to development.

For ATL and PAC PA's, it would appear from a consideration of the proximity of the major mountain ranges that diabatic heating is the only relevant *local* forcing for the primary anomalies. There have been relatively few investigations of the forced response to *midlatitude* heating anomalies. As discussed earlier, realistic midlatitude heating anomalies produce relatively weak local responses in zonally averaged linear models

(Hoskins and Karoly, 1981; Simmons, 1982). A recent study (Navarra, 1990) of anomalous forcing in a multi-level spherical model linearized about a zonally varying basic state suggests that shallow heating anomalies positioned near the east coast of Asia at midlatitudes can excite a robust midlatitude response. The model's horizontal resolution is coarse (rhomboidal truncation of 7), however, and the maximum midlatitude response (Z' ~75m at 300 mb) is still quite weak compared to observed PA's. Also, such models of the *steady* response to local forcing anomalies provide little predictive information on the expected time evolution. More theoretical and observational work will thus be necessary in order to elucidate the potential role of local forcing in PA formation.

A recent study by Nigam and Lindzen (1989) analyzes the sensitivity of forced stationary waves to modifications of the *mean flow* (with a fixed forcing distribution). Their investigation uses a high resolution primitive equation model, linearized about a zonally uniform basic state, to study variations in the orographically forced stationary waves. A key result is that modest zonal flow variations (~5 m/s) near the subtropical jet lead to relatively strong modulations in the amplitude of the stationary wave pattern in the midlatitude troposphere. Specifically, a southward shift in the subtropical jet modifies the atmospheric index of refraction allowing enhanced poleward propagation of stationary wave activity (from the latititude of the Himalayas). The linear barotropic study of Kang (1990) also attributes a similar forced wave sensitivity to modifications in the wave propagation characteristics of the basic state.

The result that basic state variations primarily affect stationary wave *amplitude* implies that the anomalous forced wave pattern will be in phase with the climatological mean stationary waves. Here we note that, in the upper troposphere, the time-mean PA patterns (as presented in Dole, 1986a) are of similar scale but are phase-shifted from the winter mean stationary wave pattern. For example, the primary anomaly associated with the time-mean PAC pattern is almost exactly in quadrature with the local climatological stationary wave structure. Irregardless, this hypothesis will be tested by examining the

fluxes of stationary wave activity (Plumb, 1985) associated with particular stationary wave patterns (as in Kang, 1990).

The above studies examined the *time-mean* response to basic state variations. A topic more relevant to PA evolution is the transient response excited during a transition between zonal flow regimes. Using a barotropic model on a sphere, DaSilva and Lindzen (1987) found that the response to tropical thermal forcing during a zonal flow transition included an excitation of westward propagating ultra-long Rossby waves. In his thesis, DaSilva (1989) considers the same process in a baroclinic model. During the transition between zonal flow regimes in the more sophisticated model, he finds that no external Rossby modes are excited. There is a transient response, however, which consists of eastward propagating and meridionally confined disturbances having zonal wavenumbers ~3-4. The total anomaly pattern during the transition, which includes the anomalous *stationary* waves, consists of a very slowly eastward propagating anomaly pattern which converges towards the anomalous stationary wave pattern. As in the steady-state theory, the final anomaly structure is associated with a modified stationary wave activity flux and can be compared directly to mature PA patterns. The transients excited in the baroclinic model bear more resemblance to developing PAC PA's than do the westward propagating external Rossby modes excited in the barotropic model. This is particularly true of the quasi-stationary growth phase of PAC development. However, the fully established anomalous stationary wave pattern is much weaker in amplitude and has much more upstream structure than observed PAC anomaly patterns.

iii. Transient eddy forcing

Although there exists a plethora of observational and theoretical studies (Shutts, 1986; Mullen, 1987; and references therein) concerned with the role of transient eddy forcing in maintaining various low frequency phenomena, there are few observational

analyses of the effects of synoptic-scale eddy forcing upon the time evolution of PA's (or other LFV). Relevant observational analyses are the recent works of Tsou and Smith (1990) and the thesis of Neilley (1990), along with the more qualitative research of Berggren et al. (1949) and Colucci (1987). The modeling studies of MacVean (1985), Hayashi and Golder (1987) and Haines and Rizzoli (1990) examine aspects of the nonlinear forcing of planetary waves.

In this thesis we will not focus explicitly on the effects of synoptic scale eddies during PA evolution; however, the fundamental dynamical picture is that systematic large-scale anomalies in potential vorticity flux divergence due to synoptic-scale eddies lead to PA formation (e.g. Shutts, 1986). The most complete observational study addressing this hypothesis is Neilley (1990). In a detailed examination of the effects of synoptic-scale eddies upon the life cycles of PA's, he determines that anomalous synoptic-scale eddy forcing plays a significant role in PA development over the North Atlantic. Over the North Pacific, the effects of synoptic-scale eddies appears to be weaker. It will prove useful to compare Neilley's results with the observational analyses of this thesis which consider other proposed development mechanisms.

C. Summary

The previous section describes several potential mechanisms proposed to explain PA development. Our understanding of the relevant importance of the various mechanisms is, however, far from complete. The observational study of Neilley (1990) suggests that anomalous synoptic-scale eddy forcing is at least partially responsible for the development of ATL PA's. Although Neilley observes that direct synoptic-scale forcing is weak during the PAC developments, Dole's (1986b, 1989) results suggest that an intensifying synoptic-scale disturbance plays an important role in initiating PAC PA's.

One potential mechanism is the instability of (or growth upon) the zonally varying

time-mean flow. The barotropic studies of Simmons et al. (1983) and Farrell (1989b) predict horizontal eddy structures, time evolution patterns and growth rates compatible with observed PAC and ATL developments. The 3-D baroclinic instability analyses of Frederiksen (1983b) are capable of explaining the initial, highly baroclinic portion of the PAC developments and better represent the downstream wave patterns observed during PAC developments. These theories predict positive conversions between the growing large-scale eddy and the time-mean flow. We will investigate this hypothesis using budgets of energy and enstrophy in Chapter V. In particular, we will examine whether direct energy and enstrophy conversions from the time-mean flow are sufficient to account for eddy growth.

Another intriguing process is the response to anomalous remote forcing. The modeling studies of Simmons (1982), Simmons et al. (1983), Branstator (1985) and others suggest that anomalous thermal forcing near specific regions in the tropics can lead to efficient excitations of particular midlatitude teleconnection patterns. These studies conclude, however, that a significant portion of the extratropical response is due to eddy/mean flow interactions at midlatitudes (Simmons et al.; Blackmon et al., 1983; Branstator; Palmer and Owen, 1986). Although there is little observational evidence for direct tropical forcing of PAC PA's (Dole, 1986b), it is quite possible that anomalous tropical forcing may be involved in the upstream variations of the East Asian subtropical jet observed prior to PAC developments. Here, we will investigate the potential role of remote forcing using wave activity flux diagnostics and tropical analyses of upper-level winds and OLR.

Other possible development mechanisms include the response to diabatic and topographic forcing anomalies and zonal flow variations. Because of the time scales associated with PA development, it is unlikely that the time evolution of PA's results from direct anomalous thermal forcing associated with midlatitude (or tropical) sea surface temperature anomalies. At this point, the significance of local internal diabatic

heating anomalies is not well understood from either a theoretical or observational perspective. In Chapter V, we estimate the effects of local, nonconservative forcing using eddy enstrophy analyses. The response to zonal flow variations is discussed in Chapter VI.

III. Methodology.

A. Introduction

The fundamental objective of this thesis is to determine the sources for the development of persistent anomalies of the extratropical Northern Hemisphere wintertime circulation. Detailed observational analyses of their time evolution are performed in order to attain this goal. As described in Chapter I, the thesis has two major parts. The goal of the first part is to provide a thorough synoptic *description* of the three-dimensional time evolution of PA's. In the second part, we then conduct specific observational diagnostics that are aimed at testing particular hypotheses for PA generation. These diagnostic analyses are motivated in part by results of the earlier synoptic analyses.

Throughout the thesis our philosophy is that the primary features of interest are those features which appear systematically in the individual cases. In this thesis, the *coherent* part of the case evolutions is isolated by compositing the individual evolutions relative to the case onset or termination times. The *systematic* aspects of the coherent evolution are then determined using simple statistical tests. The PA evolutions are described in terms of composite features that are deemed most significant. Specific diagnostics are performed in order to determine the sources for the coherent flow anomalies of the composite evolution. Thus, the evolving large-scale eddies which we describe and seek to understand are the perturbations associated with the composite flow fields. The representativeness and reproducibility of the composite results are considered in Chapter VI.

B. Data

Our primary dataset is obtained from the twice-daily (0000 UTC and 1200 UTC)

National Meteorological Center (NMC) final analyses of geopotential heights, winds and temperatures at the standard pressure levels between 1000 mb and 100 mb. For detailed discussions of the NMC analyses see DG and Trenberth and Olson (1988a). The NMC analyses incorporate ship and aircraft observations which aid substantially in improving data coverage over the North Atlantic and North Pacific regions (DG). The primary dataset consists of the twenty-four 120-day winter seasons (starting November 15) extending from 1963-64 through 1986-87. The data were spatially interpolated from the NMC octagonal grid to a 2° latitude by 5° longitude grid extending from 20 to 90°N. Obviously incorrect or missing analyses were replaced by linearly interpolated values. Less than 3% of the time series were missing.

In Chapter VI, the midlatitude observations are supplemented with simultaneous tropical analyses. These consist of satellite-derived outgoing longwave radiation (OLR) and upper tropospheric winds as analyzed by the European Centre for Medium-Range Weather Forecasts (ECMWF). OLR is a derived estimate of the total outgoing longwave radiative flux at the top of the atmosphere (see Gruber and Krueger, 1984) and is used as a measure of tropical convective activity (e.g. see Weickmann et al., 1985; Knutson and Weickmann, 1987). The data used here are obtained from daily averages of OLR calculated on a 2.5° by 2.5° grid extending from 45°S to 45°N.

A more complete dynamical picture of tropical variations is obtained by supplementing the OLR information with operational analyses of upper-level winds. A detailed comparison of the NMC and ECMWF operational analyses was recently conducted by Trenberth and Olson (1988c). One of their conclusions is that the introduction of diabatic nonlinear normal mode initialization into the ECMWF analysis scheme has led to stronger and more "realistic" patterns of tropical divergence. Recent ECMWF archives contain more analyzed quantities and have better temporal continuity (very few missing days) than the NMC archives. Also, the ECMWF analyses available at the National Center for Atmospheric Research (NCAR) are stored in a format readily

input into NCAR's Community Climate Model (CCM) processor. This provides the user with simple post-processing capabilities. Therefore we choose to use the ECMWF analyses to supplement the OLR data. These analyses have been interpolated to the 4.4° latitude by 7.5° longitude grid associated with output from an R15 (rhomboidal truncation of 15) run of NCAR's CCM (a spectral general circulation model). For a detailed discussion of the ECMWF analyses, see Trenberth and Olson (1988b).

C. Composites

The systematic aspects of PA evolution are isolated using a compositing procedure. For each set of PA cases (e.g. PAC negative, etc.), a composite evolution is determined by ensemble averaging the individual case evolutions with respect to the time that each case first exceeds/falls below the threshold M at the key point. For example, the *composite* flow five days before PA onset consists of an average of all the individual flow fields observed five days prior to onset. This would be referred to as "day -5" of the composite development. Features which show up systematically in the individual cases lead to the coherent evolution of the composite.

Composite *anomalies* are the deviations of the composite fields from the long-term climatology. For the simple height and temperature anomaly analyses of chapter IV, an anomaly is defined as a departure from the local seasonal cycle. The seasonal cycle is defined as the sum of the first four harmonics of an annual time series derived by ensemble averaging 25 years of twice-daily NMC analyses from 1963 through 1987. For all subsequent analyses, anomalies are defined as deviations from local wintertime mean values determined by averaging the fourteen 120-day winter seasons (starting Nov 15) extending from 1963/64 through 1976/77. These are the winters during which the PA's studied by Dole (1986a, 1989) occurred. We note that the height anomalies presented in Chapter IV are *not* scaled by sine latitude as in Dole (1986a). The

significance of composite anomalies is tested using a two-sided t-test.

As mentioned earlier, the primary features of interest are contained in the composite evolution. This coherent evolution is what we describe and strive to understand the sources for. One of the underlying hypotheses is that the important large-scale dynamics are contained in the composite flow fields. Unless otherwise stated, all "eddies" and "eddy" fluxes refer to perturbations derived from the composite fields. To further illustrate this, consider the quasigeostrophic potential vorticity equation:

$$\left(\frac{\partial}{\partial t} + \mathbf{v}\cdot\nabla\right) q = S$$

where q is pseudopotential vorticity, $\mathbf{v}$ is the geostrophic velocity and S is a nonconservative source term. This can be expanded as:

$$\frac{\partial}{\partial t}\langle q'\rangle = -\bar{\mathbf{v}}\cdot\nabla\langle q'\rangle - \langle\mathbf{v}'\rangle\cdot\nabla\bar{q} + \langle S'\rangle - \left(\langle\mathbf{v}'\cdot\nabla q'\rangle - \overline{\mathbf{v}'\cdot\nabla q'}\right) \qquad (3.1)$$

where: $\langle\mathbf{v}'\cdot\nabla q'\rangle = \langle\mathbf{v}'\rangle\cdot\nabla\langle q'\rangle + \langle\mathbf{v}''\cdot\nabla q''\rangle$

$(\bar{})$	represents a time-mean value
$(\,)'$	is a deviation from the time-mean
$\langle(\,)'\rangle$	is an ensemble average (composite) perturbation
$(\,)''$	represents a deviation from the ensemble average (an incoherent eddy)

The above equation is used to derive the eddy enstrophy relation used in Chapter V. The first two terms on the right hand side of the equation are linear interactions with the mean flow. <S'> is due to anomalous diabatic, frictional and non-quasigeostrophic effects. The term in parentheses represents the effects of anomalous nonlinearity. This includes the nonlinearity of the composite eddies as well as that associated with the incoherent

transients. Our primary interest will be in examining the linear terms of this equation. Although the nonlinearity of the composite fields will be explicitly calculated, the anomalous nonlinearity associated of the incoherent transients will be grouped with the nonconservative source/sink term.

In practice, the composite flow anomalies are large-scale in nature. The compositing procedure tends to filter out much of the higher frequency synoptic-scale variability. Thus, a large portion of the case-to-case variability (due to the *incoherent* transient eddies) is a result of synoptic-scale eddy activity. We note, however, that the coherent evolution may also contain synoptic-scale eddies - if they are systematic components of the time evolution. For example, Dole (1986b) notes that the unfiltered (in time) composite PAC developments include an intensifying and eastward propagating synoptic-scale transient disturbance over the western North Pacific. In general, however, the level of synoptic-scale activity in the composite evolutions is relatively small. Chapter VI further examines the usefulness and representativeness of the composite analyses by comparisons with individual cases.

Most of the composite evolutions are based upon cases originally identified by DG and examined in the 500 mb time evolution study of Dole (1989). The cases were selected during the fourteen winters of 1963/64 through 1976/77 from low-pass filtered time series of Z_θ' at the PAC and ATL key points (see Chapter II). In Chapter VI, we examine the reproducibility of the results by identifying new cases in a more recent independent dataset which includes the 10 subsequent winters of 1977/78 through 1986/87. These additional cases aid in reducing the noise of the eddy enstrophy budgets of Chapter V. Also, the newer cases are used in the investigations of possible tropical influences upon development. The onset days and durations of the cases identified in both datasets are listed in Appendix A.

D. Quasigeostrophic approximation

Quasigeostrophic (QG) approximations are often applied in analyses presented in this thesis. Fourier decomposition shows that the dominant zonal scales associated with composite PA developments are wavenumbers 1-4 (Dole, 1986b). PA's are local phenomena, however, and the zonal scale of *variation* exhibited by the composite anomalies in the key regions is $\approx 2\times10^6$ m. The meridional scale of variation is typically smaller than the zonal scale during the large-scale growth phase (see Chapter II, section A). For these scales:

$$L \approx 2 \times 10^6 \text{ m} \quad \Rightarrow \quad L/a \approx 0.3$$

$$R_o \approx 0.1$$

Where L is the horizontal scale of variation, a is the radius of the earth and R_o is the Rossby number. Thus, the motions will be governed by large-scale QG dynamics rather than by ultra-long, planetary scale dynamics. This is in accord with the observational results of Lau (1979), which suggest that even the stationary forced waves of the atmosphere should be regarded as long waves rather than ultra-long waves. As a result, we will often employ a large-scale QG scaling in our diagnostic analyses. For composite analyses, the magnitude of geostrophic wind anomalies typically differed from analyzed wind anomalies by less than 10%.

E. Analyses

The analyses of Chapter IV detail the 3-D time evolution of PA's over the PAC and ATL regions. Composite analyses are used to determine the systematic flow

anomalies associated with PA development and decay. One goal of this work is to extend Dole's (1989) 500 mb study by examining the vertical and thermal structure associated with the evolving flow anomalies. Significant anomaly patterns are identified using statistical methods. These features are then studied within the context of the full-field synoptic evolution. In order to investigate the predictability of PA decay, we compare post-development anomaly patterns to pre-decay patterns. The horizontal fluxes of heat and momentum associated with the developing composite eddy are diagnosed. Q-vectors are used to assess the secondary (ageostrophic) circulation associated with the composite.

In Chapter V, specific diagnostic methods are employed to identify anomalous sources and sinks of wave activity. Dynamical processes during the developments are investigated with both conventional energetics analyses and with local, QG eddy enstrophy budgets. QG potential vorticity analyses are also used to further interpret aspects of the large-scale evolution.

The reproducibility of our results is investigated in Chapter VI by studying PA's identified in more recent dataset. The representativeness of the composite is also demonstrated using individual case analyses. In addition, potential tropical influences upon PA development are considered using OLR data and upper-tropospheric tropical wind analyses obtained during the more recent events.

F. Hypothesis testing

The analyses of Chapter IV are descriptive in nature and provide an initial basis for testing the hypotheses for PA development. The various theories predict structures and time evolutions which can be compared with the results of Chapter IV. The diagnostics of Chapter V more directly address the development hypotheses. Wave activity fluxes are used to determine whether the sources for the large-scale developments are primarily local or remote. The energetics analyses and eddy enstrophy budgets will test whether

the wave/time-mean flow interactions are sufficient to account for the observed developments. Also, the eddy enstrophy budgets are used to deduce net local nonconservative effects (including diabatic and incoherent eddy forcing). The potential influence of anomalous tropical forcing upon the upsream jet variations observed *prior* to PAC developments is examined in Chapter VI. Some predictions of the various theories are presented below:

i) Large-scale instability/growth

The instability theories discussed in Chapter II suggest that eddy/mean flow interaction can account for the large-scale eddy developments. The theory of barotropic instability of a zonally varying flow (Simmons et al., 1983) anticipates upgradient E-vector signatures in the jet exit regions of the upper troposphere during development. Downgradient and upward eddy heat fluxes would be expected during baroclinic growth (Frederiksen, 1983b). In both cases, the sources of wave activity will be primarily local to the development region. Also, large-scale eddy/mean flow interaction should be sufficient to account for eddy growth. It is plausible that both baroclinic *and* barotropic conversions could contribute simultaneously to development, as suggested by Frederiksen's results.

ii) Anomalous forced waves

Anomalous forced waves can arise from *anomalous forcing* or *mean flow variations*. Anomalous *remote* forcing would result in an equivalent barotropic wavetrain extending into the region of development (Hoskins and Karoly, 1981). Wave activity fluxes would extend from the forcing region toward the disturbance (Plumb, 1985).

As mentioned in the previous chapter, there are few thorough studies of the

potential effects of local diabatic forcing upon PA development. If diabatic heating was responsible for PA development, however, we would expect local wave sources and positive contributions to the nonconservative source term in the enstrophy budget.

Mean flow variations lead to changes in the propagation characteristics of the atmosphere. Thus it is possible to change the stationary wave structure without actually modifying the forcing distribution. This mechanism would lead to a *redirection* of the wave activity flux associated with climatological mean stationary waves (e.g. Kang, 1990). The results of Nigam and Lindzen (1989) suggest that this results primarily in a modification of stationary wave amplitude rather than phase. Thus, the evolving PA should converge towards an anomaly pattern which is approximately in-phase with the climatological mean stationary waves.

iii) Synoptic-scale forcing

Although we do not focus upon anomalous synoptic-scale forcing, it is implicity contained in the eddy enstrophy analyses of Chapter V, as the residual "nonconservative" term of the eddy enstrophy budget includes the nonlinear effects of incoherent synoptic-scale eddies. Thus, if synoptic-scale eddies are largely responsible for PA development, we would expect a substantial positive contribution to the residual term from the incoherent eddies. Also, the wave activity analyses should indicate that the sources for development are local.

The above discussion provides a foundation for interpreting the subsequent observational analyses. We note that the mechanisms are not necessarily independent. For example, it is possible for a remotely forced wave to locally interact with the mean flow (e.g. Simmons et al., 1983; Branstator, 1985). In this case we might anticipate signatures of both remote forcing *and* eddy/mean flow interaction.

IV. Composite time evolution analyses

A. Introduction

This chapter presents the results of composite analyses of the time evolution of ATL and PAC persistent anomaly cases. As discussed previously, Dole (1986b, 1989) has performed detailed observational analyses of the 500 mb time evolution of PA's. In Dole (1986b), he also briefly examines the vertical structure of composite PAC developments. A review of this work is presented in Chapter II. Here Dole's studies are extended in order to provide a more complete picture of the systematic aspects of the time evolution of PA's. For clarity, we initially describe results for each PA type separately. Later, we will compare and contrast the different developments. Although we focus mainly on the systematic features of developments, we will also attempt to identify any significant *differences* between the anomalous flow patterns observed after development and those observed just prior to breakdown.

B. Procedure

For each type of event, we first analyze the three-dimensional composite *anomaly* structure observed during development, where an anomaly is defined as a deviation from the local seasonal trend value (see Chapter III, section C). Dole (1986a) determined that PA's exhibit maximum geopotential amplitudes near 300 mb. Therefore, results for the 300 mb level will be displayed to illustrate the time evolution of upper level height anomalies. The lower tropospheric flow evolution will be examined using 1000 mb height anomalies, and thermal anomalies are studied at 700 mb. The significance of composite anomalies is estimated using a two sided t-test with a null hypothesis of zero mean anomaly. Meridional and zonal cross sections are used to more fully describe the

vertical structure during development. The 300 mb height anomaly time evolution is found to be quite similar to that at 500 mb, as described in Dole. Therefore we do not present t-test results for 300 mb.

The full field PA evolution is studied using synoptic analyses. The lower tropospheric flow and thermal advection patterns are displayed by overlaying the 1000 mb heights with the thickness of the 1000-500 mb layer. At upper levels, we superpose the 400 mb height and pseudopotential vorticity patterns. For display purposes, the small-scale features of of the pseudopotential vorticity field are removed by filtering out fluctuations having zonal wavenumbers ≥ 12. The most significant aspects of the composite anomaly evolution are then discussed in the context of these analyses.

One problem of particular interest is the interaction of the composite eddy with the mean flow. The classical method for examining eddy/mean flow interactions in the atmosphere has been through energetics analyses, as pioneered by Lorenz (1955). In this approach, downgradient eddy fluxes of heat and momentum are related to conversions of energy between the mean flow and the eddies. In the original formulation, eddies were defined as departures from the zonally averaged flow. In some more recent studies (Simmons et al, 1983; Lau and Lau, 1984), eddies are instead defined as departures from the *zonally varying* time-mean flow (including the stationary waves). In the QG formulation, the relevant conversion terms are:

$$\text{(4.1a)} \qquad C(K, K') = -\int \left(u'v' \cdot \nabla \bar{u} + v'v' \cdot \nabla \bar{v} \right) dm$$

$$\text{(4.1b)} \qquad C(A,A') = -\int c_p \gamma \left(v'T' \cdot \nabla \bar{T} \right) dm$$

$$\text{(4.1c)} \qquad C(A',K') = -\int \left(\omega'\alpha' \right) dm$$

where: $(\bar{\ })$ = time mean
$(\ )'$ = deviation from time mean

The zonal and meridional geostrophic wind components are, respectively, u and v, T is temperature, c_p is the specific heat at constant pressure, γ is inversely proportional to the mean isobaric static stability, ω is the vertical pressure velocity and α is the specific volume. The terms A and K represent, respectively, the available potential energy and kinetic energy of the time-mean flow, and A' and K' are corresponding eddy energy terms. The integrations are mass-weighted over latitude, longitude and pressure. From 4.1, we see that downgradient fluxes of heat and momentum are associated with positive energy conversions from the time-mean flow into the anomalies. Note that, in this formulation eddies may extract mean flow energy associated with the zonal variations in the basic state.

The general usefulness of energetics analyses for diagnosing eddy-mean flow interactions in the atmosphere has been questioned (e.g. Plumb, 1983), and ambiguities of this approach are discussed in Chapter V. Although the approach has limitations, it is still useful (a) for describing characteristic structures of the growing eddies and (b) examining whether the observed developments are consistent with proposed models for PA generation (many of which are presently described in terms of energetics).

To a very good approximation, Simmons et al. (1983) show that:

$$C(K,K') = \int (\mathbf{E} \cdot \nabla \bar{u})\, dm$$

$$\text{where:} \qquad \mathbf{E} = [\, (v')^2 - (u')^2;\ -u'v' \,]$$

This is easily displayed on a pressure surface by superposing E-vectors and contours of time-mean u. *Upgradient* E-vectors imply local positive contributions to the barotropic energy conversions from the mean flow into the eddy. Phase-averaged E-vectors also

provide information on horizontal eddy structure (Hoskins et al., 1983). Zonally elongated eddies have $u'^2 > v'^2$ and westward pointing E-vectors, and the converse is true for meridionally elongated eddies. Also, E_y is related to the horizontal tilt of the eddy. For barotropic flows -E represents an effective flux of westerly momentum.

The baroclinic conversion term of (4.1b) can be depicted by overlaying vectors of eddy heat flux and contours of time-mean T. In practice, the baroclinic term is dominant in the lower troposphere, where heat fluxes are relatively strong, while the barotropic conversion term is largest near the tropopause. Therefore, for a first order look at the potential dynamical interactions of the composite eddy with the time-mean flow, we diagnose the 700 mb heat fluxes and 300 mb E-vectors of the growing composite perturbation.

Quasigeostrophic Q-vectors are used to qualitatively diagnose the secondary (ageostrophic) circulation associated with the evolving anomalies. As Hoskins et al. (1978) and Hoskins and Pedder (1980) show, Q-vectors provide considerable useful information. Hoskins and Pedder show that geostrophic frontogenesis is given by:

$$\frac{d}{dt}|\nabla\theta|^2 = 2\mathbf{Q}\cdot\nabla\theta \tag{4.2}$$

where:

$$\mathbf{Q} = -\left(\frac{\partial \mathbf{v}_g}{\partial x}\cdot\nabla\theta\,;\,\frac{\partial \mathbf{v}_g}{\partial y}\cdot\nabla\theta\right)$$

Potential temperature is denoted by θ, $\mathbf{v}_g$ is the geostrophic velocity and d/dt is the time derivative following the geostrophic flow. A frontogenetical flow is associated with Q-vectors directed up the gradient of θ. Hoskins et al. demonstrate that for adiabatic and inviscid flows on an f-plane, horizontally converging Q-vectors (on some interior tropopheric pressure level) suggest large-scale ascent. Also Q-vectors tend to point in the direction of the low-level ageostrophic motion. By plotting Q-vectors over the evolving

composite T field, one can qualitatively deduce the patterns of vertical motions as well as frontogenetical aspects of the flow field (noting that $\theta = \theta(T,p)$). Again, we will apply this diagnosis at the 700 mb level. A comparison of the Q-vector pattern with the 700 mb T ' evolution will provide an indication of $\omega'\alpha'$ in the lower troposphere.

It is important to reiterate that the fluxes described below are associated with the *composite* perturbations. This is to be distinguished from *composited* fluxes. As discussed in Chapter III, our main focus will be on the coherent aspects of the time evolution as captured in the composite analyses. For reference, the climatological- mean patterns of E-vectors, heat fluxes and Q-vectors are presented in fig. 4.0. In the next section, a detailed description of Pacific negative composite development is presented and is followed by summaries of the other PAC and ATL developments

C. Composite analyses

i. Description - PN cases.

We first examine the composite evolution of Pacific negative (PN) persistent anomaly cases. Fig. 4.1 shows the composite 300 mb geopotential height anomaly evolution. Five days prior to PN onset (day -5) a midlatitude ridge is located near the date line (fig. 4.1a). Upstream, significant negative height anomalies are found over eastern Asia at 40N. This pattern is zonally elongated, suggesting the existence of (a) significant perturbations to the upper level zonal flow near the East Asian subtropical jet stream (or EAJ) and (b) anomalous cyclonic shear in the upper-level geostrophic flow over eastern Asia. Between day -5 (fig. 4.1a) and -1 (fig. 4.1c) the midlatitude ridge over the North Pacific weakens as it retrogresses northwestward toward eastern Siberia. An intensifying synoptic-scale low, tilting from northwest to southeast, is observed northeast of Japan at day -3 (fig. 4.1b). The low propagates eastward to the date line by

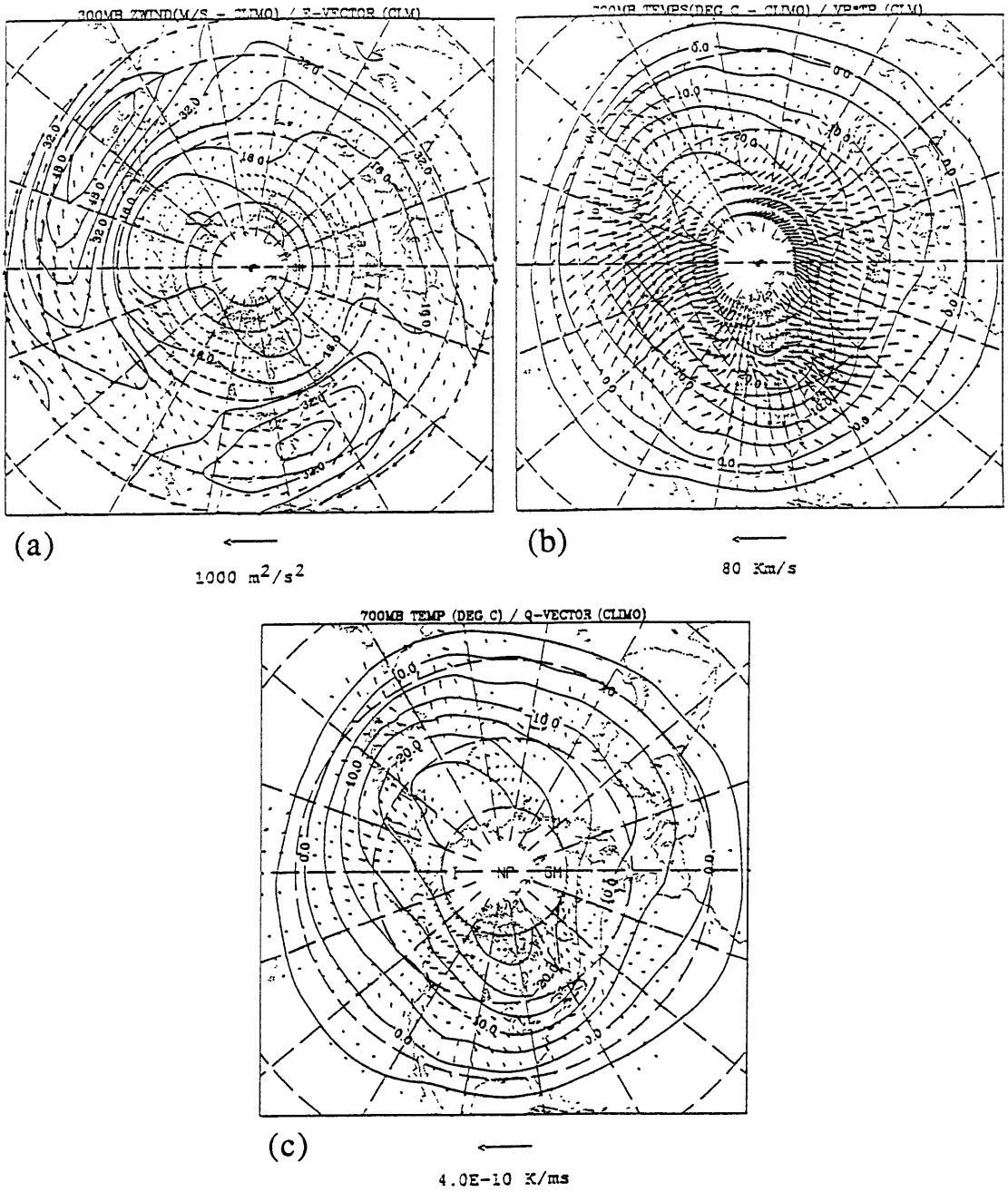

Fig. 4.0. Wintertime-mean values of (a) 300 mb zonal winds (m/s) and transient eddy E-vectors, (b) 700 mb temperature (°C) and transient eddy heat fluxes, and (c) 700 mb temperatur (°C) and mean-flow Q-vectors. A scale vector and corresponding magnitudes are displayed below each figure.

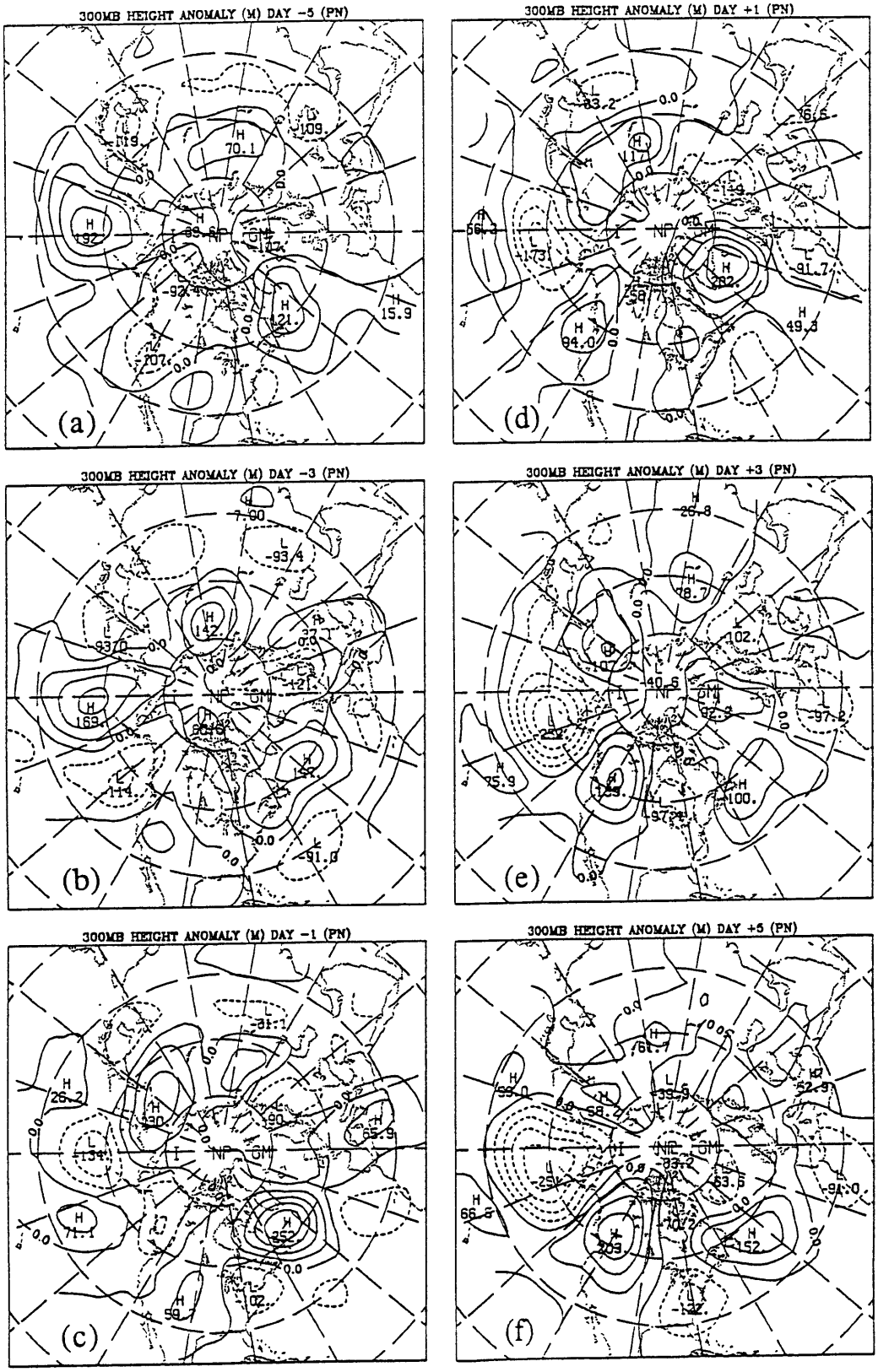

Fig. 4.1. Composite averaged 300 mb height anomalies (m) for the first 14 PN cases on days (a) -5, (b) -3, (c) -1, (d) +1, (e) +3, and (f) +5 relative to onset time.

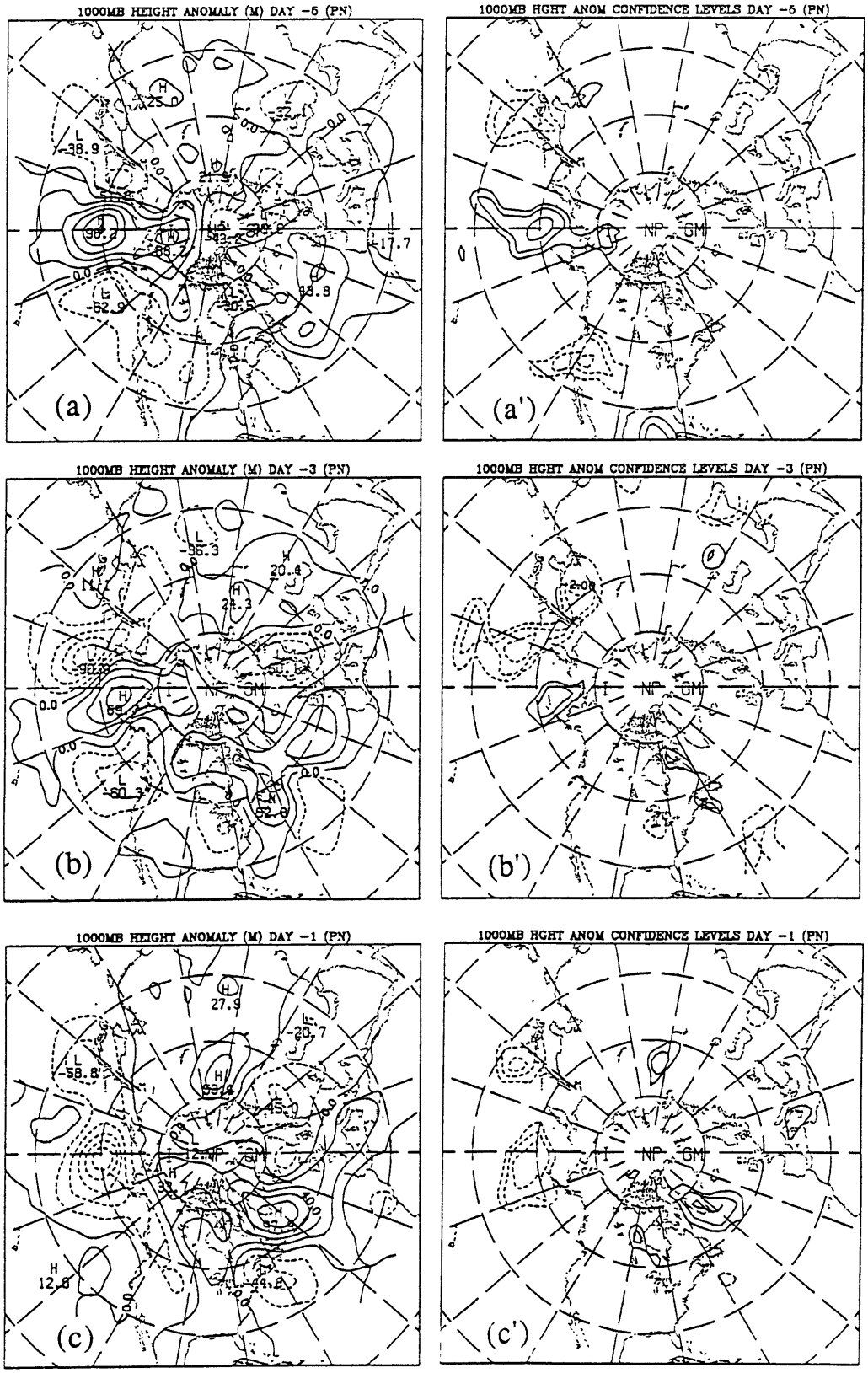

Fig. 4.2. The left column is as in Fig. 4.1 for 1000 mb height anomalies (m). Regions where composite anomalies are greater or less than zero at the 90%, 95% and 99% confidence levels are indicated in (a')-(f') with contour values of 1, 2 and 3, respectively. Dashed lines correspond to negative anomalies.

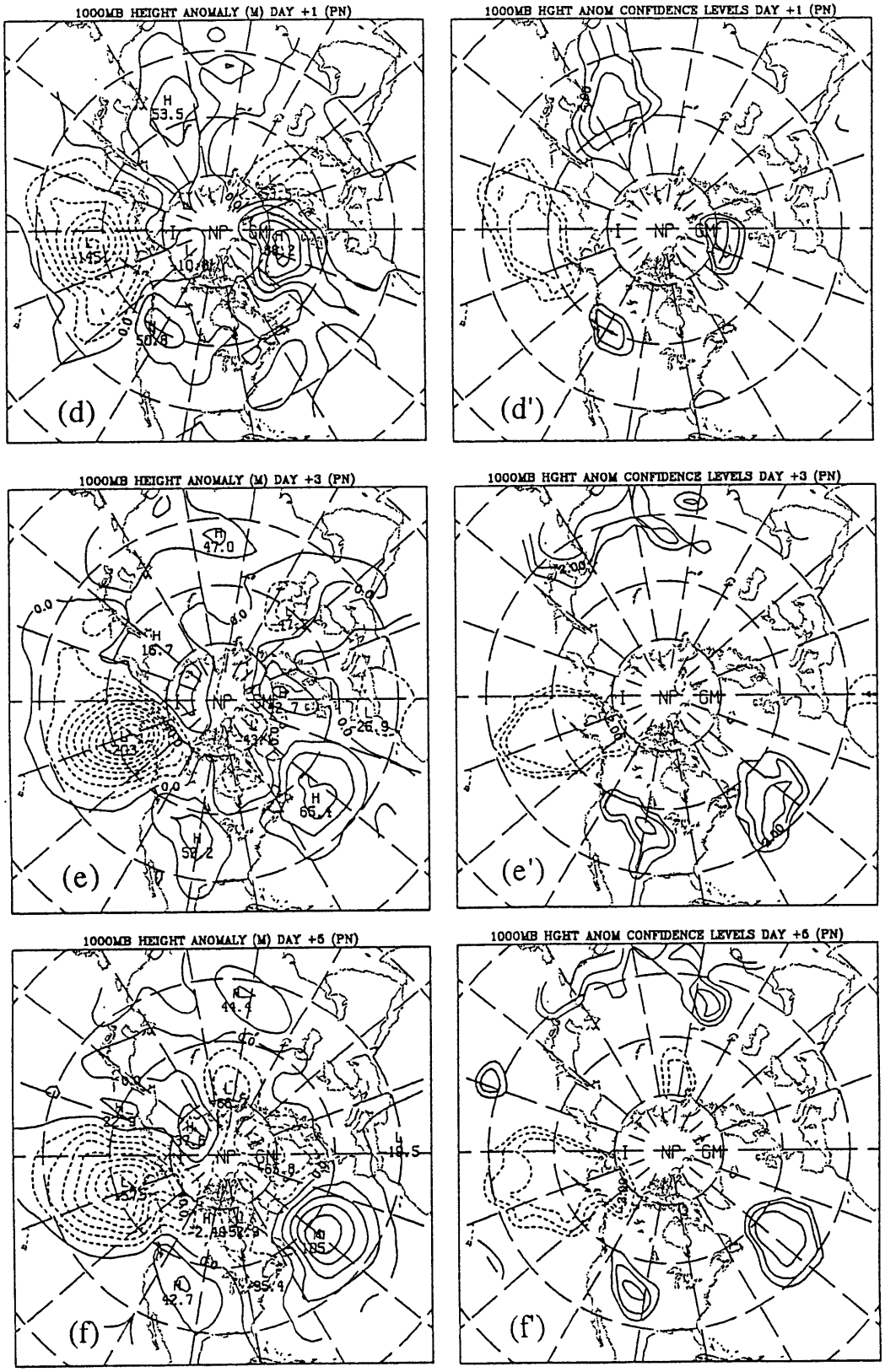

Fig. 4.2. (*Continued*)

day -1 (fig. 4.1c). After day -1, the disturbance slowly propagates into the PAC key region (near the Aleutian Islands) initiating the PA. At day +1 (fig. 4.1d), the composite low exhibits a zonally elongated structure in the exit region of the EAJ. Between days -1 and +1, significant positive anomalies form south and east of this "primary" anomaly. Also, the negative height anomalies initially observed upstream over Asia weaken at this time.

After day +1, the primary anomaly near the Aleutians becomes quasi-stationary (figs. 4.1e, f). Intensification continues, but on a larger scale than previously observed, with the meridional scale of the disturbance increasing with time. Strong ridge development occurs downstream over western North America. Subsequently, a trough forms over the eastern U.S. By day +5 (fig. 4.1f), significant positive anomalies are observed even further downstream over the North Atlantic. At this time, the pattern closely resembles the mean 500 mb PN anomaly structure of Dole (1986a).

Fig. 4.2 displays the 1000 mb height anomalies and corresponding t-test results. At day -5 (fig. 4.2a), significant positive anomalies are found below the upper-level ridge located near the date line. This signature weakens while propagating northwestward between day -5 and -1 (figs. 4.2a-c). A weak but statistically significant surface low is found southeast of Japan at day -5. This synoptic-scale surface low intensifies as it propagates northeastward to near the key region by day -1 (fig. 4.2c). Comparison with fig. 4.1b shows that the disturbance exhibits a strong westward tilt with height at day -3 (fig. 4.2b), as well as a pronounced northwest-southeast horizontal tilt. By day -1 (fig. 4.2c), the low becomes roughly equivalent barotropic (see fig. 4.1c).

By day +1 (fig. 4.2d), a large-scale anomalous cyclonic circulation covers most of the North Pacific. The disturbance remains equivalent barotropic at this time. Further strengthening of the anomalous cyclonic circulation occurs over the North Pacific, as the center of the surface low shifts slowly northeastward between days +1 and +3 (figs. 4.2d,e). The disturbance tilts southwestward with height after day +1. Downstream of

the primary anomaly center, positive height anomalies build into the west central US and over the North Atlantic ocean (figs. 4.2e,f).

Fig. 4.3 shows the 700 mb thermal anomaly evolution for the same times. Positive temperature anomalies are associated with the mid-Pacific ridge at day -5 (fig. 4.3a). This warm perturbation strengthens between day -5 and -3 (fig. 4.3b) and then retrogresses towards eastern Siberia (fig. 4.3c). Initially, most of east and southeast Asia is covered by significant cold anomalies. A portion splits off and move eastward during synoptic-scale intensification observed over the western North Pacific at day -3. Negative anomalies intensify near the key region after day +1 (figs. 4.3e,f). We note that *throughout* the latter part of the evolution, highly significant cold anomalies continue to be observed over southeast Asia.

Figs. 4.4 and 4.5 illustrate the vertical structure of the primary features during PN development, focusing on the primary anomaly. Zonal cross sections (fig. 4.4) show a strongly westward tilting low west of 170E at day -3 (fig. 4.4a), with a weakening ridge near the date line. By day 0 (fig. 4.4b) the intensifying low propagates eastward to 165W and acquires a roughly equivalent barotropic structure. Note, however, that as the development continues the large-scale disturbance reacquires a westward tilt (fig. 4.4c). The meridional sections (fig. 4.5) demonstrate that during both early and later stages of development the growing disturbance also exhibits *southward* tilts with height. This implies that, at these times, there are associated anomalous *westward* geostrophic heat fluxes. Throughout the evolution, the primary anomaly appears predominantly confined to the troposphere, with maximum geopotential amplitudes near 300 mb.

Fig. 4.6 depicts the composite 1000 mb height and 1000-500 mb thickness fields during PN development. At day -5 (fig. 4.6a), strong geostrophic cold advection occurs over the far western North Pacific. This cold advection decreases southward, indicating a strongly frontogenetical flow exists near the latitude of the EAJ. At this time, two low centers are located over the northeastern and northwestern North Pacific. During the next

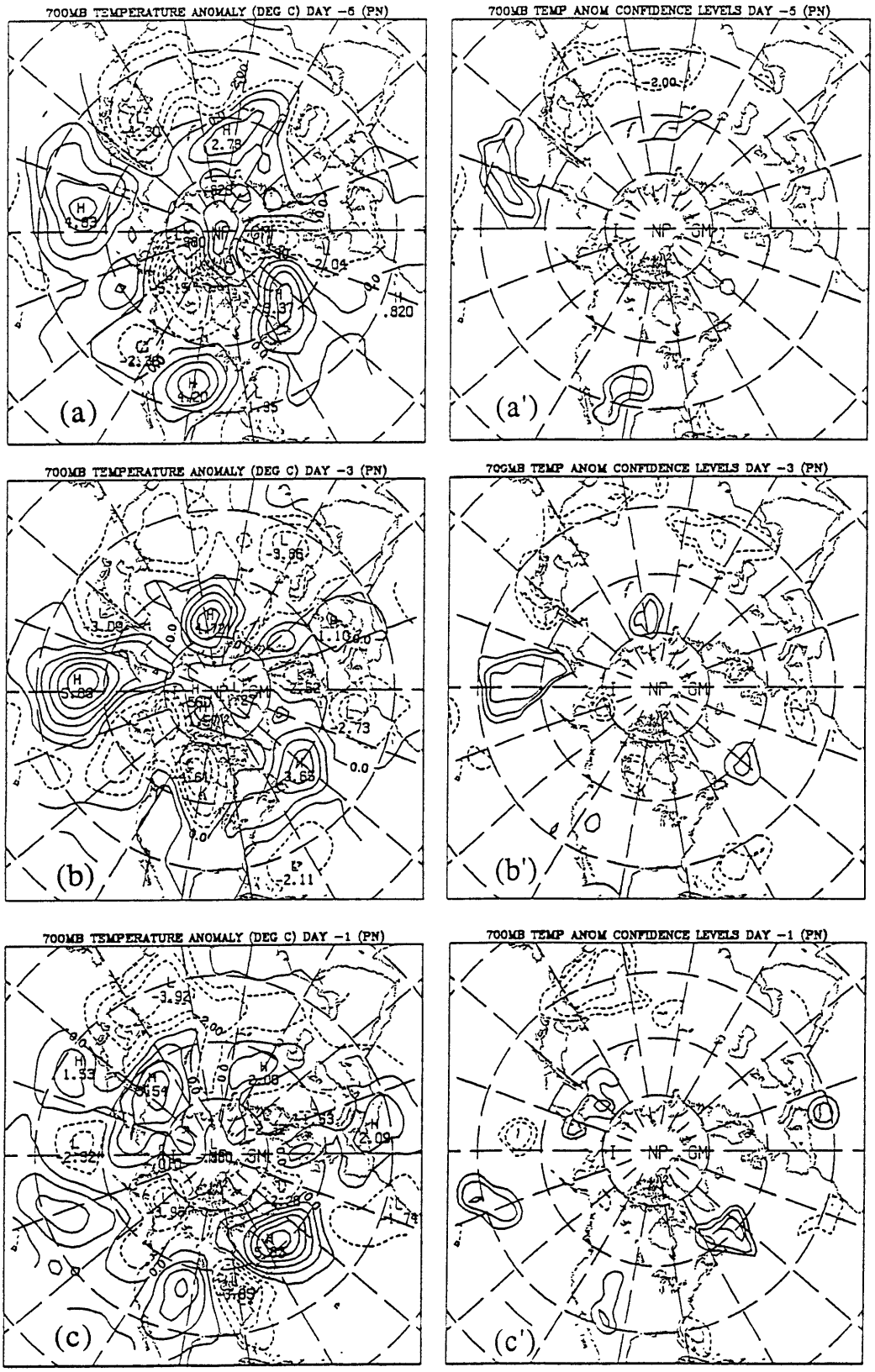

Fig. 4.3. As in Fig. 4.2 for 700 mb temperature anomalies (°C)

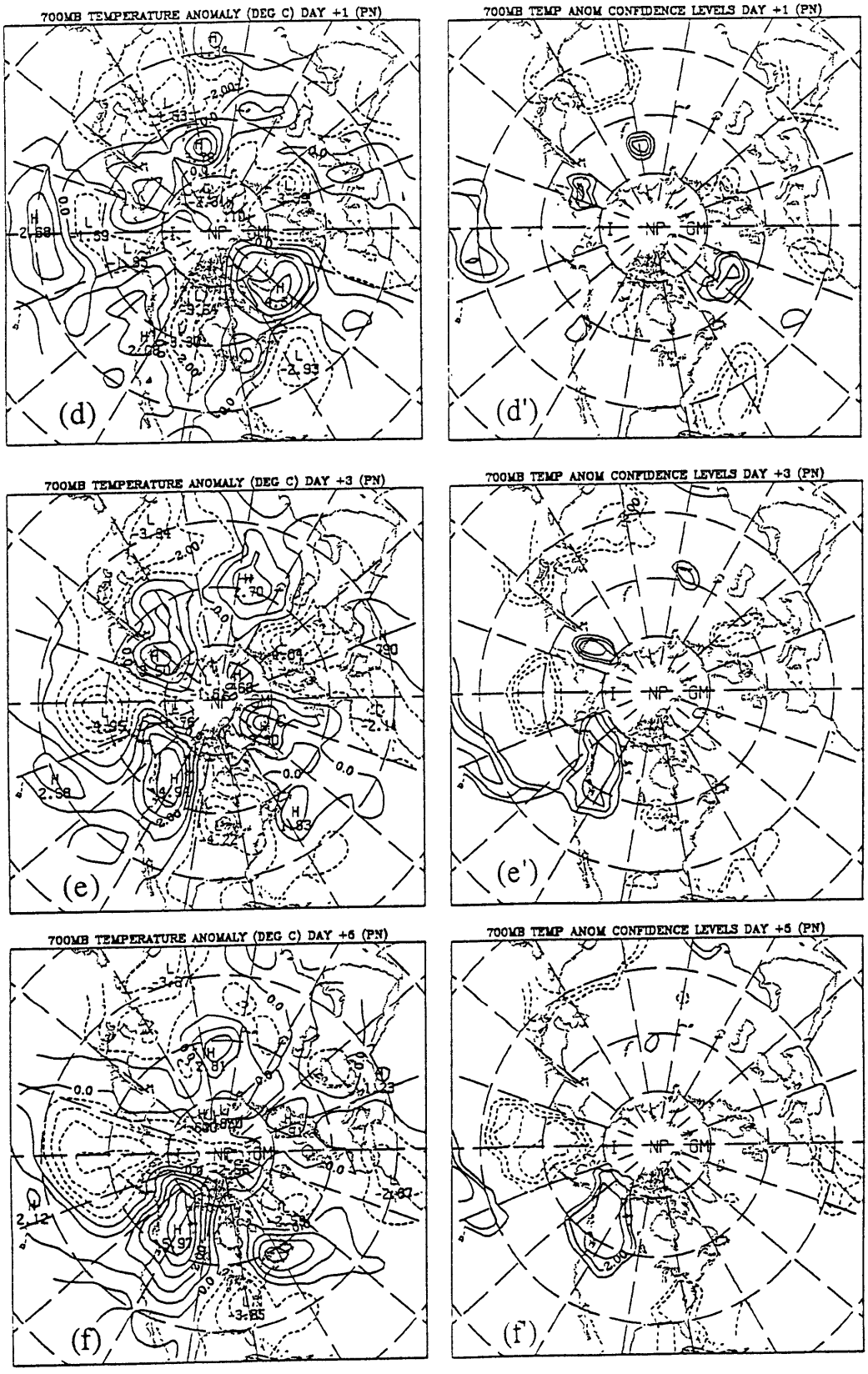

Fig. 4.3. (*Continued*)

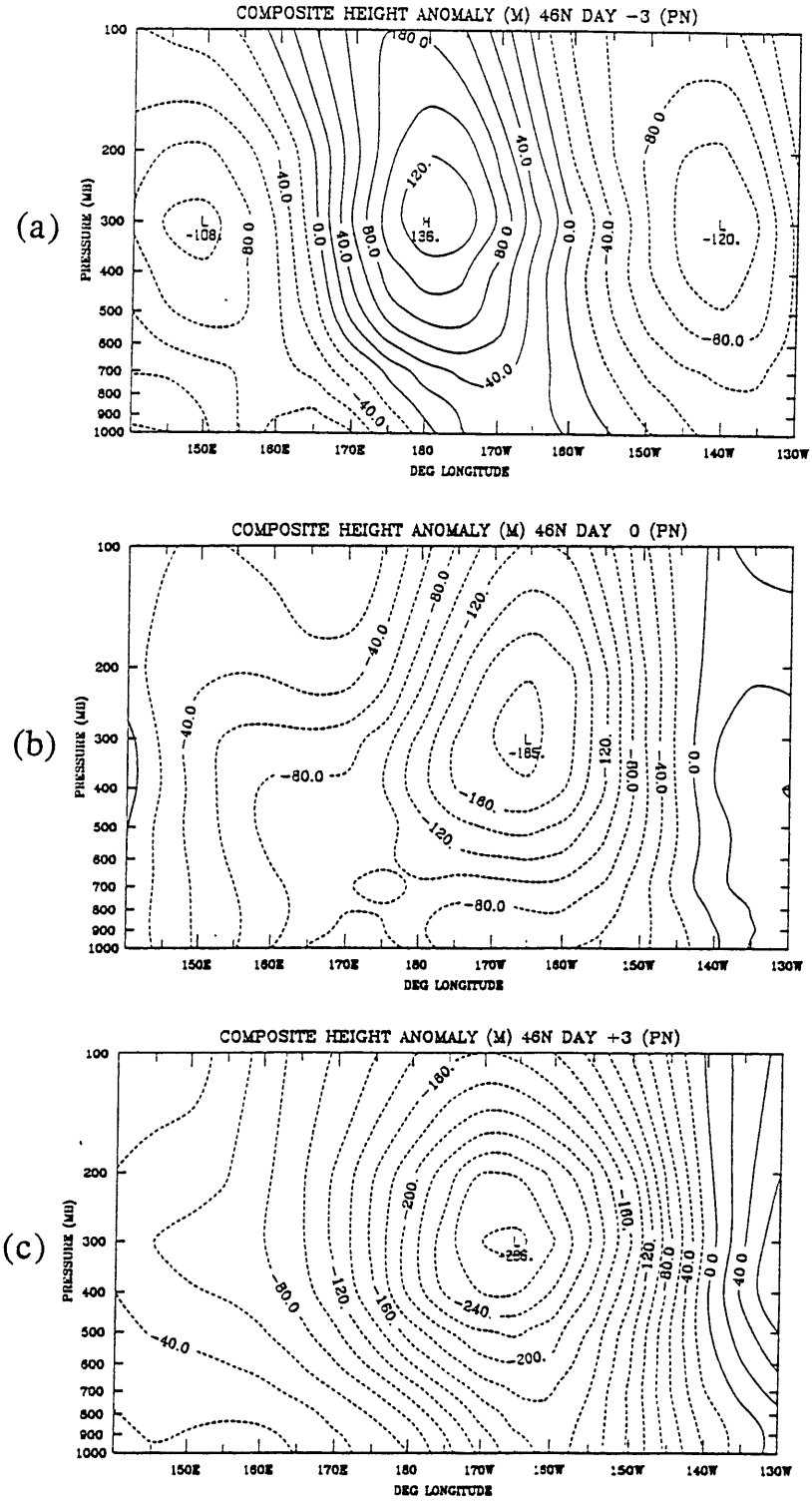

Fig. 4.4. Zonal cross sections of composite height anomalies (m) during PN development. Sections are taken at 46°N for days (a) -3, (b) 0, and (c) +3.

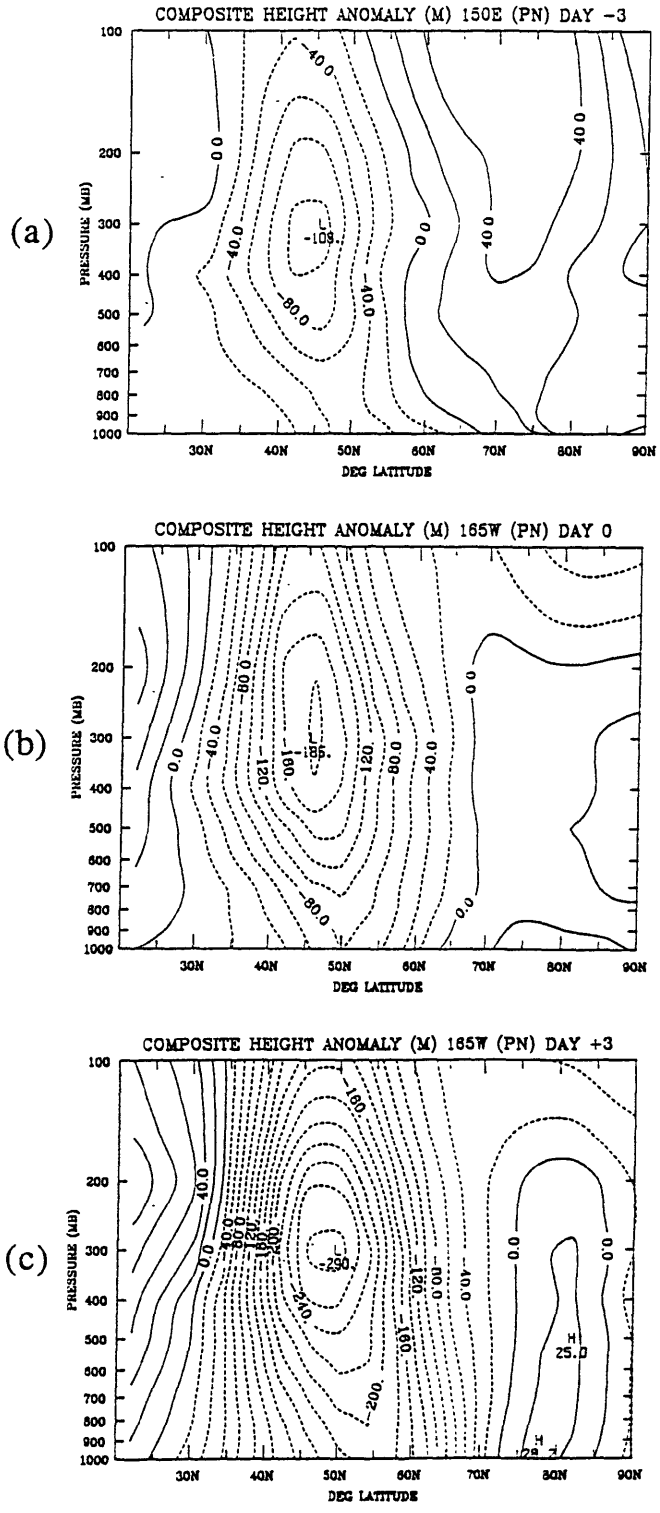

Fig. 4.5. Meridional cross sections of composite height anomalies (m) during PN development. Sections are at 150°E for (a) day -3 and 165°W for days (b) 0 and (c) +3.

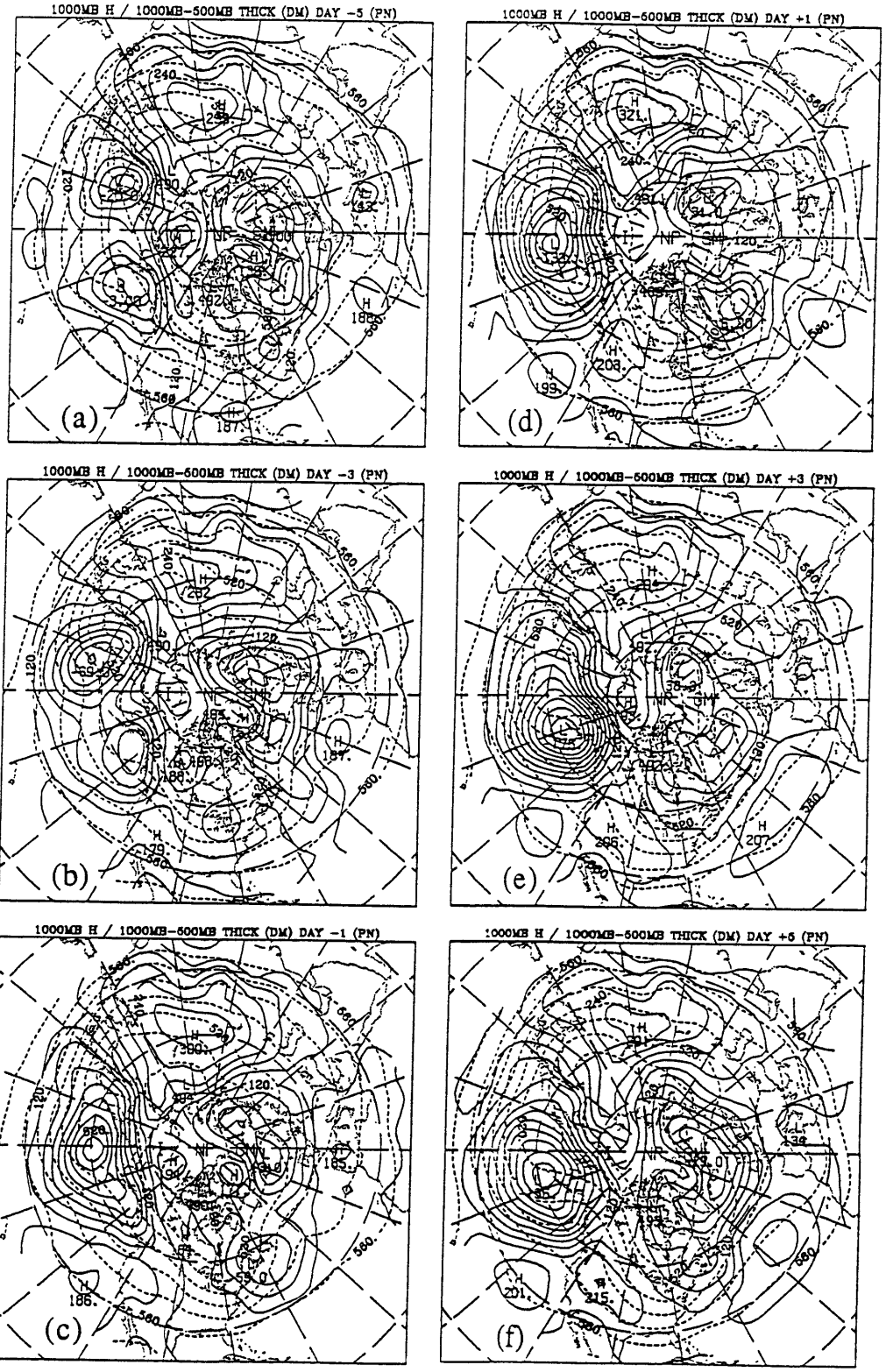

Fig. 4.6. As in Fig. 4.1 for 1000 mb heights (solid lines) and 1000-500 mb thickness (dashed lines). The contour intervals are 30 m for heights and 10 dam for thickness.

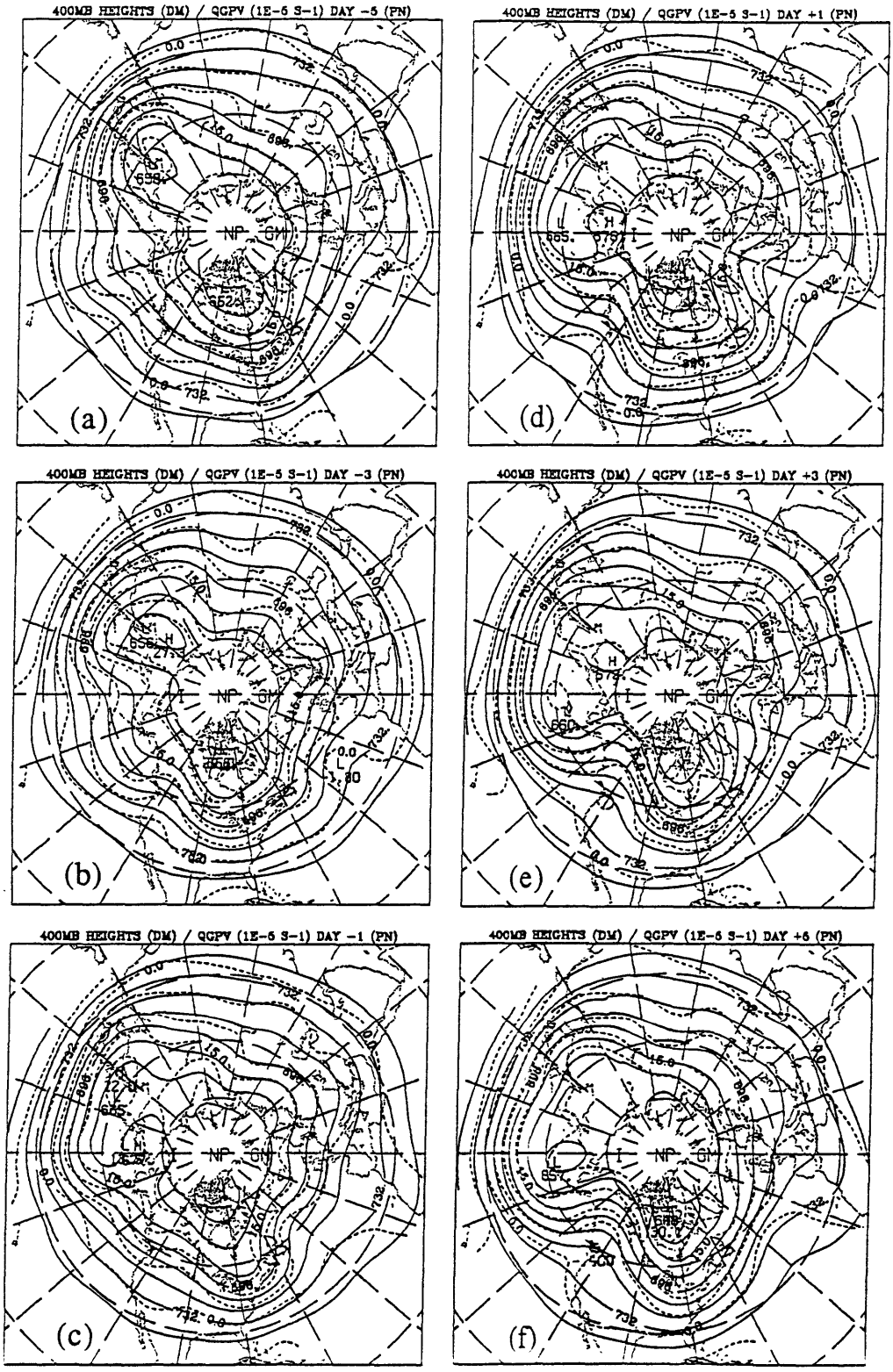

Fig. 4.7. As in Fig. 4.1 for 400 mb heights (solid lines) and psuedo-potential vorticity (dashed lines). Contour intervals are 12 dam for heights and 5×10^{-5} s^{-1} for vorticity.

two days, the eastern low weakens and the western low intensifies while propagating eastward in a strong baroclinic zone over the western North Pacific. Note the northwest-southeast tilt and the geostrophic thermal advections associated with this feature at day -3 (fig. 4.6b). At this time, strong cold advection is found in the storm's southwest quadrant with weaker warm advection to the northeast. By day -1 (fig. 4.6c), the intensifying and eastward propagating surface low amalgamates with the decaying eastern low, resulting in a markedly zonally elongated structure.

Two days later (day +1), an anomalously strong cyclonic circulation spans the North Pacific basin (fig. 4.6d). Strong cold advection extends southward and eastward from the Asian continent to the date line. Warm advection strengthens northeast of the surface low, near the region of upper-level ridge development. After day +1, the developing surface low propagates slightly northeastward, and becomes quasi-stationary near 165W at day +3 (fig. 4.6e). Downstream, surface high pressure builds into the western US and over the North Atlantic at 40N.

Fig. 4.7 displays the 400 mb heights and pseudopotential vorticity fields for the PN cases. The evolution begins with a deeper than normal trough and higher than normal potential vorticity over the east coast of Asia and a weak ridge over the central North Pacific (fig. 4.7a). An embedded short wave in the upper-level flow (indicated by a ridge in the potential vorticity) is found west of Japan at this time. At day -3 (fig. 4.7b), the upper wave is located upshear of the developing surface low, with positive pseudopotential vorticity advection over the surface center at this time. Again, note the northwest-southeast tilt of the trough, suggesting a southward flux of westerly momentum into the latitude of the intensifying upper-level jet. The EAJ subseqently intensifies and extends eastward over the western North Pacific (fig. 4.7c).

The jet continues strengthening over the central North Pacific after onset and extends eastward to 160W by day +1 (fig. 4.7d). Ridge development begins over the west coast of North America at this time. Further downstream, the later evolution is

characterized by trough development over the eastern US and weak ridge building over the North Atlantic (fig. 4.7e). A strong upper-level jet spans almost the entire North Pacific at day +5 (fig. 4.7f).

The 300 mb E-vectors associated with PN development are displayed over contours of time-mean u in fig. 4.8. For the Pacific composites, E-vectors and heat fluxes are displayed in two day intervals from day -3 to day +3. In general, significant flux patterns were not observed until day -3 or thereafter. After day +3, the large-scale flux patterns exhibit little change. Therefore we do not display days -5 or +5.

For PN, the early evolution is characterized by a relatively weak and disorganized E-vector pattern. At day -3 (4.8a), weakly downgradient E-vectors are observed on the north side of the EAJ over the western North Pacific, consistent with the noted northwest-southeast horizontal disturbance tilt described earlier. Weak, upgradient E-vectors are located in the jet exit two days later (fig. 4.8b). A strong, coherent upgradient pattern is observed in the exit region from day +1 onward, consistent with the zonally-elongated eddy structure in this region. Through day +3 (fig. 4.8d), this pattern intensifies, with strong E-vector divergence south of the Aleutians, where time-mean u is weak, and strong convergence upstream in the EAJ. This is consistent with an effective eastward flux of zonal momentum and conversions of kinetic energy from the time-mean flow into the growing anomalies.

Fig. 4.9 displays the corresponding 700 mb heat fluxes associated with the composite. Strong downgradient heat fluxes occur at day -3 (fig. 4.9a) in association with the growing synoptic-scale disturbance. During days -1 (fig. 4.9b) and +1 (fig. 4.9c), heat fluxes over the North Pacific are weak and largely rotational, consistent with the observed equivalent barotropic eddy structure. By day +3 (fig. 4.9d), however, a robust large-scale flux pattern emerges, which has, in addition to rotational fluxes, significant *downgradient* heat fluxes over a large portion of the North Pacific. Near the date line, there is a notable westward component to the flux pattern. Note that the

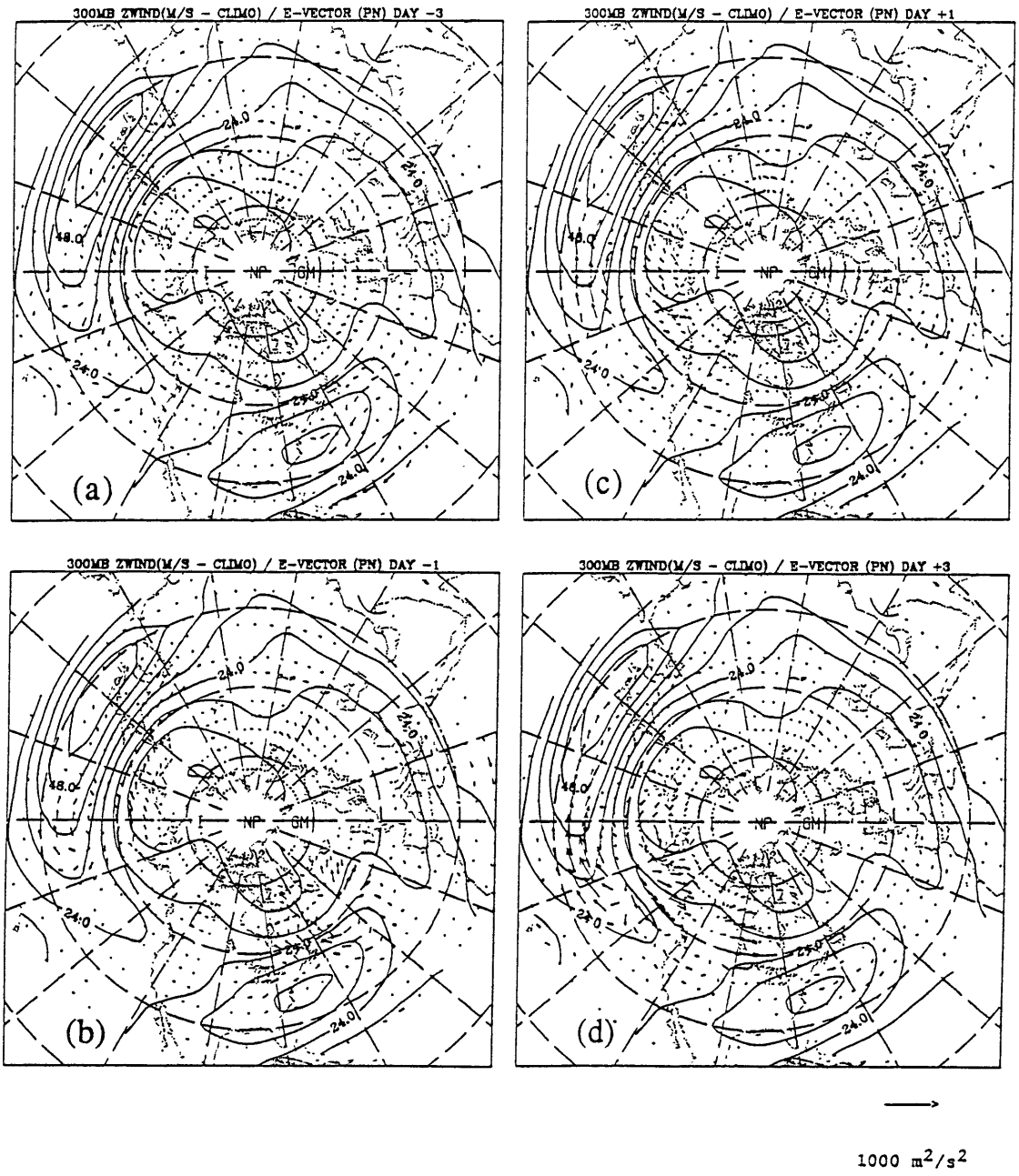

Fig. 4.8. Time evolution of E-vectors derived from 300 mb composite anomaly fields for the first 14 PN cases. E-vectors are displayed at days (a) -3, (b) -1, (c) +1 and (d) +3 along with the wintertime-mean 300 mb zonal wind (m/s). A scale vector and corresponding magnitude are displayed in the lower right-hand portion of figure.

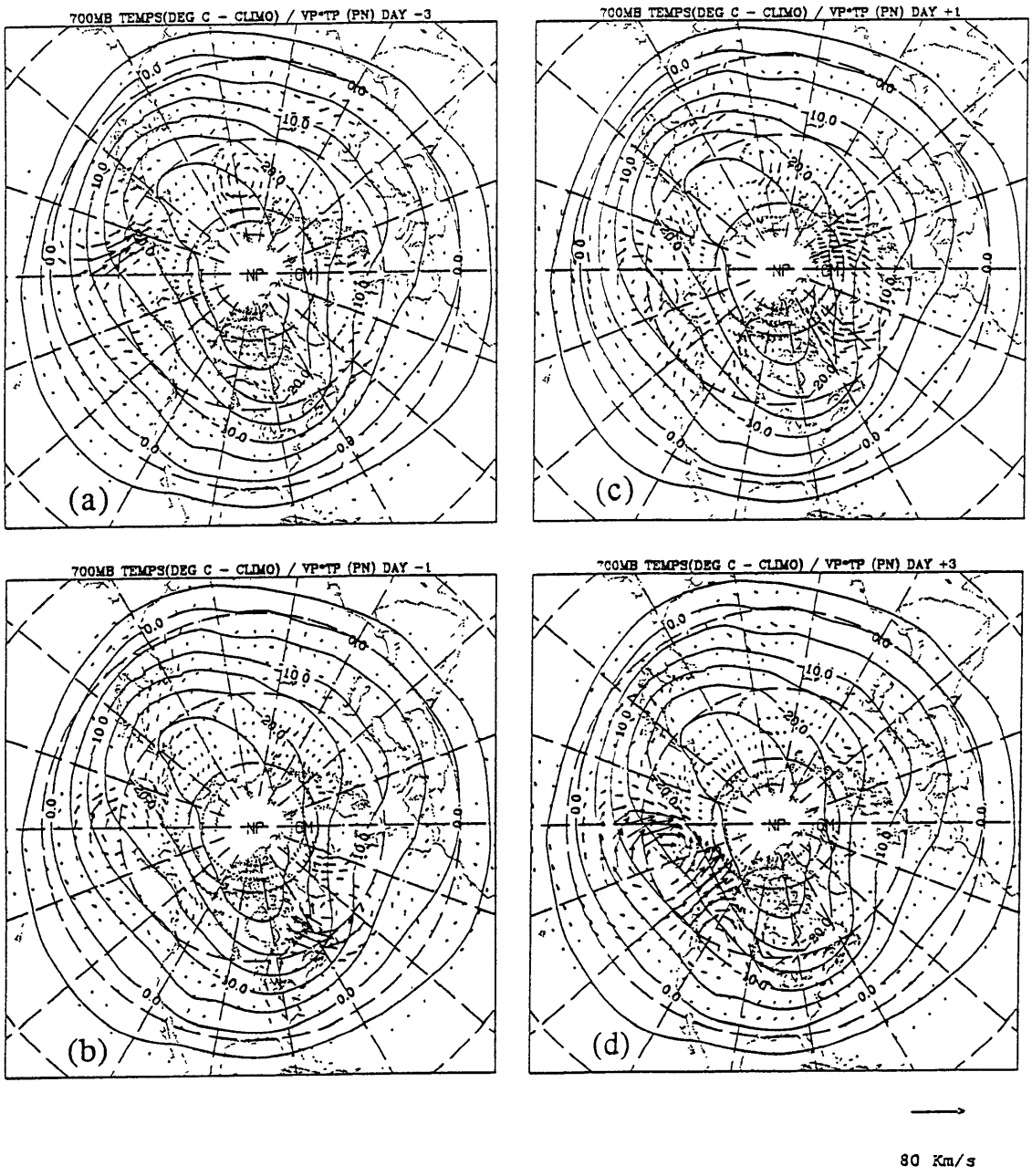

Fig. 4.9. As in Fig. 4.8 for 700 mb heat fluxes and wintertime-mean temperature (°C).

large-scale development of heat fluxes *follows* the upper-level E-vector intensification. In the context of the energy cycle, the downgradient heat fluxes observed at days -3 and +3 suggest that there are positive baroclinic conversions of available potential energy from the mean flow into the growing eddy.

Finally, we examine the 700 mb Q-vector patterns during the development. In fig. 4.10, Q-vectors are displayed over the evolving composite temperature field for days -5, -3, -1 and +3 (Note the chosen lag times *differ* from the heat flux and E-vector analyses). The Q-vectors are obtained from the *total* composite flow field (mean plus anomaly), unlike the heat fluxes and E-vectors, which are derived from the composite anomalies alone. Throughout the evolution, the Q-vectors are directed towards higher temperature over extreme southeast Asia, indicating that a strongly frontogenetical flow exists near the region of initial upper-level jet intensification. Initial frontogenesis rates, as given by equation (4.2), are locally nearly twice the values associated with the climatological mean flow. At day -3 (fig. 4.10b), Q-vectors diverge from the west and converge into the eastern portion of the developing low, suggesting that $-\omega'T'$ is positive - i.e. that there is an upward heat flux in this region. Weaker signatures exist over the North Pacific at day -1 (fig. 4.10c). At day +3 (fig. 4.10d), however, Q-vectors diverge from a thermal trough found east of the date line and converge into the developing downstream thermal ridge, suggesting a net upward vertical eddy heat flux during later stages of the evolution.

Composite analyses of PN decay (not shown) indicate there are also systematic precursors to the breakdown. Four days prior to the breakdown of the primary center, the composite anomaly evolution exhibits synoptic-scale ridge development at midlatitudes near Japan. This is manifested synoptically by a significant weakening of the frontogenetical circulation observed near the east coast of Asia. A *weakening* of the upper-level zonal flow near the EAJ then occurs as the evolving ridge propagates southeastward during days -3 to -1. Simultaneously, the significant cold anomalies found upstream over southeast Asia after PN development (see fig. 4.3) weaken and

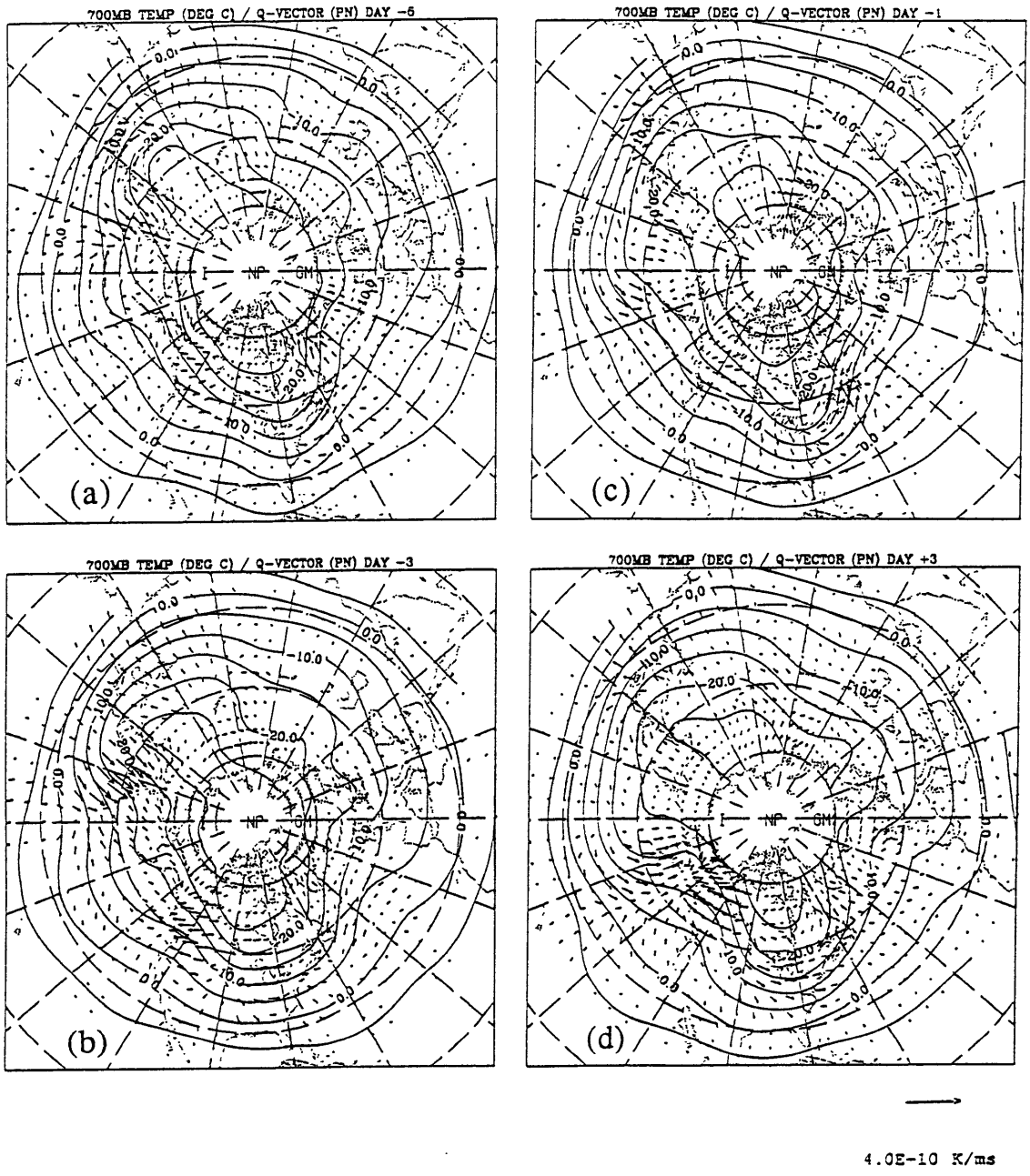

Fig. 4.10. Time evolution of Q-vectors derived from the *full* 700 mb composite fields for the 14 PN cases. Q-vectors are displayed at days (a) -5, (b) -3, (c) -1, and (d) +3 with the composite 700 mb temperature field (contour interval of 5°C). A scale vector and corresponding magnitude are shown in the lower right-hand portion of figure.

become insignificant. Thereafter, the primary anomaly contracts zonally, acquires a northwest-southeast elongated tilt and then quickly weakens as it propagates northwestward away from the key region.

ii. Summary - PN cases

The results indicate that PN development is preceded by negative anomalies in upper-level geopotential height and lower tropospheric temperature over eastern and southeastern Asia. The structures are associated with enhanced upper-level cyclonic shear and static stability (not shown) over eastern Asia. The results suggest that there are positive anomalies in upper-tropospheric potential vorticity over this region. Prior to development, stronger than normal geostrophic zonal flow is also observed near the EAJ. An anomalous ridge over the North Pacific results in relatively weak upper-level flow and a split low feature near the ocean surface.

The early evolution is characterized by synoptic-scale cyclone development over the western North Pacific. At day -3, the disturbance tilts strongly westward with height and has associated downgradient and upward heat fluxes. A strongly frontogenetical flow is observed to the west of the developing low. The disturbance also exhibits a northwest-southeast horizontal tilt on the north side of the climatological mean jet. Thus the eddy acts both baroclinically and barotropically to increase the upper-level zonal flow near the axis of the mean jet. After day -3, the intensifying low evolves into an equivalent barotropic and zonally elongated disturbance which propagates slowly eastward into the jet exit region. The subtropical jet intensifies and extends eastward during this time, as high potential vorticity air is advected eastward over the ocean.

After onset, the disturbance becomes quasi-stationary and continues to develop on a large-scale. Strong eastward fluxes of zonal momentum develop in the jet exit region at day +1. Subsequently, the disturbance acquires a westward tilt with height and

large-scale downgradient and upward heat fluxes form. A strengthening basin-wide cyclonic circulation is observed at the surface at this time. At upper levels, the cases are associated with an anomalously strong jet stream which extends across most of the North Pacific. Downstream, anomalous ridge building occurs first over western North America, and is followed by trough digging to the east. Further downstream, ridge development subsequently occurs over the North Atlantic.

iii. Summary - PP cases

The composite evolution of the Pacific positive cases (PP) is summarized next. Selected analyses for PP development are presented in figs. 4.11-4.16.

The PP composite development exhibits a weak anomaly signature 5 days prior to onset (fig. 4.11a). A westward-tilting anticyclonic disturbance of synoptic scale appears near Japan at day -3 (figs. 4.11b, 4.12a). The disturbance is characterized by a small amplitude surface perturbation and weak downgradient heat fluxes (fig. 4.16a). The anticyclone then intensifies while propagating eastward to the date line. This results in an upper-level split flow (fig. 4.14c) and a split Aleutian Low near the surface (figs. 4.13c) at day -1. At this time, the disturbance retains a strong westward tilt with height and exhibits a southwest-northeast horizontal tilt on the north side of the mean jet (fig. 4.11c). The upper-level momentum fluxes associated with the disturbance at this time would tend to weaken the subtropical jet stream over the central North Pacific. Upstream trough development is observed over Siberia during the early stages of evolution (figs. 4.11a,c).

During onset a large-scale and primarily downgradient heat flux pattern forms over the North Pacific (fig. 4.16c) as the westward tilting disturbance enters the key region (fig. 4.12b). After onset (day +1), the primary anomaly pattern acquires a zonally elongated structure in the jet exit region (fig. 4.11d). In conjunction with this, a coherent

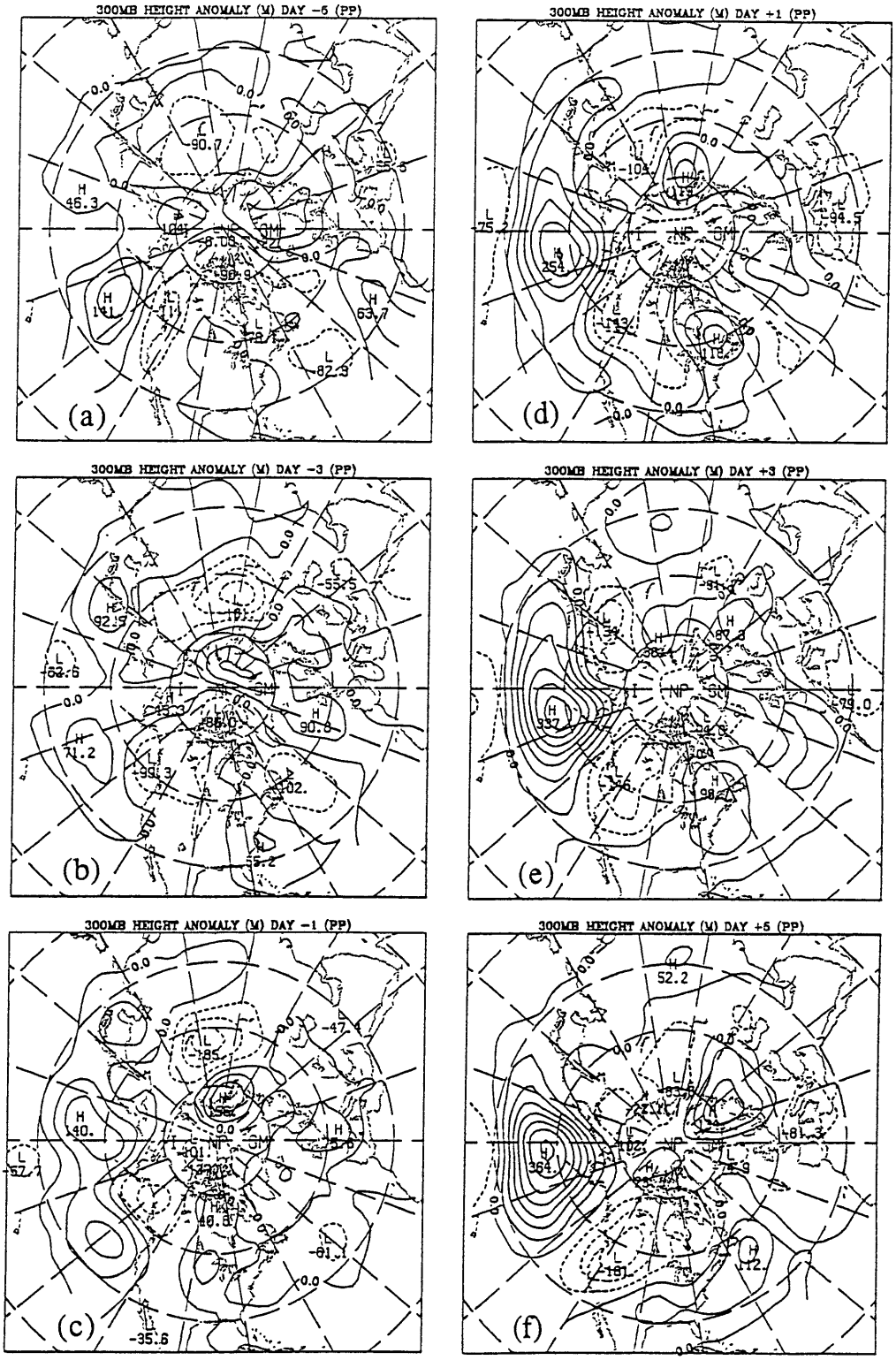

Fig. 4.11. As in Fig. 4.1 for the first 15 PP cases.

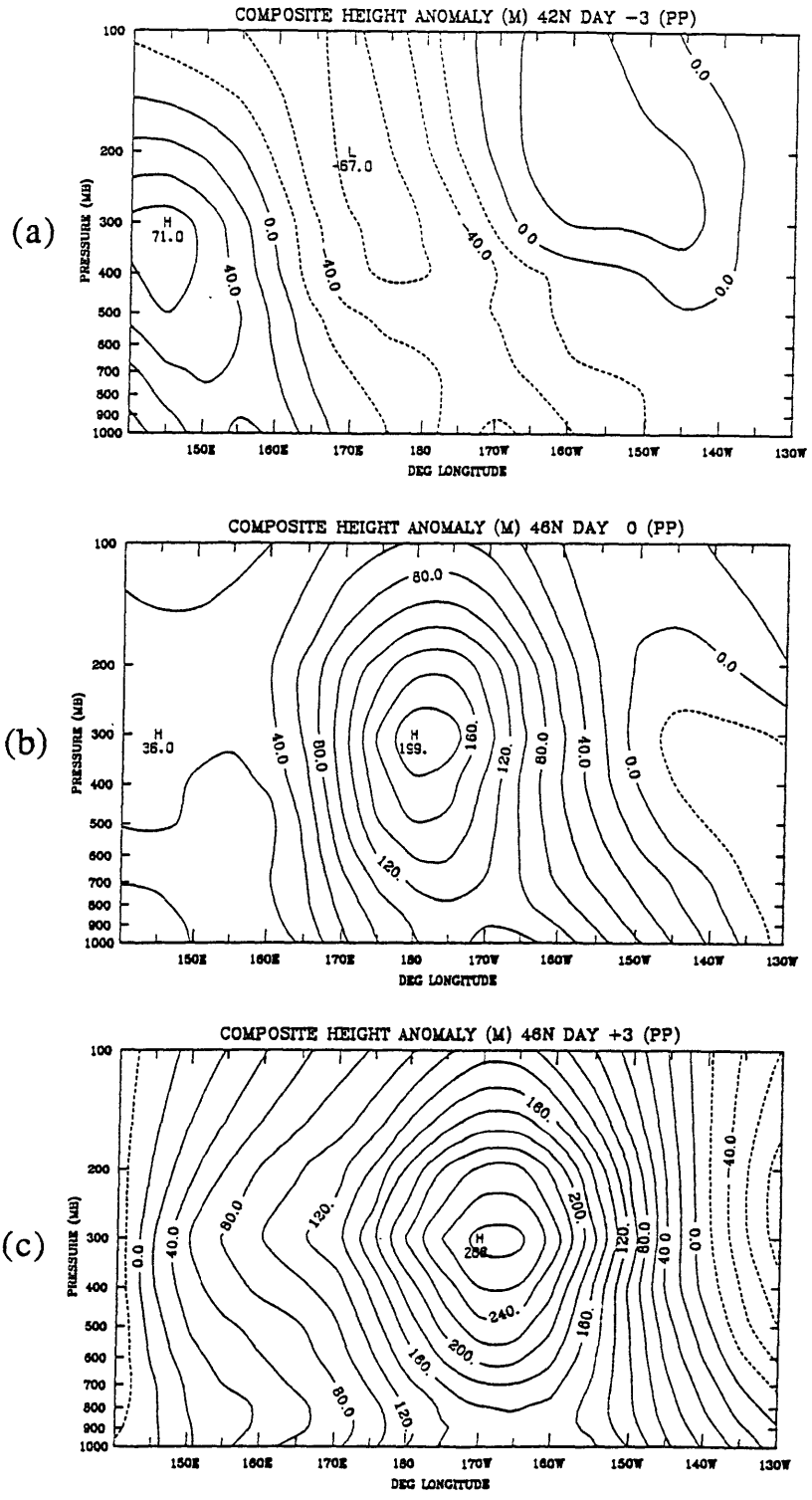

Fig. 4.12. As in Fig. 4.4 for PP development. Sections are taken at 42°N for day -3 and 46°N for days 0 and +3.

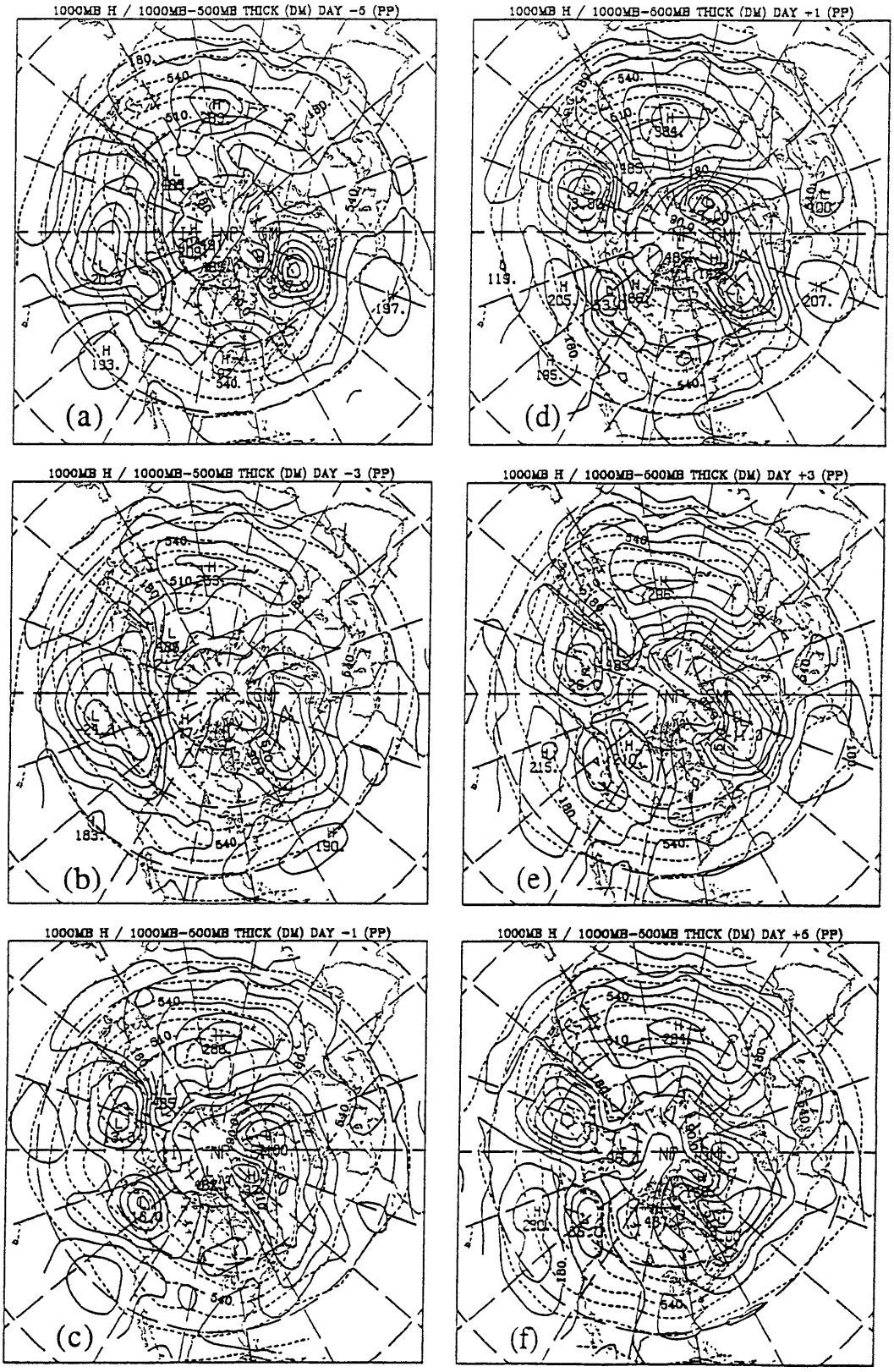

Fig. 4.13. As in Fig. 4.6 for the first 15 PP cases.

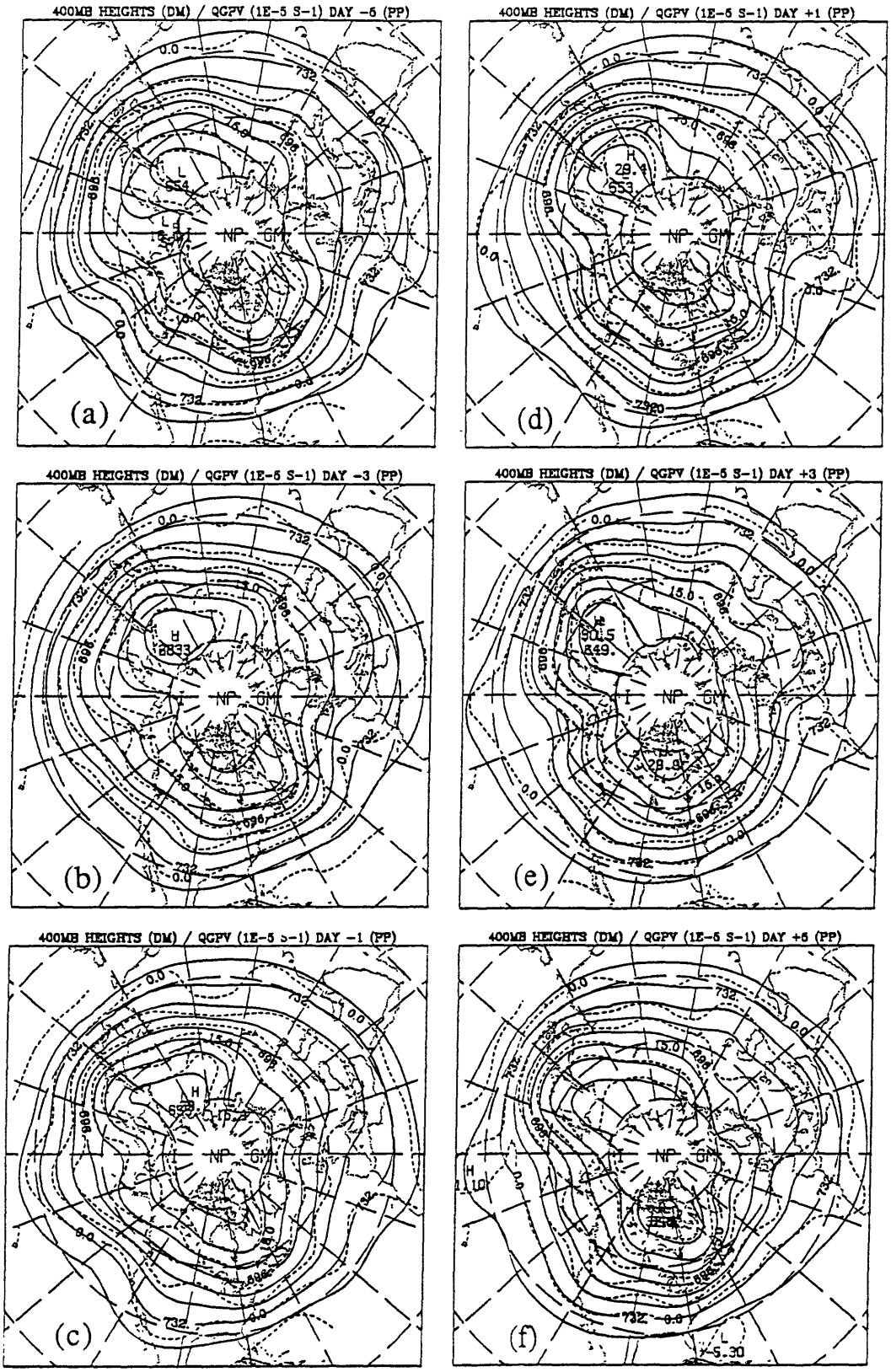

Fig. 4.14. As in Fig. 4.7 for the first 15 PP cases.

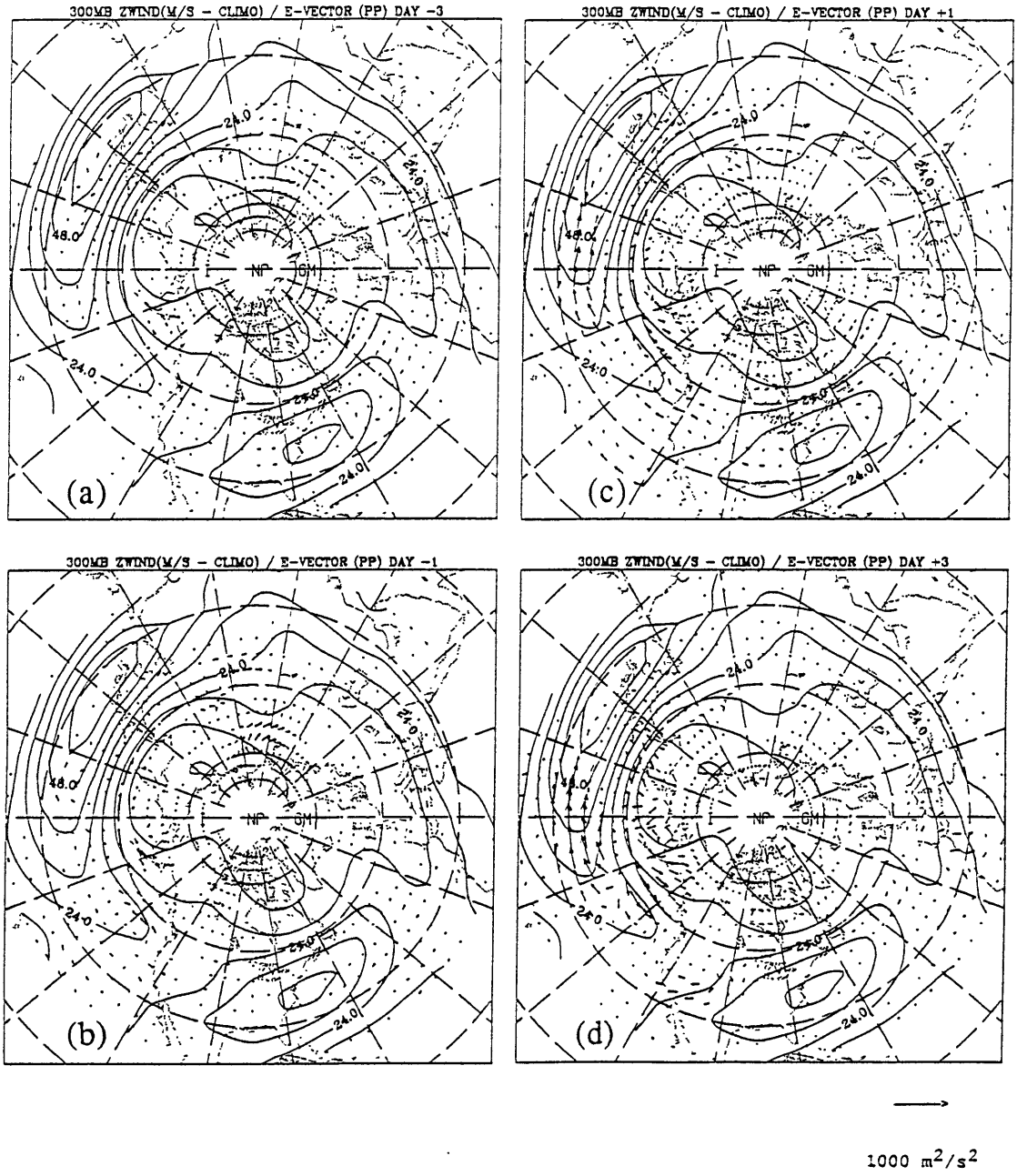

Fig. 4.15. As in Fig. 4.8 for the first 15 PP cases.

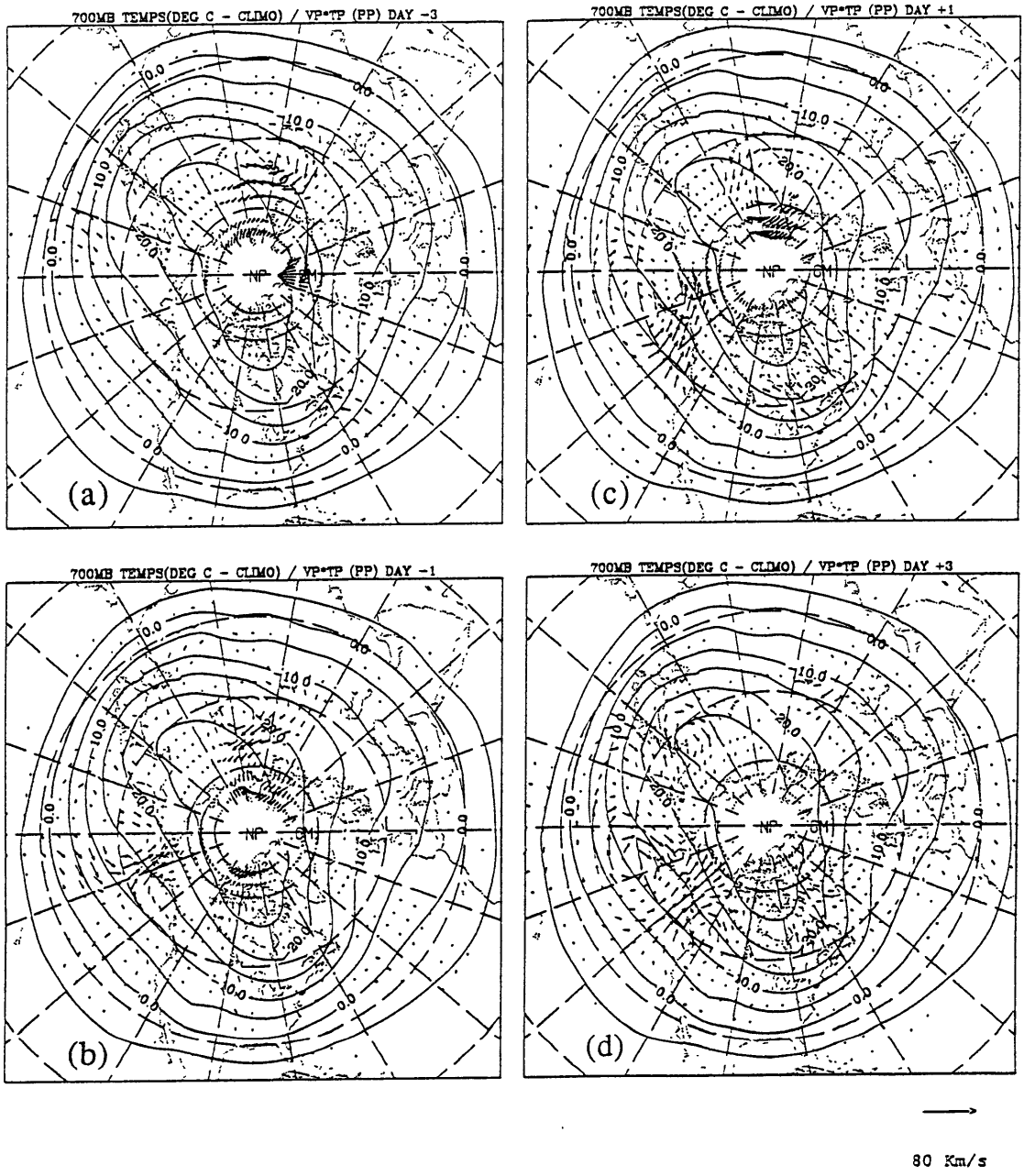

Fig. 4.16. As in Fig. 4.9 for the first 15 PP cases.

upgradient E-vector pattern develops in this region (fig. 4.15c). After day +1, the disturbance becomes quasi-stationary and amplifies on a large-scale. At upper levels over the North Pacific, this results in a relatively weak subtropical jet and a strengthened jet at mid to high latitudes (figs. 4.14e, f). Near the surface, the Aleutian Low is split by an anticyclone which extends southeastward from the key region (fig. 4.13f). Over North America the upper-level flow becomes more zonally oriented than normal but little significant surface change is observed.

During the early stages of development the PP cases, like the PN cases, are characterized by synoptic-scale development over the western North Pacific. For the PP cases, however, the surface disturbance and lower tropospheric heat fluxes are relatively weak. Also unlike PN development, the eastward propagating disturbance retains a westward tilt with height during onset. After day 0, the development of large-scale heat fluxes *precedes* the formation of upgradient E-vectors in the jet exit region, opposite to the PN development. Despite these differences, however, the fully developed large-scale heat flux and E-vector patterns of PP strongly resemble their PN counterparts. Vertical heat fluxes (not shown) during PP development appear much weaker than during PN.

Unlike for the PN cases, there appear to be few systematic *precursors* to PP decay (not shown). The composite anomaly pattern found five days before decay is almost identical to the post-development pattern. Between days -5 and -3 the western portion of the primary anomaly weakens and the center of the anomaly moves slightly north. The primary anomaly then contracts zonally and, at day -1, is elongated from northwest to southeast on the north side of the climatological mean jet. Thereafter, the eddy quickly dissipates while propagating northwestward. The evolution after day -1 of PP breakdown resembles PN breakdown.

iv. Summary - AN cases

Selected analyses for the composite development of the first thirteen Atlantic negative (AN) cases are presented in figs. 4.17-24. AN development is preceded by a pronounced large-scale high over low anomaly pattern over the eastern North Atlantic (fig. 4.17a) which is opposite to the anomaly pattern which subsequently develops. Synoptically, a strongly diffluent "blocking" flow is observed over the eastern North Atlantic (fig. 4.21a). The early stages of AN development are characterized by a synoptic-scale baroclinic development near the Canadian maritimes (figs. 4.20a,b). At day -4, the synoptic cyclone tilts westward with height (fig. 4.19a) and is associated with an anomalous frontogenetical circulation to the southwest (fig. 4.24a) and upper-level jet intensification (figs. 4.21a,b) to the south. Thereafter (days -3 to -1), the Atlantic ridge weakens east of Greenland as the synoptic disturbance propagates eastward to combine with the large-scale low initially found south of the key region (fig. 4.17b,c). This leads to a zonally elongated cyclonic disturbance over the North Atlantic by day -1 (fig. 4.17c). During this time, upper-tropospheric ridge building occurs upstream over the eastern North Pacific and trough digging occurs over North America. An anomalous surface ridge over western Canada (not shown) is associated with enhanced cold advection (fig. 4.23b) and cold air buildup over the central North American continent (fig. 4.18c). As noted for the PN cases, the early evolution suggests that positive upper-level potential vorticity anomalies form over the upstream continent prior to large-scale development.

Large-scale development ensues over the North Atlantic after day 0 (figs. 4.17d-f). A strong downgradient E-vector pattern develops in the upper level jet exit region (fig. 4.22d). In the middle troposphere, downgradient and upward heat fluxes appear in the region of strong mean thermal gradients near the Canadian maritime provinces (figs. 4.23d, 4.24d). The development leads to an anomalously strong Icelandic surface low (fig. 4.20f), with enhanced cold advection and geostrophic

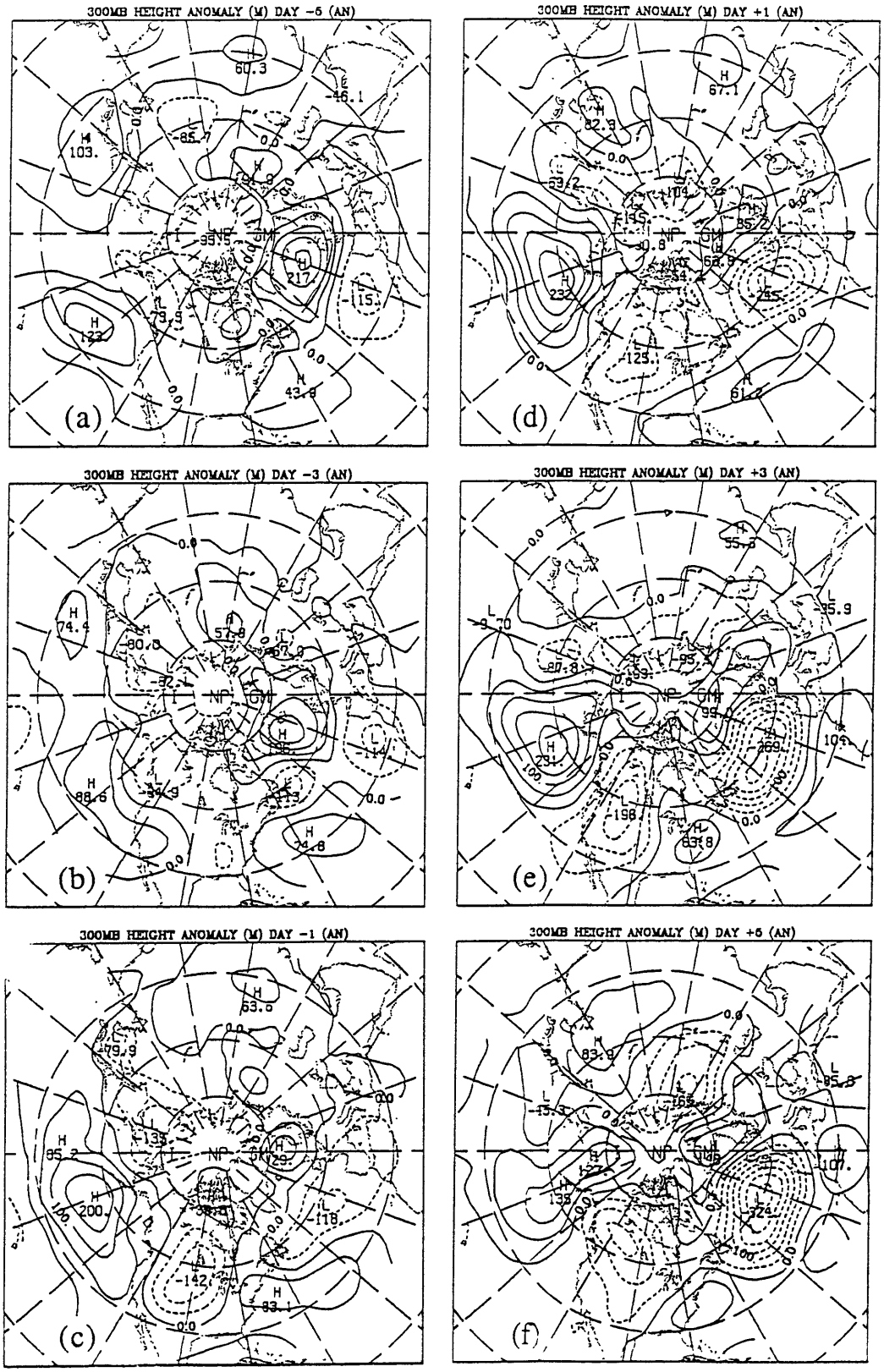

Fig. 4.17. As in Fig. 4.1 for the first 13 AN cases.

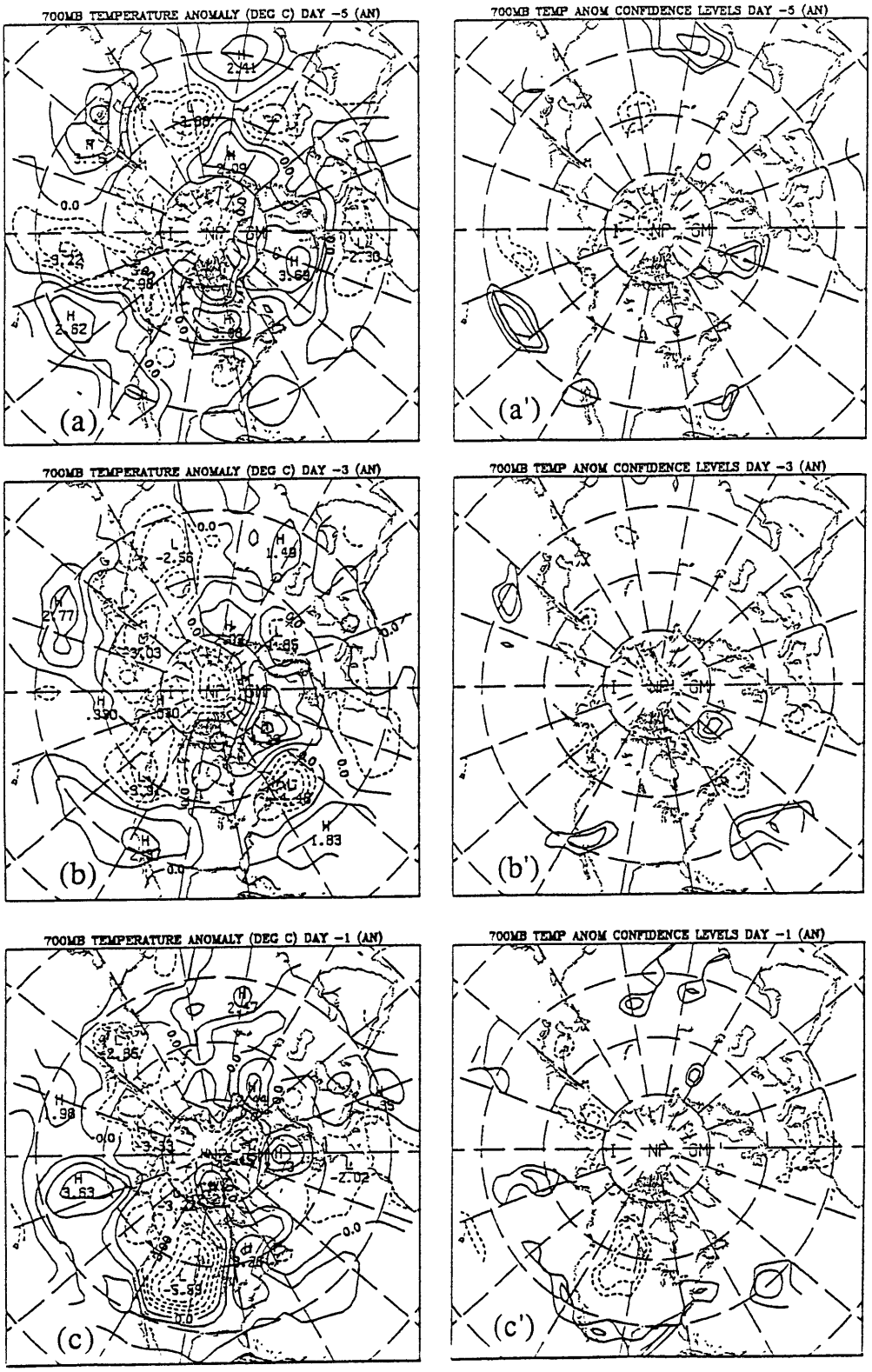

Fig. 4.18. As in Fig. 4.3 for the first 13 AN cases.

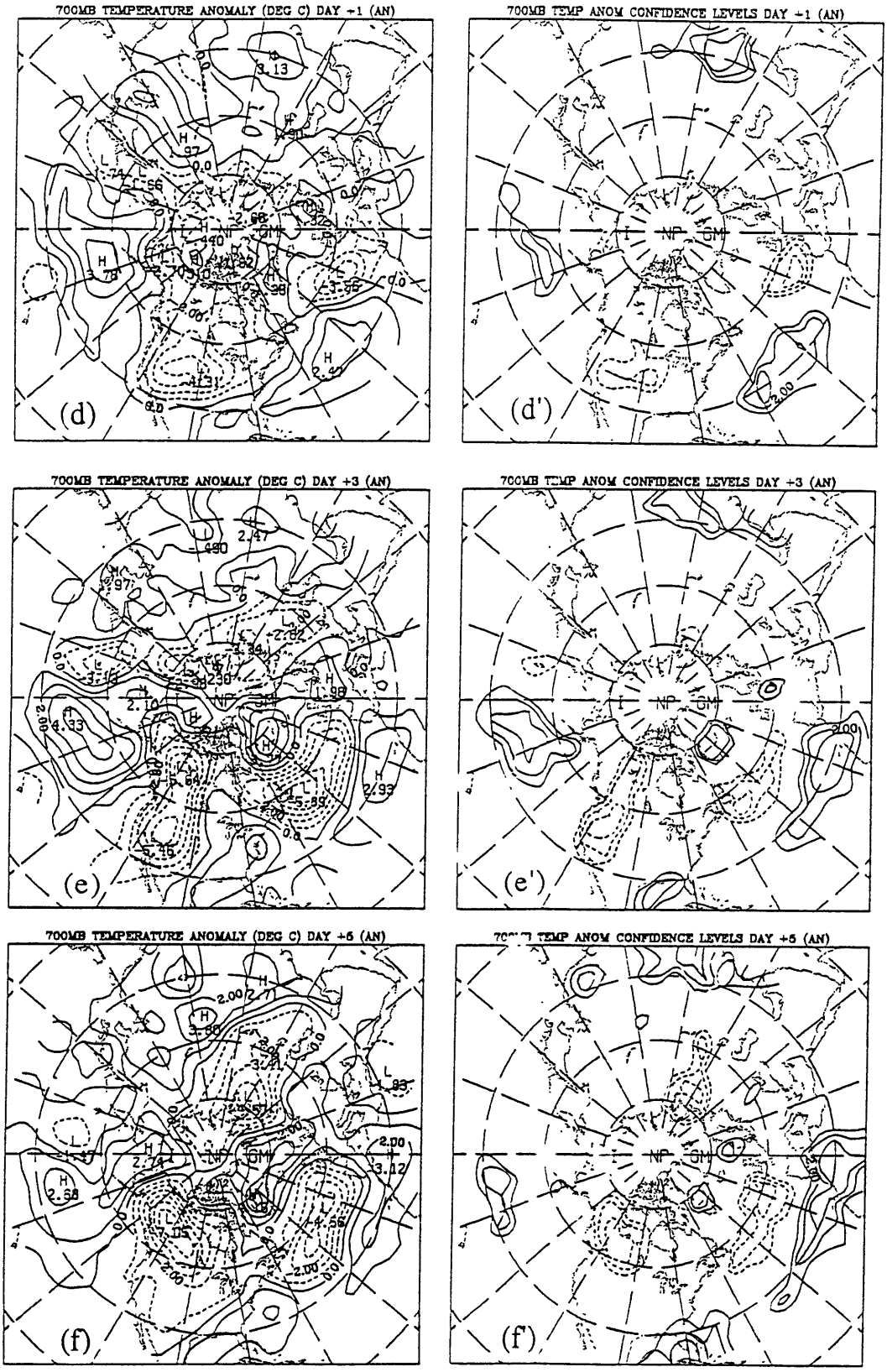

Fig. 4.18. (*Continued*)

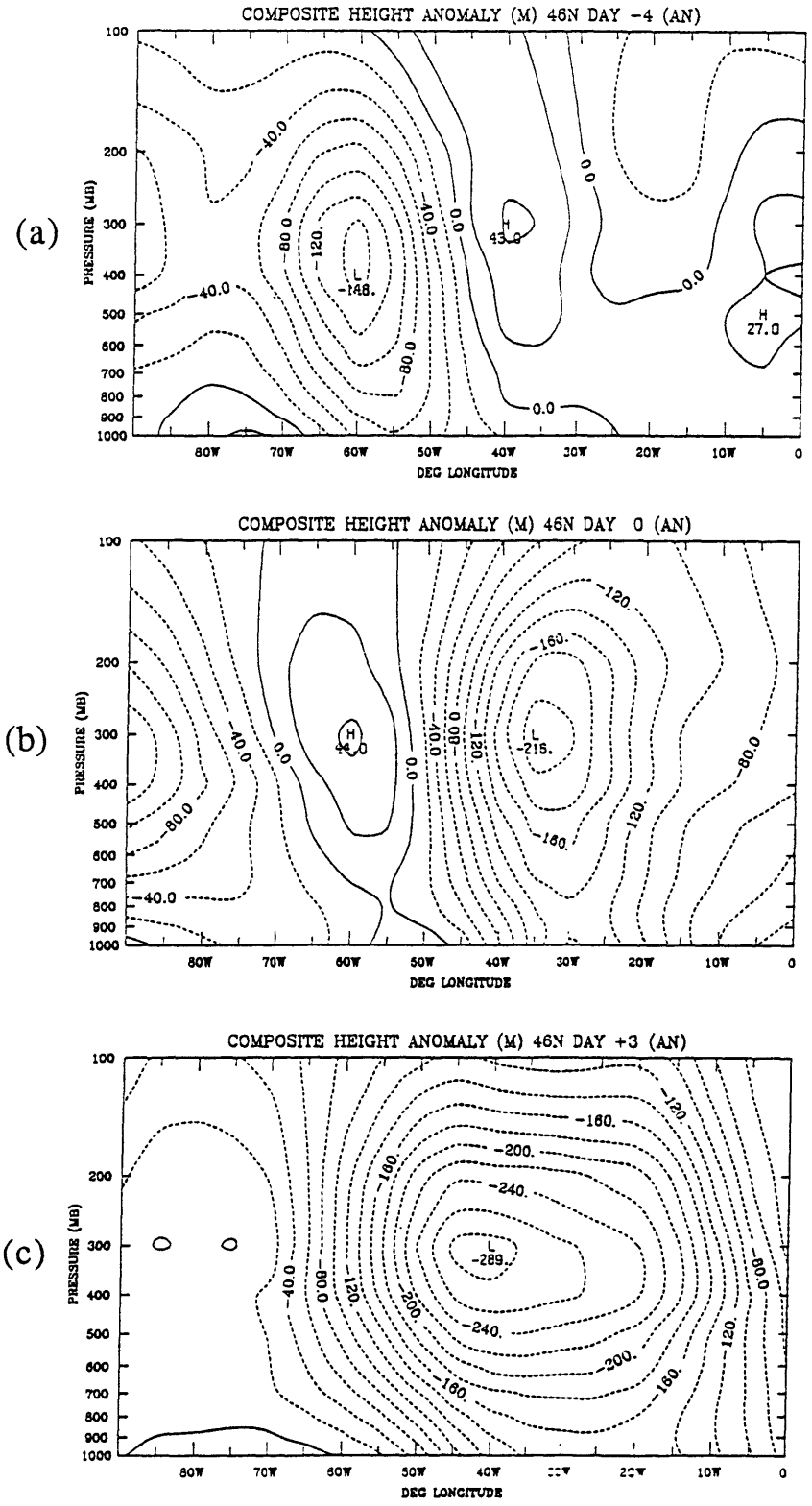

Fig. 4.19. As in Fig. 4.4 for days -4, 0 and +3 of AN development. Sections are taken at 46°N.

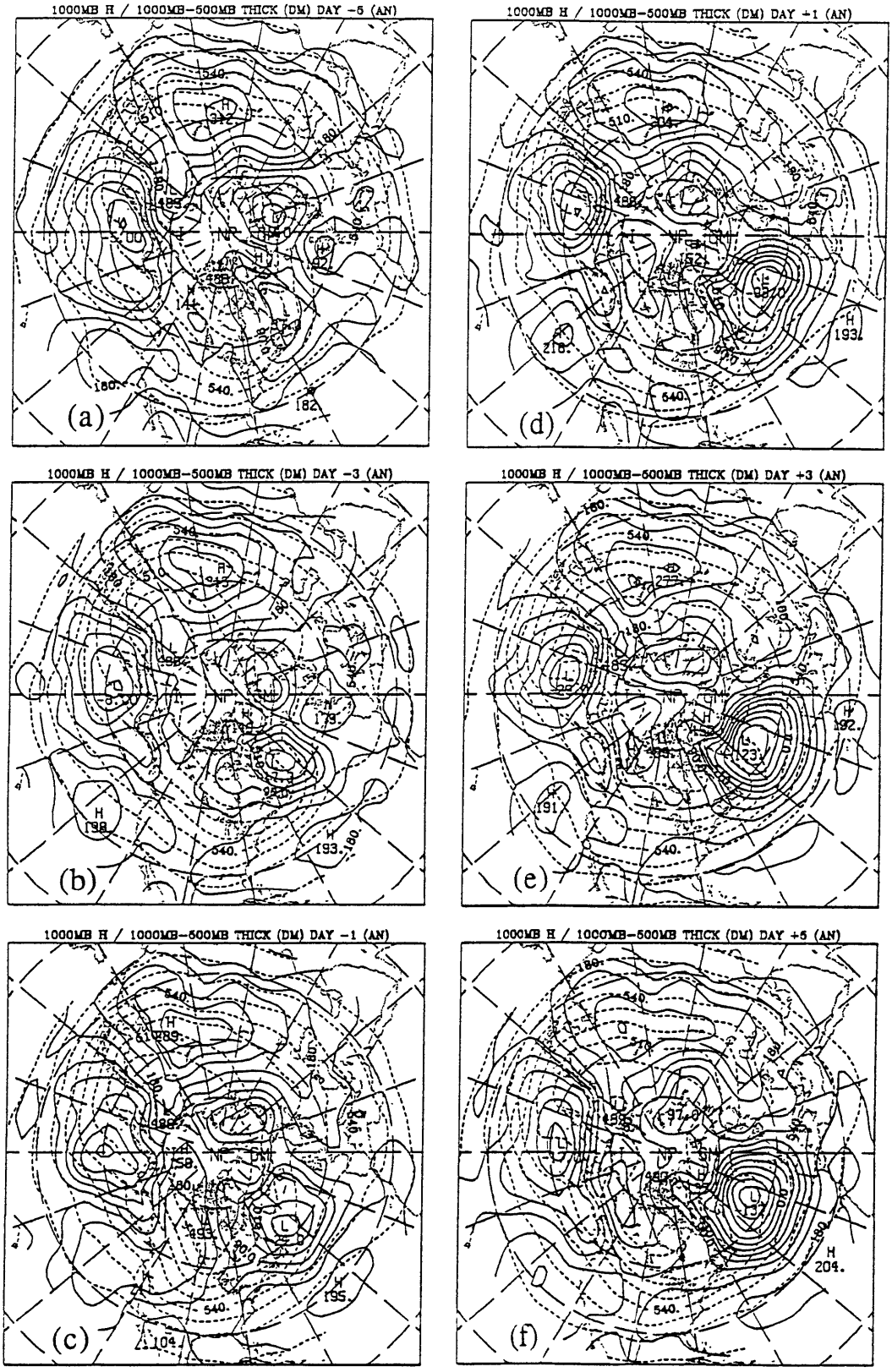

Fig. 4.20. As in Fig. 4.6 for the first 13 AN cases.

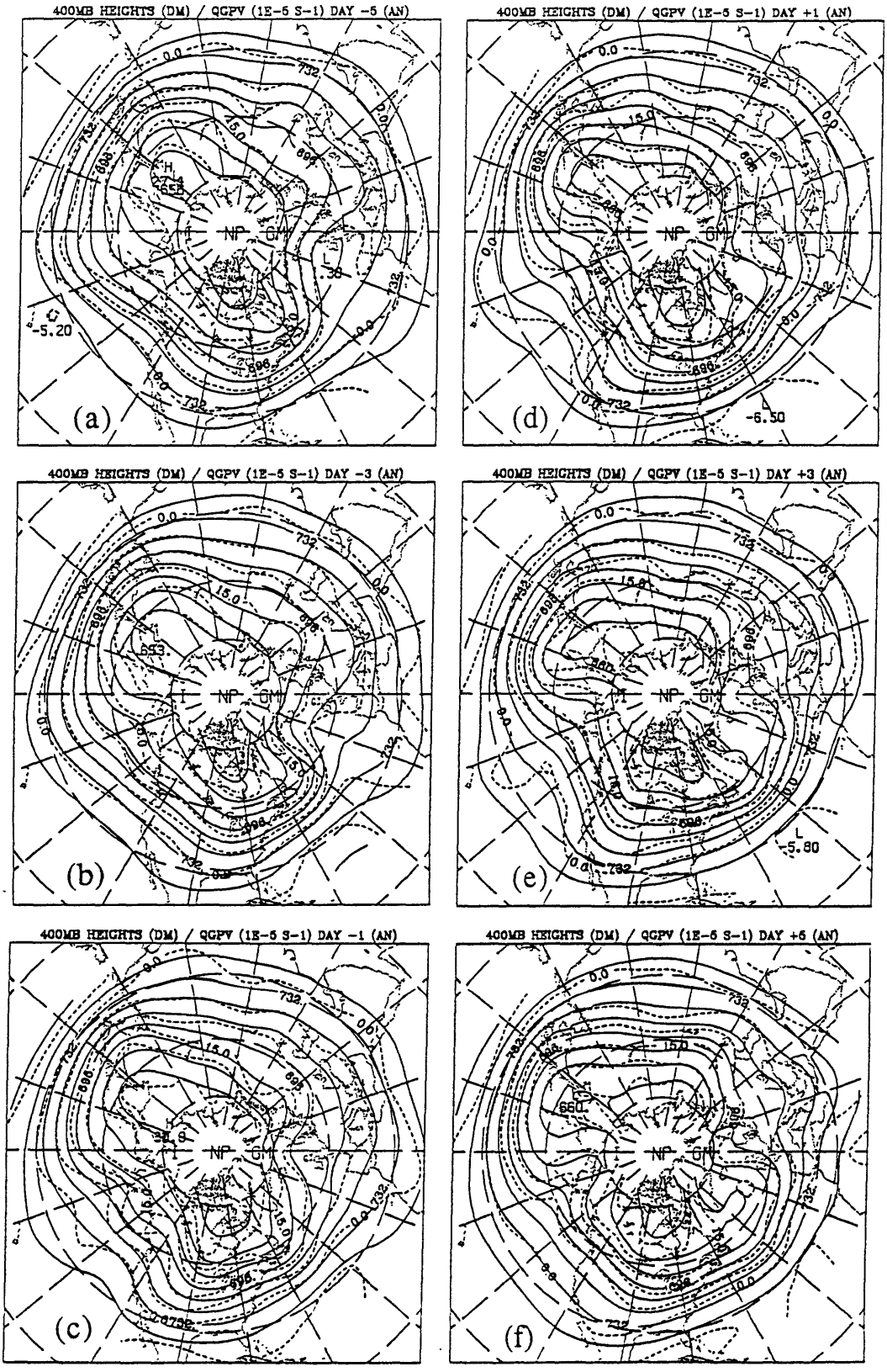

Fig. 4.21. As in Fig. 4.7 for the first 13 AN cases.

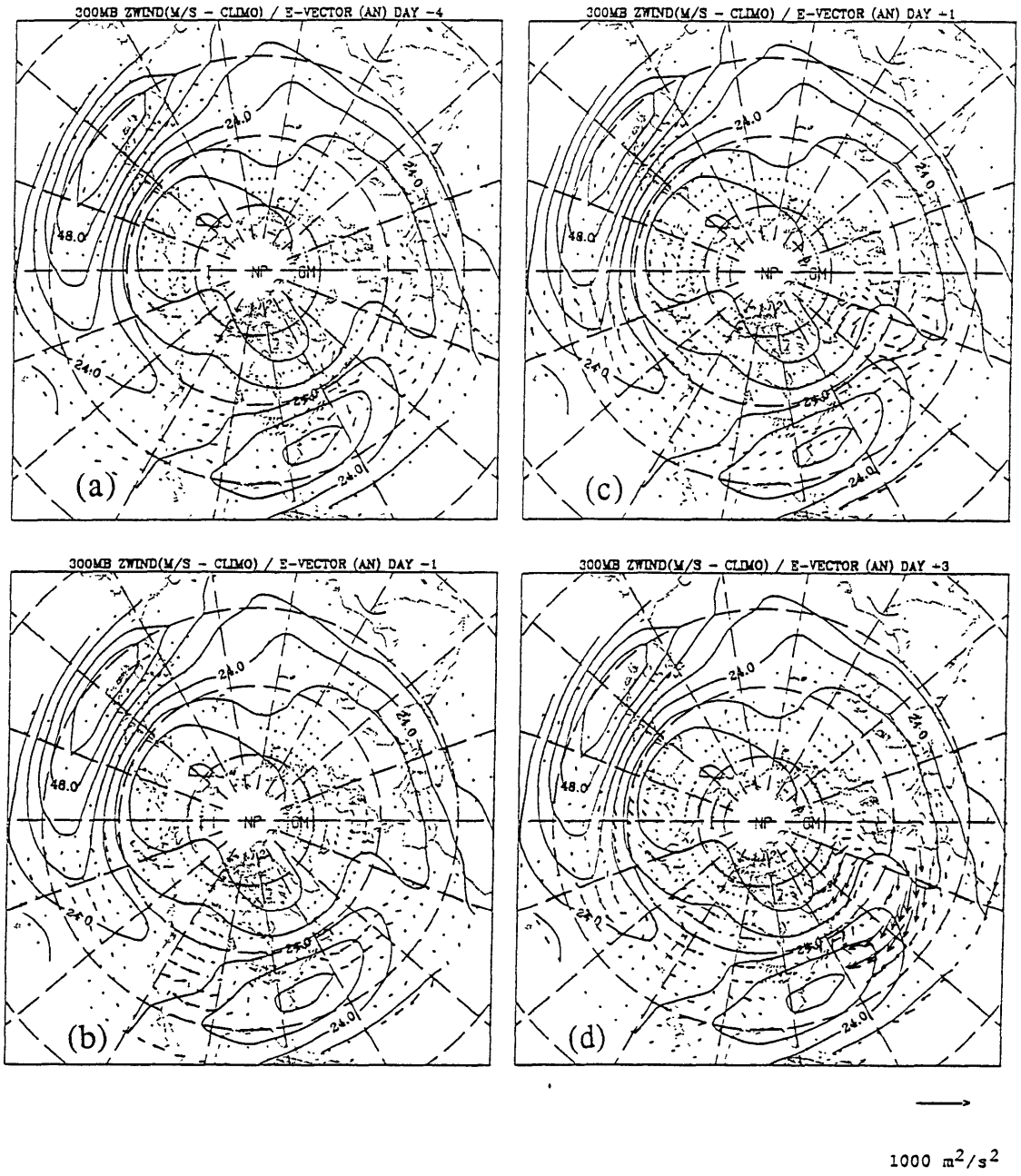

Fig. 4.22. As in Fig. 4.8 for days -4, -1, +1 and +3 of AN development.

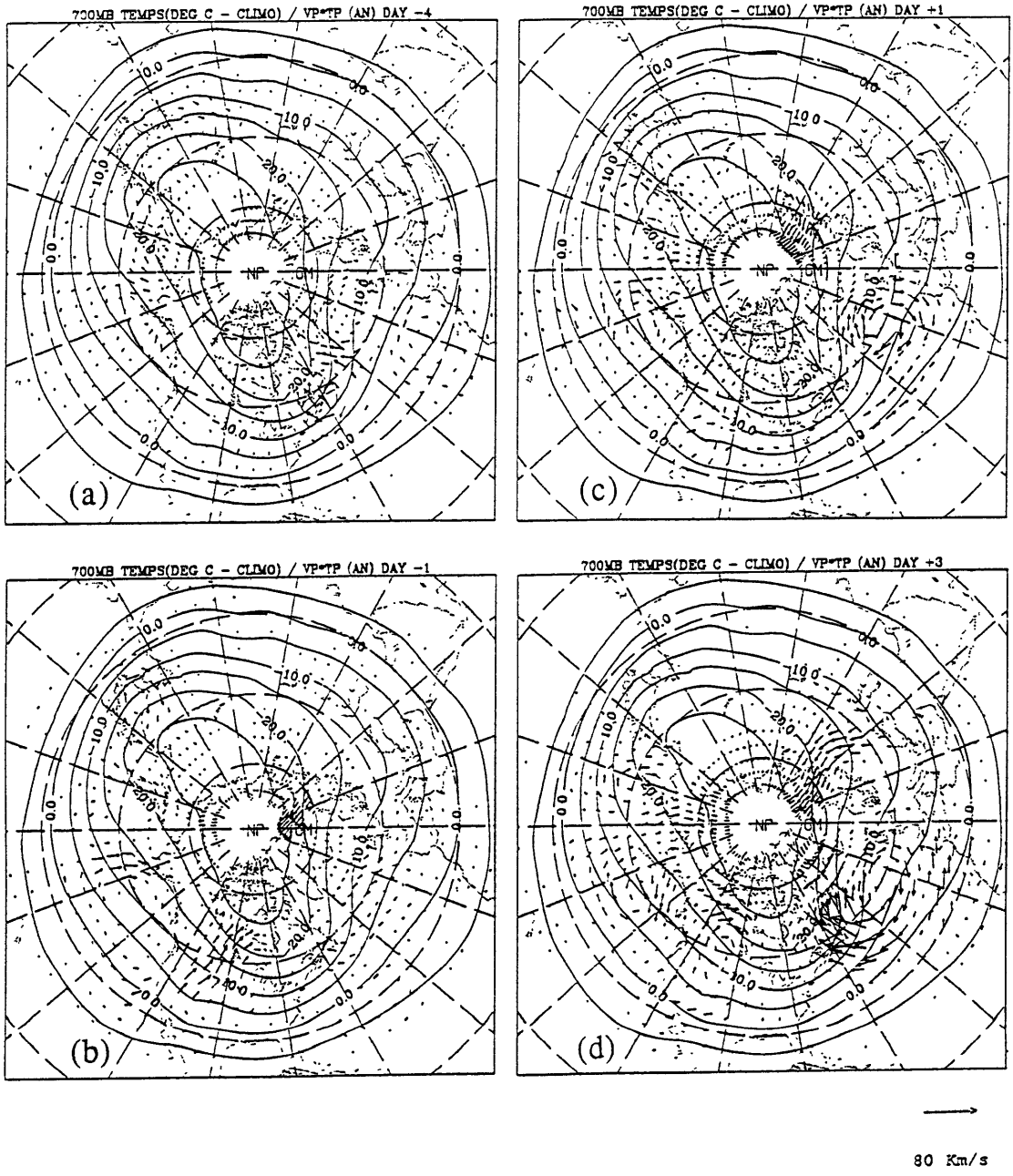

Fig. 4.23. As in Fig. 4.9 for days -4, -1, +1 and +3 of AN development.

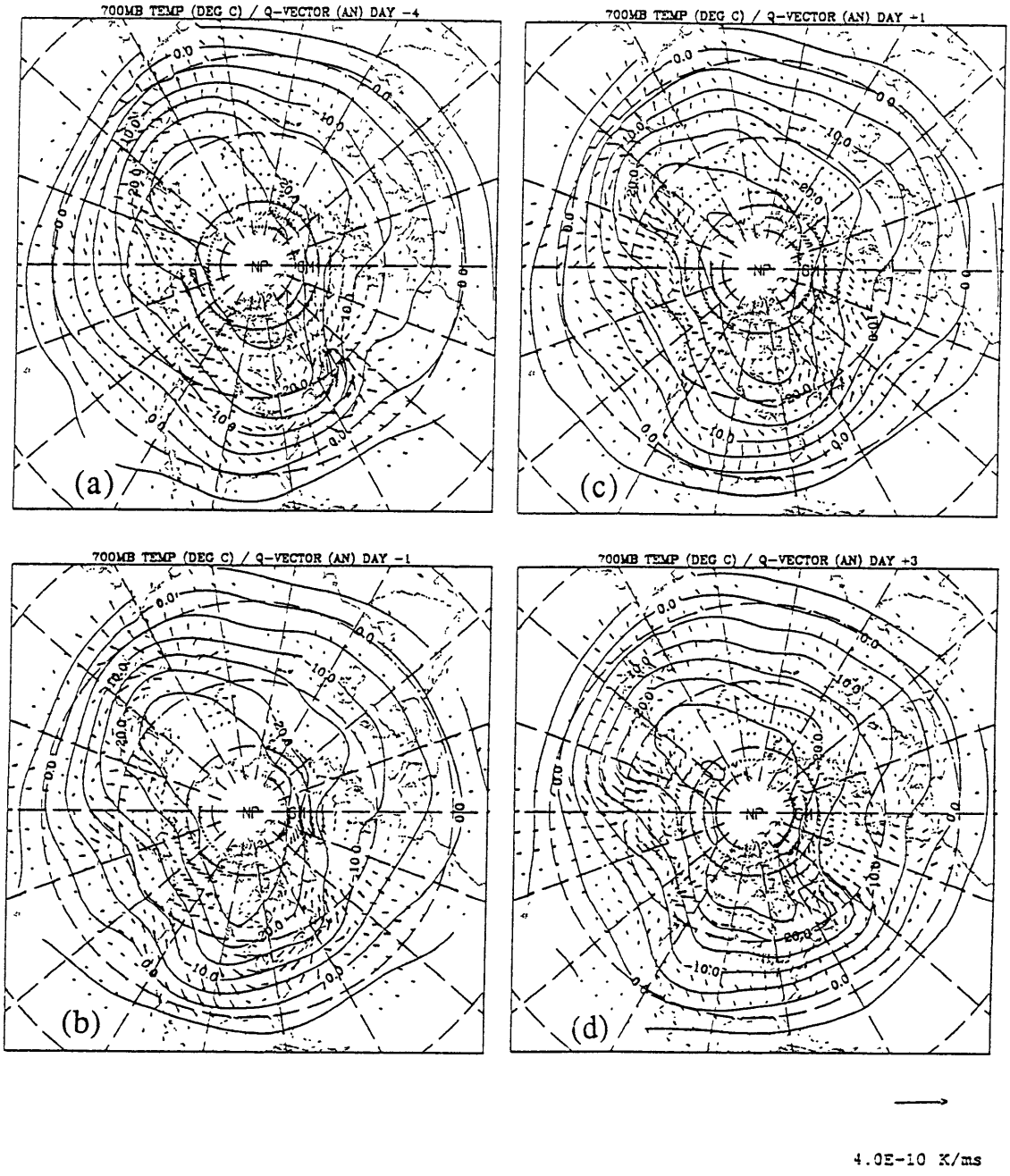

Fig. 4.24. As in Fig. 4.10 for days -4, -1, +1 and +3 of AN development.

frontogenesis over the western North Atlantic. At upper-levels, the subtropical jet intensifies and extends eastward to span the North Atlantic basin (fig. 4.21f). A weak anomaly "wavetrain" pattern subsequently develops at upper levels downstream of the key region (fig. 4.17f).

AN breakdown (not shown) has remarkable similarities to the behavior seen in PN cases. Six days prior to breakdown a surface ridge develops near the east coast of the US. The anomalous ridge propagates southeastward to the subtropical North Atlantic. As for PN, this results in a *weakening* of the frontogenetical circulation over the western oceanic region. Thereafter, the western portion of the upper-level primary anomaly pattern weakens. This leads to a "rounder" perturbation structure which subsequently decays. Simultaneously, there is a weakening of the upper-tropospheric potential vorticity anomaly pattern found upstream over North America.

v. Summary - AP cases

Figs 4.25-4.30 display selected analyses of Atlantic positive (AP) composite development, which consists of an ensemble of 13 cases. At upper levels, composite AP development begins with a coherent train of westward tilting and meridionally elongated synoptic-scale waves (figs. 4.25a, 4.26a). The wavetrain extends from the eastern North Atlantic upstream to North America and has associated northward heat fluxes (fig. 4.30a) and eastward directed E-vectors (fig. 4.29a). Except for the easternmost ridge, the wave pattern weakens between days -5 and -3 (fig. 4.25b). The ridge propagates downstream towards western Europe. Prior to onset (days -3 to -1), a synoptic-scale trough develops over the southwest North Atlantic (figs. 4.25b,c). At the same time, the ridge over Europe amplifies and begins retrogressing towards the key region. Weak warm advection develops over the North Atlantic to the west of the ridge (fig. 4.30b).

The primary anomaly propagates northwestwards toward the key region and

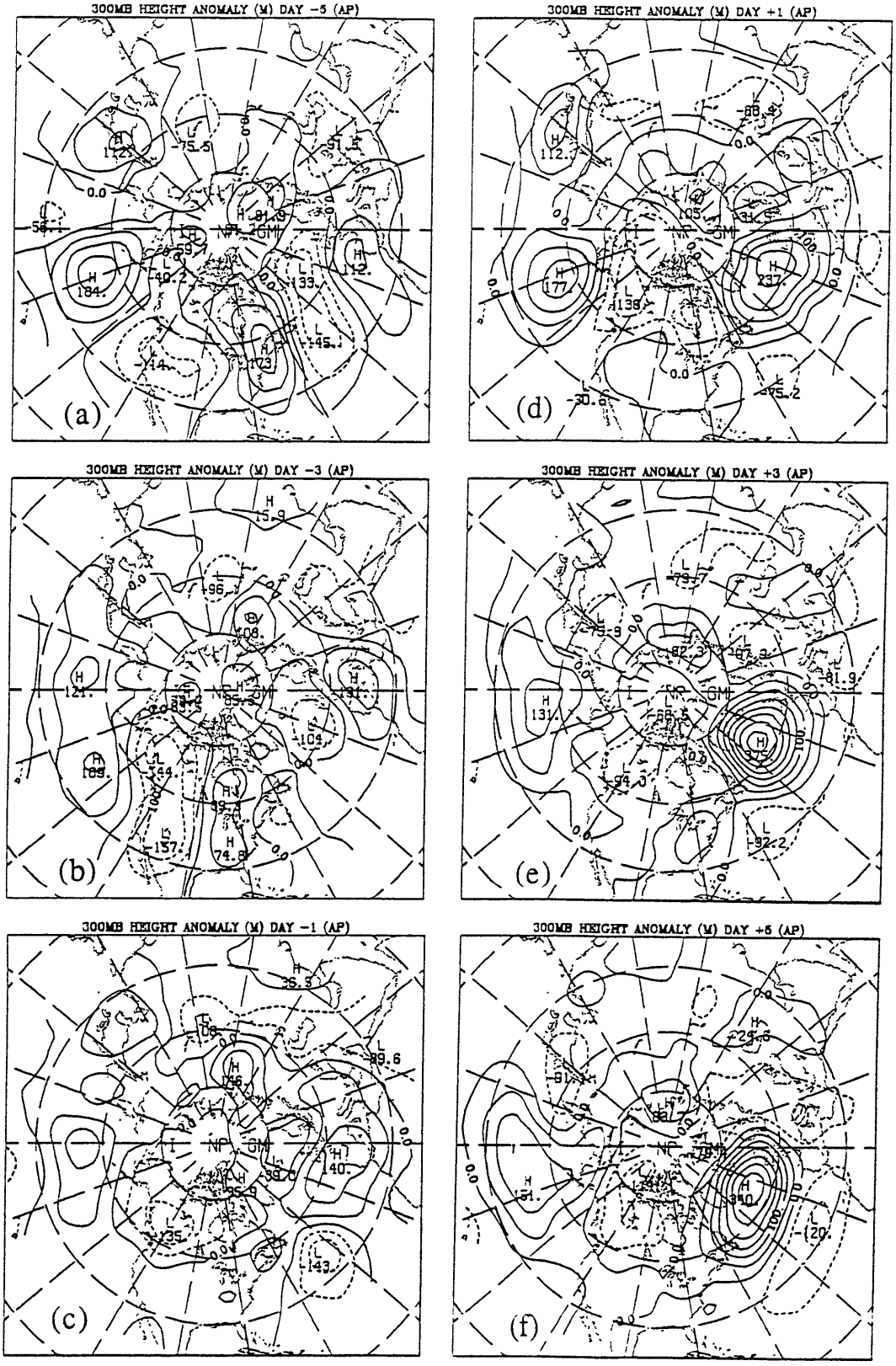

Fig. 4.25. As in Fig. 4.1 for the first 13 AP cases.

(a)

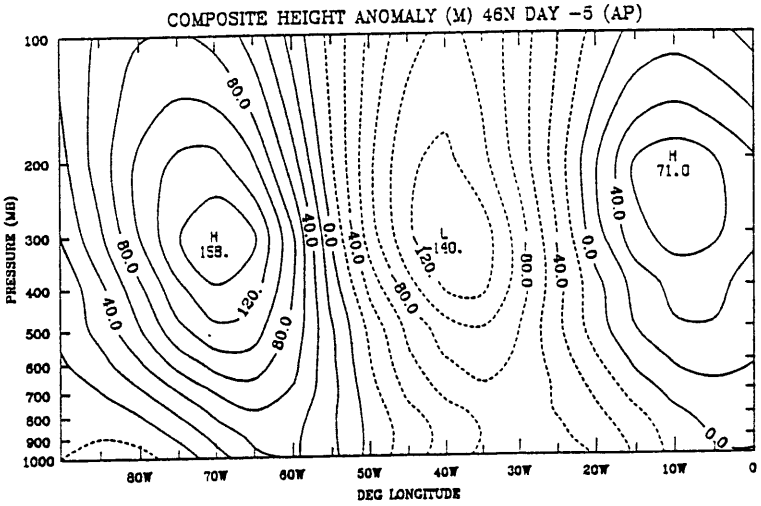

(b)

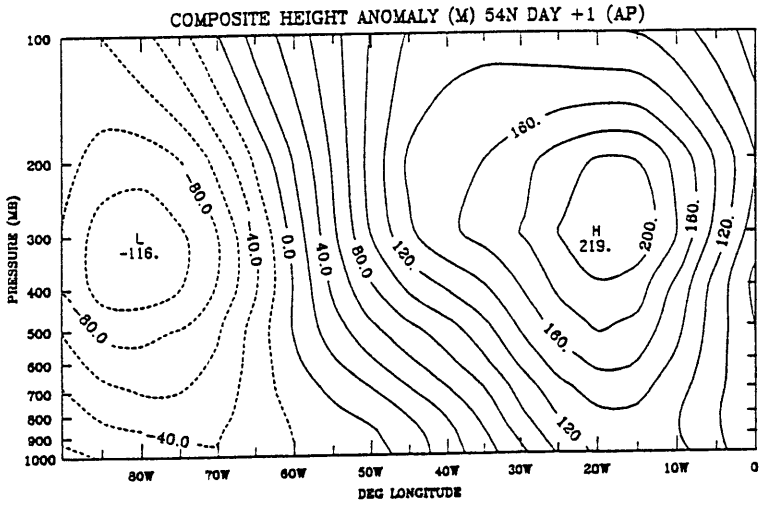

(c)

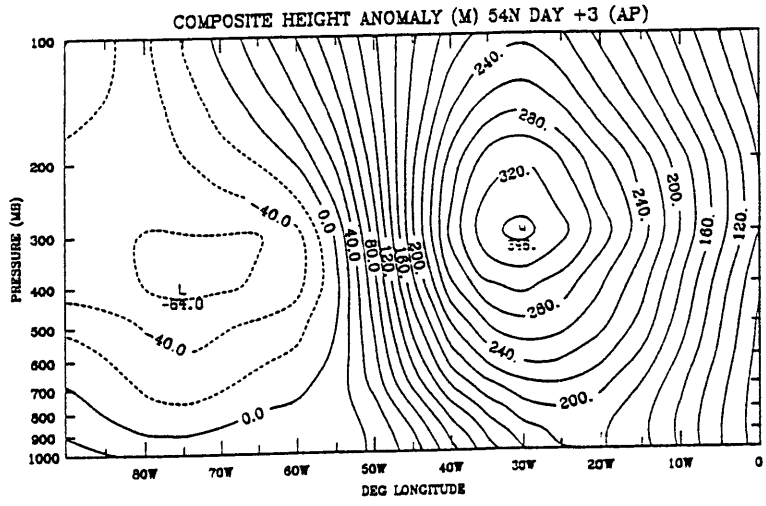

Fig. 4.26. As in Fig. 4.4 for days -5, +1 and +3 of AP development. Sections are taken at 46°N for day -5 and 54°N for days +1 and +3.

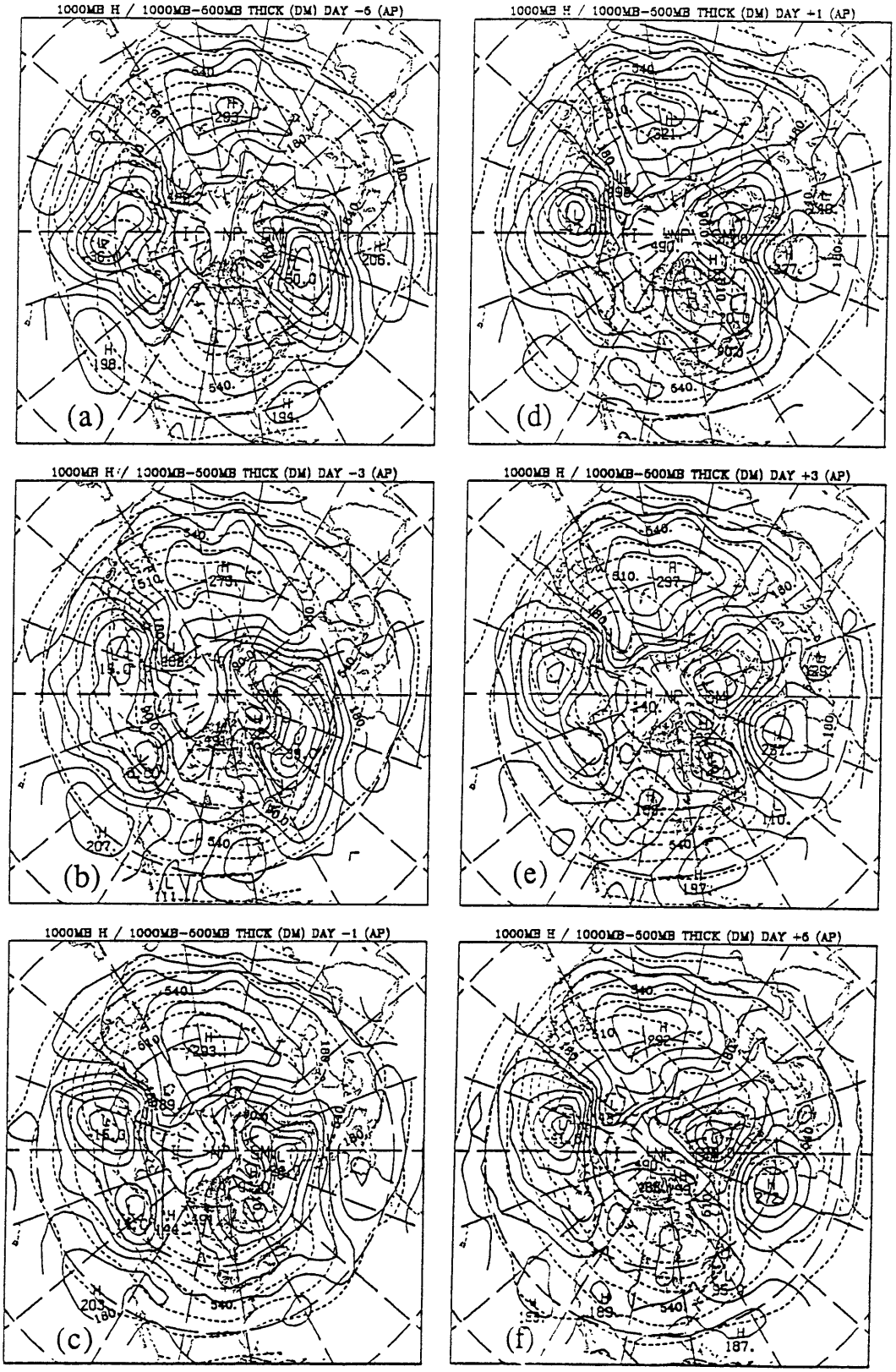

Fig. 4.27. As in Fig. 4.6 for the first 13 AP cases.

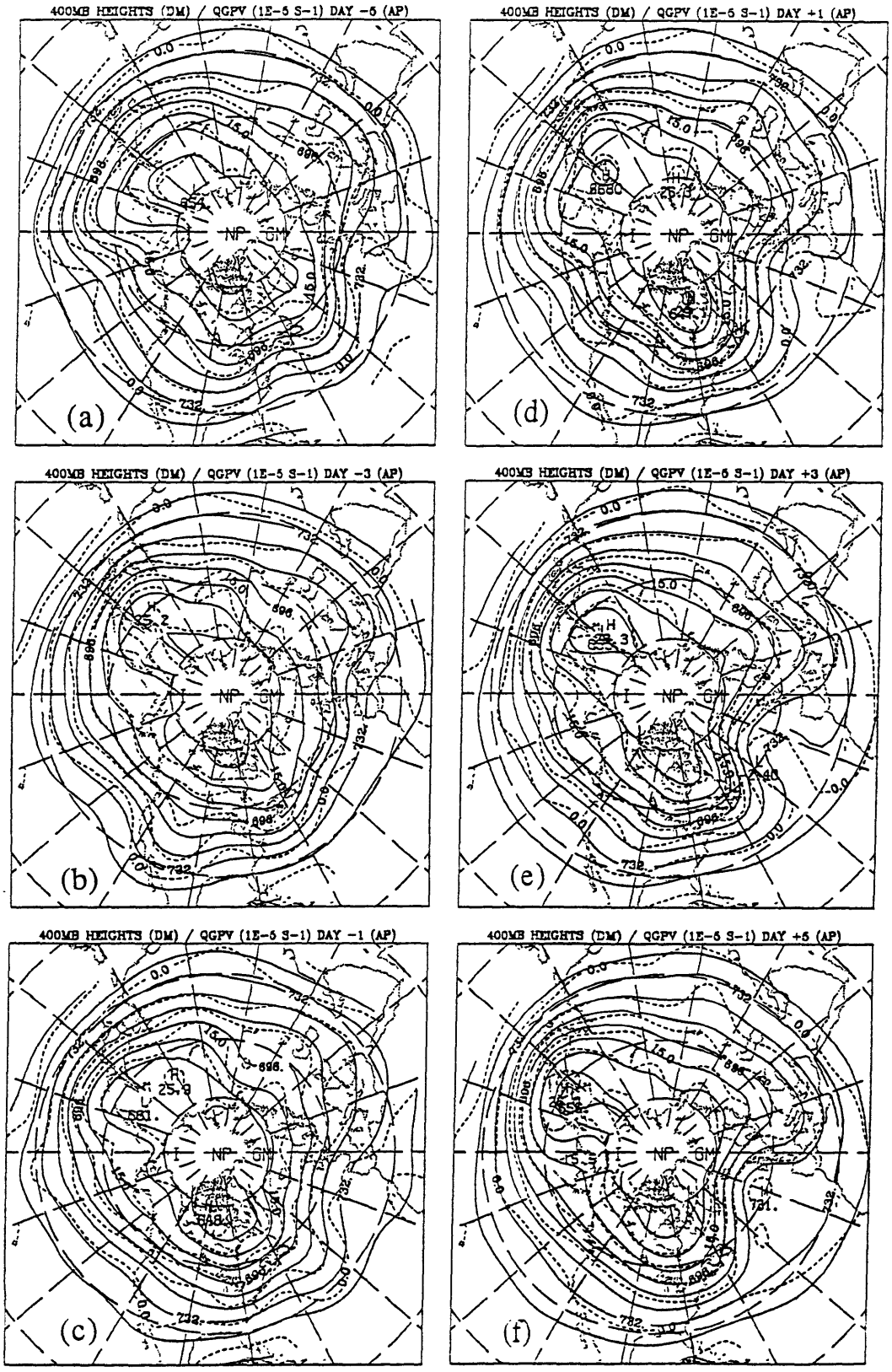

Fig. 4.28. As in Fig. 4.7 for the first 13 AP cases.

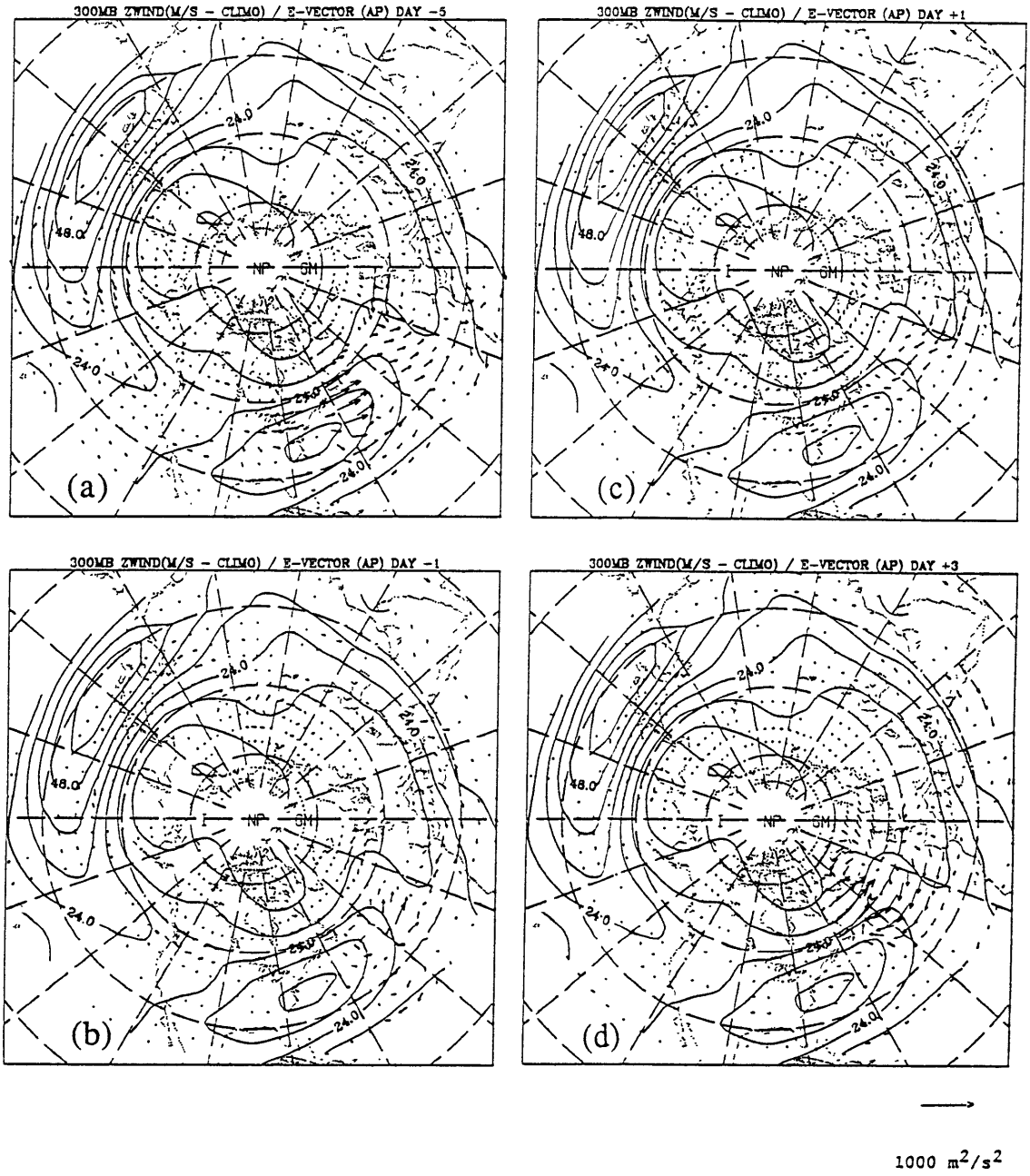

Fig. 4.29. As in Fig. 4.8 for days -5, -1, +1 and +3 of AP development.

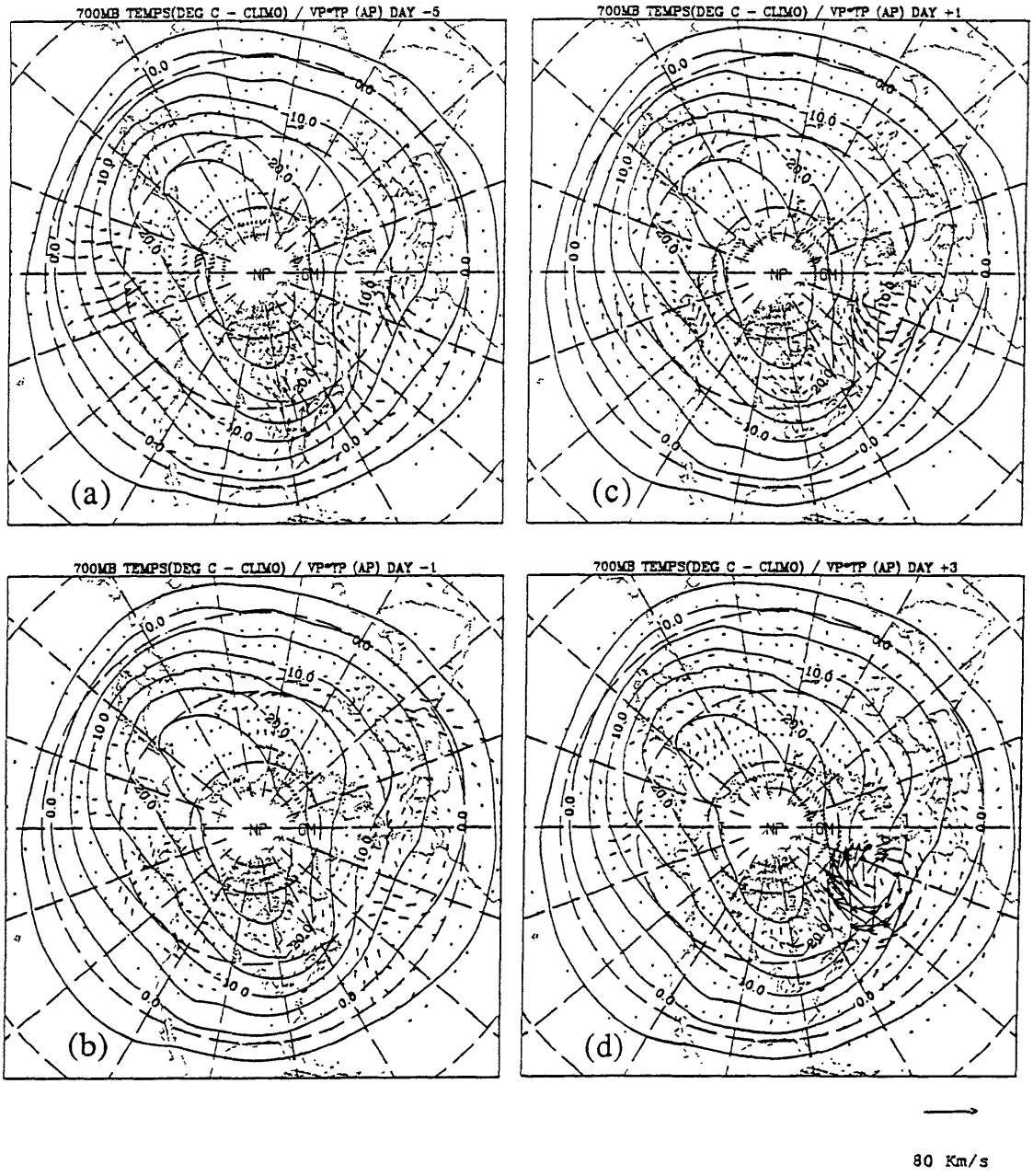

Fig. 4.30. As in Fig. 4.9 for days -5, -1, +1 and +3 of AP development.

intensifies during AP onset (figs. 4.25c,d). Warm advection strengthens on the west side of the ridge (figs. 4.30c,d), while a primarily upgradient E-vector pattern develops to the south (figs. 4.29c,d). The disturbance is zonally elongated and westward tilting in the jet exit region at day +1 (figs. 4.25d,4.26b). The ridge experiences large-scale development after day +1 and becomes quasi-stationary near the key region (figs. 4.25d,e) . As found in the other composite developments, strong downgradient heat and momentum fluxes are observed during the later stages of development. Like PP development, Q-vector analyses (not shown) suggest that vertical eddy heat fluxes are weak and predominantly upward. The development ultimately results in a strongly split upper-level flow field (4.28f), with pronounced surface high pressure located over the eastern North Atlantic at midlatitudes (4.27f).

Little difference was found between the composite fields observed after AP development and those analyzed prior to breakdown. The primary anomaly weakens in situ prior to day 0 of the breakdown. After day 0, the disturbance continues to weaken while propagating northwestward away from the key region.

D. Summary.

AN and PN developments are preceded by upstream intensifications of the subtropical jet stream and by a buildup of anomalously high potential vorticity in the upper-troposphere over the upstream continent. The upstream jet intensifications are associated with enhanced frontogenetical circulations in the lower troposphere. AN and PN developments are also initially characterized by anomalous ridges near the key regions. As AP development begins, a coherent synoptic-scale wavetrain is found over most of the Northern Hemisphere.

During the early stages of AN and PN evolution, synoptic-scale cyclogenesis occurs over the western oceanic regions. The eastward propagating disturbances tilt

westward with height and have associated downgradient and upward heat fluxes. During this time, the upper-level subtropical jet stream extends eastward and intensifies in association with strong geostrophic frontogenesis located to the southwest of the cyclone. Synoptic-scale *ridge* development takes place during early PP development. The anticyclone also propagates eastward and tilts westward with height but exhibits a smaller amplitude and weaker heat fluxes than its negative counterparts. Early AP development is characterized by a decay of the initial coherent wavetrain.

The PAC cases intitiate as the intensifying synoptic-scale disturbance approaches the key region. A large-scale anomaly retrogresses northwestwards over the eastern North Atlantic during onset of the ATL cases. During AN onset the large-scale anomaly amalgamates with the eastward propagating synoptic-scale disturbance. *In all cases, a large-scale zonally elongated perturbation structure is found in the jet exit region after onset.* The PP, AN, and AP cases exhibit westward tilts with height at this time (day +1).

Thereafter, the composite disturbances become quasi-stationary near the key region and experience large-scale intensification. In all cases, the perturbations exhibit zonally elongated and westward tilting structures near the exit region of the climatological-mean subtropical jet. The eddy structures are associated with large-scale patterns of upgradient E-vectors and downgradient heat fluxes. The negative cases also exhibit significant upward heat fluxes during this time. For the ATL developments, the large-scale heat flux and E-vector signatures develop simultaneously. For PN (PP) developments, however, the large-scale E-vector (heat flux) pattern precedes the formation of the large-scale heat flux (E-vector) pattern.

In all cases, large-scale development occurs *locally* near the key region. The upgradient E-vector and downgradient heat flux patterns suggest that there are strong barotropic and baroclinic conversions from the time-mean flow into the eddies. This is consistent with the theories of large-scale instability of (or growth upon) the time-mean

flow. The later stages of the PAC evolutions are remarkably similar to certain stages in the evolution of the most unstable mode associated with barotropic instability of the time-mean 300 mb flow (Simmons et al., 1983). We note, however, that there are also strong baroclinic signatures, indicated by the downgradient and upward heat fluxes and the westward tilts of the large-scale disturbances. This is more in accord with a mixed type of instability as in Frederiksen (1983b). The viability of these mechanisms is examined in more detail in the following chapter.

V. Eddy sources and wave-mean flow interaction.

A. Introduction.

In this chapter specific diagnostic analyses are performed in an attempt to identify the principal mechanisms responsible for the PA developments. Wave activity fluxes are used to locate wave sources and sinks, and to diagnose propagation characteristics during the developments. These analyses will aid in determining whether the sources for development are primarily local or remote to the key regions. In particular, the possible *direct* influences of anomalous tropical forcing upon PA formation will be examined. Budgets of energy and enstrophy are also performed to assess the potential role of large-scale wave-mean flow interaction during PA development. Finally, potential vorticity analyses are used to further elucidate particular aspects of PA formation and breakdown.

As described in Chapter IV, the time evolution of PA's appears to be essentially a two stage process. Until just after onset (day +1), composite flow anomalies are, in general, transient and propagating. Thereafter, the primary anomaly patterns remain quasi-stationary near the key region as large-scale development occurs. For the purposes of this chapter, we will refer to days -5/0 as the "transient" phase and days +1/+5 as the "stationary" phase of PA development. This aids in selecting appropriate diagnostics. Most large-scale PA *development* appears to occur on or after day 0. Therefore, our main focus will be upon determining the mechanisms responsible for this portion of the evolution.

As described in Chapter II, fully developed PA's exhibit maximum geopotential height anomalies near 300 mb. Dole (1982) notes that PA's are associated with large potential vorticity anomalies near the tropopause. Analyses of pseudo-potential vorticity (q) during PA development (discussed later) suggest that local *anomalies* in q are comparable between 300 and 400 mb. A similar result was obtained by Holopainen and

Fortelius (1987b), who show a vertical profile of the hemispherically averaged eddy potential enstrophy during February 1979. An eddy measure of particular interest to us will be wave activity (a function of q'). As will be demonstrated below, wave activity is scaled by pressure and normalized by the magnitude of the horizontal gradient of pseudopotential vorticity. Near the PAC key region, for example, this leads to a reduction in wave activity of 40% between 400 and 300 mb (for a vertically uniform profile of q'). At mid-latitudes, anomalies and horizontal gradients of q fall off sharply below 400 mb. This suggests that the level of maximum transient eddy wave activity is found near 400 mb at midlatitudes. The observational analyses of Plumb (1985) indicate that this is true for both band-pass and low-frequency eddies. Consequently, we will concentrate particularly upon the sources for wave activity at the 400 mb level.

B Wave activity flux diagnostics

Plumb (1985, 1986) has recently generalized the Eliassen-Palm flux relationship obtained for zonal mean flows (e.g. see Edmon et al., 1980) to three dimensions. In Plumb's approach, this involves deriving a local conservation relation for some appropriate measure of eddy activity. Under certain constraints, local changes in wave activity are related to the convergence of a three-dimensional wave activity flux and/or local nonconservative sources or sinks. For almost-plane waves the wave activity flux is parallel to group velocity. Wave activity fluxes are therefore useful for identifying sources, sinks and propagation characteristics of eddies.

The conservation relation for transient eddies is given in Plumb (1986). For small-amplitude, quasi-geostrophic transients on a time-mean flow which varies slowly in space, M_T is a flux of wave activity in the conservation relation:

$$(5.1) \qquad \frac{\partial M}{\partial t} + \nabla \cdot \mathbf{M}_T = S_M$$

where:

$$M = \frac{p}{p_0} \cdot \frac{\overline{q'^2}}{2} \cdot \cos\phi \,/\, |\, \nabla_H \bar{q} \,|$$

$$\mathbf{M}_T = \mathbf{M}_R + \bar{\mathbf{v}}\, M$$

$$\mathbf{M}_R \approx \frac{p \cos\phi}{p_0} \left[\frac{\overline{v'^2 - u'^2}}{2} - \frac{R p^{\kappa} \overline{\theta'^2}}{2H \frac{d\bar{\theta}}{dz}} \; ; \; -\overline{u'v'} \; ; \; \frac{\overline{fv'\theta'}}{\frac{d\bar{\theta}}{dz}} \right]$$

Here, an overbar represents a time-average and a prime a deviation from a time average. Geostrophic velocity is given by $\mathbf{v} = (u, v)$, p is pressure (with p_0 a reference pressure), q is pseudopotential vorticity, θ potential temperature, ϕ latitude and $z = -H \ln(p/p_0)$. Also, R is the gas constant, H is the scale height, f is the coriolis parameter and $\kappa = R/c_p$ where c_p is the specific heat at constant pressure. M is the transient eddy wave activity and S_M is a nonconservative source/sink term due to diabatic, frictional and non-QG effects.

For a conservative flow, local changes in wave activity are related to the divergence of $\mathbf{M}_T$. The wave activity flux, $\mathbf{M}_T$, is parallel to group velocity for almost-plane waves. The approximate expression for $\mathbf{M}_R$ is valid for flows in which the horizontal gradient of time-mean q is primarily meridionally oriented. A detailed discussion of the derivation and application of this relation is contained in Plumb (1986).

An important distinction between $\mathbf{M}_T$ and other measures of eddy propagation (e.g. the E-vector of Hoskins et al., 1983) is that it is related to the *total* group velocity rather

than the group velocity relative to the mean flow. In fact, Plumb found that the horizontal component of $\mathbf{M}_T$ is dominated by mean flow advection, with both high frequency and low frequency eddies tending to propagate upward and *downstream* in the troposphere. Upward fluxes are strongest in the low to mid-troposphere while horizontal fluxes are most pronounced in the upper troposphere. Because of the dominance of mean flow advection, calculation of $\mathbf{M}_T$ is quite sensitive to the quality of eddy enstrophy statistics. As a result, Plumb concluded that his flux climatology may be inaccurate. Apparently unrealistic sources of transient eddy wave activity were found, for both synoptic-scale and low frequency eddies, near the entrance regions of the storm tracks in the *upper* troposphere. The diagnostic therefore needs to be applied with considerable caution. In this section, we will use this diagnostic, and compare our results with results contained in the composite analyses of Chapter IV. The term "propagation" will be often be used interchangeably with "flux" in the following discussions.

Transient eddy flux patterns for the PAC and ATL cases averaged over days -5/0 are displayed in figs. 5.1 and 5.2, respectively. Figure 5.1a overlays the horizontal flux in the upper troposphere (400 mb) and contours of lower tropospheric vertical flux (700 mb) for PN development. We see that, at early stages of the development, a robust upward and downstream wave activity flux pattern is located over the western North Pacific. At 400 mb, the flux converges into the key region. This pattern is consistent with the general picture obtained in Chapter IV, with early PN development characterized by synoptic-scale cyclogenesis over the western Pacific and eastward propagation toward the key region. The downstream signature in fig. 5.1a is associated with upper-level ridge development to the south of Greenland (see fig. 4.1). Fig. 5.1b shows a vertical profile of the vertical flux averaged horizontally over the North Pacific basin. We see that the average flux is upward at all levels, with maximum values at 700 mb and convergence above.

Similar analyses for PP evolution (figs. 5.1c,d) show that the early stages of

development are characterized by weak eastward fluxes of wave activity in the upper troposphere over the North Pacific. Upward propagation is observed over a broad region with a local maxima near the key region. A *vertical* convergence of wave activity is found near the key region. Over Siberia a well-defined flux pattern is observed in association with an eastward propagating and intensifying trough (see fig. 4.11). As for PN, the areal averaged wave activity flux is primarily trapped in the troposphere with the strongest vertical fluxes near the surface (fig. 5.1d).

Figure 5.2 displays parallel analyses for the early portions of AN and AP developments. AN (figs. 5.2a,b) exhibits upward and downstream wave activity flux over the western North Atlantic, as observed over the western North Pacific during PN development. The pattern is apparently related to coherent cyclogenesis over the western ocean region. Horizontal flux convergence is found near the key region in the upper troposphere. An upstream signature is observed near the region of cold air mass/upper trough development over western North America. AP development (figs. 5.2c,d) is typified by a nearly hemispheric pattern of upward and eastward transient eddy fluxes. This is consistent with the observation in Chapter IV (see also Neilley, 1990) that the early portion of AP development contains a coherent, synoptic-scale wave train extending over a large portion of the Northern Hemisphere. Unlike PN and AN, there is no organized *convergence* of wave activity into the key region. The suggestion is that there is a high *level* of transient eddy activity in the composite flow field. The vertical profiles of vertical flux (averaged over the North Atlantic region) for AN and AP show patterns qualitatively similar to PN and PP.

Although somewhat noisy, the diagnostic results are consistent with and lend support to the analyses of Chapter IV. The early portions of AN and PN development are characterized by upward and eastward fluxes of wave activity from a region of *coherent* synoptic-scale cyclogenesis over the western oceans. In the upper troposphere, the eastward flux continues to the key regions where horizontal convergence is found. PP

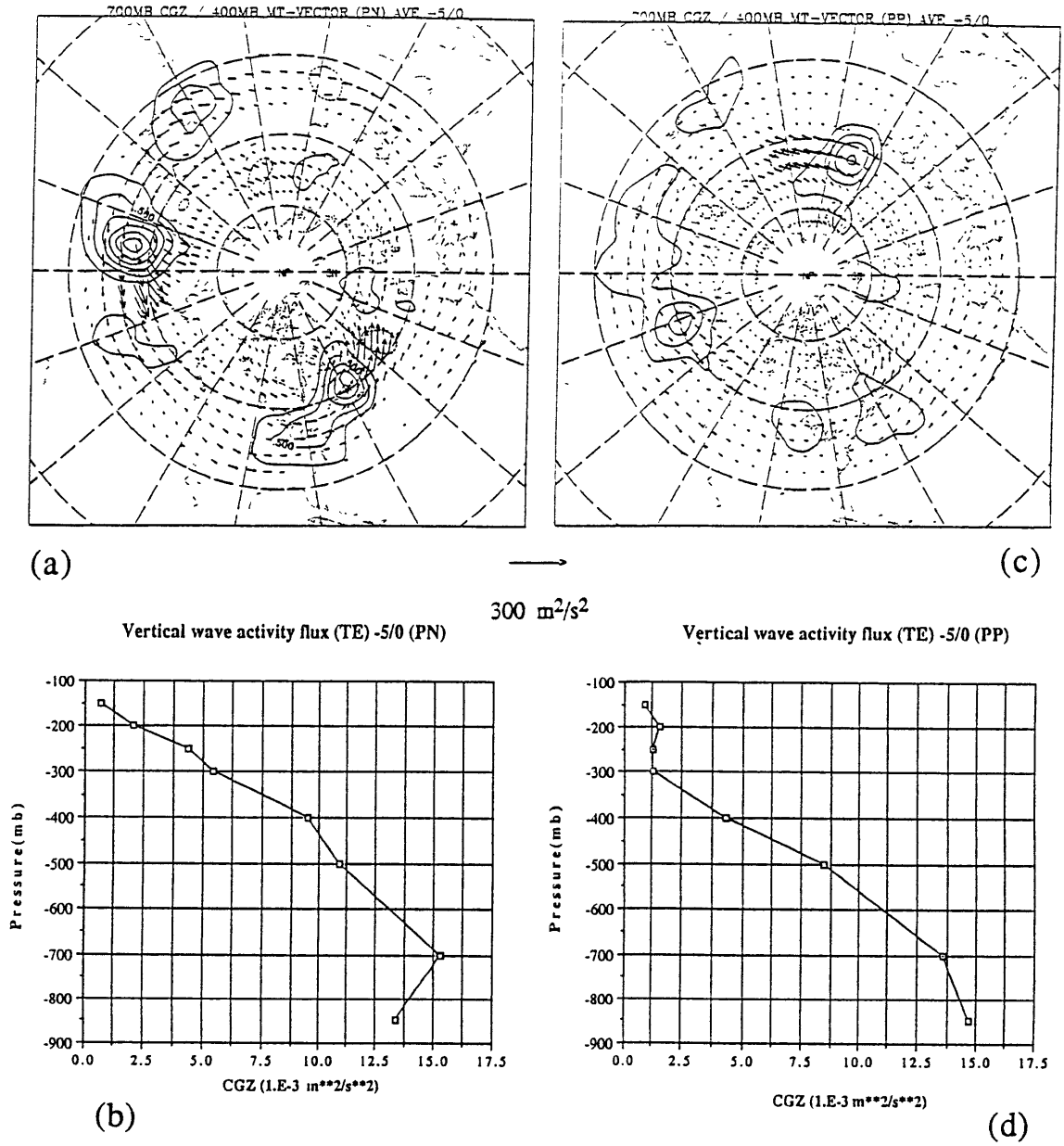

Fig. 5.1. Horizontal wave activity flux at 400 mb superimposed upon contours of the 700 mb vertical wave activity flux (contour interval: .025 m^2/s^2) for days -5 to 0 of (a) PN development and (c) PP development. Vertical profiles of the areal averaged vertical wave activity flux for (b) PN and (d) PP. The averaging area encompasses the midlatitude North Pacific region and is bounded by the latitudes 34°N and 78°N and the longitudes 140°E and 100°W. A scale vector is displayed for the horizontal flux.

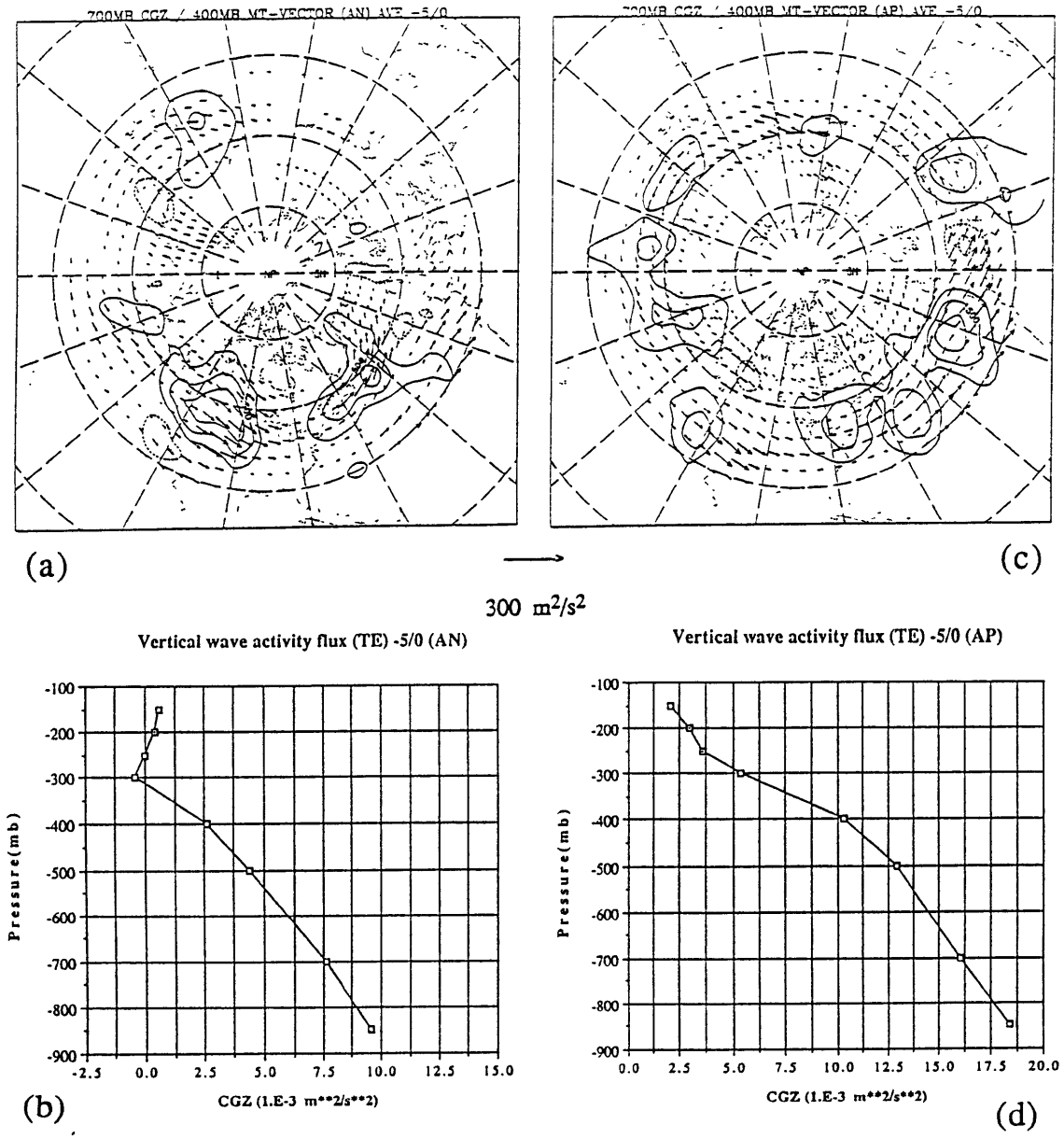

Fig. 5.2. As in Fig. 5.1 but for days -5 to 0 of (a), (b) AN development and (c), (d) AP development. Averaging area is the North Atlantic region and is bounded by the latitudes 34°N and 78°N and the longitudes 80°W and 20°E.

development exhibits a *vertical* convergence of wave activity near the key region. This is appears related to local baroclinic development near the key region (see fig. 4.16b). AP development exhibits a high level of coherent transient eddy activity during transient development. This is consistent with Neilley (1990) whose results show that there is a high level of synoptic-scale eddy activity during AP onset. In all cases there is little significant flux into the stratosphere.

Composite flow anomalies are quasi-stationary near the key regions during the latter stages of development (days +1/+5). Plumb (1985) derived an analogous local conservation relationship for *stationary* waves on a sphere. For linear, quasi-geostrophic stationary waves on a slowly varying zonal-mean flow, $\mathbf{F}_S$ is a flux of stationary wave activity in the relation:

$$\frac{\partial A_S}{\partial t} + \nabla \cdot \mathbf{F}_S = C_S \qquad (5.2)$$

As in the transient eddy formulation, the stationary wave activity A_S is related to the potential enstrophy of the waves. C_S is a non-conservative source/sink term and $\mathbf{F}_S$ is a 3-D flux of stationary wave activity:

$$\mathbf{F}_S = \frac{p\cos\phi}{p_0}\begin{bmatrix} v'^2 - \dfrac{1}{2\Omega a \sin 2\phi}\dfrac{\partial(v'\Phi')}{\partial\lambda} \\ -u'v' + \dfrac{1}{2\Omega a \sin 2\phi}\dfrac{\partial(u'\Phi')}{\partial\lambda} \\ \dfrac{2\Omega\sin\phi}{S}\left[v'T' - \dfrac{1}{2\Omega a \sin 2\phi}\dfrac{\partial(T'\Phi')}{\partial\lambda}\right] \end{bmatrix} \qquad (5.3)$$

In this formulation, ( )' is an average deviation from a *zonal* mean flow. Φ is geopotential,

λ is latitude, T is temperature, a is the radius of the Earth, Ω is the Earth's rotation rate and S is areal average static stability. Other symbols are defined in reference to equation (5.1).

For steady, conservative waves $\mathbf{F}_S$ is nondivergent. In the case of slowly varying, almost-plane waves $\mathbf{F}_S$ is parallel to group velocity. Unlike the transient eddy formulation, one potential source/sink in C_S is QG forcing by transient eddies. $\mathbf{F}_S$ has proven useful in diagnosing 3-D propagation characteristics of stationary waves in both observational studies (Plumb, 1985; Karoly et al., 1989) and modelling studies (Mo et al., 1987; Kang, 1990). As with any technique, however, care must be taken in its application. First, it is important to eliminate any zonally symmetric components of stationary flow anomalies before analysis. In the upper troposphere, horizontal Rossby wave propagation tends to be directed along potential vorticity gradients near the tropopause. Since the height of the tropopause varies considerably with latitude, care must be taken in choosing an appropriate pressure level to study horizontal propagation characteristics (Karoly et al.). Also, $\mathbf{F}_S$ is a nonlinear function of the wave variables. Thus, the wave flux associated with stationary flow *anomalies* is not necessarily the same as the anomalous stationary wave flux. Kang's modelling study includes an example where anomalous $\mathbf{F}_S$ divergence is not due to a local, anomalous wave source but rather results from a local *redirection* of wave activity flux emanating from a fixed remote source. Indeed, variations in the refractive index of the atmosphere can lead to such signatures (e.g. Nigam and Lindzen, 1989). Taking these into consideration, we apply $\mathbf{F}_S$ to the latter, quasi-stationary phase of PA development.

Selected analyses based on the climatological mean flow are presented for reference in fig. 5.3. In fig. 5.3a, the vertical component of $\mathbf{F}_S$ (hereafter FSZ) at 700 mb is contoured over vectors of the horizontal component of $\mathbf{F}_S$ (hereafter FSH) at 400 mb. As Plumb (1985) demonstrated, there is a strong upward flux of wave activity in the lower troposphere near eastern Asia and over the North Atlantic. In the upper troposphere, FSH

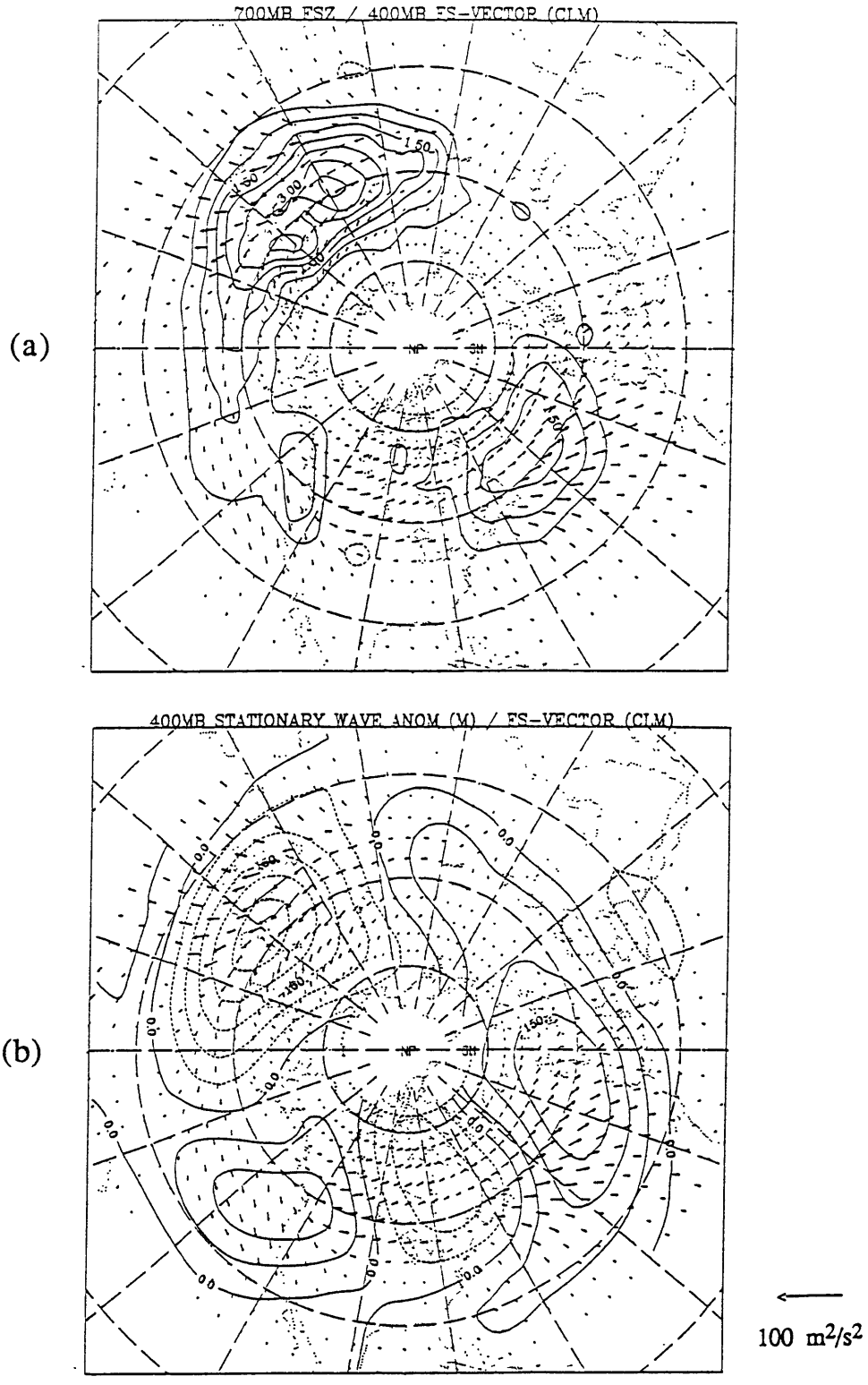

Fig. 5.3. FSH at 400 mb overlays (a) 700 mb FSZ (contour interval: .05 m^2/s^2) and (b) 400 mb stationary wave pattern (contour interval: 50 m), for *the wintertime-mean stationary waves*. A scale vector and corresponding magnitude is shown for FSH.

(c)

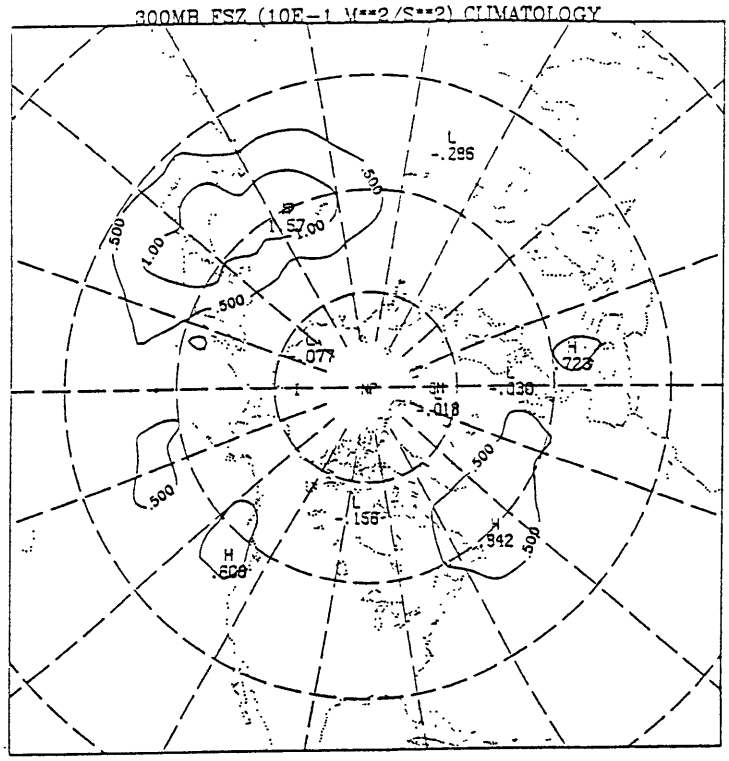

(d)

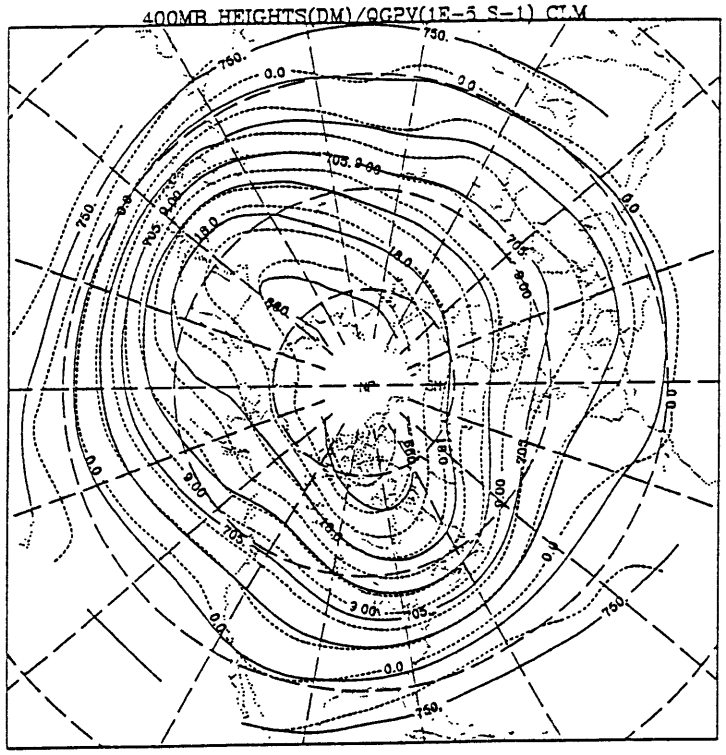

Fig. 5.3. (*cont.*) (c) 300 mb FSZ (contour interval: .05 m^2/s^2) for the wintertime-mean stationary waves. (d) 400 mb wintertime-mean heights (solid lines) and q (dashed lines). Contour intervals: 15 dam for heights; 3×10^{-5} s^{-1} for q.

streams southeastward over the North Atlantic and both northeastward and southeastward from the east coast of Asia. Plumb's results suggest that the climatological stationary waves (1) have relatively small contributions from tropical forcing, (2) are only weakly forced by the Rocky Mountains and (3) are strongly influenced by the Himalayas and by local, non-orographic effects near the storm tracks (presumably due to the direct or indirect effects of transients, the latter associated with diabatic processes). Fig. 5.3b displays FSH and the climatological stationary waves for 400 mb. The 300 mb FSZ pattern (fig. 5.3c) is qualitatively similar to that at 700 mb but is considerably weaker in magnitude. Figure 5.3d shows the 400 mb pseudopotential vorticity and geopotential height fields of climatology, to be discussed later.

Analyses of $\mathbf{F}_S$ are displayed in figs. 5.4-5.7 for the stationary phase of PA development. In these analyses, stationary wave anomalies are defined as composite flow anomalies averaged over days +1 to +5. The flow anomalies project only weakly on wavenumber 0. Therefore the time-averaged flow anomalies are a very good approximation to the anomalous stationary waves. Our primary concern is in diagnosing anomalous fluxes of stationary wave activity. This is achieved by calculating the flux of the total stationary wave pattern (which includes climatology) and subtracting out the flux associated with the climatological mean waves. This leads to a net, anomalous flux that is distinct from the flux associated with the wave anomalies. As mentioned earlier in this chapter, our main focus is on the level of maximum wave activity, which at mid-latitudes is near 400 mb. In practice, the 400 mb level appears close enough to the subtropical tropopause in order to capture the *qualitative* nature of upper tropospheric wave propagation at these latitudes. This was checked by examining $\mathbf{F}_S$ near the subtropical tropopause. It is important to consider this when diagnosing potential tropical sources. Unlike for the climatological waves, in our analyses $\partial A_S/\partial t$ can be (and is) nonzero. Local changes in wave activity are then due to either a convergence of the flux of stationary wave

activity $\mathbf{F}_S$ or to local nonconservative or transient eddy processes.

Fig. 5.4 displays components of the net $\mathbf{F}_S$ patterns associated with the stationary phase of PN development. Figure 5.4a displays 700 mb FSZ together with 400 mb FSH. The most prominent features are the strong upwards and downstream flux anomalies near and to the east of the PAC key region. The 400 mb FSH and averaged 400 mb height anomaly patterns (fig. 5.4b) indicate that, in the upper troposphere, the anomalous flux is directed eastward from the key region towards the downstream ridge and trough. Note that, south of the key region, FSH points southeastward toward the subtropics. The 300 mb FSZ pattern (fig. 5.4c) exhibits net upward propagation but it is considerably weaker than at 700 mb. This is more clearly demonstrated in fig. 5.4d, which displays the areal average values of FSZ. Although there is a net upward flux at 300 mb, it decays with height and is an order of magnitude smaller than FSZ in the lower troposphere, with strong vertical convergence near 400 mb. The diagnostics concisely suggest that there is an anomalous local source of wave activity during the later stages of PN development. Wave activity propagates upward, eastward and southward from the local source. The flux is primarily confined to the troposphere, with little evidence for direct tropical forcing of the flow anomalies.

The analyses for PP, displayed in fig. 5.5, suggest a qualitatively different behavior. There is anomalous upward flux over eastern Siberia and, in the upper troposphere, an eastward horizontal flux from Siberia towards the PAC key region, where horizontal convergence and anomalous downward propagation is observed. Horizontal convergence extends zonally along the axis of the mean ridge (fig. 5.5b). The pattern suggests that anomalous forcing from a remote upstream source may contribute to the large-scale development. Also, a weak northward wave flux from the subtropics is found to the east of the date line. At 300 mb, the dipole in FSZ remains evident, albeit weaker in amplitude. Because of the dipole nature of the vertical flux pattern, the areal averaged FSZ is much

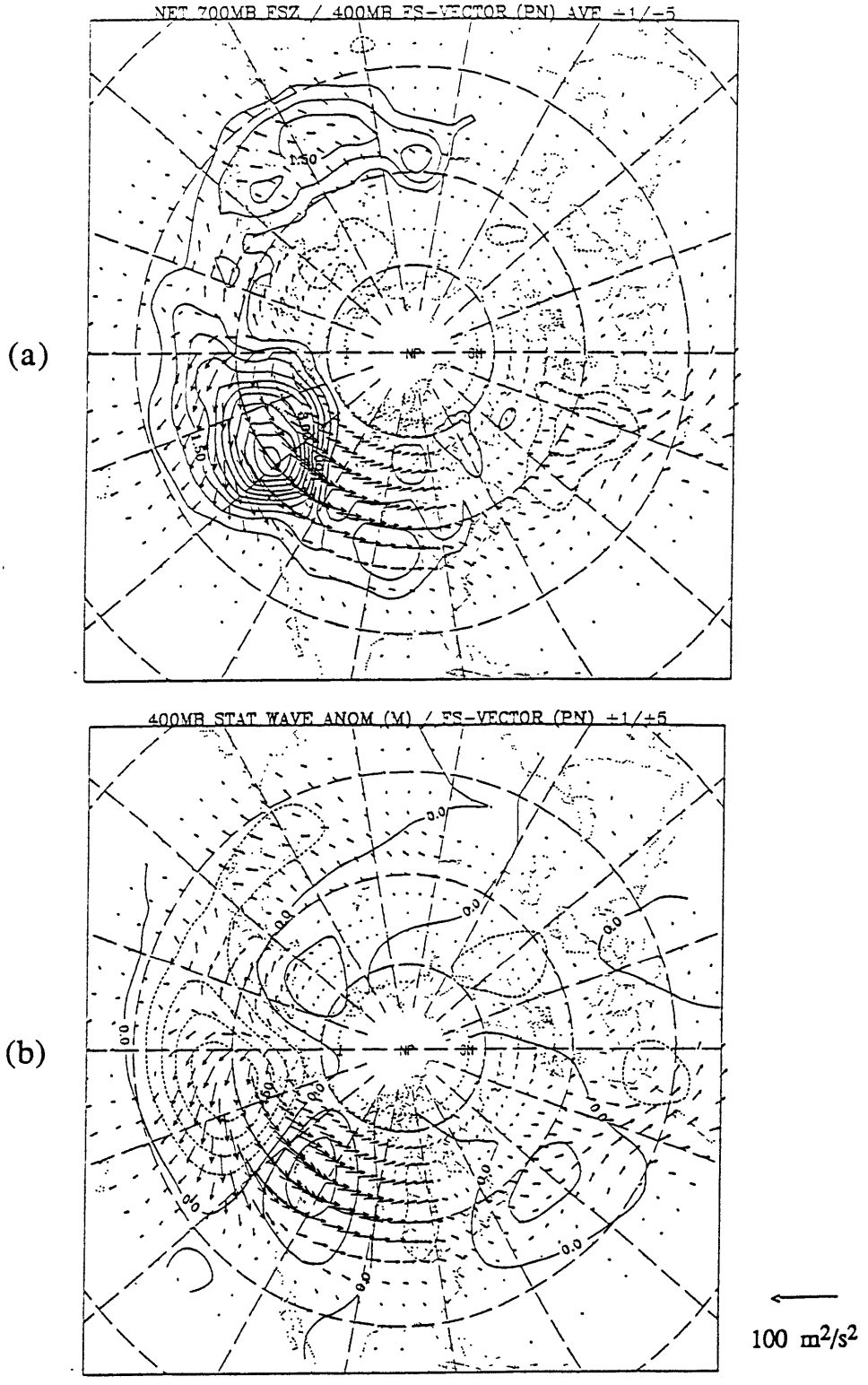

Fig. 5.4. Anomalous FSH at 400 mb overlays (a) 700 mb FSZ anomalies (contour interval: .05 m^2/s^2) and (b) 400 mb stationary wave anomalies (contour interval: 50 m) for days +1 to +5 of PN development. A scale vector is shown for FSH.

(c)

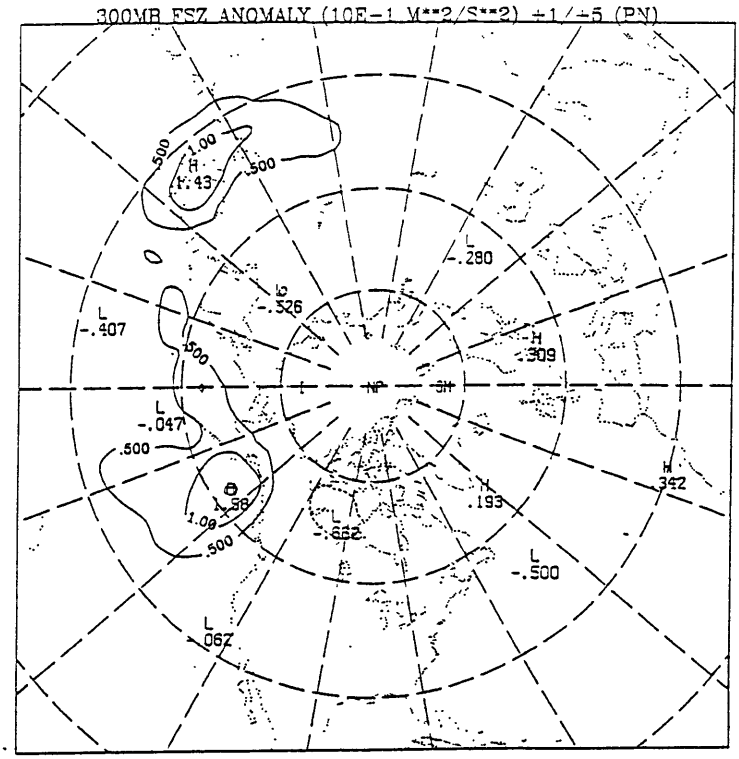

Vertical wave activity flux (SE) +1/+5 (PN)

(d)

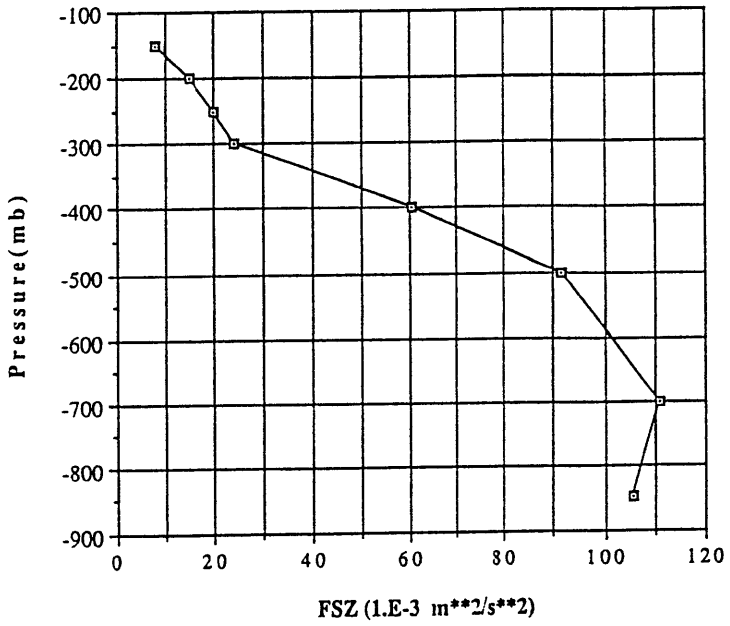

Fig. 5.4. (*cont.*) (c) 300 mb FSZ anomalies (contour interval: .05 m^2/s^2) and (d) vertical profile of areal averaged FSZ anomalies, for days +1 to +5 of PN development. Averaging area is the same as in Fig. 5.1.

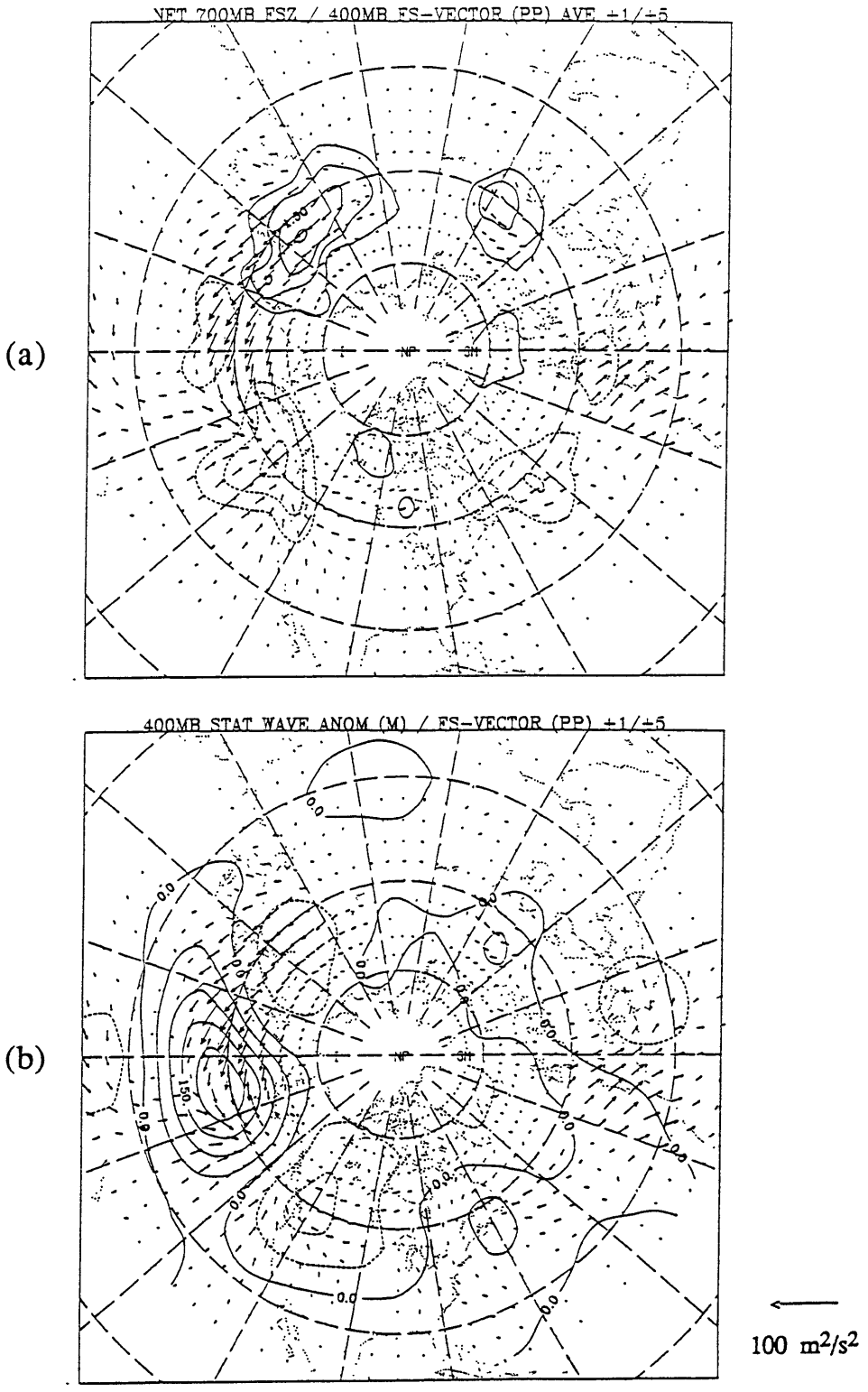

Fig. 5.5. As in Fig. 5.4 for days +1 to +5 of PP development. Averaging area for (d) is bounded by the latitudes 34°N and 78°N and the longitudes 90°E and 100°W.

(c)

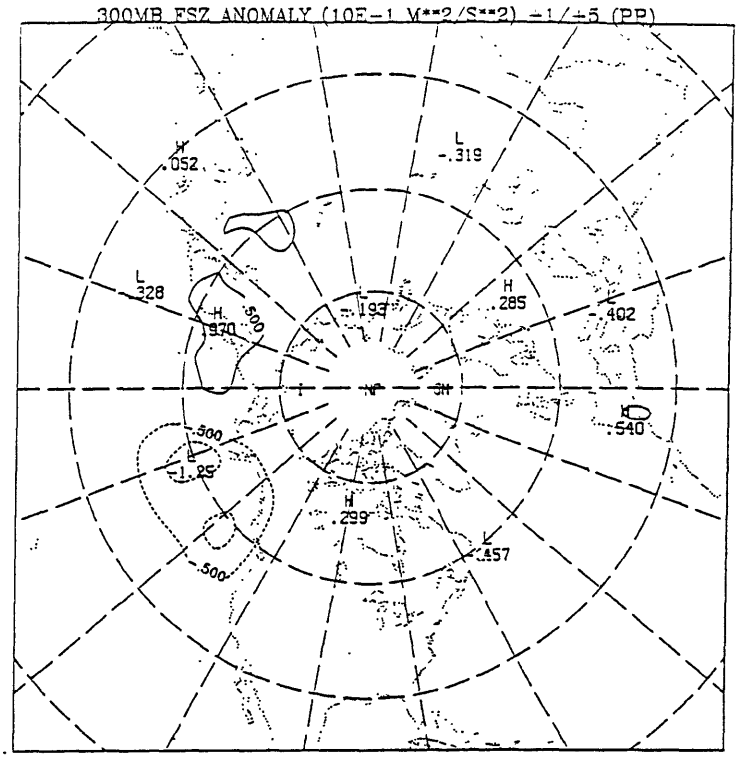

Vertical wave activity flux (SE) +1/+5 (PP)

(d)

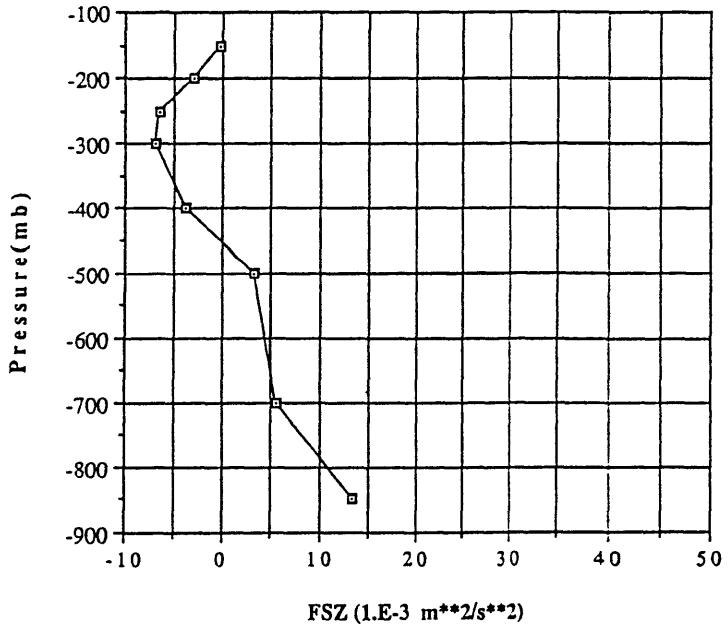

Fig. 5.5. (*Continued*)

smaller than for PN. A net *downward* anomalous flux in the lower stratosphere weakens with height.

The upstream source appears to be related to an upper level trough which develops over Siberia during the early stages of PP development (see fig. 4.11 and discussion). During the later stages of PP evolution, the trough is stationary near the east coast of Asia and weakens, consistent with a loss of stationary wave activity. Neilley (1990) has shown that enhanced synoptic-scale wave activity is found upstream of the key region during PP onset. Thus a possible contributor towards the anomalous remote source is upstream transient eddy forcing. A redirection of wave activity flux seems unlikely when comparing figs. 5.3a and 5.5a. Anomalous eastward flux is not accompanied by anomalous northward flux over the southwestern North Pacific, where strong southward fluxes are observed in the climatological pattern (e.g. see Kang, 1990).

Even though there is evidence for remote forcing, this does not preclude the possibility that local sources may also contribute positively towards development. In other words, $\partial A_S/\partial t$ can also be influenced by C_S in equation (5.2). The zonal orientation of the horizontal convergence pattern in fig. 5.5b suggests that the remote source contributes towards forming a zonally elongated anomaly pattern. Such a pattern could also interact, locally, with the time mean flow. These interactions will be further examined in the following two sections of this chapter.

The anomalous $\mathbf{F}_s$ fields associated with AN development are shown in fig. 5.6. Note the strong positive anomalies in 700 mb FSZ on the east and west sides of the large-scale low. Although only a weak FSH pattern is found in the upper troposphere, there is an anomalous northeastward flux of wave activity from the northeastern portion of the low towards an anomalous ridge located over Scandinavia (fig. 5.6b). A robust upstream signature is observed in association with ridge development which occurs over the eastern North Pacific. The 300 mb FSZ pattern shows very little structure over the

North Atlantic region. As for PN, the areal averaged FSZ is strongest in the lower troposphere with large convergence near 400 mb. Very little vertical wave flux is found above the tropopause.

AP (fig. 5.7) exhibits a strong anomalous flux pattern over the North Atlantic. Large positive values of FSZ are observed in the low troposphere west of the key region (fig. 5.7a). FSH diverges above this region, flowing eastward toward the Greenwich meridian where horizontal flux convergence and downward propagation is observed. Some anomalous flux is directed southeastward to northern Africa. Upward flux anomalies are observed at 300 mb south of Greenland. Horizontally averaged values of FSZ suggest a weak, but consistent, upward flux of wave activity above 300 mb. Unlike the other PA's, the largest average values of FSZ are found near 500 mb. Vertical convergence occurs in the 300-400 mb layer. For both AP and AN cases, then, *the main source of wave activity appears to be local to the development region.*

In summary, $\mathbf{F}_s$ diagnoses suggest that *local* sources are responsible for the large-scale, quasi-stationary portion of PN, AN and AP developments. PP development shows some evidence for remote forcing from an upstream source located near eastern Siberia. A weak flux of wave activity from the subtropical North Pacific is also evident for PP. Otherwise, there is very little evidence of direct forcing from the tropics during PA formation. All four PA's appear to be primarily trapped in the troposphere. AP shows the most consistent upward propagation into the stratosphere. PN and AN exhibit the strongest anomalous vertical fluxes, peaking in the lower troposphere.

C. Energetics analyses.

One major hypothesis for PA formation discussed previously is that the development is due to a large-scale instability of the time-mean flow. One classical approach toward assessing the possible role of instabilities in the developments is through the energetics

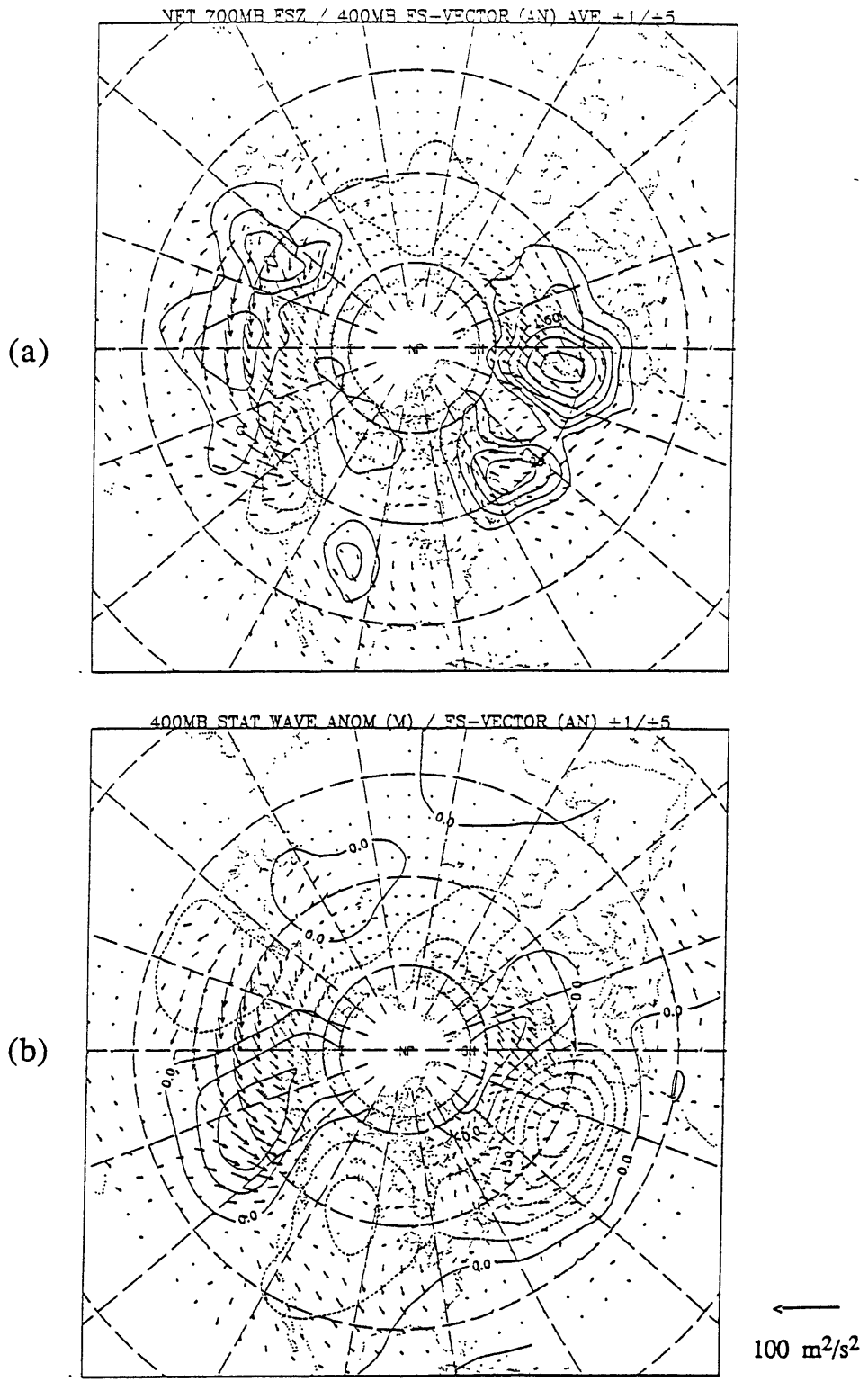

Fig. 5.6. As in Fig. 5.4 for days +1 to +5 of AN development. Averaging area for (d) is the same as in Fig. 5.2.

(c)

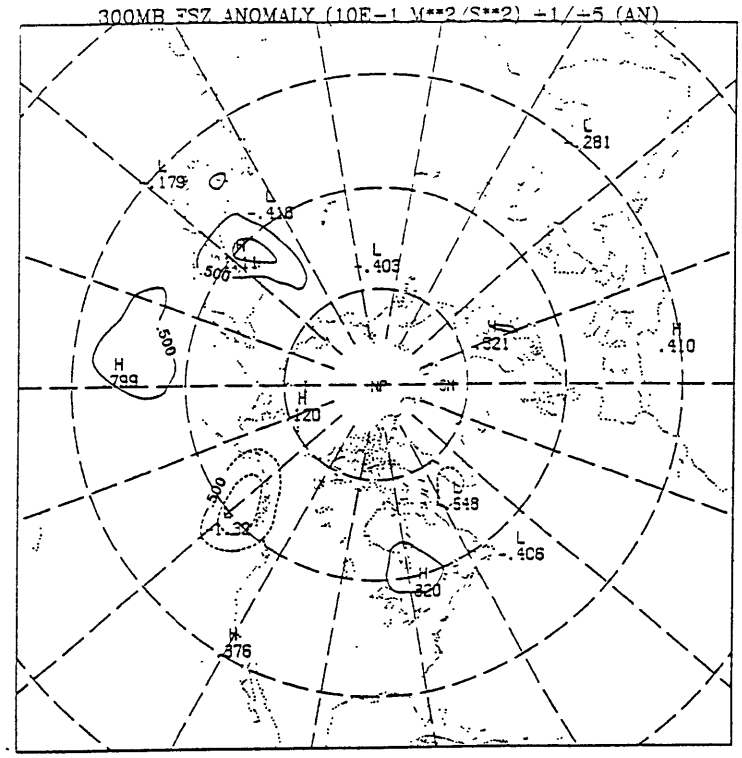

Vertical wave activity flux (SE) +1/+5 (AN)

(d)

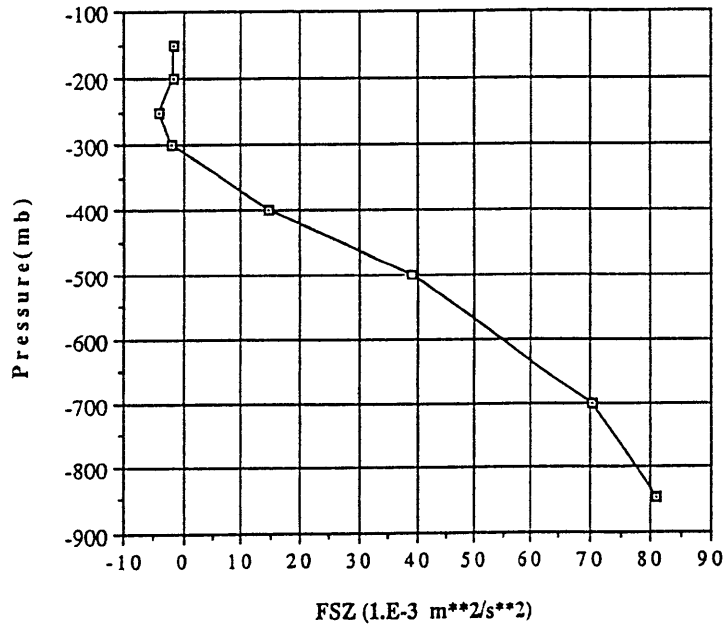

Fig. 5.6. (*Continued*)

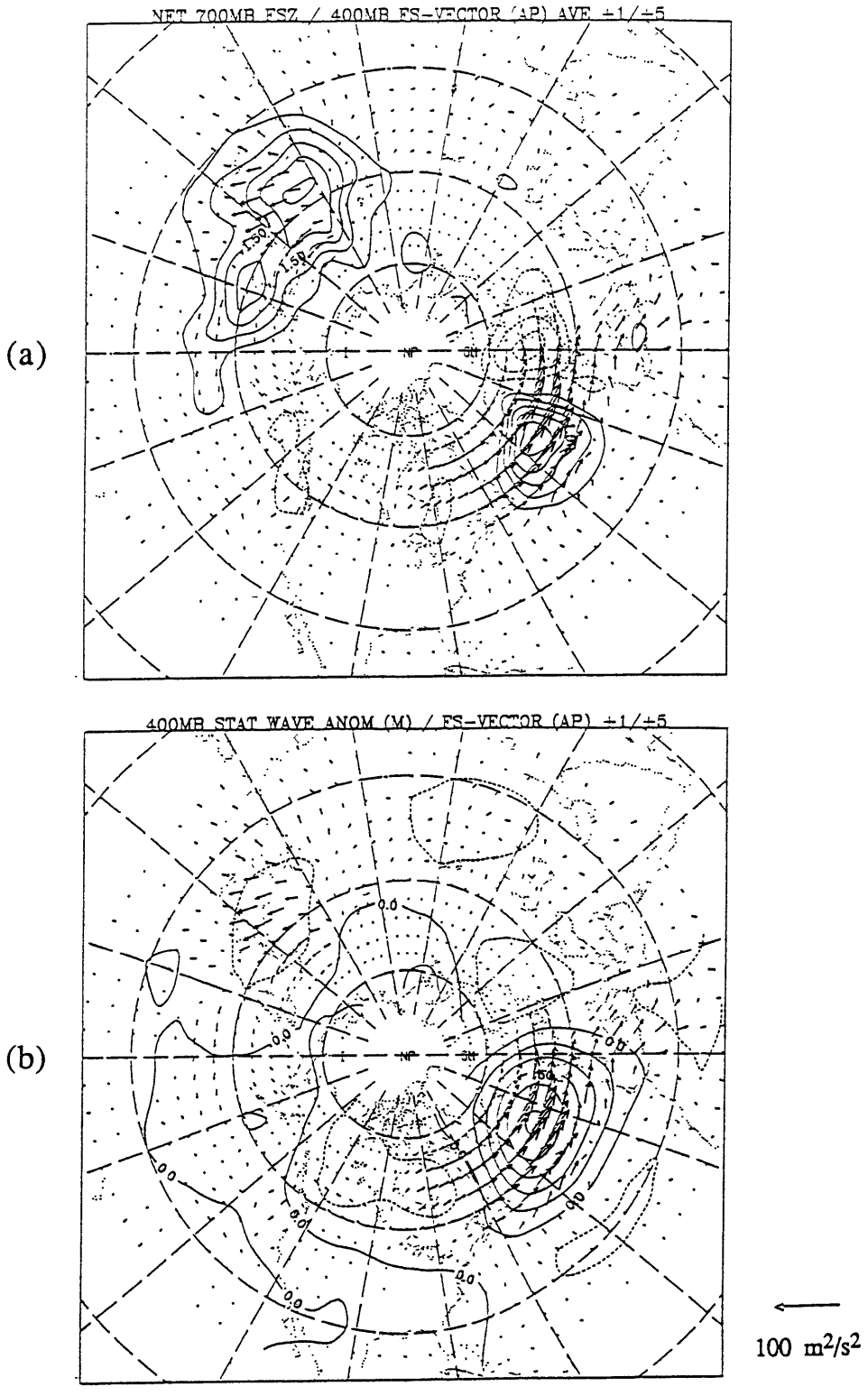

Fig. 5.7. As in Fig. 5.4 for days +1 to +5 of AP development. Averaging area for (d) is the same as in Fig. 5.2.

(c)

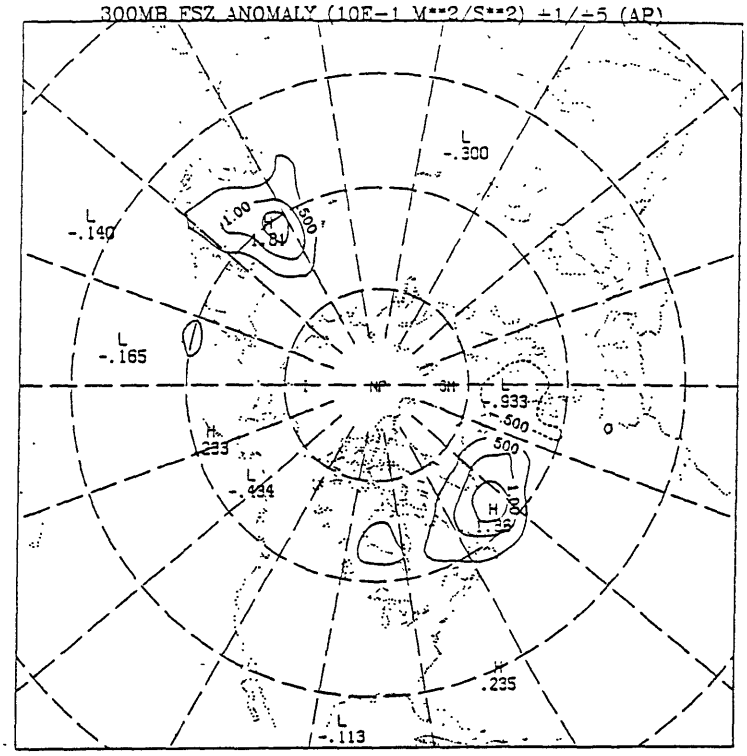

Vertical wave activity flux (SE) +1/+5 (AP)

(d)

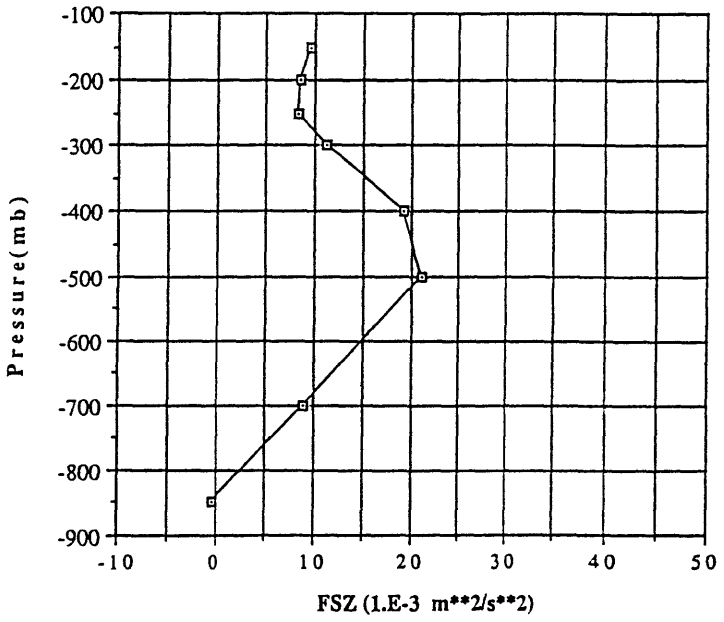

Fig. 5.7. (*Continued*)

cycle, as discussed in Chapter IV. The E-vector, heat flux and Q-vector analyses of Chapter IV provide preliminary, qualitative information on possible energy conversions associated with the growing eddies. In this section the energetics analyses are extended to quantitatively compare the volume integrated energy conversions of equation (4.1) to time series of integrated energy changes. Our aim is to determine if the energy conversions are consistent with the proposed instability mechanisms. A *lack* of consistency would provide strong evidence against these mechanisms.

The composite PA flow anomalies tend to be regionally confined. This isolation is even more prominent for the energy terms (quadratic quantities) of the composite eddies. Here, the volume of integration is chosen in order to isolate the region of eddy (and hence eddy energy) growth. We do not assess boundary fluxes of *composite* energy. Clearly, there can be additional dynamical contributions to development due to boundary fluxes and/or nonlinear interactions associated with the *incoherent* eddies (which are *not* regionally confined). However, our aim here is to determine whether the internal, downgradient fluxes of heat and momentum associated with the *composite eddy* are sufficient to account for changes in the energy associated with the composite anomalies.

At the outset, it is important to note that there are certain ambiguities associated with the energetics method of studying eddy-mean flow interactions. For example, Plumb (1983) demonstrates that when the traditional energy cycle is applied to a steady, upward propagating topographically forced wave, one finds a series of eddy "conversions" qualitatively similar to those of a developing baroclinic wave. Unlike a growing baroclinic wave, however, the energy *tendencies* are identically zero and the "conversions" are an artifact of the analysis scheme. Large *changes* in both kinetic and potential energy take place during PA development. The question is whether the conversions of equation (4.1), due to downgradient fluxes by the composite anomalies, can account for these changes. Despite the ambiguities, the energy cycle associated with PA development can be compared for consistency with the models discussed in Chapter II. A more fundamental and less

ambiguous way of studying eddy-mean flow interaction is examined in the next section.

The conversions of equation (4.1) are analyzed during PN and PP development, with the perturbation quantities obtained from the *composite* eddy fields. Conversions 4.1a and 4.1b are straightforward to calculate. Conversion 4.1c, however, involves vertical velocity anomalies which are difficult to determine from observations. In this study, ω' is estimated as a residual in the thermodynamic equation, neglecting diabatic heating anomalies. This approximation is probably worst near the east coast of Asia during PN development, where the observed anomalously strong cold advection is likely to lead to significant diabatic heating anomalies near the Kuroshio. A comparison of the adiabatically estimated vertical velocities with Q-vector analyses suggests, however, that a reasonable correspondence is found east of this region over the central and eastern North Pacific.

Integrations are performed horizontally over a domain bounded by the latitudes 26°N and 78°N and the longitudes 140°E and 100°W. A vertical average is then performed in the layer between 850 and 150 mb. Time series are presented in figs. 5.8 and 5.9 for PN and PP, respectively.

Figure 5.8a displays the vertically averaged barotropic conversions and eddy kinetic energy (EKE) changes for PN development. Note the strong correlation between the two time series during development. On average, the conversions are sufficient to account for the increases in EKE. The early portion of development is characterized by negative barotropic conversions. This is consistent with the analyses of Chapter IV in which the composite perturbation at day -3 exhibits a northwest to southeast horizontal tilt on the north side of the mean jet, suggesting that barotropic eddy decay is likely. Increasing conversions are observed thereafter, as the disturbance attains a zonally elongated structure in the jet exit region (e.g. see fig. 4.8c,d). The barotropic conversions strongly exceed observed EKE changes by day +4. At this time, strong Ekman damping is anticipated and some energy leakage occurs via Rossby wave radiation through the eastern boundary (100°W).

Fig. 5.8:

(a) Time series of the horizontally integrated and vertically averaged barotropic energy conversions associated with the composite eddies (open squares) and the rate of change of composite eddy kinetic energy (solid squares) during PN development. The integration/averaging domain is discussed in the text. Units are 10^{-4} m^2/s^3. A three-point binomial filter was applied to the time series for display purposes.

(b) Time series of the two baroclinic conversion terms C(A,A') (open squares) and C(A',K') (solid squares) associated with the heat fluxes of the composite eddies during PN development. The integration and averaging is performed as in (a). The units are 10^{-4} m^2/s^3. The time series is lightly smoothed using a three-point binomial filter.

(c) Time series of the summed energy conversions C(K,K') and C(A',K') (open squares) and the time rate of change of eddy kinetic energy (solid squares) during the large-scale phase of PN development. The integration and averaging regions are as in (a). The units are 10^{-4} m^2/s^3 and the time series is lightly smoothed using a three-point binomial filter.

(a)

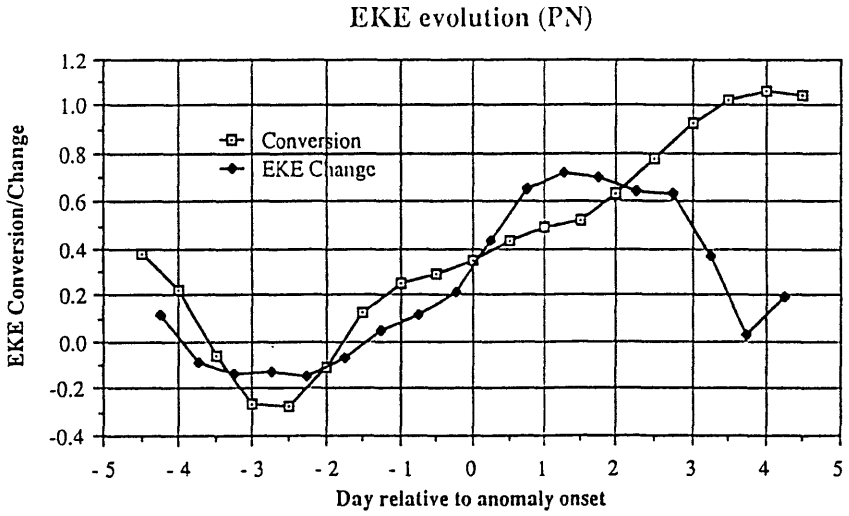

(b)

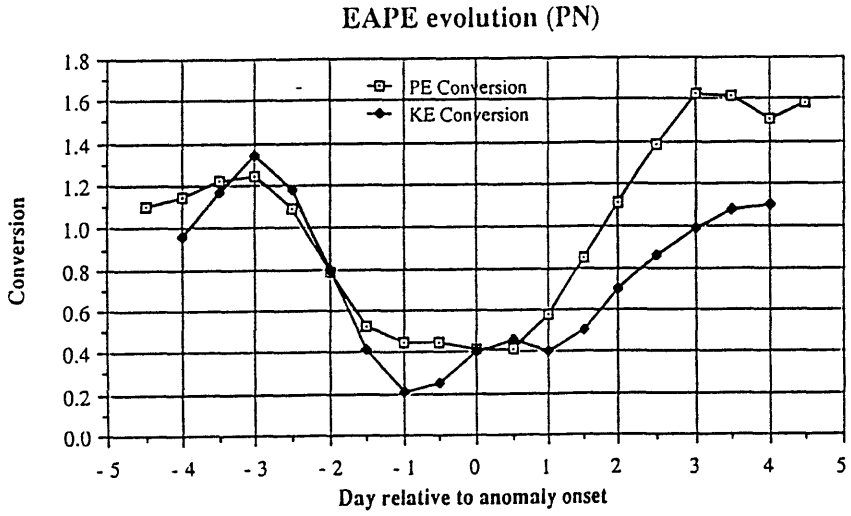

(c)

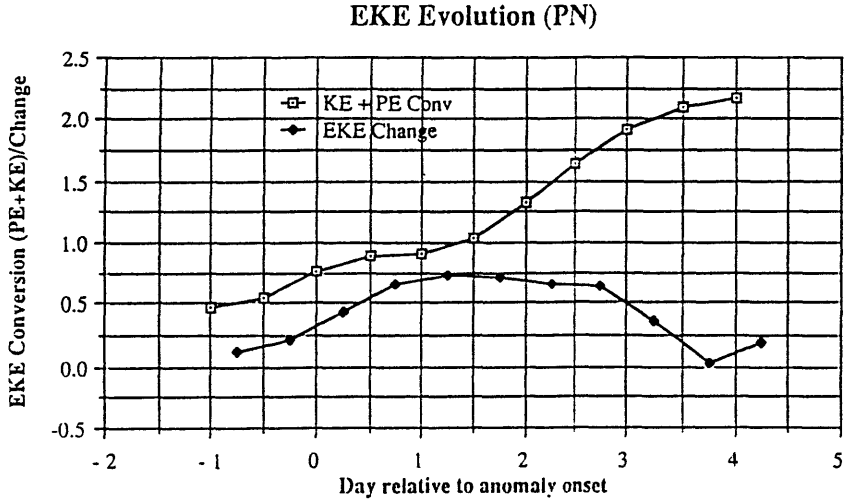

Fig. 5.8. (See caption on previous page)

The baroclinic conversions C(A,A') and C(A',K') are displayed in fig. 5.8b (see equation (4.1) for formulation of the conversions). Consistent with the heat flux and Q-vector analyses of Chapter IV (figs. 4.9a and 4.10b), strong positive conversions are found at day -3 in association with synoptic-scale cyclogenesis over the western North Pacific. At this time, the conversion to EKE slightly exceeds the conversion to eddy available potential energy (EAPE). Both conversions weaken as the onset day approaches and the composite eddy acquires an equivalent barotropic structure. After day +1, however, increasing downgradient and upward heat fluxes result in increasingly strong positive baroclinic conversions. The conversion to EAPE exceeds the conversion to EKE during this time, consistent with the energetics of baroclinic wave development. Time series of vertically averaged EKE changes and the summed conversions C(K,K') and C(A',K') are displayed in fig. 5.8c for the period of large-scale development. Note that *the summed conversions are sufficient to account for the large-scale growth.*

Corresponding time series for PP development are shown in fig. 5.9. Barotropic conversions are relatively weak until after day 0. Prior to day +1, the barotropic conversions are *not* sufficient to account for EKE changes. Thereafter, barotropic conversions significantly exceed EKE changes. The positive barotropic conversions are consistent with the strong upgradient E-vector pattern associated with the disturbance during this time (see fig. 4.15c,d).

The time series of baroclinic conversions exhibit small peaks at day -1, when strong heat fluxes are observed near the key region (fig. 4.16b). A secondary surge of positive C(A,A') occurs after day +1. During the latter part of evolution, the conversion to EAPE far exceeds the conversion to EKE. This result was suggested by the Q-vector analyses discussed in the previous chapter (not shown) which indicated that only weak upward heat fluxes occur during PP development. C(A',K') is large enough, however, that the *summed* conversions displayed in fig. 5.9c are sufficient to account for EKE changes during PP development. Unlike during PN development, strong baroclinic conversions

(a)

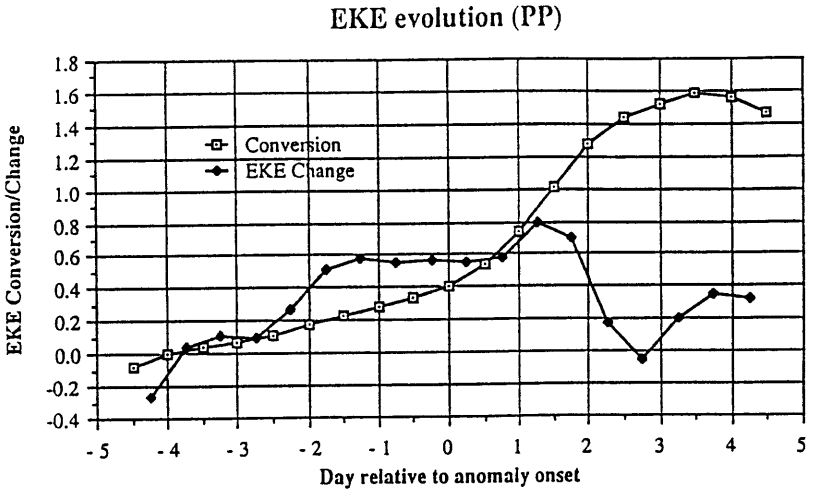

(b)

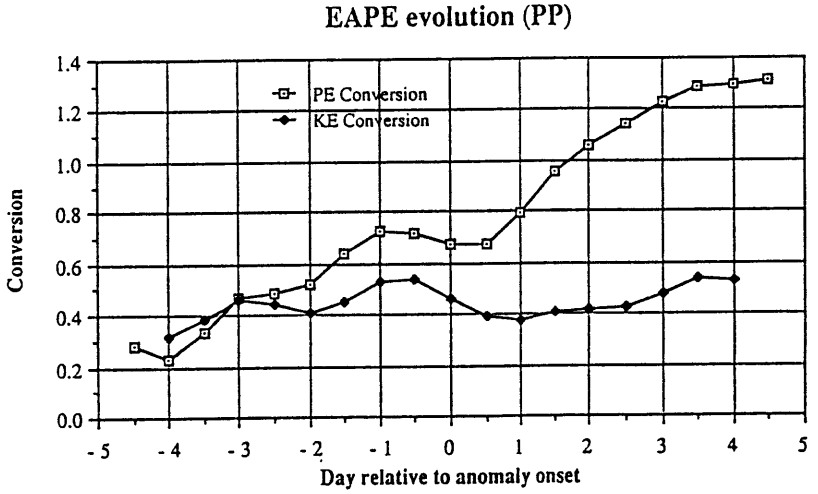

(c)

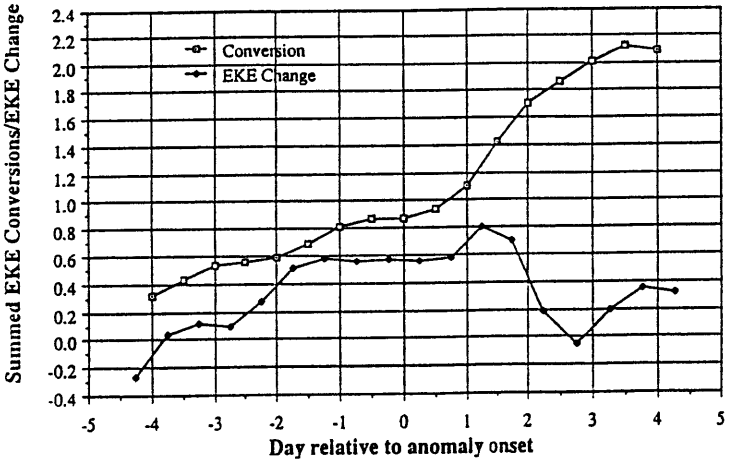

Fig. 5.9. As in Fig. 5.8 for PP development.

precede barotropic conversions during the large-scale phase of PP development.

The downgradient heat fluxes which occur at large scales during PA development are substantial when compared to climatological values. This appears surprising when one considers the relatively small vertical phase tilts found during the later stages of PA development (e.g. figs 4.4c and 4.12c) and the body of evidence which suggests that low frequency eddies appear to be predominantly "equivalent barotropic" in nature (Blackmon et al., 1979; Dole, 1986a; Schubert, 1986). A simple thought experiment helps to reconcile this apparent discrepancy. Consider a plane wave with no meridional variation:

$$\psi' = Z_0 \, e^{i(kx + mz - kct)} \, g / f$$

Where ψ' is the perturbation streamfunction, Z_0 is the wave amplitude (geopotential height) and f is the coriolis parameter. The phase averaged meridional heat flux is given by:

$$\langle v'T' \rangle \propto \left\langle \frac{\partial \psi'}{\partial x} \frac{\partial \psi'}{\partial z} \right\rangle \propto \frac{(Z_o)^2}{L_x L_z}$$

Where $\langle \, \rangle$ is some phase averaging operator, L_x is zonal wavelength and L_z is the vertical wavelength. For a growing "synoptic-scale" disturbance:

Z_0	~	90 m	-peak standard deviation at 300 mb
L_x	~	4000 km	-zonal wavenumber 7 at mid-latitudes
L_z	~	40 km	-allows 1/4 wavelength shift between the surface and 300 mb (12.5 degrees longitude)

The values of Z_0 and L_x are taken from the observational studies of Blackmon et al. (1977 and 1984a). For day +3 of PN development:

Z_0	~	290 m	-maximum value of Z' at 300 mb (fig. 4.4c)
L_x	~	9000 km	-zonal wavenumber 3 at mid-latitudes
L_z	~	150 km	-allows 1/15 wavelength shift between the surface and 300 mb (7.5 degrees longitude)

These values are estimated from the analyses of Chapter IV (in particular, fig. 4.4c). Using the above values:

$(Z_0)^2/(L_xL_z)$	=	5.1E-8	-for typical synoptic-scales
$(Z_0)^2/(L_xL_z)$	=	6.2E-8	-for day +3 of PN development

Although the large-scale wave pattern has a vertical phase shift of only 1/15 wavelength between the surface and tropopause, its associated heat fluxes are comparable to, and may exceed, the heat fluxes of a growing synoptic-scale "baroclinic" wave. The quadratic amplitude factor compensates for the effects of reduced vertical tilt. Clearly, this suggests that the descriptor "equivalent barotropic" must be qualified somehow to account for this. The results of Lau and Holopainen (1984) and Schubert (1986) also suggest that there are significant heat fluxes associated with low frequency variations at mid-latitudes.

To summarize, the energetics analyses suggest that coherent eddy-mean flow interactions are sufficient to account for PN and PP developments. Although the analyses do not prove that instability occurs, they are *consistent* with that possibility. For PN, the early stages resemble synoptic-scale baroclinic growth. After day 0, large-scale development is initially accompanied by increasingly large positive barotropic conversions. Subsequently, strong baroclinic conversions occur, consistent with observed increases in EAPE and EKE. During large-scale PP development, large-scale baroclinic conversions *precede* barotropic conversions. The two evolutions are remarkably similar during latter

stages of development. The main difference is that PN exhibits a stronger "baroclinic" signature while PP has a stronger "barotropic" signature. Because of the qualitative consistency between the results of this section and the following section, we will omit a description of the energetics of ATL developments in this section.

D. Potential enstrophy analyses.

A more fundamental, and less ambiguous, approach towards studying atmospheric dynamics is through the framework of potential vorticity. This is thoroughly discussed by Hoskins et al. (1985). In this section, the eddy-mean flow problem is examined in terms of *quasigeostrophic* pseudopotential vorticity. The wave activity diagnoses of section B are based upon this quantity. The cornerstone of quasigeostrophic (or QG) theory is the QG potential vorticity equation:

$$(\frac{\partial}{\partial t} + \mathbf{v}_g \cdot \nabla) q = S$$

where:

$$q = f + \frac{1}{f_o} \nabla^2 \Phi + f_o \frac{\partial}{\partial p} (\frac{1}{\sigma} \frac{\partial \Phi}{\partial p})$$

$$\sigma = \sigma(p)$$

Here f is the coriolis parameter, σ is the static stability parameter, Φ is geopotential, $\mathbf{v}_g$ is the geostrophic velocity, q is the QG potential vorticity and S is a nonconservative source/sink of q. For adiabatic and inviscid QG flows, q is conserved following the geostrophic flow. Dividing the dependent variables into time-mean and perturbations and multiplying by q' one can derive the following, unaveraged, potential enstrophy equation:

$$\left(\frac{\partial}{\partial t} + \bar{\mathbf{v}} \cdot \nabla\right) \frac{(q')^2}{2} + \mathbf{v}'q' \cdot \nabla \bar{q} = q'S' - q'(\mathbf{v}' \cdot \nabla q' - \overline{\mathbf{v}' \cdot \nabla q'})$$

where geostrophic velocity is now denoted by v. The term in parentheses on the right hand side represents anomalous nonlinear effects. Illari and Marshall (1983) show that for:

$$\bar{\psi} = \bar{\psi}(\bar{q})$$

One can reformulate the mean advection of eddy enstrophy as:

$$\bar{\mathbf{v}} \cdot \nabla \frac{(q')^2}{2} = -\frac{1}{2}\left[\mathbf{k} \times \nabla \left(\frac{d\bar{\psi}}{dq}(q')^2\right)\right] \cdot \nabla \bar{q} = -(\mathbf{v}'q')_R \cdot \nabla \bar{q}$$

This defines a rotational potential vorticity flux, $(\mathbf{v}'q')_R$, which *exactly balances* the mean flow advection of eddy enstrophy. Substitution into the eddy enstrophy equation leads to:

$$\frac{\partial}{\partial t}\frac{(q')^2}{2} = -(\mathbf{v}'q')_* \cdot \nabla \bar{q} + q'S' - q'(\mathbf{v}' \cdot \nabla q' - \overline{\mathbf{v}' \cdot \nabla q'})$$

where: $(\mathbf{v}'q')_* = (\mathbf{v}'q') - (\mathbf{v}'q')_R$

This localizes the equation and isolates a *residual flux* $(\mathbf{v}'q')_*$ which is a dynamically significant "conversion" flux related to eddy-mean flow interactions. *For linear and conservative waves, downgradient* $(\mathbf{v}'q')_*$ *implies local eddy growth.* The residual flux is related to the divergence of Plumb's $\mathbf{M}_T$ vector.

We have determined the eddy enstrophy budget during the PA developments.

Consistent with our earlier discussion, our primary focus is on the 400 mb level. Unlike the previous energetics approach (whose interpretation is complicated by large fluxes of energy), a localization in the vertical is possible with an eddy enstrophy budget. Fig. 5.3d (in section B of this chapter) overlays contours of time-mean ψ and q at 400 mb. A remarkable correspondence is found between the two fields, strongly suggesting that, to a very good approximation, $\psi = \psi(q)$ for the climatological mean flow near this level. Thus we will use the reformulated eddy enstrophy relation. The appropriate equation for the composite eddies (derived from equation 3.1) is:

$$\frac{\partial}{\partial t}\frac{\langle q' \rangle^2}{2} = -(\langle v' \rangle \langle q' \rangle)_* \cdot \nabla \bar{q} + \langle q' \rangle \langle S' \rangle - \langle q' \rangle(\langle v' \cdot \nabla q' \rangle - \overline{v' \cdot \nabla q'}) \qquad (5.4)$$

(a) (b) (c) (d)

where <( )> is an ensemble (i.e, composite) average. Like Plumb's $\mathbf{M}_T$ diagnoses (see section B), this analysis is sensitive to the quality of the eddy enstrophy statistics. In particular, term (b) contains the derived rotational flux, which depends upon horizontal derivatives of eddy enstrophy. In order to reduce the noise of the calculation we have constructed composites consisting of ensemble averages of PA's occuring during the winters 1963/64 to 1986/87. Unlike the previous analyses, the composites used in this section also include additional events identified in an independent dataset extending from 1978 through 1987 (see section C of Chapter III).

The static stability parameter used here is derived from climatological mean temperature fields and is an areal average over the region north of 22°N. This results in values of σ which are typical for mid-latitudes. The $d\psi/dq$ relationship was calculated from the mean values of ψ and q at 400 mb. In practice, $d\psi/dq$ is a strong function of latitude and only a weak function of longitude. Zonally averaged values of $d\psi/dq$ were used to calculate the rotational flux of q. The approximations and numerical analyses

involved in determining the rotational flux were checked by a direct comparison of $-(v'q')_R \cdot \nabla q$ with the mean flow advection of eddy enstrophy. The correspondence is remarkable, lending further support to the use of equation (5.4).

The eddy enstrophy budget is applied at 400 mb during the latter portion of PN development for the 23 PN cases listed in Appendix A. Figs. 5.10 and 5.11 display the time averaged results during the period of large-scale development (days +1/+5). Fig. 5.10a displays the average local changes in eddy enstrophy. We note increases near the PAC key region and downstream over far western Canada, where ridge development is observed. Vectors representing the total eddy q-flux, $(v'q')$, are overlayed contours of time averaged eddy enstrophy in fig. 5.10b. Note the large flux component which rotates around the local maxima in eddy enstrophy. The following figure displays the derived rotational flux, $(v'q')_R$. A comparison of 5.10b and 5.10c suggests that the rotational flux, which acts to balance mean flow advection of eddy enstrophy, comprises a large portion of the total flux field. The residual q-flux, $(v'q')_*$, is displayed in fig. 5.10d along with the time mean field of q. A downgradient residual flux is observed near the key region and over northwestern North America, implying eddy enstrophy growth via net downgradient q-fluxes. Note, in particular, that *positive local conversions are observed in the regions of eddy growth.*

The conversion is depicted quantitatively in fig. 5.11a. Although there is not a perfect spatial correlation between 5.10a and 5.11a, conversion magnitudes are large compared to regional enstrophy changes. The discrepancy between the two fields is due to terms (c) and (d) of equation (5.4). For PN development, a very good approximation to term (d) is the nonlinearity associated with the composite. Mathematically:

$$\langle q' \rangle \left(\langle \mathbf{v}' \cdot \nabla q' \rangle - \overline{\mathbf{v}' \cdot \nabla q'} \right) \approx \langle q' \rangle \langle \mathbf{v}' \rangle \cdot \nabla \langle q' \rangle$$

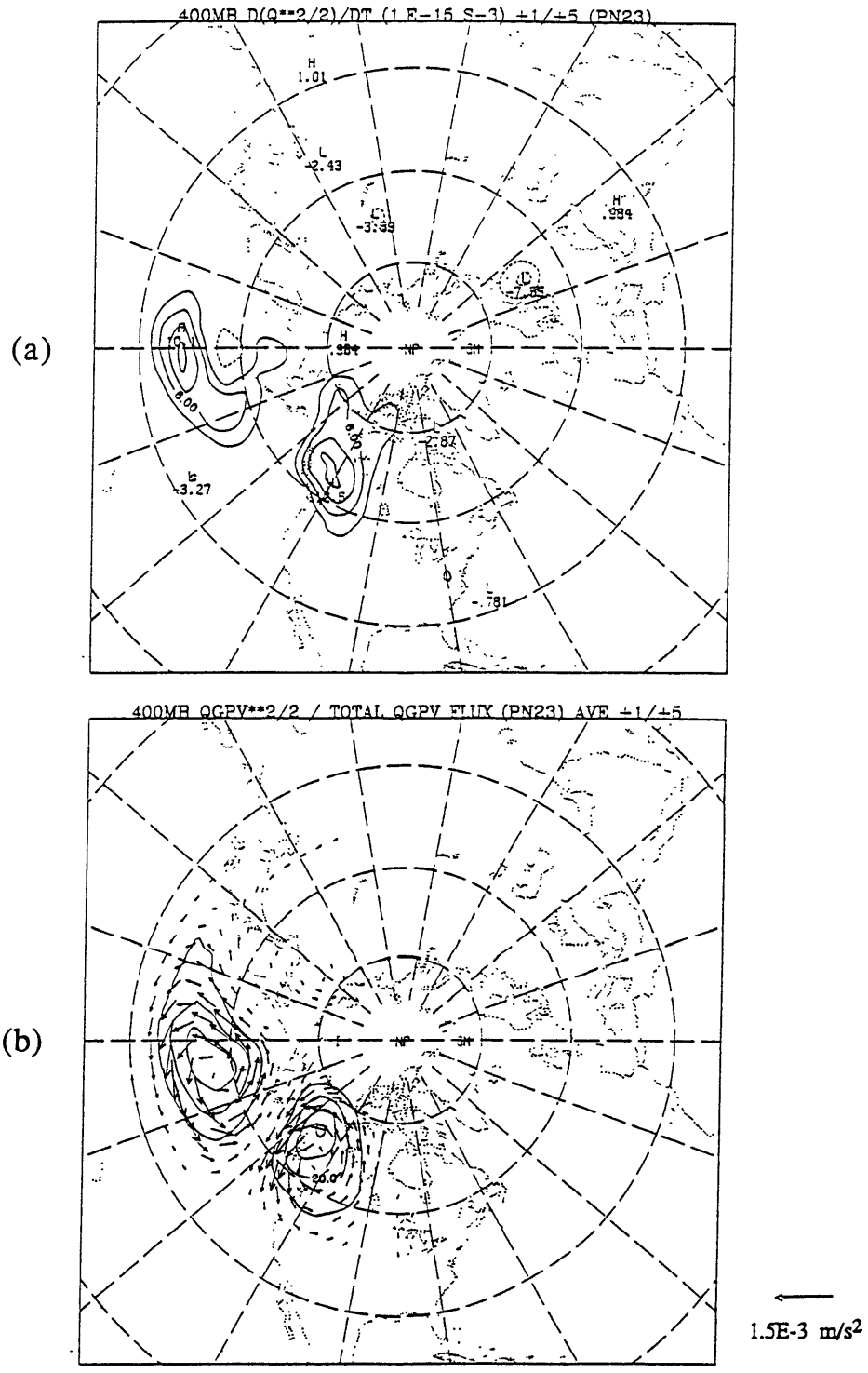

Fig. 5.10. (a) 400 mb eddy enstrophy change (contour interval: 3×10^{-15} s^{-3}) between days +1 to +5 of the 23 case PN composite development. (b) 400 mb eddy enstrophy (contour interval: 10×10^{-10} s^{-2}) and total q flux averaged over days +1 to +5 of PN development. A scale vector and corresponding magnitude are shown in lower right.

(c)

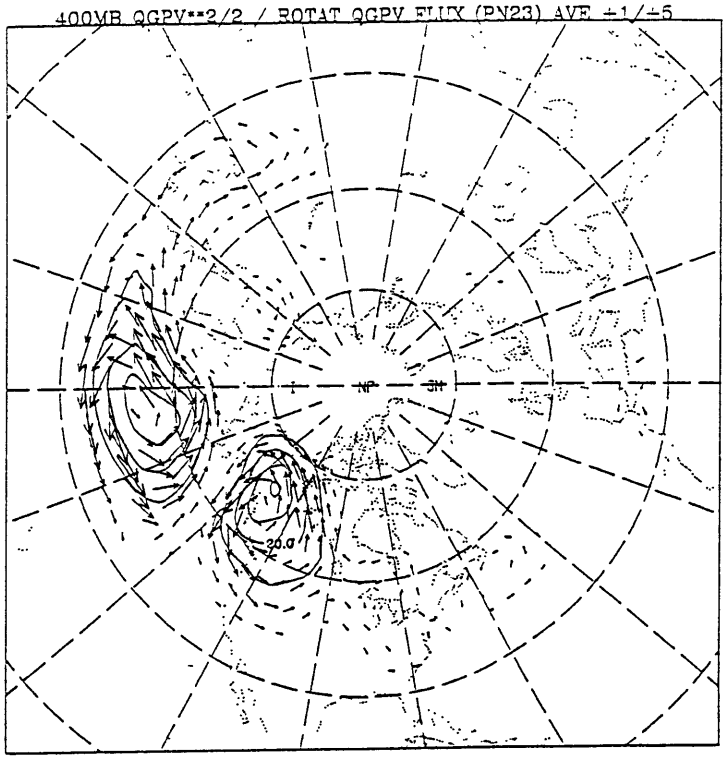

(d)

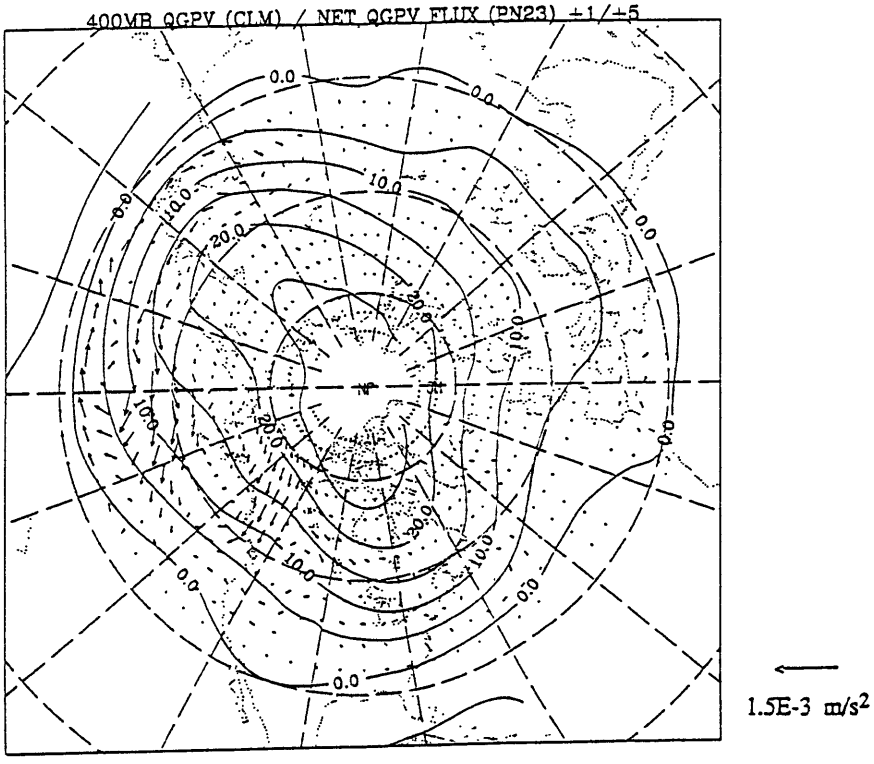

Fig. 5.10. (*cont.*) (c) Time averaged 400 mb enstrophy (contour interval: 10×10^{-10} s^{-2}) and rotational q flux for days +1 to +5 of PN development. (d) 400 mb net q flux, averaged over days +1 to +5 of PN development, and climatological-mean q (contour interval: 5×10^{-5} s^{-1}). A scale vector and magnitude are presented for q fluxes.

(a)

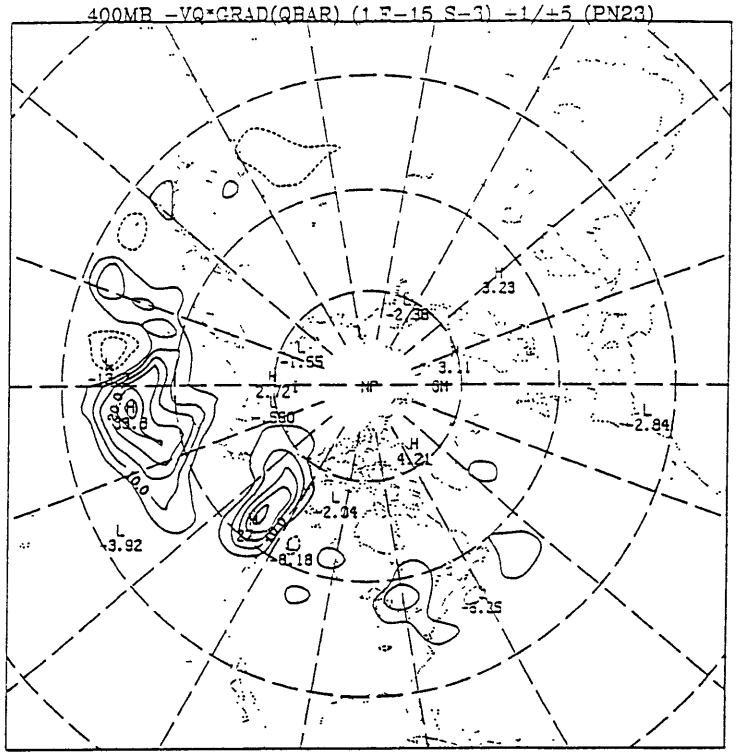

(b)

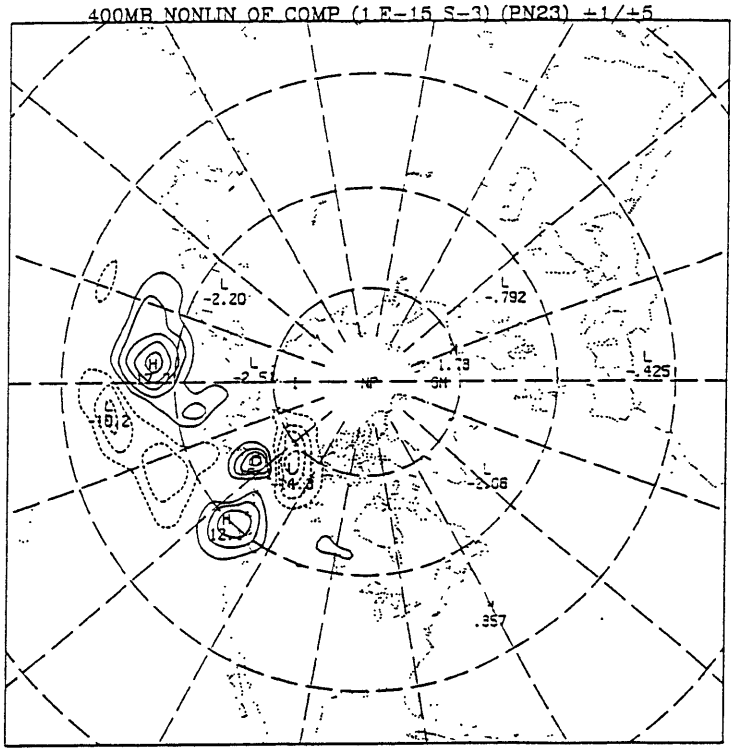

Fig. 5.11. Time averaged 400 mb (a) eddy enstrophy conversion (contour interval: 5×10^{-15} s^{-3}) and (b) composite nonlinearity (contour interval: 3×10^{-15} s^{-3}) during days +1 to +5 of PN development.

(c)

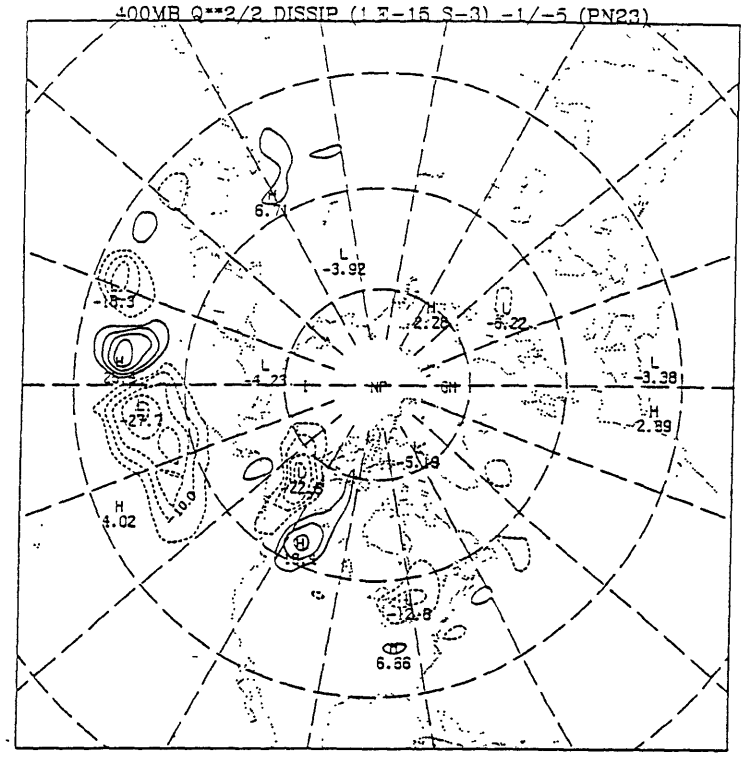

(d)

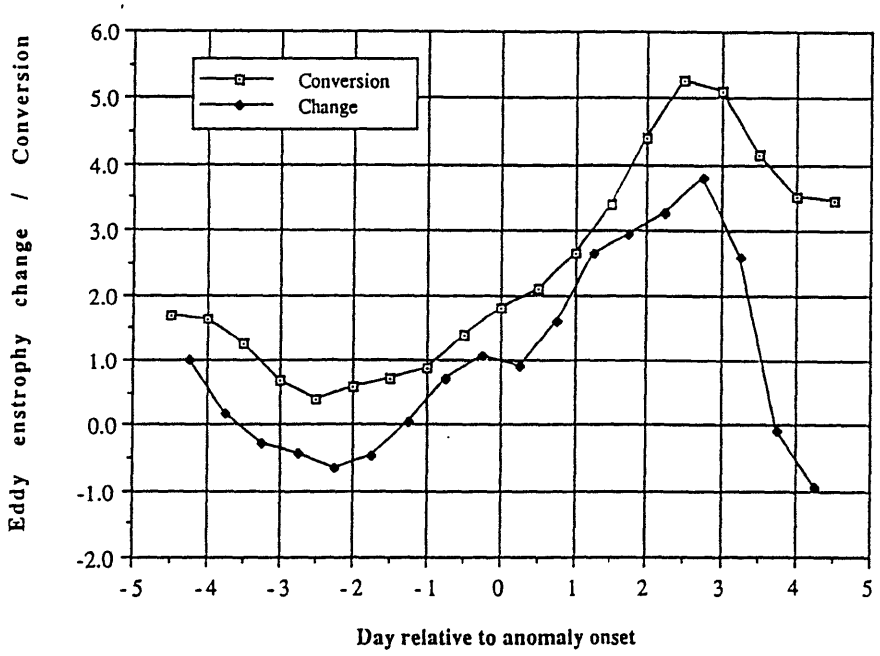

Fig. 5.11. (*cont.*) (c) 400 mb residual dissipation (contour interval: 5×10^{-15} s^{-3}) averaged over days +1 to +5 of PN development. (d) Time series of areally averaged 400 mb enstrophy conversion (open squares) and enstrophy change (solid squares) during PN evolution. Units are 10^{-15} s^{-3} and a three-point binomial filter is applied.

This implies that the nonlinearity associated with the *incoherent transients* is similar to climatological values during PN development. The *anomalous* nonlinearity is thus primarily associated with the composite (or coherent) eddies. This term is shown in fig. 5.11b and consists of local maxima and minima of comparable magnitude. The areally averaged effects of this term are small compared to the enstrophy change and eddy conversion terms. In essence, term (d) acts to *redistribute* eddy enstrophy horizontally over the domain.

Combining terms (a), (b) and (d), one can determine term (c) as a residual. Term (c) is shown in fig. 5.11c for PN. Note that this nonconservative source/sink term acts mainly to *dissipate* eddy enstrophy over the domain. This is most likely due to diabatic and frictional processes. Strong Ekman damping is likely to occur over the North Pacific during the later stages of PN development as a strong anomalous circulation develops in the boundary layer. The cyclonic nature of the low level circulation suggests that Ekman damping would lead to upward motion and possible diabatic heating below the upper-level q anomalies found near the key region. Diabatic heating would then result in a nonconservative downward transport of potential vorticity towards the boundary layer where it can be effectively dissipated. Near the local maxima in mean eddy enstrophy (e.g. see fig. 5.10b or 5.10c) there are dipole-like features in the dissipation pattern. We speculate that these may be due to non QG effects such as vertical advection of static stability near the tropopause. The main conclusion, however, is that *the net effect of the incoherent transients and nonconservative processes is to oppose eddy growth.*

A time series of areal averaged conversion and enstrophy change is shown in Fig 5.11d for PN development. Note that throughout the evolution the conversions are sufficient to account for eddy enstrophy changes. Table 1 summarizes the various terms in equation (5.4) averaged over days +1 to +5 of PN evolution. The averaging region is between 34°N and 78°N and 140°E to 100°W. The term d' refers to the approximated value of d.

Table 1:	PN (+1/+5)				
Term from eqn (5.4):	a	b	c	d'	
Areal Average:	1.8	4.1	-2.2	-0.1	(1.E-15 S-3)

As suggested previously by the energetics analyses, eddy-mean flow conversions appear to be sufficient to account for eddy growth. Nonconservative processes tend to oppose eddy growth. The nonlinear term redistributes eddy enstrophy horizontally but contributes little towards the areal averaged potential enstrophy budget.

The time evolution of the residual flux pattern is shown in fig. 5.12. A weak signature appears over the western North Pacific at day -3. By day +1, downgradient fluxes are found to the east of the Date Line. This is in the region where an upgradient E-vectors pattern develops (fig. 4.8c,d). Downgradient residual q-fluxes become prominent near the key region and over northwest North America at day +3. Recalling fig. 4.9d, a large-scale heat flux pattern is observed at this time, with strong downgradient heat fluxes found near and to the east of the key region.

An important question to address is the quality of the results. As mentioned earlier, these analyses may be subject to considerable noise. One of the most sensitive quantities to analyze is the conversion (term (b) of equation 5.4) which involves the derived rotational flux. In order to assess the "noise" of the calculation, the residual flux and conversion were calculated using a composite derived from a subset of 14 of the 23 PN cases. The analyses are displayed in fig. 5.13 and should be compared to figs. 5.10d and 5.11a.

The results obtained using the subset of cases appear less smooth, as one might expect. In particular, we note many small-scale features outside the region of interest in the conversion pattern of fig. 5.13b. The additional 9 cases lead to a pattern (fig. 5.11a) in which these small scale features are considerably reduced (e.g. upstream near southeast Asia). The signatures found near the key region and downstream over western Canada, however, remain strong. Indeed, the areal averaged conversion changes by less than 0.2E-15. The basic results therefore appear to be quite robust.

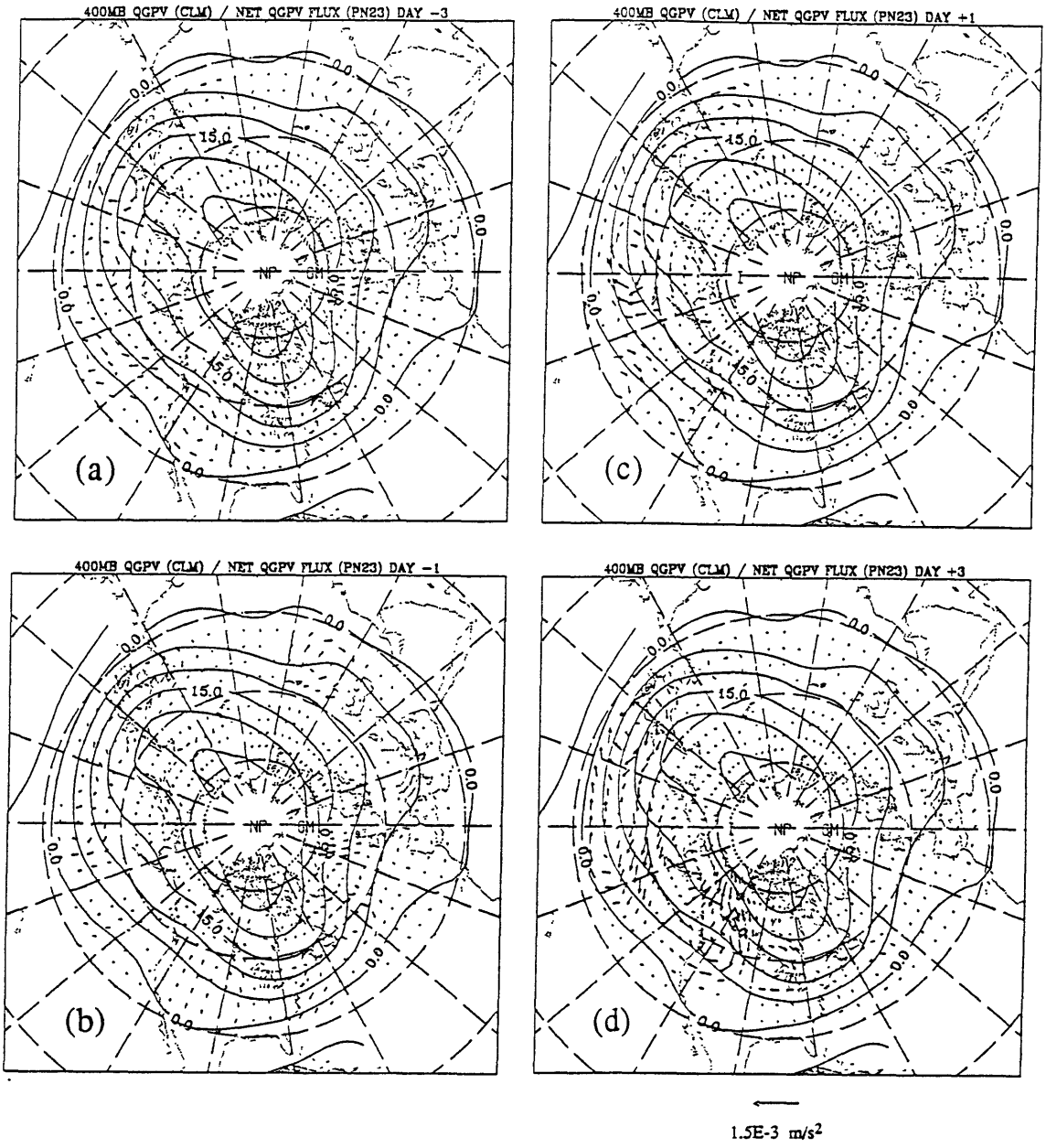

Fig. 5.12. Net q flux superimposed upon contours of wintertime-mean q (contour interval: 5×10^{-5} s^{-1}) for days (a) -3, (b) -1, (c) +1 and (d) +3 of PN time evolution. Zonal wavenumbers greater than 12 were removed before analysis. A scale vector and magnitude are displayed below (d).

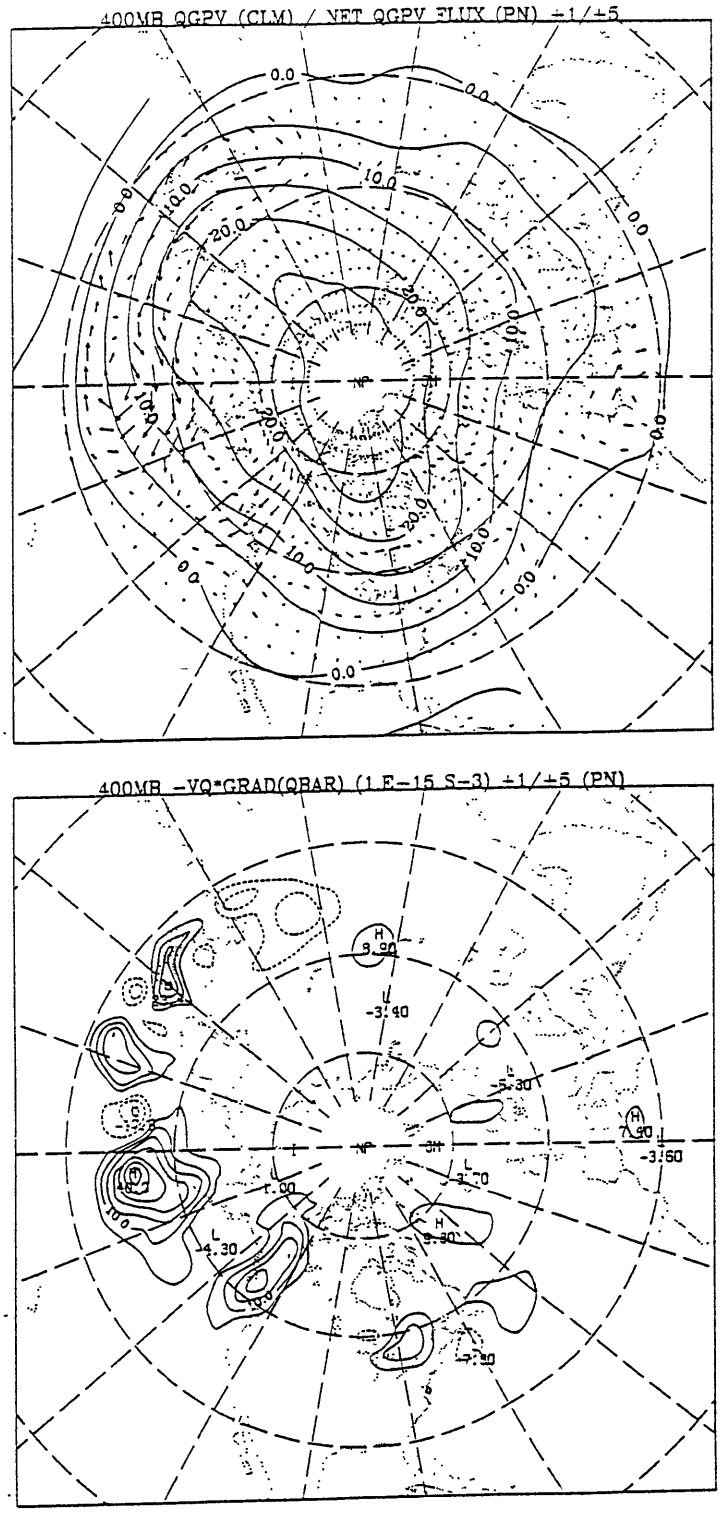

Fig. 5.13. (a) As in Fig. 5.10d and (b) as in Fig. 5.11a using composite fields derived from the *first fourteen* PN cases.

The enstrophy analyses provide us with a picture of large-scale development which is quite similar to the energetics picture. A detailed comparison, however, does show differences. Some of the differences may be attributable to differences in composites. Also, the enstrophy budget is applied at one pressure level whereas, in the energetics analyses, vertical integrations are performed. Overall, though, the correspondence between the two analyses is quite good. The eddy enstrophy analysis has certain distinct advantages, however, such as its fundamental link to atmospheric dynamics and its local applicability. Nonconservative processes are also more clearly depicted within this framework.

Selected analyses averaged over days 0 to +5 of PP development are shown fig. 5.14. The PP composite consists of 21 cases, listed in Appendix A. Eddy enstrophy changes are found to occur in roughly the same regions as PN. The pattern of residual q-fluxes (fig. 5.14b) bears a striking resemblance to that of PN. Strong conversions are found near the key region with weaker conversions downstream over North America. A comparison of figs. 5.14a and 5.14c suggests that strong dissipation must occur near the key region. Time series of areal averaged conversions and eddy enstrophy changes are shown in fig. 5.14d. A strong correlation is found between the two time series. As for the PN cases, it appears that *during PP development eddy-mean flow conversions are more than sufficient to account for development.*

Fig. 5.15 displays the time series of the residual q-flux patterns. The early evolution is characterized by an eastward propagating transient pattern. Downgradient fluxes are found near the date line at day -1. After day 0, large downgradient fluxes develop south of the key region. Weaker downgradient fluxes are found over western Canada at day +3. We summarize the large-scale growth for the PP development in Table 2, where the averaging area is the same as for PN.

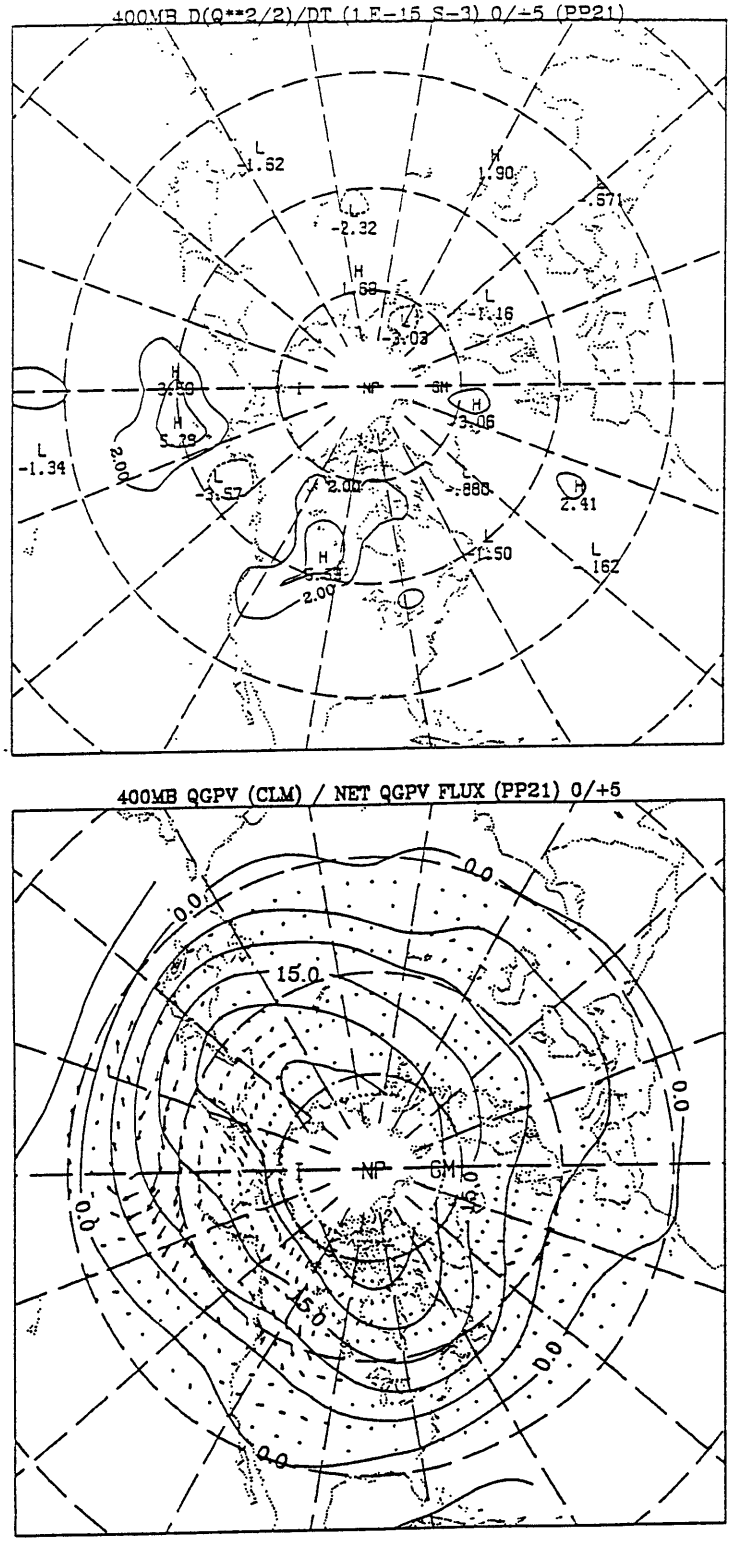

Fig. 5.14. (a) 400 mb eddy enstrophy change (contour interval: 2×10^{-15} s^{-3}) and (b) net q flux, averaged over days 0 to +5 of the 21 case PP composite development. The climatological-mean q field (contour interval: 5×10^{-5} s^{-1}) is also shown in (b). A scale vector and corresponding magnitude are shown in lower right.

(c)

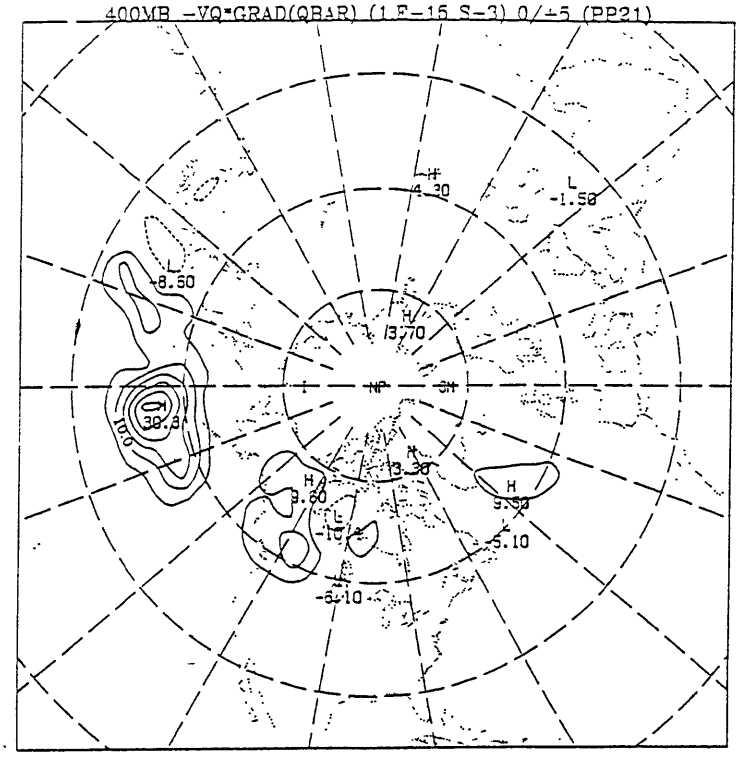

(d)

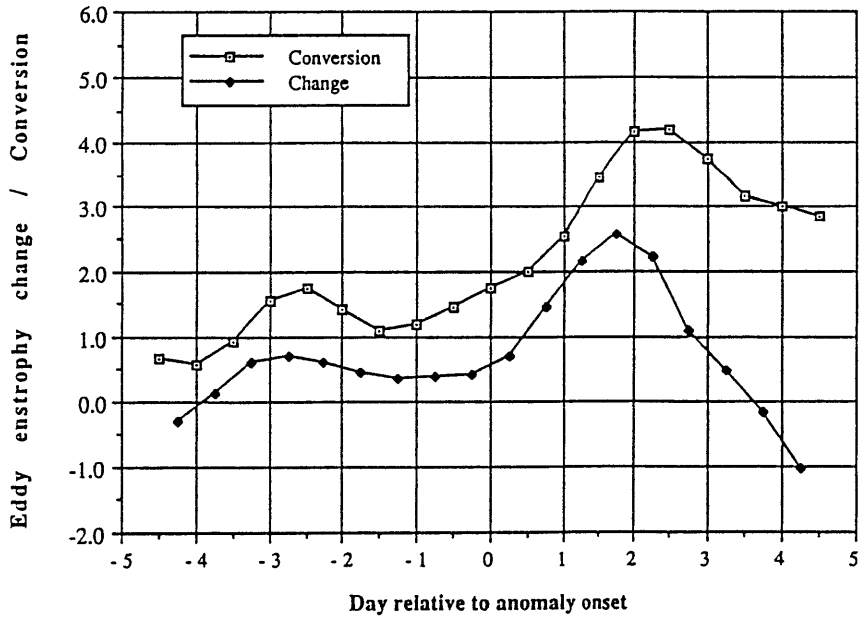

Fig. 5.14. (*cont.*) (c) 400 mb eddy enstrophy conversion (contour interval: 5×10^{-15} s^{-3}) averaged over days 0 to +5 of PP evolution. (d) Time series of areally averaged 400 mb enstrophy conversion (open squares) and eddy enstrophy change (solid squares) during PP evolution. Units are 10^{-15} s^{-3} and a three-point binomial filter is applied.

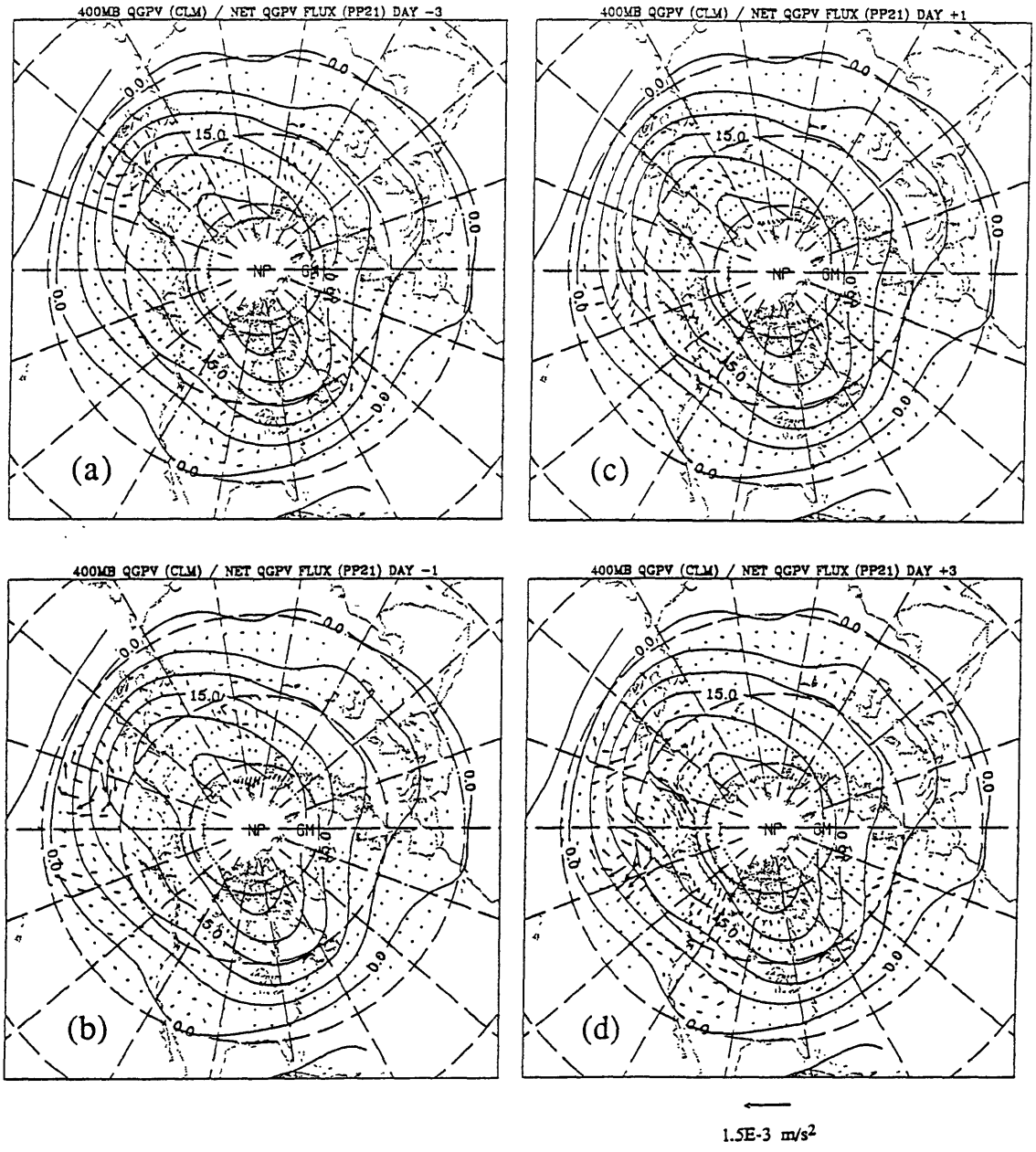

Fig. 5.15. As in Fig. 5.12 for the 21 case PP composite development.

Table 2: PP (0/+5)

Term from eqn (5.4):	a	b	c	d'	
Areal Average:	0.8	3.1	-2.4	0.1	(1.E-15 S-3)

For PP and the following cases we continue to approximate term d of equation (5.4) by the nonlinearity associated with the composite, d'. Thus term c, calculated as a residual, will include the anomalous nonlinearity associated with incoherent eddies. The effects of the incoherent transients (which involves many temporal and spatial scales) have been crudely estimated for PP. Unlike PN, incoherent transients are strongly dissipative during PP development and contribute significantly towards c. This is consistent with the results of Neilley (1990) who found that there is net dissipation of the slowly varying flow by synoptic-scale eddies in the upper troposphere during PP development.

The results for AN development are displayed in fig. 5.16. The AN composite is constructed from 20 cases. Local increases in eddy enstrophy are found near the ATL key region (south of Iceland) and upstream over western Canada, where trough development occurs. Downgradient residual q-fluxes are found east of Newfoundland and further downstream near the key region. This leads to the double maxima observed in the conversion pattern of fig. 5.16c. Note the negative conversions found south of Newfoundland. Areal averaged conversions are sufficient to account for eddy growth when *time averaged over days 0 to +5*. This is illustrated in Table 3, which displays averages over the latitudes 34°N and 78°N and the longitudes 80°W and 20°E:

Table 3: AN (0/+5)

Term from eqn (5.4):	a	b	c	d'	
Areal Average:	1.1	1.8	-0.7	0.0	(1.E-15 S-3)

The time series in fig. 5.16d demonstrate, however, that during the early stages of large-scale development (~ days 1-2) the conversions are barely sufficient to account for

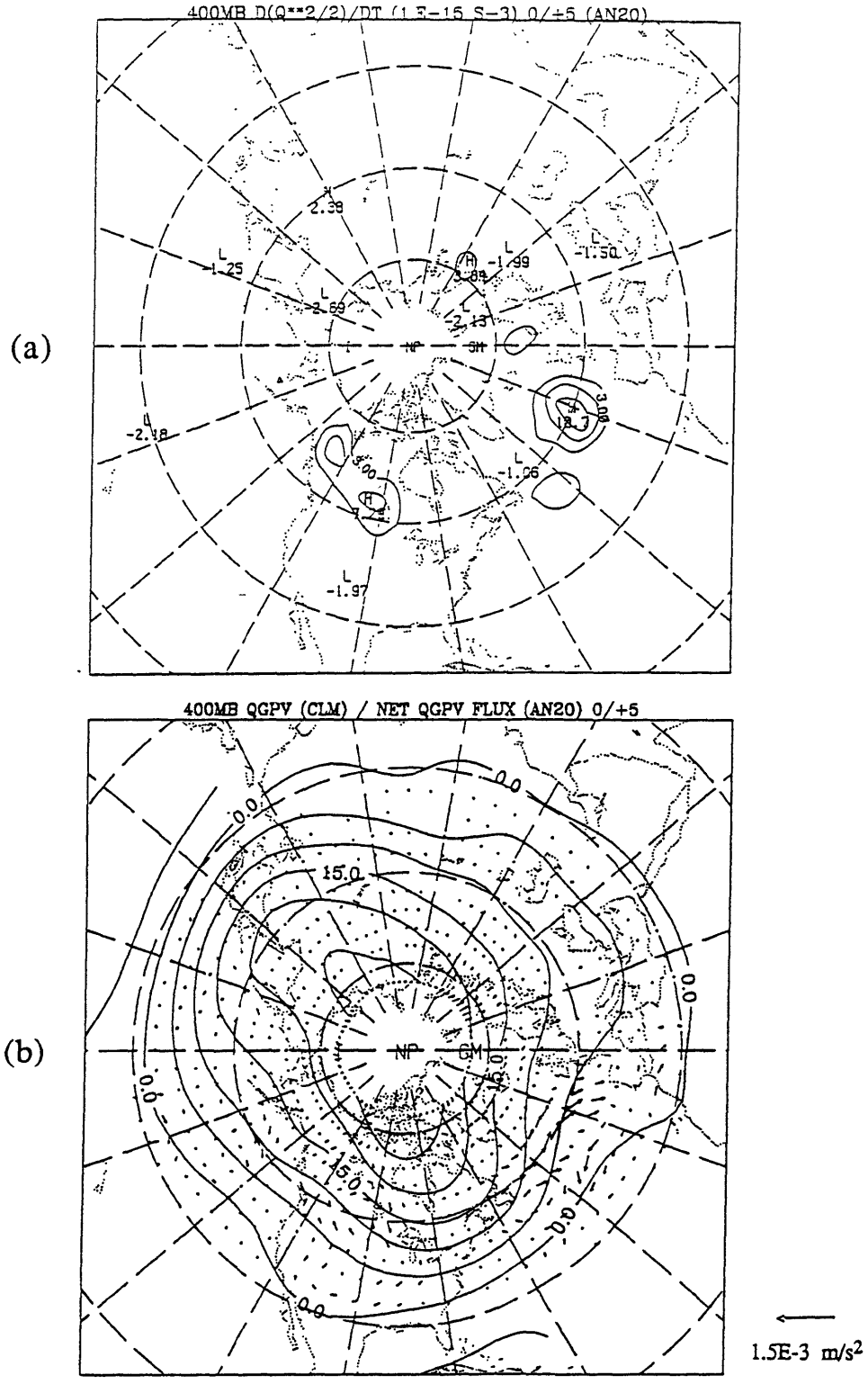

Fig. 5.16. As in Fig. 5.14 for the 20 case AN composite development. Contour interval in (a) is 3×10^{-15} s^{-3}. Averaging area for (d) is outlined in text.

(c)

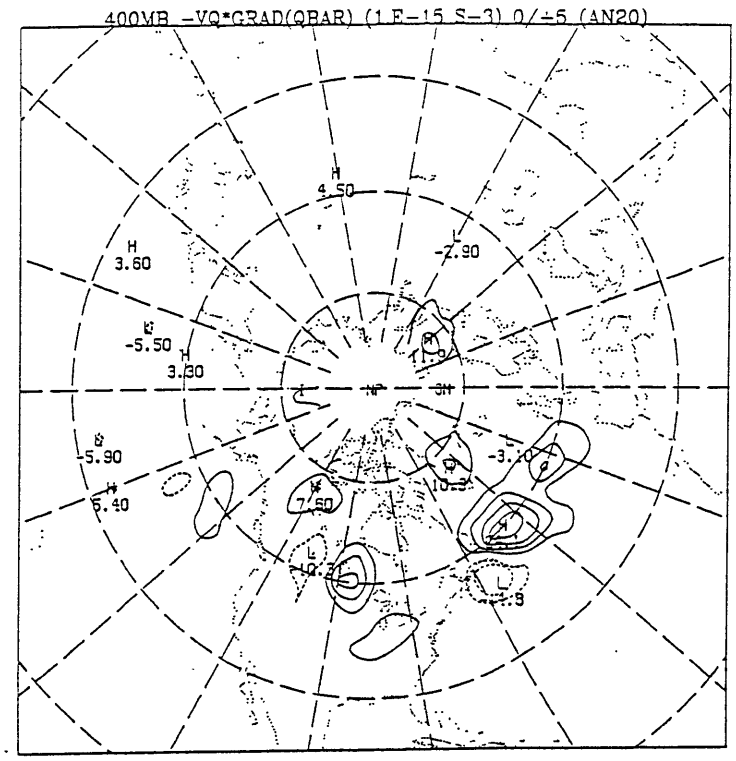

400 mb eddy enstrophy evolution (AN)

(d)

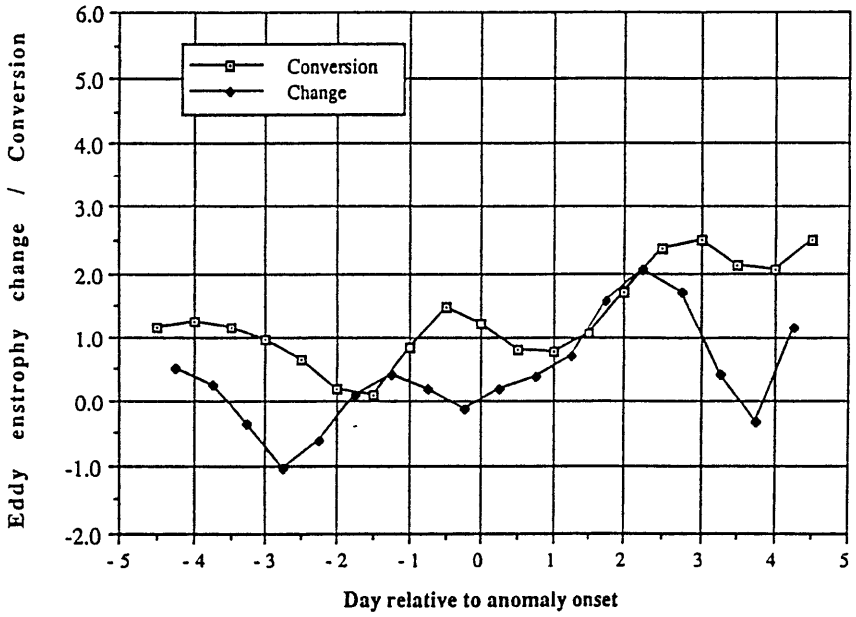

Fig. 5.16. (*Continued*)

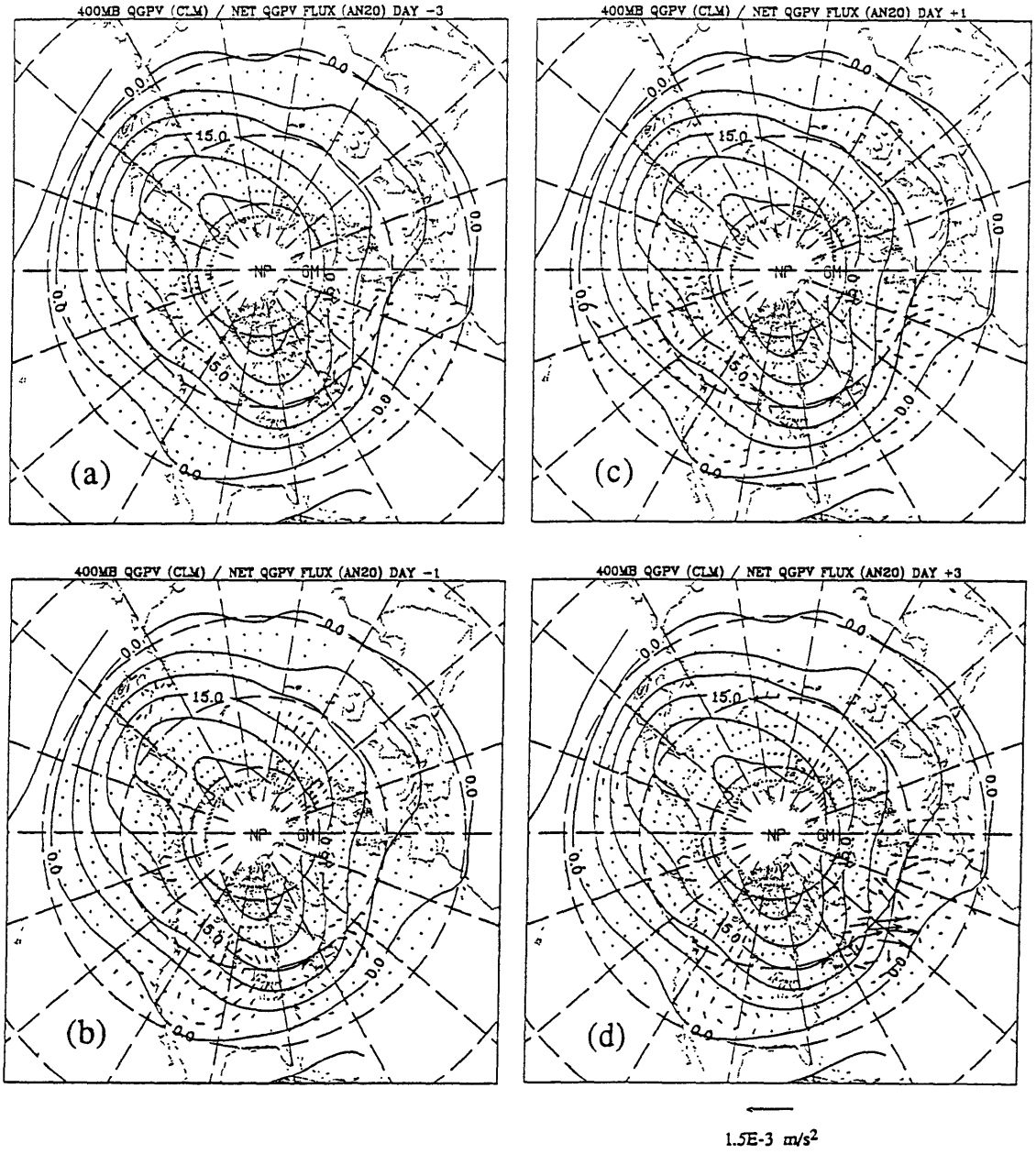

Fig. 5.17. As in Fig. 5.12 for the 20 case AN composite development.

growth. For nonzero dissipation, the suggestion is that there must be some additional source during this time. After day +3, however, conversions exceed the observed changes. Overall, however, the two time series are more weakly correlated than during PAC developments.

The time evolution of the residual flux patterns is shown in fig. 5.17 for AN. At day -3, a rotational signature is observed near Newfoundland in association with a mature synoptic-scale cyclone (e.g. see fig. 4.20b). Weak downgradient fluxes are observed south of Greenland at day -1. This corresponds well to the upgradient E-vector signature found in fig. 4.22b. After onset (day +1) a small rotational signature is found south of the key region over the North Atlantic. Two days later, however, strong downgradient residual fluxes are found southwest and east of the key region. This is consistent with the day +3 E-vector and heat flux analyses of figs. 4.22d and 4.23d.

The AP composite evolution consists of an ensemble of 18 cases. AP eddy enstrophy analyses are shown in figs. 5.18 and 5.19. The 400 mb AP eddy enstrophy evolution (fig. 5.18d) suggests that, unlike the other three developments, the period of maximum enstrophy change occurs *during* onset. Thus, we choose to study days -2 to +2 of AP development for the time averaged analyses of fig. 5.18.

A broad region of eddy enstrophy increases is observed over the North Atlantic. Although weak in amplitude, a consistent downgradient residual q-flux is observed west of the key region during this time. A comparison of the conversions (fig. 5.18c) to the changes (fig. 5.18a) shows a fairly good correspondence. The areal averaged conversions exceed the enstrophy changes during the onset period. This is summarized in Table 4:

Table 4: AP (-2/+2)

Term from eqn (5.4):	a	b	c	d'	
Areal Average:	0.8	1.5	-0.8	0.1	(1.E-15 S-3)

Once again, the results suggests that large-scale eddy-mean flow interaction contributes

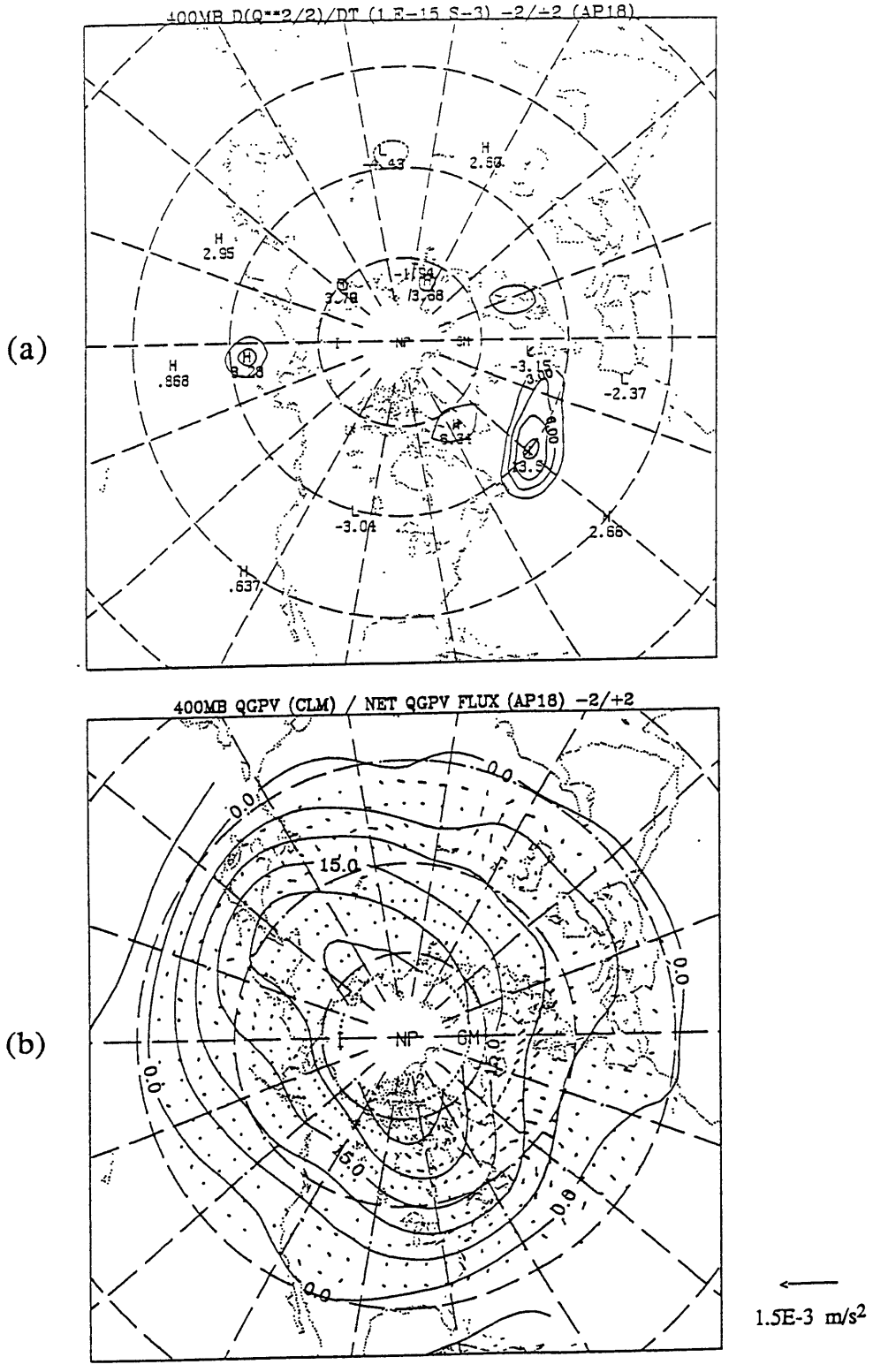

Fig. 5.18. (a), (b) and (c) are as in Fig. 5.14 for days -2 to +2 of the 18 case AP composite development. (d) As in Fig. 5.14 for AP. Averaging area outlined in text.

(c)

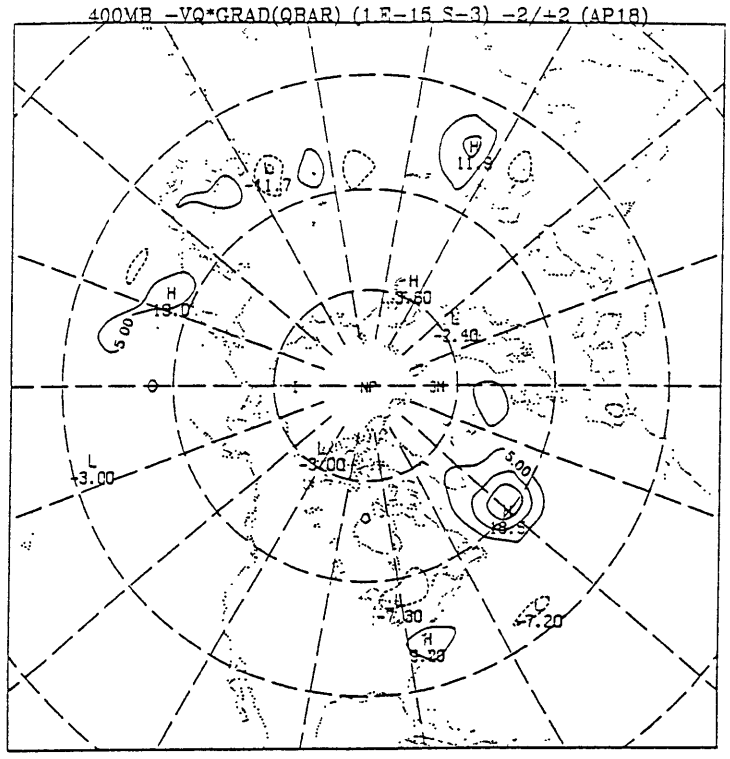

400 mb eddy enstrophy evolution (AP)

(d)

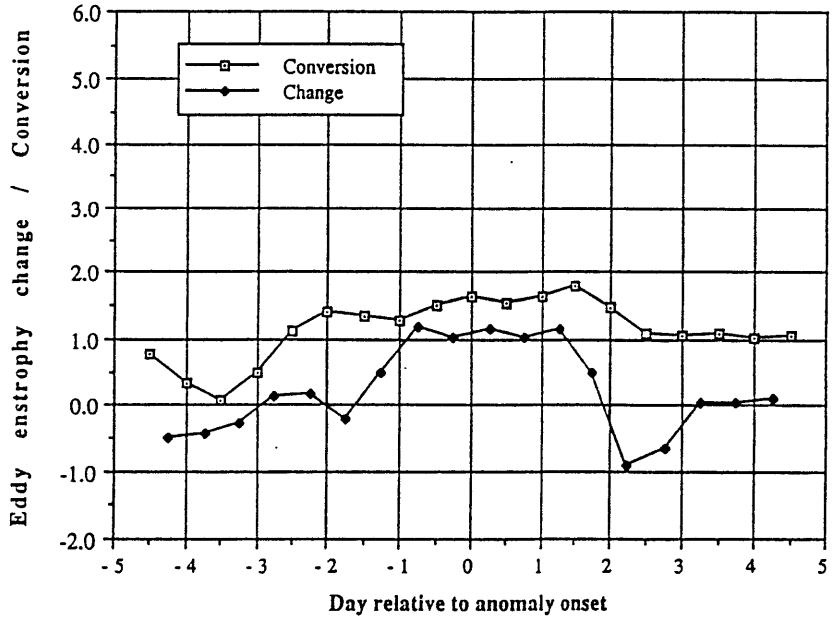

Fig. 5.18. (*Continued*)

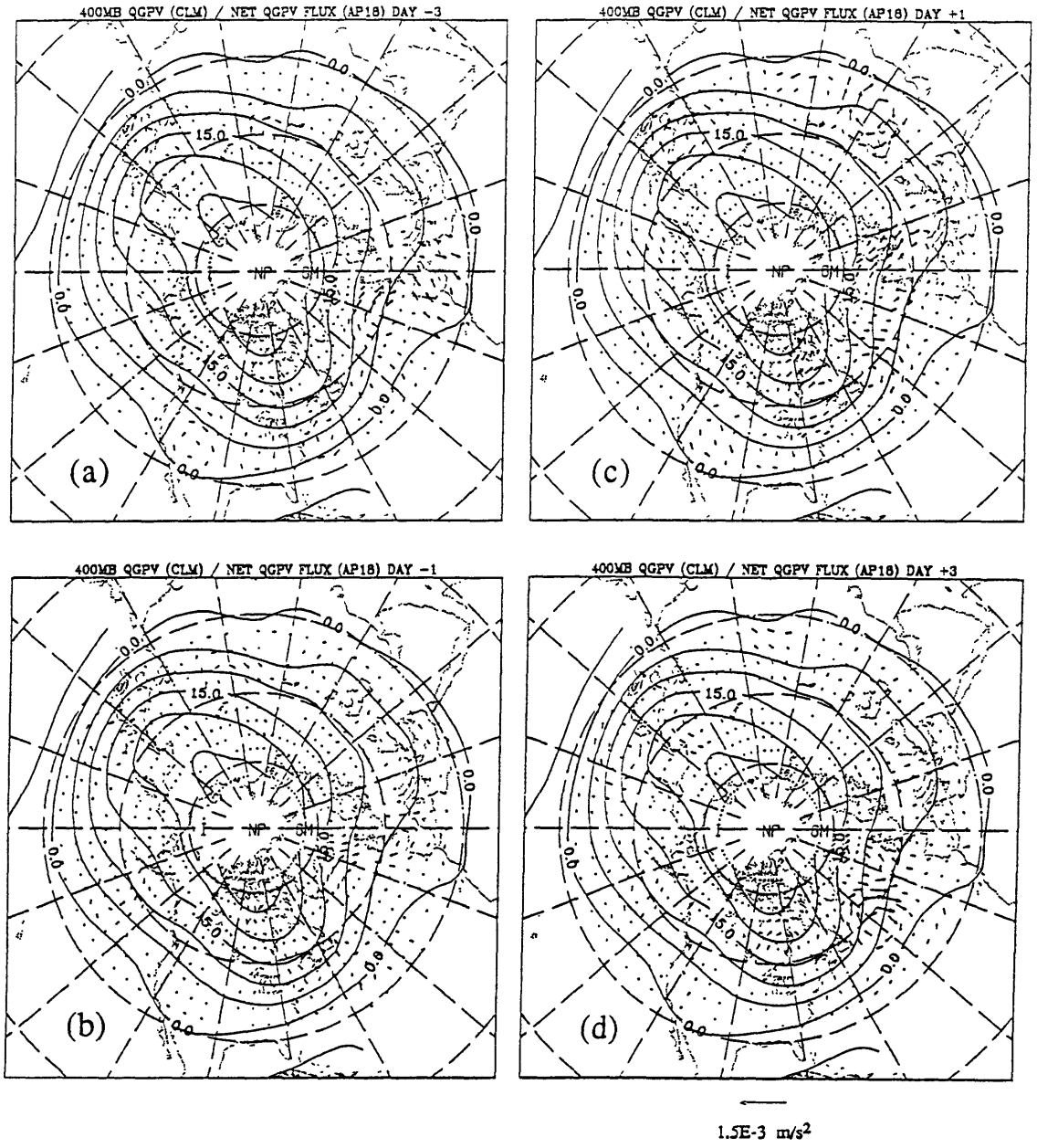

Fig. 5.19. As in Fig. 5.12 for the 18 case AP composite development.

significantly towards PA development. Figure 5.19 shows little structure until day +1, when downgradient q-fluxes are found to the southeast of Greenland. A stronger flux pattern is observed two days later. The day +3 pattern contains a large rotational flux component, however, including both downgradient and upgradient components. During both AN and AP developments, the incoherent eddies are likely to contribute partially towards term (c).

In summary, large-scale eddy-mean flow interaction appears likely to play a dominant role in PA development. For the PAC developments there is very good spatial and temporal correspondence between conversions and changes in potential enstrophy. The conversions are more than sufficient to account for the enstrophy changes. The residual dissipation (including the nonlinear effects of the incoherent eddies) locally opposes development. The eddy enstrophy results are qualitatively consistent with the energetics analyses of the previous section, and suggest remarkable similarity between the dynamics of PN and PP development.

There is less correspondence between enstrophy conversions and changes during AN development. During the early stages of large-scale development, conversions are not sufficient to cover both enstrophy changes and additional dissipative effects. Coherent eddy-mean flow interaction is likely to play a major role during the later stages of development, however, as strong downgradient residual q-fluxes develop. During AP development, most of the potential enstrophy changes occur around day 0. Enstrophy conversions exceed changes during this time, with good spatial correspondance between the two fields. The *ratio* of enstrophy conversion to change, however, is weaker during ATL developments than for PAC developments. This is demonstrated in Table 5, the first line of which show the ratio of areal averaged conversions to enstrophy changes:

Table 5: Development summary

PA type:	PN	PP	AN	AP	
Conversion ratio:	2.3	3.7	1.7	1.8	(unitless)
Dissip. time scale:	5	3	7	7	(days)

The table suggests that coherent eddy-mean flow interaction plays a stronger role in the PAC than in the ATL developments. This is consistent with Neilley (1990) who found that forcing by synoptic-scale incoherent eddies is likely to be more significant during the ATL developments than during the PAC developments. The second line of Table 5 displays estimated dissipation time scales for PA development. This is the ratio of the average eddy enstrophy to term (c), the residual dissipation. Dissipation time scales are ~5-6 days, with relatively stronger dissipation for the PAC developments. These time scales are somewhat smaller than the 10 day scale estimated by Holopainen and Fortelius (1987b) in their study of transient eddy activity of Feb 1979.

E. Quasigeostrophic potential vorticity analyses

As mentioned in the previous section, a fundamental way of studying atmospheric dynamics is with potential vorticity (PV) analyses. For adiabatic and inviscid flows, PV is conserved following the motion. Also, given suitable boundary and balance conditions, one can invert the PV distribution and deduce the associated flow field. Conservation and invertibility allow for a complete description of atmospheric dynamics based on the three-dimensional distribution of PV. Hoskins et al. (1985) demonstrate how PV principles can be used to concisely and simply conceptualize Rossby wave propagation and shear instability in the atmosphere.

For quasigeostrophic (QG) flows pseudopotential vorticity (q) is conserved following the geostrophic flow (in the absence of diabatic and frictional processes). Hoskins et al. outline the conservation and balance relations for QG flows. Choosing a reference field $q_{ref} = f$ where f is the Coriolis parameter, the balance condition for deviations from this reference field is:

$$q - q_{ref} = \frac{1}{f_o} \nabla^2 \Phi' + f_o \frac{\partial}{\partial p} \left(\frac{1}{\sigma} \frac{\partial \Phi'}{\partial p} \right) \qquad (5.5)$$

where: $$\mathbf{v}_g = \frac{\mathbf{k} \times \nabla \Phi'}{f_o}$$

Φ' is a deviation from a reference geopotential, $\Phi_{ref}(p)$, which is a function of pressure only. Also, f_o is a standard value of the coriolis parameter, $\mathbf{v}_g$ is the geostrophic velocity and σ is the static stability parameter. This relationship between q' and Φ' is linear and allows one to examine the circulations associated with individual components of the q' distribution seperately. Hoskins et al. demonstrate that the potential temperature (θ) field on the lowest pressure surface can be treated as a delta-function contribution to the interior q distribution. Surface θ anomalies can than be thought of as potential vorticity perturbations which propagate along a background potential temperature gradient. For the Earth's atmosphere, positive surface θ anomalies are associated with anomalous cyclonic circulations and negative anomalies with anomalous anticyclonic circulations.

This framework provides a method of looking at the flow associated with various components of the potential vorticity field, including the possibly important contributions due to surface θ anomalies. In particular, one can use this methodology to investigate the relationship between upper-tropospheric potential vorticity anomalies and surface θ anomalies. A QG analysis is applied to PA evolution. We treat the time-mean flow as a balanced basic state and examine how the composite flow is influenced by upper and lower tropospheric anomalies in q.

The analysis routine, provided by Chris Davis at MIT, inverts equation (5.5) for a given distribution of q'. The routine inputs geopotential heights, calculates q' at each level and then uses a relaxation technique to invert a subset of the q' distribution and find its

associated Φ' field. A lower boundary is defined midway between the two lowest pressure levels. The thickness between these two levels is used to determine a "surface" θ distribution appropriate for the intermediate pressure level. Thus, lower tropospheric thickness anomalies are treated as surface θ anomalies. In our case, the two lowest pressure levels are 1000 and 850 mb. The lower boundary condition (925 mb) becomes $\partial\Phi'/\partial p = 0$. An analogous procedure is followed at the upper boundary, located between 100 and 150 mb. The perturbations are required to vanish at the lateral boundaries.

In practice, the most important q anomalies are found near the lower boundary and the tropopause. These are regions of substantial horizontal gradients of time-mean q or surface θ. Also, values of q' tend to decay away from the tropopause. Thus, there is a logical partitioning between upper and lower tropospheric waves. Here we examine how upper-tropospheric q anomalies influence the lower-tropospheric flow and vice-versa. During composite PA development, anomalies in q at 500, 400, 300 and 250 mb significantly influence the surface circulation. Together these form the "upper-PV" distribution. Also, q anomalies at the surface and 850 mb are grouped to represent the effective "lower-PV" distribution, which is primarily due to surface θ. In general, 700 mb q anomalies are weak and have little influence upon the tropospheric circulations during the evolutions.

Figure 5.20 displays the surface geostrophic winds due to upper q anomalies and the 850 mb temperature field during PN development. The 850 mb temperatures are closely related to lower tropospheric thickness and are used as a proxy for the "surface θ" distribution. Fig. 5.21 superimposes the 400 mb geostrophic flow associated with lower q anomalies over the 400 mb composite q field. A comparison of these two figures allows one to examine how upper and lower level q anomalies influence one another.

At day -3, we observe a signature consistent with cyclogenesis over the western North Pacific. The upper level q anomalies (upper q') has an associated southeasterly flow

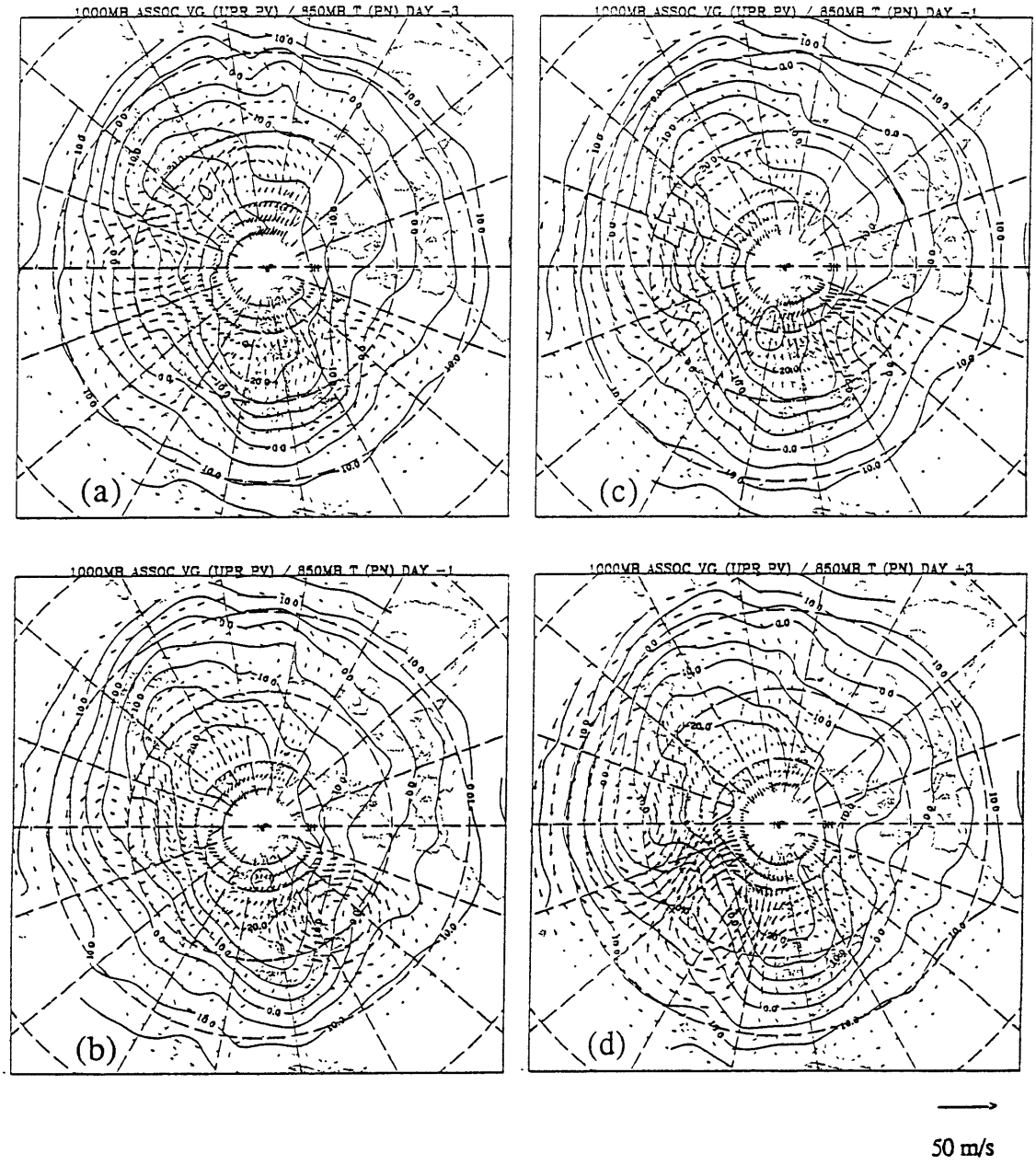

Fig. 5.20. Composite 1000 mb geostrophic winds (associated with upper-tropospheric pseudopotential vorticity anomalies - see text for details) and the 850 mb temperature field (contour interval: 5°C) for days (a) -3, (b) -1, (c) +1 and (d) +3 of the 14 case PN composite development. A scale vector and magnitude are provided for the winds.

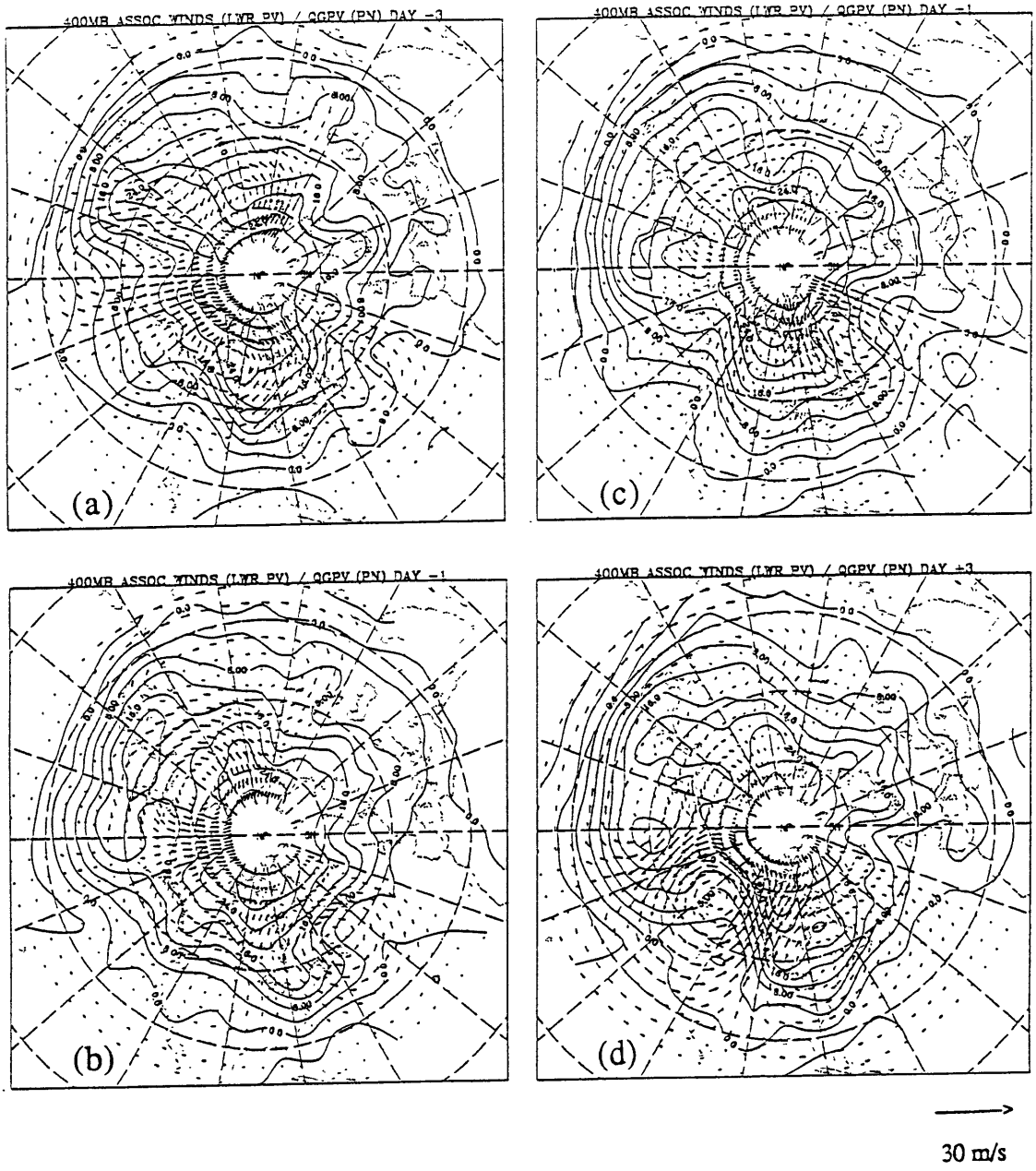

Fig. 5.21. Composite 400 mb geostrophic winds (associated with lower-tropospheric pseudopotential vorticity anomalies - see text for details) and 400 mb pseudopotential vorticity (contour interval: 4×10^{-5} s^{-1}) for days (a) -3, (b) -1, (c) +1 and (d) +3 of the 14 case PN composite development. A scale vector is provided for the winds.

near the developing surface low (fig. 5.20a). The resulting warm advection would tend to enhance the surface warm anomaly (e.g. fig. 4.3b) and its associated cyclonic circulation. At 400 mb (fig. 5.21a), the lower level q anomalies (lower q') result in anomalous northwesterly flow which acts to deepen the upper level trough (which appears as a ridge in the q field). Thus, there appears to be a mutual intensification between the upper and lower waves at this time.

Two days later, the overall pattern weakens considerably over the North Pacific. A weak cyclonic circulation is found near the surface (fig. 5.20b), in association with the upper q'. This intensifies during onset as the upper level disturbance grows. Note the developing warm advection over the eastern North Pacific after day 0 (fig. 5.20c). This is associated with thermal ridge development at 850 mb to the east of the key region (fig. 5.20d). By day +3, the surface warm anomaly is quite pronounced (e.g. fig. 4.3e) and has an associated cyclonic circulation which penetrates to the 400 mb level (fig. 5.21d). We note associated northerly flow (and positive q advection) in the eastern portion of the upper-level trough and southerly flow (and negative q advection) in the downstream ridge. This tends to enhance upper-level q' magnitudes in this region, which are qualitatively indicated by the 300 mb composite height anomaly pattern in fig. 4.1. Thus, at day +3, the flow associated with upper q' is tending to enhance the surface ridge while the flow associated with lower q' is tending to strengthen the upper wave. This suggests that a mutual intensification is occuring, but on a much larger scale than associated with typical synoptic-scale cyclogenesis.

Note that the influence of the upper wave *precedes* that of the lower wave. The surface circulation associated with the upper wave leads to the surface warm anomaly, which subsequently interacts with the upper wave. The sequence relates well to the relative time evolution of the baroclinic and barotropic conversions during PN development. After upper-tropospheric barotropic development begins (e.g. fig. 4.8c), an associated cyclonic circulation penetrates to the surface. Thereafter, a surface warm anomaly develops

downshear of the upper level trough and large-scale baroclinic intensification occurs (e.g. fig. 4.9d). Apparently, the upper wave experiences a baroclinic "self-development" after initial barotropic development.

Figs. 5.22 and 5.23 display the analogous analyses for the PP cases. Initially, only weak associated flows are observed (figs. 5.22a, 5.23a). At day -1, however, we observe an anticyclonic circulation (due to lower PV) near the key region at 400 mb (fig. 5.23b). The associated southerly flow found near the date line tends to build the ridge over the central North Pacific. Only a weak surface signature is observed at day -1 (fig. 5.22b). By day +1, the 400 mb circulation has shifted eastward and strong southeasterly flow is found near the key region (fig. 5.23c), which continues to help intensify the upper level ridge. At this time, an anticyclonic circulation (due to upper PV) penetrates to the surface of the North Pacific (fig. 5.22c). This results in northwesterly flow and cold advection to the east of the key region, intensifying surface cold anomalies (not shown) located over northwestern North America, which are largely responsible for the upper level anticyclonic circulation. Thus, the upper level flow associated with lower q' tends to build the upper ridge while the surface circulation associated with upper q' tends to deepen the surface anomaly pattern. As for the PN cases, a large-scale mutual intensification appears to occur during the latter stages of development. Unlike PN, however, the influence of the lower wave precedes that of the upper wave.

Similar analyses for the Atlantic cases (not shown) show a less organized behavior. During the later stages of AN development, the surface circulation due to upper q' advects cold air southeastward from the North American continent towards the central North Atlantic. At this time, however, the circulation associated with lower q' interacts incoherently with the developing upper level wave. During the later stages of AP development, the associated circulations are approximately in quadrature with the large-scale wave patterns near the key region. Thus, little potential exists for the associated circulations to enhance the large-scale anomaly patterns for the AP cases.

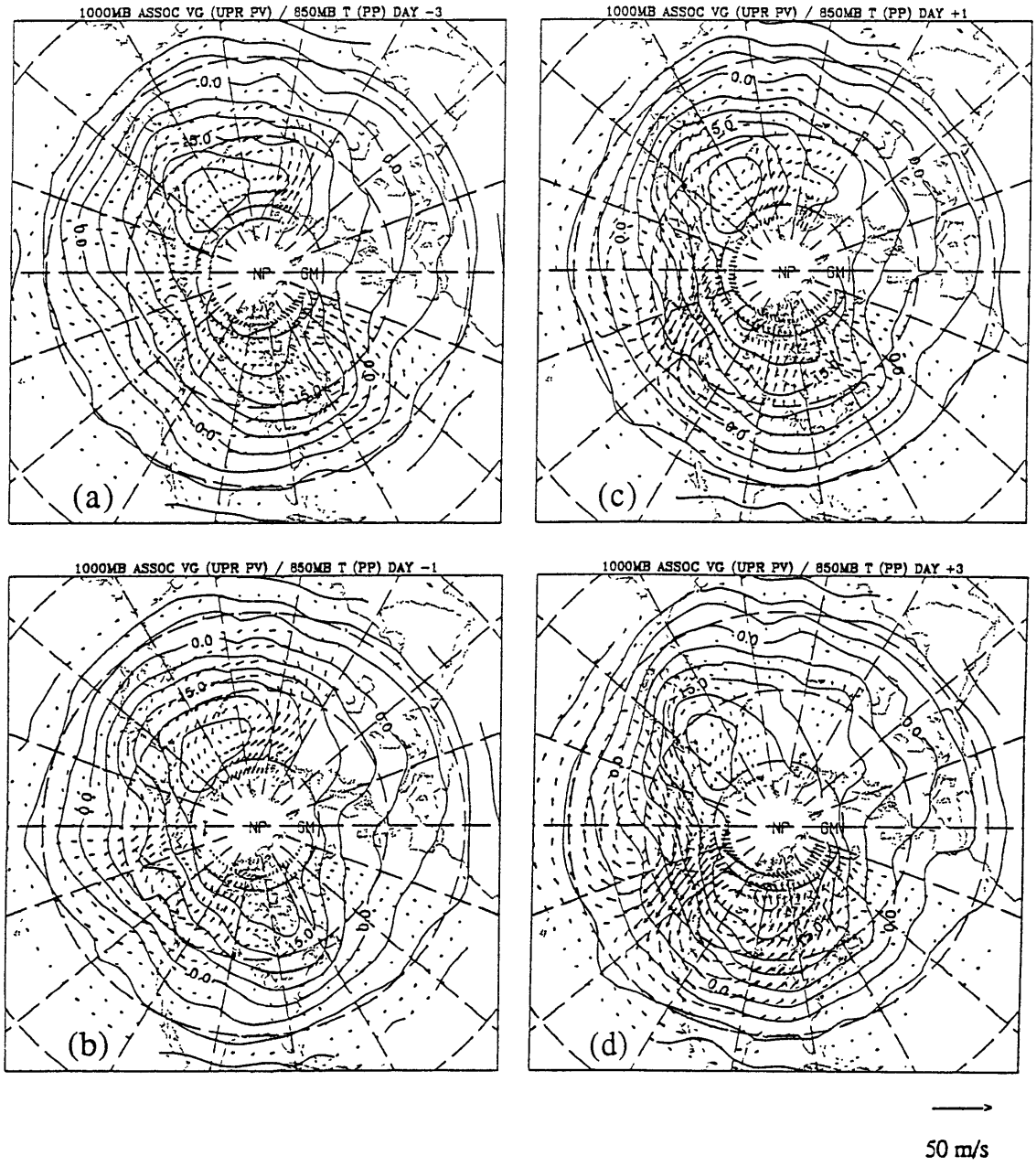

Fig. 5.22. As in Fig. 5.20 for the 15 case PP composite development.

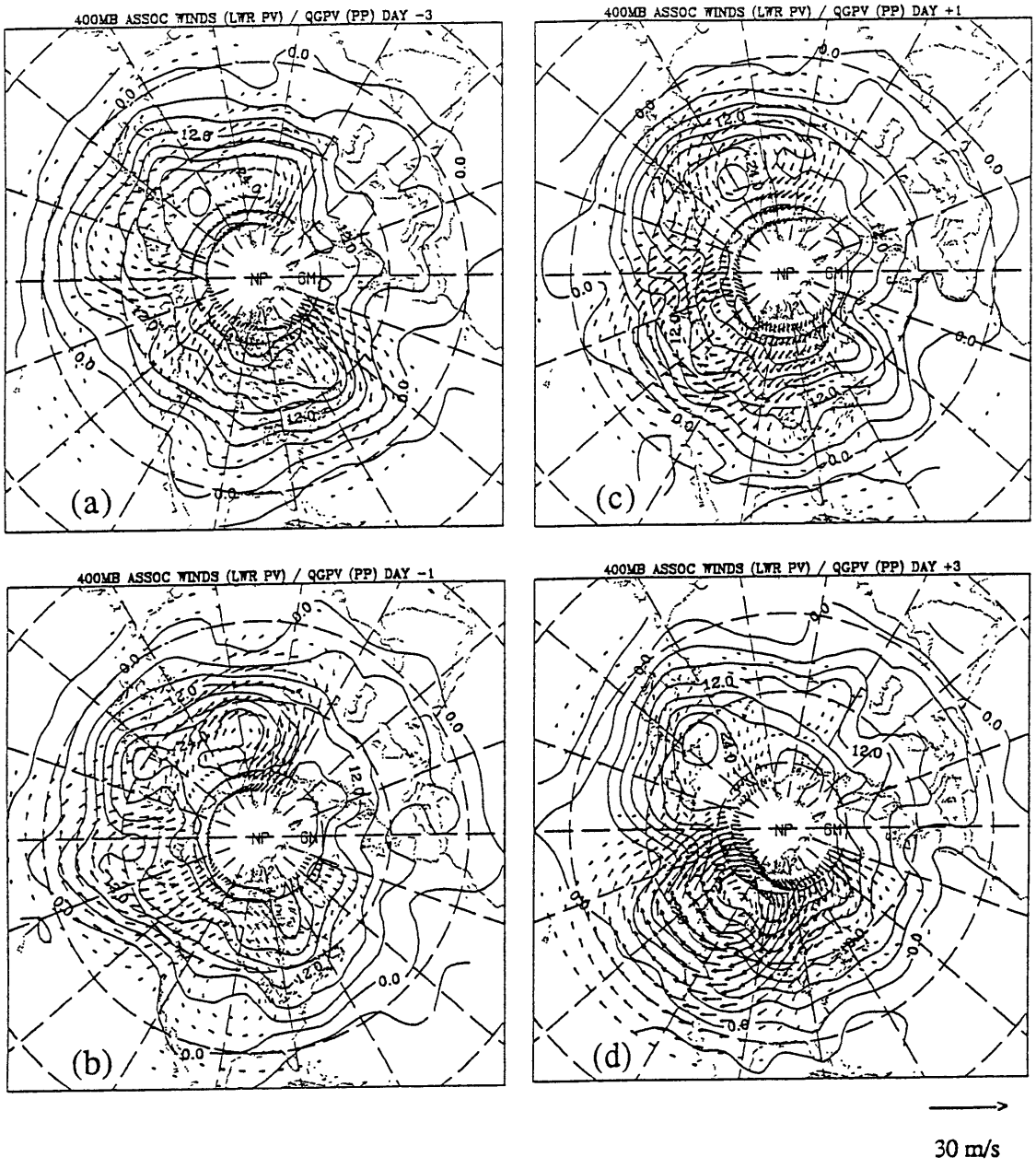

Fig. 5.23. As in Fig. 5.21 for the 15 case PP composite development.

F. Summary.

A wealth of information is provided by the diagnostic analyses of this chapter. Wave activity flux analyses provide information on regional sources and sinks of wave activity. *Transient eddy* flux analyses are applied to the early stages of PA evolution. During the early portions of AN and PN development an apparent source of wave activity is found over the western ocean regions, in association with synoptic-scale cyclogenesis upstream of the key region. Wave activity propagates upwards from the cyclogenesis region and downstream towards the key region where horizontal flux convergence occurs. Early PP development is characterized by a *vertical* flux convergence at 400 mb over the key region. A relatively high level of coherent transient eddy activity is suggested by the AP analyses, but no organized convergence is observed.

Stationary wave activity flux analyses indicate that the main sources for the large-scale, quasi-stationary portions of PA development are local to mid-latitudes. There is little evidence that anomalous tropical forcing contributes significantly towards PA growth. Sources for PN, AN and AP developments are also primarily local to the key regions. During PP development, however, there is some evidence for anomalous remote forcing from an upstream source found over eastern Siberia. Also, there is a sign of weak anomalous forcing from the subtropical North Pacific for the PP cases. All four types of PA's are predominantly trapped in the troposphere.

Energetics analyses performed during PAC evolutions indicate that the developments are *consistent* with a large-scale instability. Local baroclinic and barotropic energy conversions are sufficient to account for eddy kinetic energy changes during evolution. Although both types of conversions play important developmental roles, baroclinic conversions are largest for the PN cases while barotropic conversions appear more important for the PP cases.

Potential enstrophy analyses are performed during large-scale development. They

also indicate that conversions from the time-mean flow contribute significantly towards PA development. *In all cases, eddy enstrophy conversions are sufficient to account for the observed potential enstrophy changes.* The ratio of conversion to eddy enstrophy change is largest during PAC developments. *Residual nonconservative and anomalous nonlinear processes oppose development in all cases.* Like the energetics analyses, the results are consistent with a large-scale instability of the time-mean flow.

Pseudopotential vorticity analyses suggest that the large-scale baroclinic conversion pattern observed during the later stages of PN development may be due to a baroclinic "self-development". The circulation associated with the upper wave produces surface warm anomalies downshear of the upper level trough. Subsequently, there is an apparent mutual intensification between the upper and lower q anomalies. Similar analyses during the later stages of PP development indicate that an analogous mutual intensification appears to occur for oppositely signed q anomalies.

VI. Supplemental time evolution analyses.

A. Introduction

The synoptic and diagnostic analyses of the previous two chapters are based upon ensemble averaged flow fields. In this chapter, the *reproducibility* of the ensemble evolution is investigated in an independent dataset. In addition, the *representativeness* of the composite is studied using individual case analyses. These are demonstrated using the PN cases. Lastly, we will briefly study the potential role of tropical forcing in the formation of the upstream precursors to the PN developments.

B. Reproducibility in an independent dataset

The statistical analyses of Chapter IV (and of Dole, 1989) provide an initial indication of the systematic components of the composite evolution. Parallel analyses of PA's identified in an independent dataset provide a further means of assessing reproducibility. In order to do this, Dole and Gordon's (1983) analyses are extended to identify PA's in a more recent observational dataset. Nine additional PN cases were identified at the PAC key point during the winters 1977/78 through 1986/87 (see Appendix A). Selected composite analyses for these cases are presented in figs. 6.1, 6.2 and 6.3. These should be compared to figs. 4.1, 4.6 and 4.7, respectively.

Overall, a very good correspondence is found between the two composite evolutions. The primary difference is that the early portion of the development in the new composite lags the previous ensemble evolution by 1-2 days. This appears to be due to the initial presence of a strong low over the eastern North Pacific, which partially contributes to shifting the threshold crossing time at the key point. Prior to large-scale development, upstream jet intensification occurs to the south of Japan (figs 6.1b, 6.3b)

and high values of potential vorticity are found in the upper troposphere over the east coast of Asia (fig. 6.3b). Synoptic-scale cyclogenesis then occurs over the western North Pacific (figs. 6.2b,c). Strong cold advection and geostrophic frontogenesis forms on the western side of the cyclone at this time. The disturbance propagates eastward during onset, subsequently amalgamating with the easternmost low (fig. 6.1d). This leads to a quasi-stationary, zonally elongated and westward tilting perturbation in the jet exit region. Large-scale development occurs at this time.

It appears, then, that the primary features of development are indeed reproducible in an independent dataset. There is some suggestion, however, that there may be more than one way to produce the favored large-scale perturbation structure, with more evidence here for an amalgamation of two disturbances than seen previously. It seems likely that the key to large-scale development is the establishment of a properly configured perturbation in the jet exit region.

C. Case analyses

Although the composite features appear to be reproducible, it is also necessary to demonstrate that the composite results are also representative of the main process occurring in individual cases. Is there a reasonable correspondence between the key features determined from case and composite analyses? In order to demonstrate this, we present a case study of PA development. Selected analyses for the time evolution of PN case 12 are presented in figs. 6.4-6.8. Except for the analyses of fig. 6.8, the data are not spatially filtered in any way.

The 300 mb height anomaly evolution is shown in fig. 6.4 for days -3, -1, +1 and +3 of PN12 development. Figs. 6.5 and 6.6 contain additional, synoptic analyses for the same times. A split surface low is found over the North Pacific at day -3 (fig. 6.5a). The westernmost low tilts from northwest to southeast at this time. Strong cold

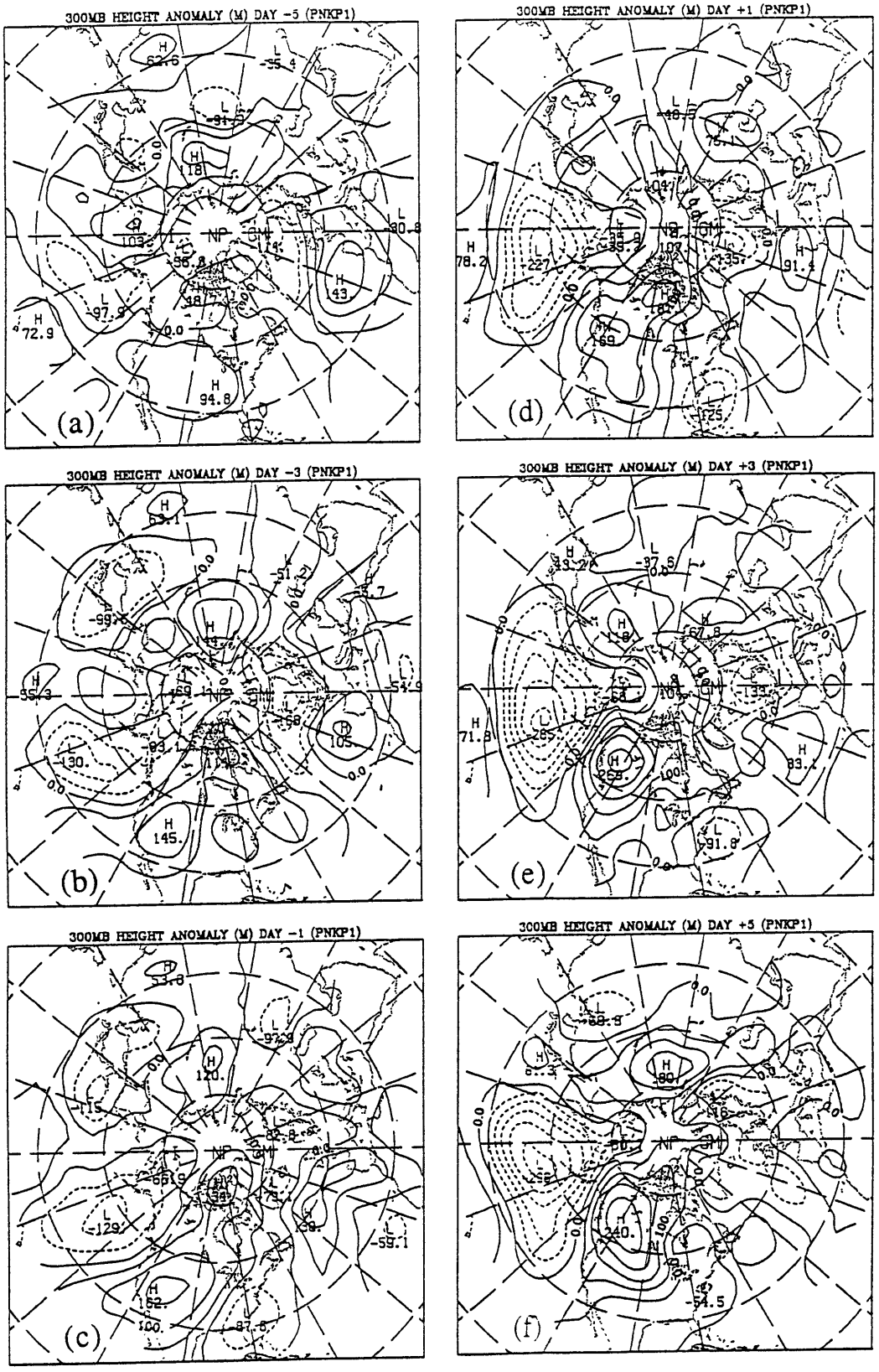

Fig. 6.1. As in Fig. 4.1 for the last 9 PN cases.

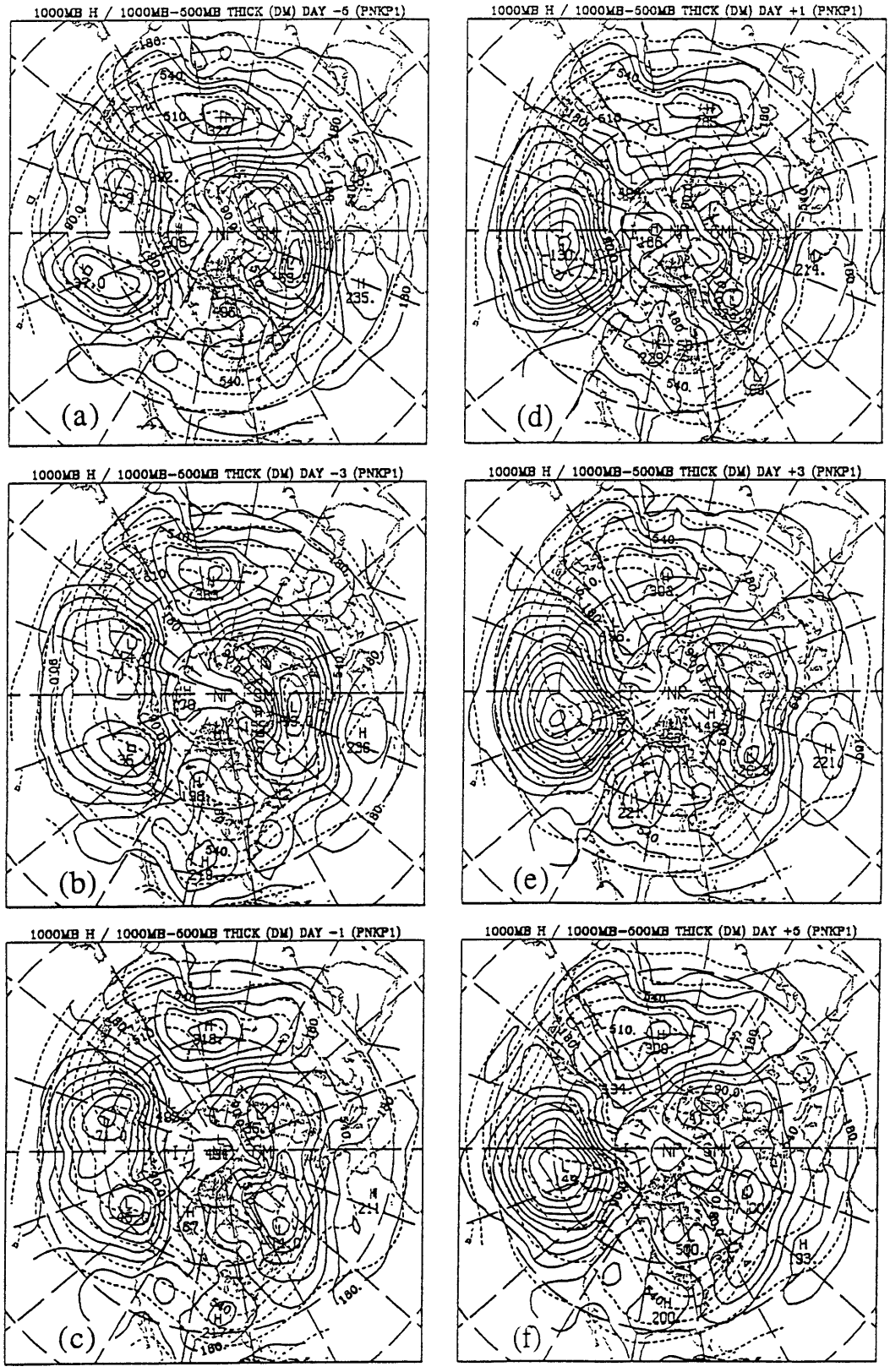

Fig. 6.2. As in Fig. 4.6 for the last 9 PN cases.

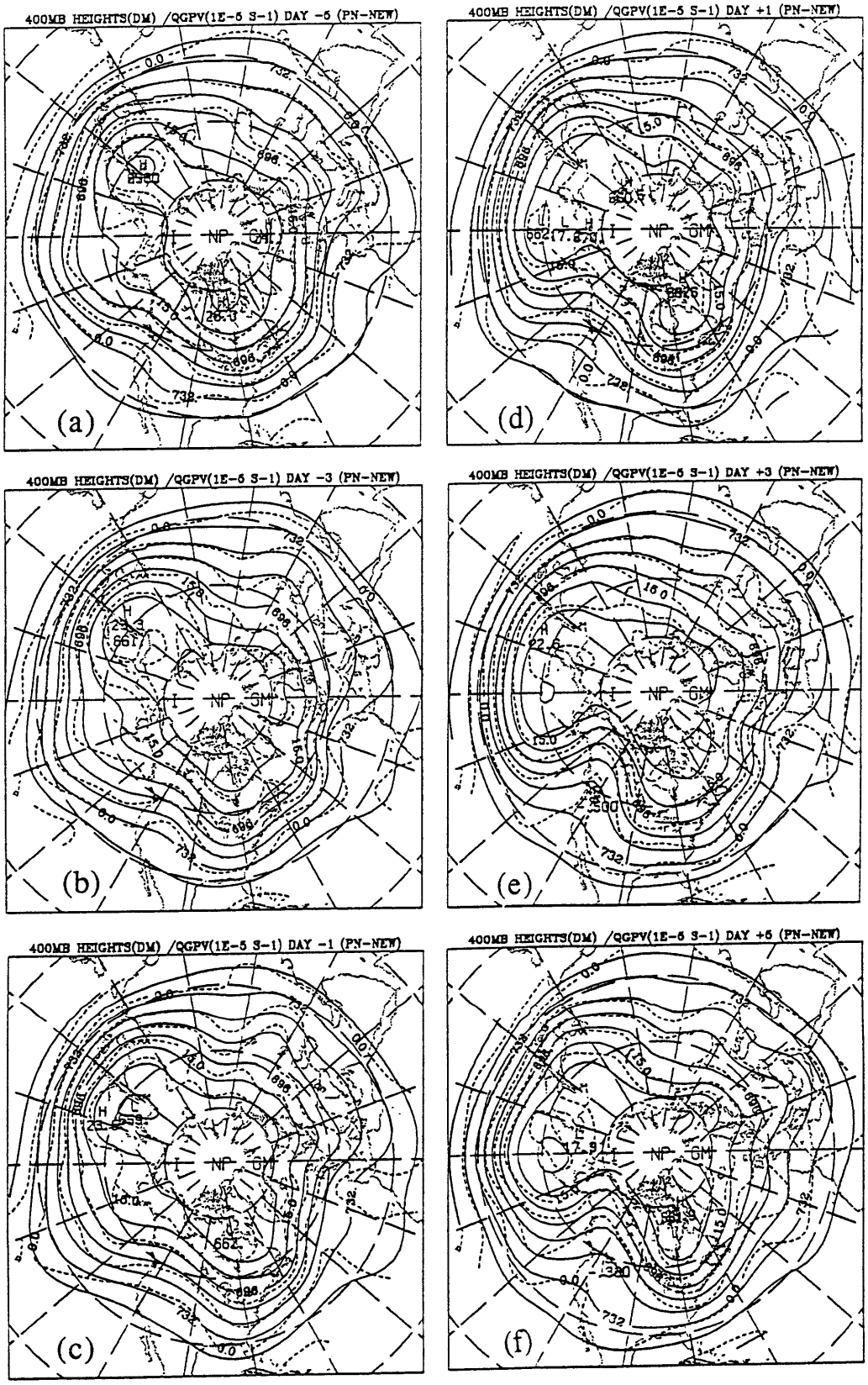

Fig. 6.3. As in Fig. 4.7 for the last 9 PN cases.

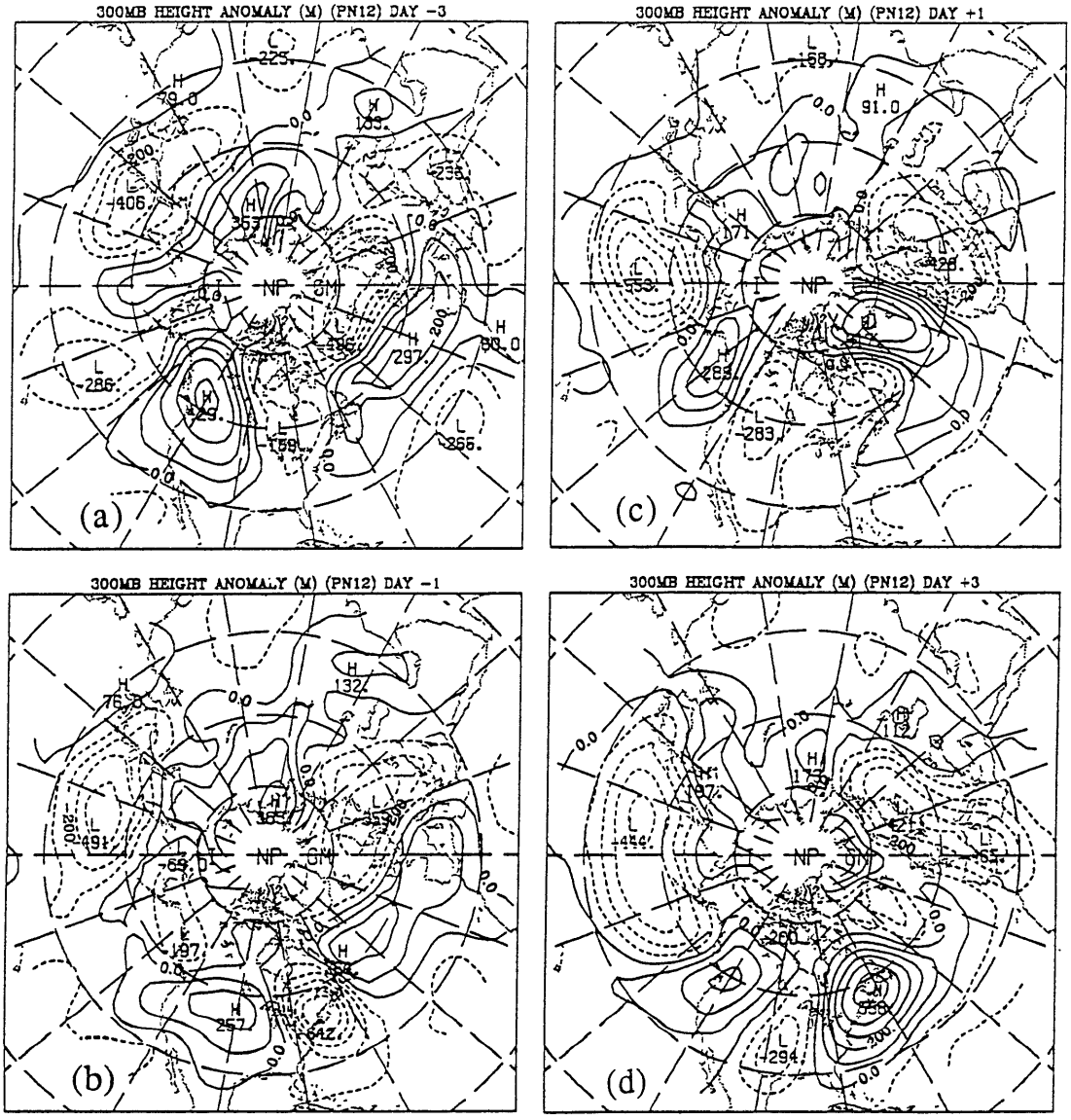

Fig. 6.4. As in Fig. 4.1 for days (a) -3, (b) -1, (c) +1 and (d) +3 of PN12 development.

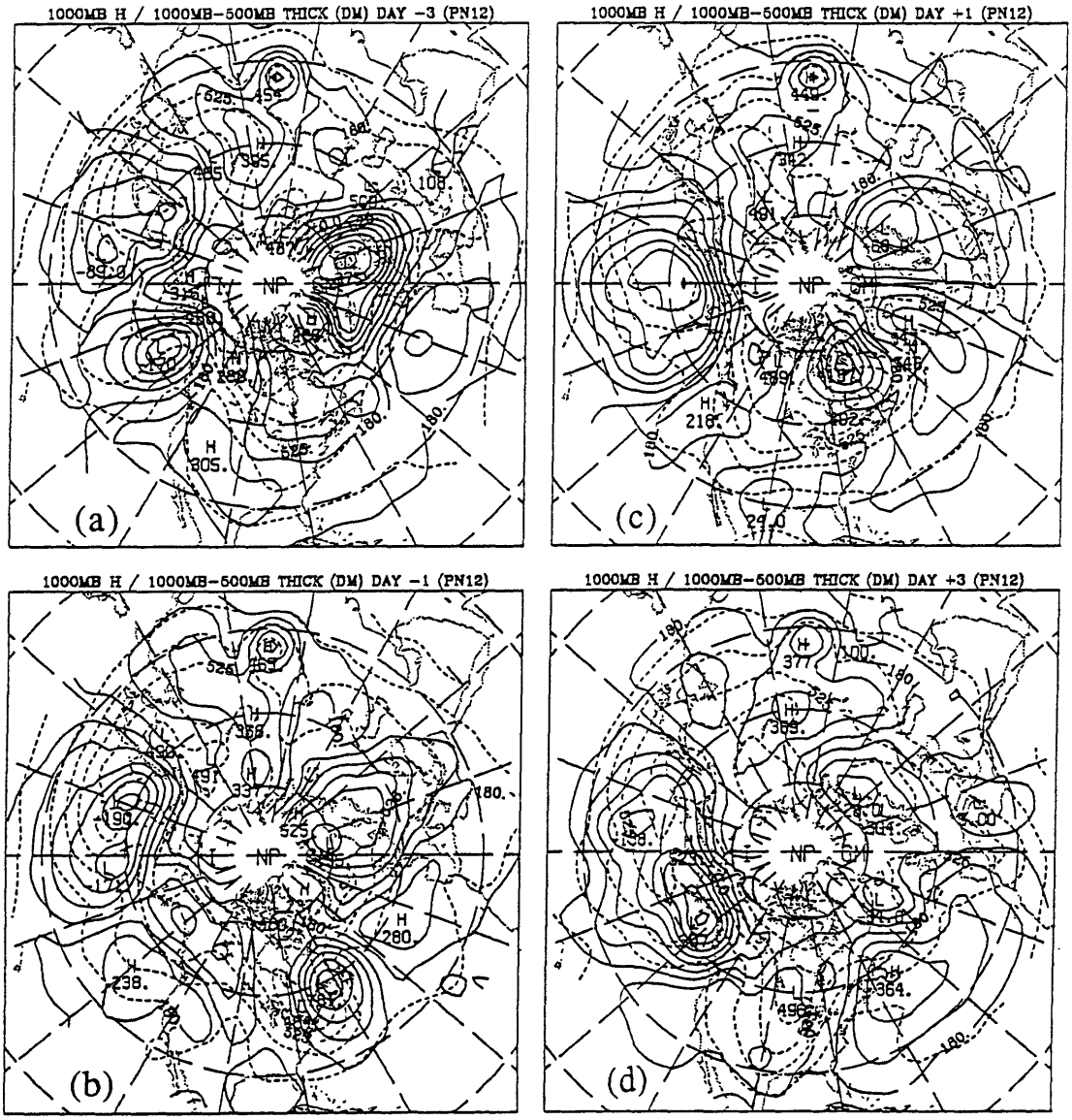

Fig. 6.5. As in Fig. 4.6 for days (a) -3, (b) -1, (c) +1 and (d) +3 of PN12 development. The contour intervals are 60 m for heights and 15 dam for thickness.

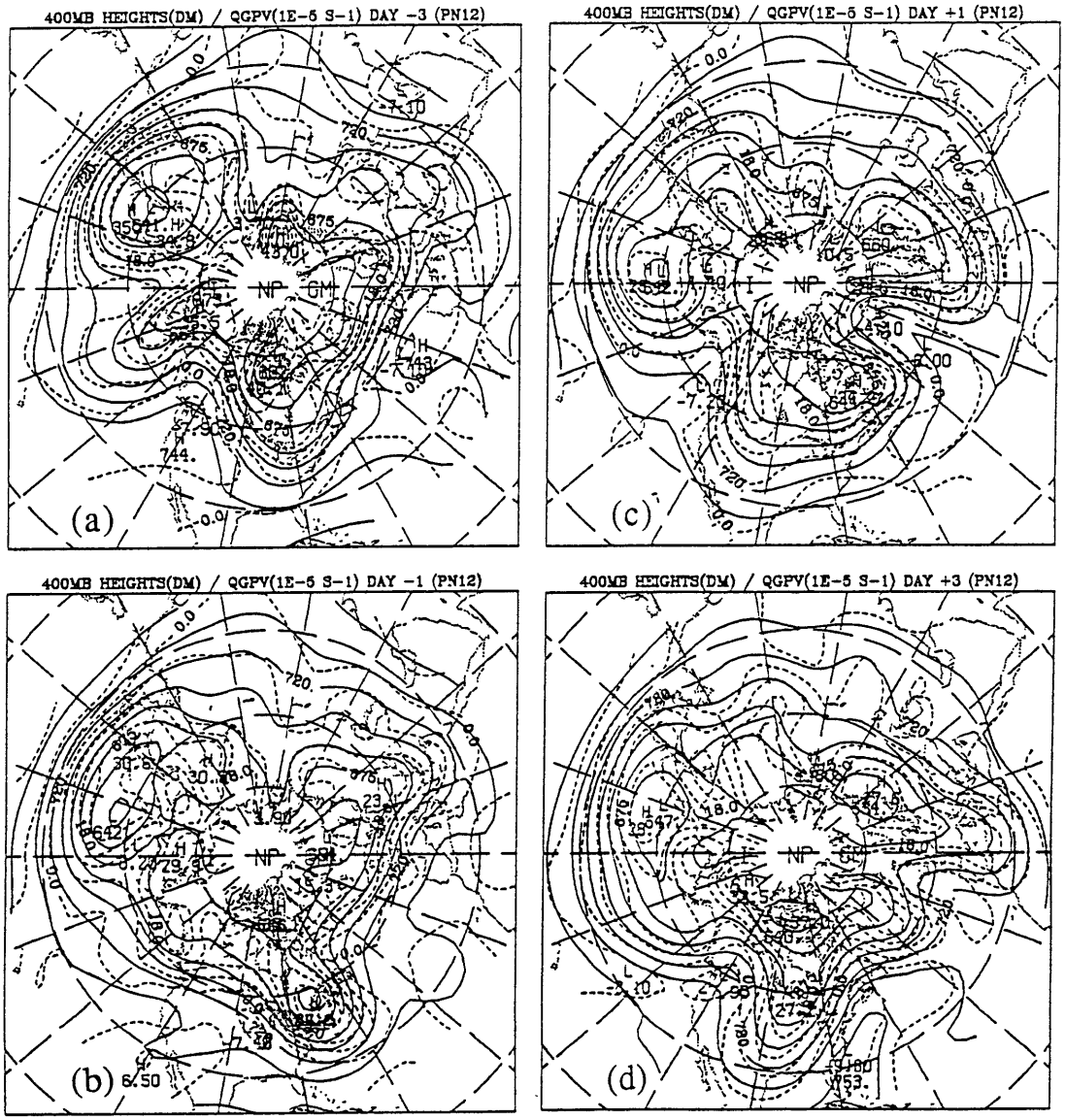

Fig. 6.6. As in Fig. 4.7 for days (a) -3, (b) -1, (c) +1 and (d) +3 of PN12 development. The contour intervals are 15 dam for heights and 6×10^{-5} s^{-1} for vorticity. Zonal wavenumbers greater than 12 have been removed.

advection is observed in the southwest portion of the disturbance and there is weak potential vorticity advection over the surface center (fig. 6.6a). At upper levels, an intensified subtropical jet is located over the southwest North Pacific (fig. 6.6a).

Two days later, the now zonally elongated disturbance intensifies and propagates eastward towards the jet exit region (fig. 6.4b). Strong cold advection extends from the Asian continent eastward towards the Date Line (fig. 6.5b) and decreases southward underneath the intensifying upper level jet. Positive potential vorticity advection is found over the eastern portion of the surface trough (fig. 6.6b) at this time, leading to an eastward extrusion of high potential vorticity over the central ocean.

Considerable surface development takes place during PA onset. By day +1, an intense basin-wide surface cyclone extends over most of the North Pacific (fig. 6.5c). For comparison, note the scale of the low found west of Greenland at this time. Increasing warm advection in the northeast quadrant of the cyclone is associated with upper-level ridge development near and to the south of Alaska at this time(figs. 6.4c and 6.5c). By day +3, a strong upper level jet spans most of the subtropical North Pacific (fig. 6.6d).

Good qualitative agreement is found between the case and composite analyses. The major differences found here are that the case exhibits larger perturbation amplitudes, has a shorter development time scale and contains more small-scale structure. All of these discrepancies can be partially attributed to the smoothing effect of the compositing procedure. The qualitative aspects of the large-scale evolution of this case, however, are accurately represented in the ensemble analyses.

This is tested further by examining diagnostic analyses of the later stages of PN12 development. Anomalous fluxes of stationary wave activity are presented in fig. 6.7 for days 0 to +5 of PN12 development. Although there is some sign of an anomalous northward flux from the subtropics over the far western North Pacific, the primary source of wave activity appears to be located over the central North Pacific at

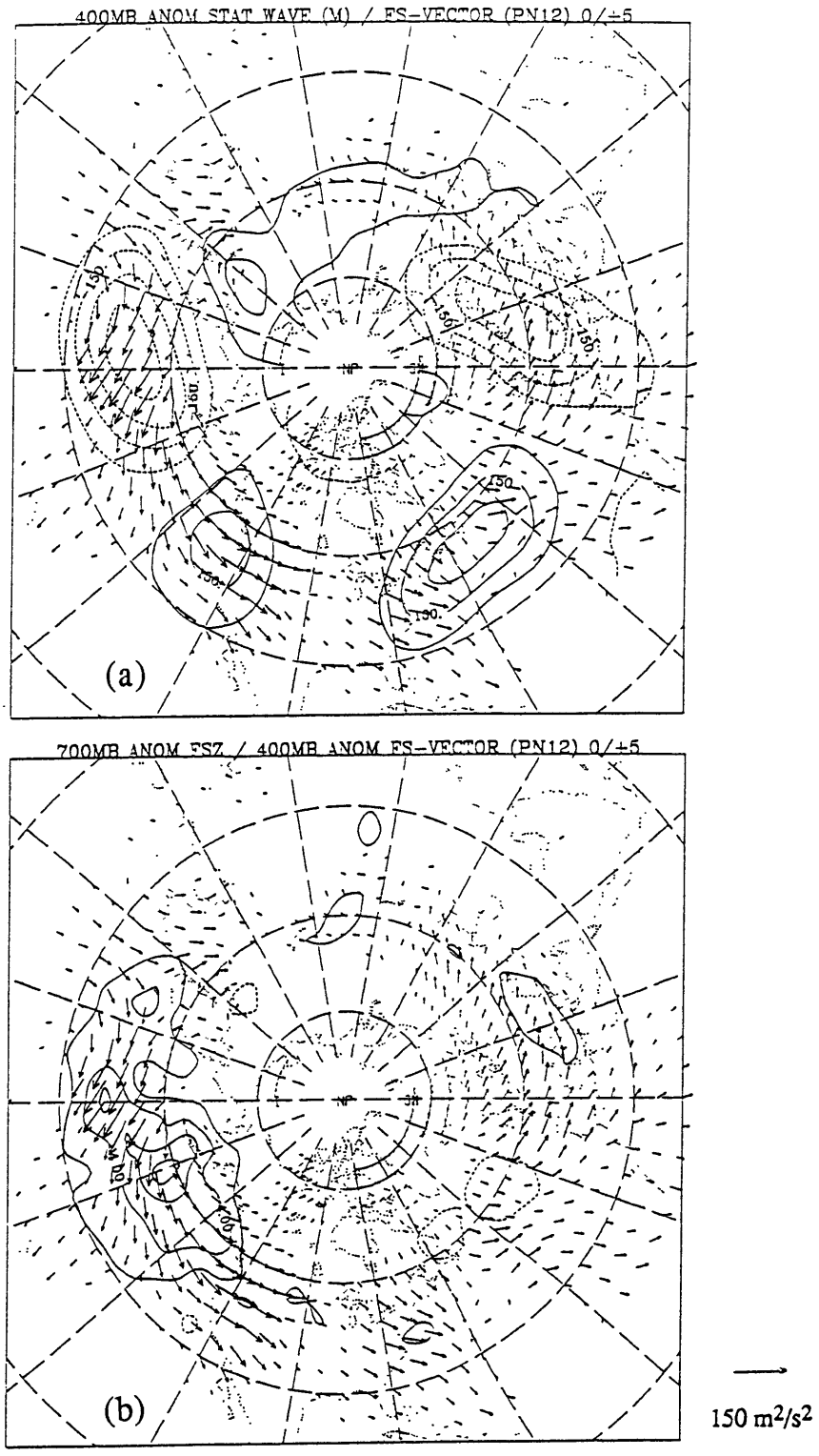

Fig. 6.7. (a) As in Fig. 5.4b (contour interval: 75 m) and (b) as in Fig. 5.4a (contour interval: 0.2 m^2/s^2) for days 0 to +5 of PN12 development. A scale vector and corresponding magnitude for FSH are displayed in the lower right.

midlatitudes. An anomalous upward and downstream flux emanates from the region of large-scale development and extends southeastward towards the subtropical North Pacific and eastward towards a downstream ridge located over the west coast of North America.

Fig. 6.8 displays the 400 mb residual potential vorticity flux (6.8a) and the associated local enstrophy conversions (6.8b) averaged over days 0 to +5 of PN12 development. In order to reduce small scale noise, wavenumbers greater than 12 were removed from the data prior to analysis. Over the central North Pacific we find strong downgradient fluxes in a region of large horizontal gradients of time-mean q, leading to large local eddy enstrophy conversions. Weaker downgradient fluxes are found downstream near Alaska. Again, a good correspondence is found between the case and ensemble results, although the pattern associated with the individual case is shifted slightly upstream when compared to the composite signature.

We also note a prominent downgradient flux pattern over central Europe in fig. 6.8a. However, these fluxes are found in a region of relatively weak horizontal gradients of time-mean q. Thus, local conversions are considerably weaker than found over the North Pacific. It appears, then, that the existence of large conversions depends upon appropriate perturbation structures existing in regions of significant time-mean potential vorticity gradients.

Further case analyses were also performed (not shown). In particular, analyses of the time evolution of the first 14 PN cases were compared individually with the composite development described previously (figs. 4.1-4.10). The following criteria were subjectively chosen to evaluate the degree of correspondence between the individual case and composite evolutions.

1) Prior to development, the magnitude of areal averaged thermal and upper-level height anomalies over southeast Asia should be comparable to (and may exceed) the areal averaged composite values.

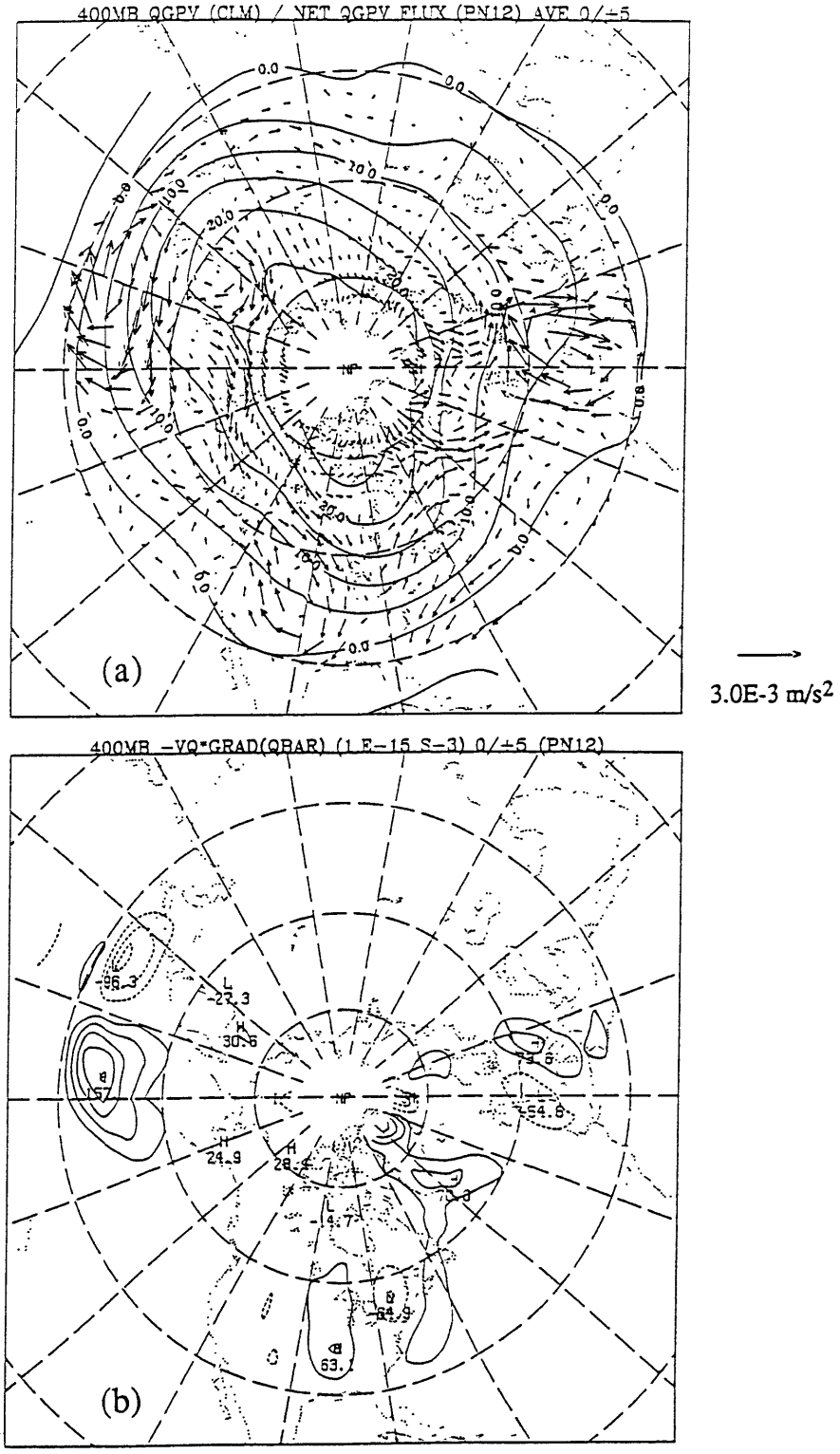

Fig. 6.8. (a) As in Fig. 5.14b and (b) as in Fig. 5.14c (contour interval: 30×10^{-15} s^{-3}) for PN12 development. A scale vector and corresponding magnitude are displayed for the q-fluxes. Zonal wavenumbers greater than 12 were removed before analysis.

2) Synoptic-scale cyclogenesis should be observed over the western North Pacific before large-scale development.

3) A basin-wide surface circulation should be obtained during the later stages of development.

The second criterion was satisified in all 14 PN cases. Using the criteria jointly we find that in seven (cases 2, 3, 5, 9, 11, 12 and 14) of the fourteen PN cases there is a good correspondence to the composite evolutions. In three other cases (4, 7 and 13), the differences appear to be attributed to temporal phase shifts between the case and composite evolutions. This could be due to extraneous features located near the key region around the time of onset. Thus, a majority of the individual cases exhibit developmental features which are similar to those of the composite evolution.

D. Tropical forcing of precursors.

The role of anomalous remote forcing during PA *development* was investigated using wave activity flux analyses in Chapter V. However, we have not yet studied the potential influence of remote forcing upon the formation of the *precursors* to PA development. In particular, the robust upstream precursors to PN development are found at longitudes where (a) strong variations in tropical convection occur and (b) the subtropical jet stream penetrates to low latitudes. It is therefore also of interest to study the potential role of anomalous tropical convection in producing the EAJ variations observed prior to PN development.

Further composite analyses (not shown) show that the upstream precursors to the PN cases intensify in a quasi-stationary manner during days -8 to -4. Here we apply stationary wave activity flux analyses during this time, in order to diagnose the sources and sinks of wave activity. Fig. 6.9 displays the 400 mb stationary wave and horizontal

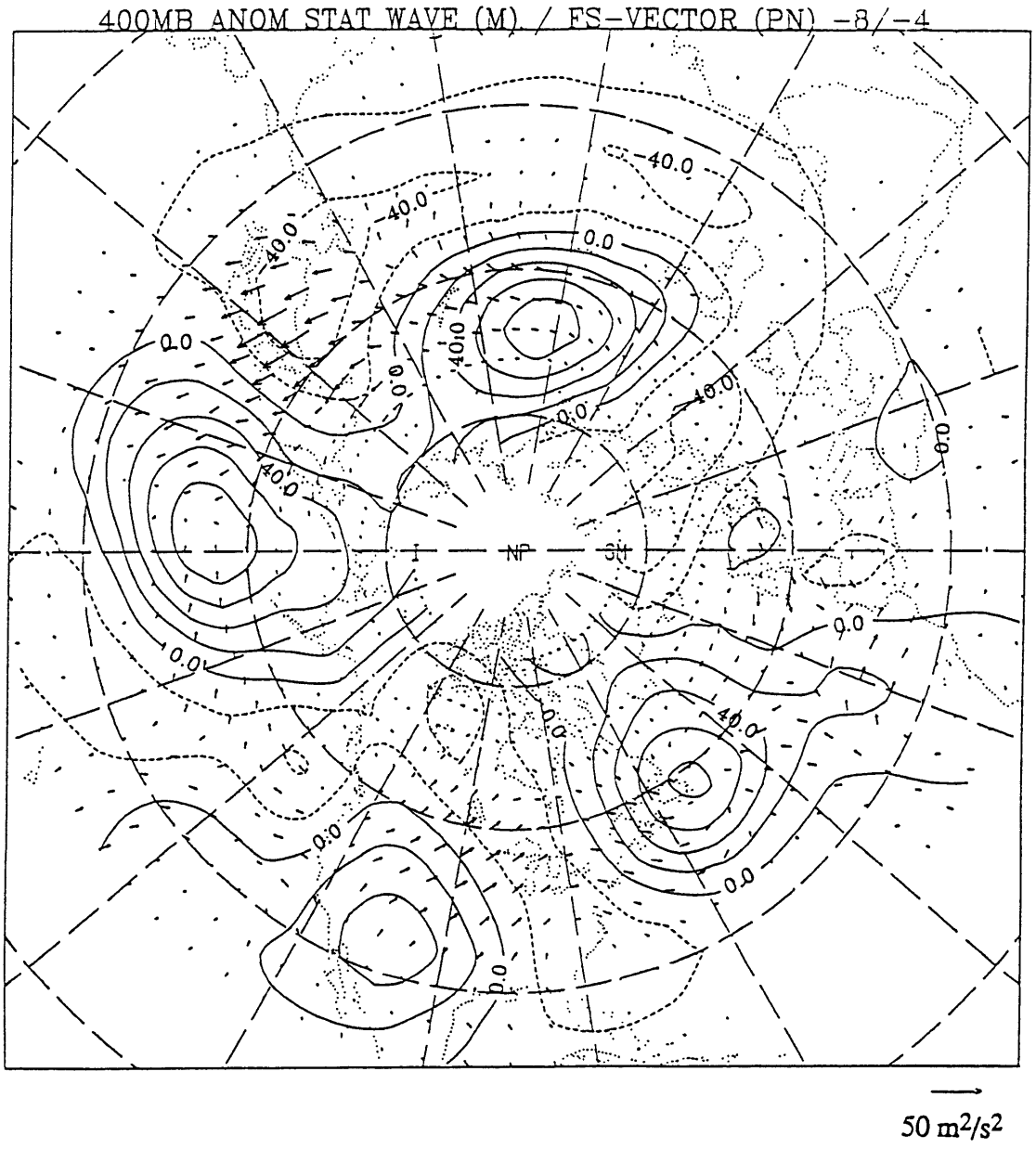

Fig. 6.9. As in Fig. 5.4b for days -8 to -4 of PN development. Contour interval is 20 m for the composite height anomalies and a scale vector is displayed for FSH.

F_S anomalies for days -8 through -4 of PN time evolution. We see that there is an anomalous flux extending southeastward from a ridge located over the Soviet Union. Horizontal flux divergence occurs near this ridge and in the northeast portion of a broad trough found over southern Asia. There is, however, no evidence of an anomalous wave activity flux emanating from the tropics.

As a further check, we looked for systematic tropical flow variations near southeast Asia during this time. Before 1980, tropical analyses are relatively sparse and of poor quality. For more recent years, global operational analyses are available from the ECMWF and NMC. As discussed in Chapter III, diabatic normal mode initialization has improved the quality of the analyzed divergent wind fields in the tropics during this time. Satellite derived analyses of outgoing longwave radiation (OLR), used as a measure of tropical convection, extend prior to 1980. Composite equatorial analyses of OLR, upper tropospheric streamfunction and upper tropospheric divergent winds were therefore constructed for 8 cases of PN development occuring during the winters of 1979/80 through 1986/87. These cases comprise 8 of the 9 cases used in the composite analyses of section B of this chapter. Thus, the figures in this section can be compared to those of section B. Our objective is to determine whether there are systematic tropical flow anomalies near southeast Asia during days -8/-4 of PN time evolution.

Fig. 6.10 displays 200 mb composite streamfunction anomalies for days -8, -6 and -4 of PN development. We note the development of a ridge over extreme southeast Asia between days -8 and -4. The ridge is associated with an upper level jet intensification between 25°N and 40°N over southeast Asia. During this time, a low intensifies over the Arabian Sea and ridge development occurs near 40°N over the western North Pacific.

Fig. 6.11 displays composite OLR anomalies for the same times. The anomalies are seasonally detrended running 5-day averages. This isolates intraseasonal OLR variations and eliminates daily variations associated with small scale convection.

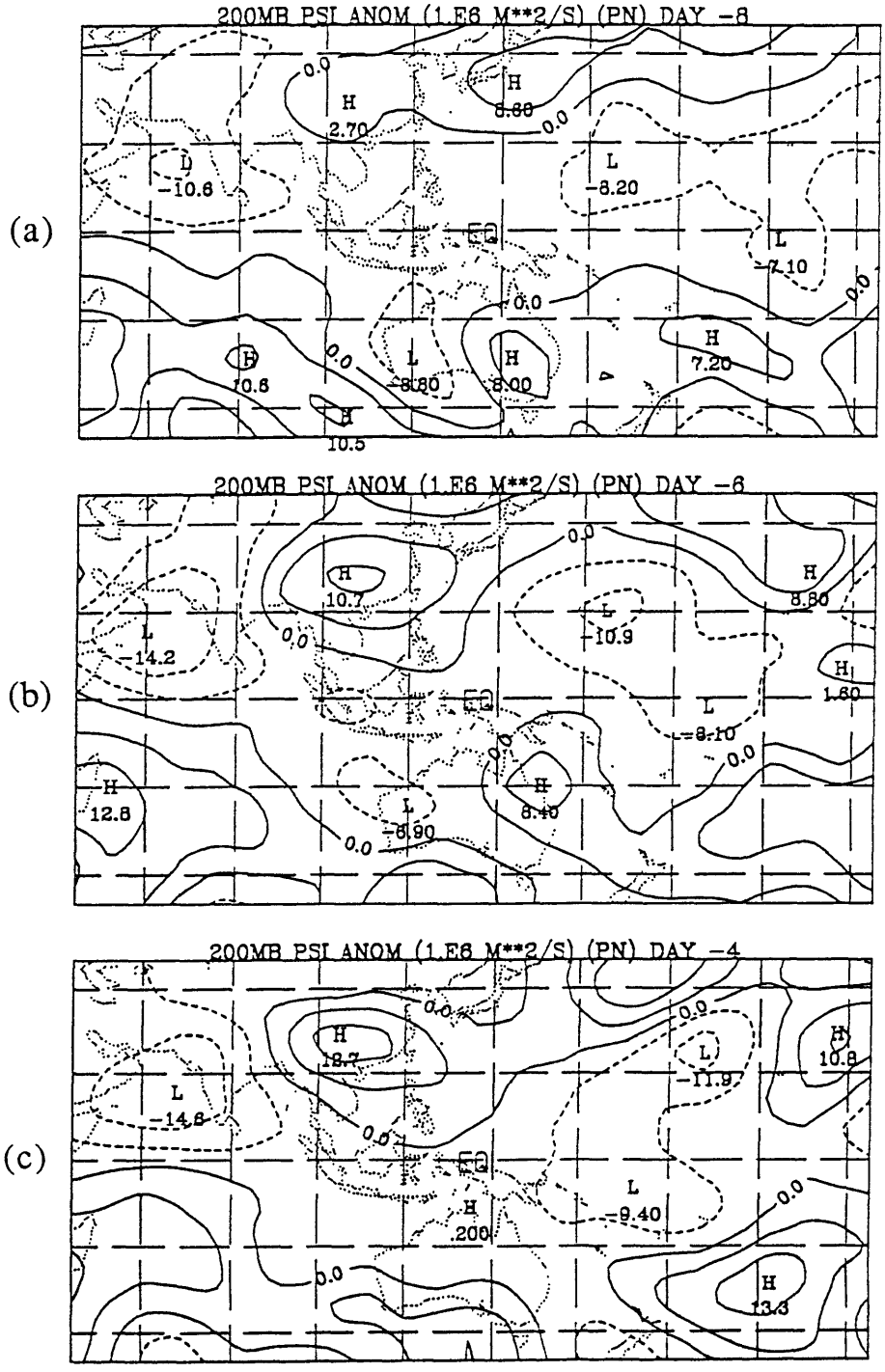

Fig. 6.10. Composite averaged 200 mb streamfunction anomalies (contour interval: 5×10^6 m^2/s) for days (a) -8, (b) -6 and (c) -4 of the 8 case PN composite development

Large-scale enhanced convection (indicated by *negative* OLR anomalies) is found north of Indonesia and over the Bay of Bengal during this time. Local maxima are 25-30 Watts/m^2. The distribution of OLR variations in these regions is highly negatively skewed (values of skewness approach -3 over the Bay of Bengal) and does not lend itself to simple statistical tests. For comparison, however, typical variations of running 5-day averages in more convectively active (and less skewed) regions are 25-35 Watts/m^2. Suppressed convection is observed over the equatorial Indian Ocean.

The OLR analyses are supplemented by composite anomalies in the 200 mb divergent wind field as displayed in fig. 6.12. A pattern of upper-level divergence develops over the northern portion the Bay of Bengal after day -8 (fig. 6.12a). By day -4, the pattern of divergence extends southeastward to Indonesia. The magnitude of the divergent winds, however, are less than ~2 m/s in this region. Also, the anomalous divergence near the Bay of Bengal is observed to develop *simultaneously* with the streamfunction anomalies over southeast Asia. This appears inconsistent with the anomalous convection forcing the jet intensification to the north. The most prominent signature in fig. 6.12 is the upper level divergence found near 40°N to the east of Japan at day -4 (fig. 6.12c). The outflow pattern is located over a region of anomalous warm advection in the lower troposphere (figs. 6.2a,b) that is associated with the extratropical development described previously.

Although there is some sign of anomalous tropical forcing near southeast Asia, the signal is relatively weak. The wave activity flux analyses also provide no indication of anomalous remote forcing from the tropics. The Q-vector analyses of Chapter IV suggest that the upper level jet intensification may instead be due to local enhancements in geostrophic frontogenesis. So, although it is possible that anomalous tropical forcing may play a prominent role in certain individual cases, the results presented here suggest that the role of systematic anomalous tropical forcing is likely to be modest in most of the developments. Further study will, however, be necessary to fully clarify the role of

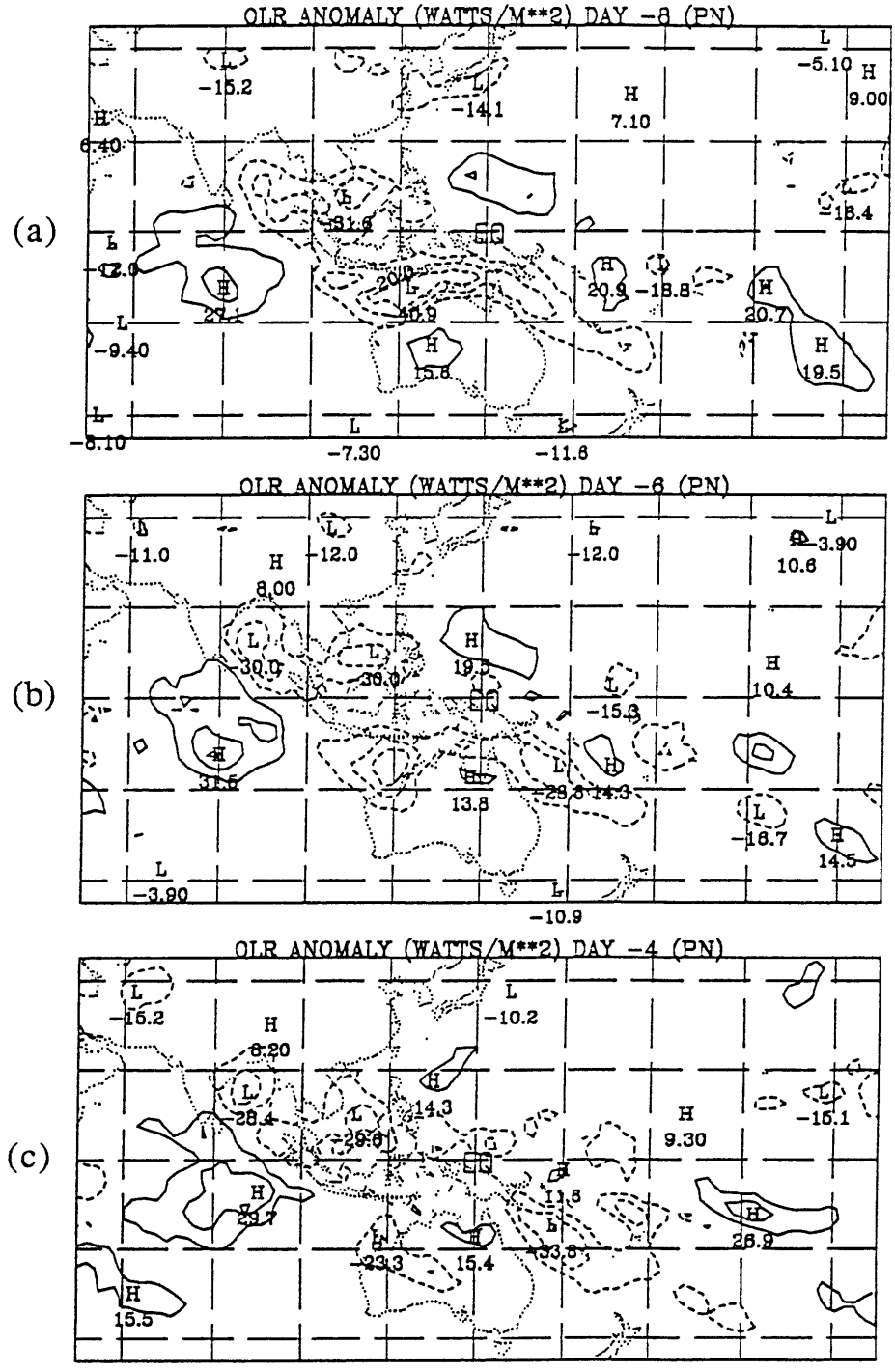

Fig. 6.11. Composite averaged OLR anomalies (contour interval: 10 Watts/m^2) for days (a) -8, (b) -6 and (c) -4 of the 8 case PN composite development. Composite anomalies are derived from seasonally detrended running 5-day averages.

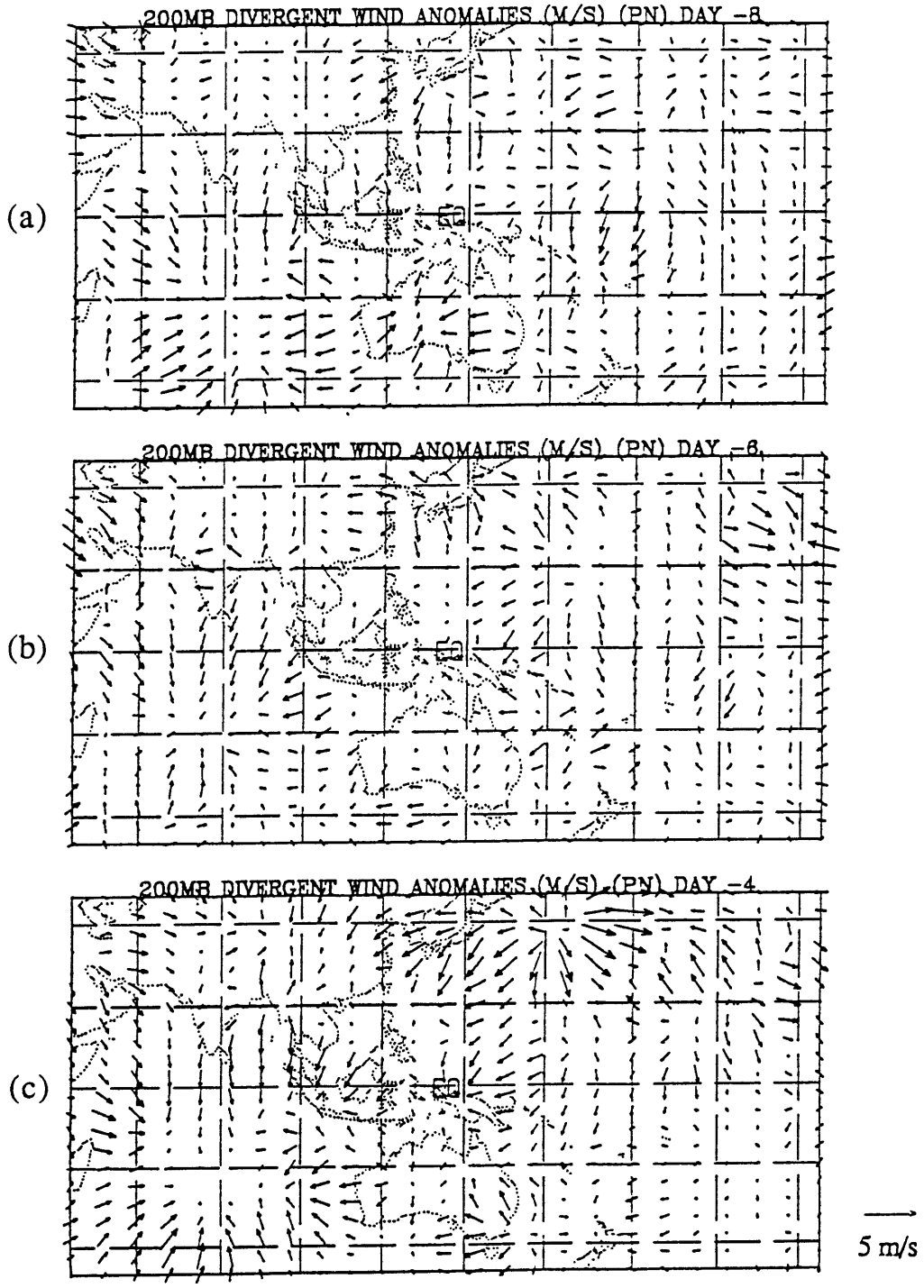

Fig. 6.12. Composite averaged divergent wind anomalies for days (a) -8, (b) -6 and (c) -4 of the 8 case PN composite development. A scale vector and corresponding magnitude are displayed in lower right for the wind field.

tropical forcing in the development of low frequency circulation anomalies.

E. Summary

In this chapter we have demonstrated the reproducibility and representativeness of the composite results using the PN cases. Composite analyses of cases identified in an independent dataset reproduce the primary features of composite time evolution. Individual case analyses show that, in most cases, large-scale features are accurately represented by the composite fields. Roughly three-fourths of the case evolutions have a good correspondence with the composite development. Lastly, composite tropical analyses indicate that there are weak systematic tropical flow anomalies near southeast Asia prior to PN developments.

VII. Discussions and Conclusions.

A. Summary of main features.

Persistent anomalies (PA's) contribute significantly towards intraseasonal, low frequency variability (LFV) in the midlatitude troposphere and are often associated with persistent extremes in surface weather (Dole, 1986a). Thus, PA's are of considerable scientific and practical interest. Although there have been a number of observational studies concering the time-averaged characteristics of particular mid-latitude low frequency phenomena (e.g. Shutts, 1986; Dole, 1986a; Mullen, 1987; Holopainen and Fortelius, 1987a), there have been relatively few studies of the *time evolution* of midlatitude LFV. As a result, our understanding of the processes responsible for their time evolution is currently quite limited. In this thesis, we have attempted to bridge this gap by extending Dole's (1989) 500 mb analyses with detailed synoptic and diagnostic analyses of the life cycles of PA's. Our main objective has been to identify the primary sources for PA development.

This objective is pursued in two parts. In Chapter IV, we thoroughly document the typical three-dimensional flow structures and associated eddy fluxes observed during the time evolution of PA's. Chapter V then provides specific diagnostic analyses of PA development which are aimed at identifying the main sources for developments. The results of Chapters IV and V together are then used for examining the viability of various hypotheses of PA development. Chapter VI investigates further the reproducibility and representativeness of the main composite results.

Ensemble analyses of PA evolution suggest that there are a number of parallels among the various PA evolutions, as well as some important differences. Negative PA's over the North Pacific and North Atlantic are preceded by the upstream intensification of

the subtropical jet and by the buildup of anomalously cold surface air and anomalously high upper-tropospheric potential vorticity over the upstream continents. In both cases, anomalous geostrophic frontogenesis occurs in advance of the developments along the axis of the intensifying subtropical jet. Near the key regions, the AN and PN cases are initially characterized by pre-existing positive height anomalies. Prior to AP development, a coherent wavetrain of synoptic-scale disturbances is found over a large portion of the Northern Hemisphere.

During the early portions of AN and PN evolution coherent synoptic-scale cyclogenesis occurs over the western ocean regions. These westward tilting and eastward propagating disturbances have associated downgradient and upward heat fluxes. Enhanced cold advection and geostrophic frontogenesis are found in the southwestern portion of the developing surface cyclones. Eastward extrusions of high potential vorticity air from the upstream continent are associated with the synoptic-scale developments.

During early PP development, a synoptic-scale *anticyclone* develops over the western North Pacific. This eastward propagating anticyclone also tilts westward with height. Large-scale ridge amplification occurs over western Europe during the early stages of the AP developments.

For the PAC cases, PA onset occurs as the eastward propagating synoptic disturbance approaches the key region and acquires a zonally elongated structure. At the time of onset (day 0), the PN cases have approximately equivalent barotropic vertical structures, while the PP cases exhibit westward tilts with height. For the ATL cases, PA onset occurs as a large-scale anomaly pattern retrogresses northwestward towards the key region from the eastern North Atlantic. During AN development, an eastward propagating cyclone amalgamates with the retrogressing large-scale low.

In all cases, a zonally elongated perturbation structure develops in the climatological mean jet exit region at the time of onset. This is associated with westward

pointing E-vectors in the upper tropospheric jet exit regions. Prominent large-scale heat flux patterns are also observed at this time for the PP, AN and AP cases, but not for the PN cases.

After onset, the primary anomaly patterns become quasi-stationary near the key regions while undergoing large-scale growth. In all cases, zonally elongated anomaly structures continue in the jet exit regions. In addition, at the later stages of development all four cases exhibit upshear tilts with height upstream of the key points. These structures are, therefore, associated with both upgradient E-vector and downgradient heat flux patterns over large areas near the key region. The E-vectors and heat flux patterns found at the later stages of development suggest that there are positive barotropic and baroclinic energy conversions from the time-mean flow into the growing eddies.

Significant differences among the cases are also found during large-scale developments. During PAC developments, large downgradient heat fluxes occur *downstream,* as well as upstream, of the key point. The negative PA cases exhibit strong upward heat fluxes, while the positive cases have only weak vertical heat fluxes. For the ATL cases, the large-scale heat flux and E-vector patterns form simultaneously. During the PN evolution an upgradient E-vector signature develops prior to the large-scale heat flux pattern, with the converse true for the PP developments.

Diagnoses of wave activity fluxes indicate that the main sources for PA development are located in mid-latitudes. In particular, *there is little evidence that anomalous tropical forcing contributes directly to the large-scale growth.* The sources for PN, AN and AP evolution are also primarily local to the development region. During PP development, there is some evidence for anomalous remote forcing from eastern Siberia. In all four cases, wave activity appears to be predominantly confined to the troposphere.

Energetics and potential enstrophy budget analyses were used to study the possible role of interactions between the large-scale eddy and the time-mean flow during

large-scale development. *In all cases, conversions from the time-mean flow into the anomalies are more than sufficient to account for the observed eddy developments.* The role of eddy conversions appears to be relatively greater during the PAC developments than during the ATL developments. This is consistent with the results of Neilley (1990), who found that synoptic-scale eddy forcing is relatively larger during the ATL developments. In all cases, potential enstrophy analyses indicate that the residual forcing, composed of anomalous nonconservative and nonlinear eddy processes, tends to oppose the developments.

Pseudopotential vorticity analyses suggest that part of the large-scale baroclinic intensification found during the later stages of the PAC developments results from a mutual interaction between upper and lower tropospheric waves. In particular, the later stages of PN development include an apparent baroclinic "self-development" after initial upper- tropospheric barotropic intensification.

Similar composite analyses of PA's derived from a more recent independent dataset reproduce the primary features obtained in the earlier composite results. Individual case analyses confirm the representativeness of the composite evolution. Although individual cases do show differences, roughly three-fourths of the cases exhibit all of the major features of the composite. The major differences between the case and composite evolutions appear to be related to the spatial and temporal smoothing associated with the compositing procedure.

B. Discussion of proposed mechanisms.

As mentioned previously, there have been few detailed observational studies examining potential mechanisms for the development of low frequency circulation anomalies. Qualitatively similar E-vector patterns to ours were obtained by Hoskins et al. (1983) for the *time averaged* low-pass eddies of the winter of 1979/80. Schubert (1986)

also finds that there are significant baroclinic and barotropic conversions from the time-mean flow for particular *global modes* of low frequency variability (determined from his EOF analyses). Karoly et al. (1989) examine the stationary wave activity fluxes associated with dominant midlatitude teleconnection patterns. Their results suggest primarily midlatitude sources for these patterns, which are closely related to our *mature* PA structures.

We now consider potential mechanisms for the developments. One mechanism discussed in Chapter II is the response to anomalous topographic or diabatic forcing. The wave activity analyses suggest that *remote* forcing anomalies play a small role in most of the developments. There is some evidence that remote processes contribute to PP development, apparently related to upstream trough development over Siberia.

If local forcing anomalies were primary contributors to development, we would expect local wave sources and significant positive contributions to the anomalous nonconservative source/sink term in the eddy enstrophy budget. Although the sources of wave activity are local, the residual term in the enstrophy budget *opposes* development in all cases, suggesting that there is no large *direct* contribution by diabatic or other nonconservative processes. For the PAC cases, wave activity fluxes do not indicate that there is significant forcing by the Rocky Mountains.

One possible mechanism that has been proposed is that zonal mean flow variations (for a fixed forcing distribution) lead to anomalous forced waves. The steady-state analysis of Nigam and Lindzen (1989) predicts that such forced wave anomalies would be in phase with the climatological mean stationary wave pattern. We note that during PA development, however, the composite anomaly patterns converge to structures which are *not* in phase with the climatological mean stationary waves. In the upper troposphere, the mature PAC anomaly patterns are almost in quadrature with the climatological-mean waves. DaSilva (1989) examines the time-dependent problem in a baroclinic model. He

finds a transitional evolution which broadly resembles PAC development. His mature anomaly pattern has a much weaker amplitude and a stronger upstream signature, however, than observed during the later stages of the PAC developments.

Although we have not focused upon the response to anomalous synoptic-scale eddy forcing, its effects are implicitly contained in the residual term of the eddy enstrophy budget. As mentioned previously, this term opposes development, suggesting that there is no large positive contribution to this term by the incoherent transients.

The large-scale eddy structures found near the jet exit regions during development do appear to be particularly efficient in extracting energy/enstrophy from the time-mean flow. Eddy fluxes of heat and momentum both make significant contributions to the downgradient residual q-flux patterns observed in the upper troposphere during the developments. In the energetics framework, both baroclinic and barotropic conversions contribute significantly towards eddy growth. These results are consistent with a mixed instability of (or growth upon) the time-mean flow, as in Frederiksen (1983b). Evidence in support of this view is strongest for the PAC cases.

We note that even though anomalous nonconservative or nonlinear effects appear to be dissipative during the developments, it is conceivable that they could still play an important *indirect* role during the developments (e.g. Held et al., 1986). That is, nonconservative and/or nonlinear processes could help force large-scale eddy structures which in turn can efficiently extract energy/enstrophy from the time-mean flow. Even in this case, however, the proximate sources for development will still be due to the direct conversions from the time-mean flow.

C. Conclusions

Our primary results, then, strongly suggest that (a) sources for development are predominantly midlatitude and local to the region of development and that (b) interactions

of the coherent eddies with the time-mean flow are sufficient to account for eddy growth. These results support the hypothesis that PA development is primarily due to a large-scale instability of (or growth upon) the three-dimensional time-mean flow.

We have focused on attempting to identify the primary mechanisms responsible for PA *development.* Significant large-scale conversions continue, however, five days after PA onset. We speculate that similar large-scale eddy/time-mean flow interactions may also play an important role in the *maintenance* of PA's. Indeed, the AN and PN breakdowns are preceded by an upstream weakenings of the subtropical jet stream (and associated horizontal gradients of pseudopotential vorticity). It is possible that, for these cases, large positive conversions from the time-mean flow into the anomalies continue as long as the strong upstream jet is maintained.

The results provide some encouragement for mid- to long-range forecasting of PA development. At least in principle, large-scale dynamical processes such as described here can be represented by numerical forecast models. Insofar as the developments are due to large-scale instabilities of the zonally varying time-mean flow, skillful predictions will depend significantly on the ability of forecast models to properly simulate the zonal mean flow and the time-mean stationary waves. Conversely, a strong climate drift will likely be detrimental to proper forecasting of both the onset and time evolution of PA's. We note, however, that some of our results suggest that synoptic-scale disturbances may also play an important role in the initial stages of PA developments. If this is the case, then extended-range predictions of PA development may ultimately be limited by our ability to correctly forecast synoptic-scale developments several days in advance.

Appendix A

Case Dates

The following is a list of the PAC and ATL persistent anomaly cases used in constructing the composite analyses of the thesis. Cases were selected from low-pass filtered data over the 23 winters from 1963-64 through 1986-87. In these analyses, winter is defined as the 120-day period beginning November 15. The key points used were 50N 25W for the ATL cases and 46N 170W for the PAC cases.

Pacific Negative Cases:

Onset date and time	Duration (in days)
16 Dec 63 00Z	17.0
24 Jan 64 00Z	12.5
09 Jan 65 00Z	12.0
30 Jan 67 00Z	12.0
05 Feb 68 00Z	30.0
22 Nov 69 00Z	17.0
16 Dec 69 12Z	17.5
28 Jan 70 12Z	25.5
04 Feb 71 12Z	15.5
17 Dec 73 00Z	11.0
16 Dec 75 12Z	12.0
24 Jan 76 00Z	10.5
10 Dec 76 00Z	15.0
01 Jan 77 00Z	52.5
10 Feb 78 00Z	28.5
04 Feb 80 00Z	11.0
28 Dec 80 12Z	22.5
11 Dec 81 00Z	12.5
13 Jan 83 12Z	56.0
30 Dec 84 00Z	14.0
17 Dec 85 00Z	11.5
26 Jan 86 00Z	19.5
06 Dec 86 12Z	26.5

Pacific Positive Cases:

Onset date and time	Duration (in days)
10 Dec 64 00Z	10.0
23 Dec 64 12Z	14.0
21 Dec 65 00Z	13.0
10 Feb 66 00Z	25.0
29 Dec 67 12Z	20.5
09 Dec 68 12Z	11.5
31 Dec 68 00Z	15.0
23 Jan 69 00Z	16.5
16 Dec 70 00Z	13.5
17 Jan 71 12Z	10.0
24 Feb 71 12Z	10.5
08 Dec 71 12Z	17.0
16 Feb 72 12Z	11.5
22 Feb 74 12Z	12.5
01 Jan 75 00Z	20.0
12 Dec 78 12Z	14.0
03 Feb 79 12Z	14.0
01 Dec 79 00Z	11.0
25 Dec 81 00Z	10.0
13 Dec 84 12Z	14.5
02 Feb 85 12Z	14.5

Atlantic Negative Cases:

Onset date and time	Duration (in days)
09 Dec 63 12Z	12.0
13 Feb 64 12Z	17.5
31 Dec 65 12Z	11.5
17 Jan 66 00Z	42.5
18 Jan 67 00Z	11.5
12 Feb 67 12Z	13.5
08 Jan 69 00Z	18.5
08 Jan 70 00Z	20.5
04 Jan 71 00Z	23.5
05 Jan 72 12Z	12.0
30 Jan 72 12Z	13.0
01 Jan 74 00Z	14.0
24 Jan 74 00Z	10.0
01 Dec 77 00Z	11.0
15 Feb 78 12Z	16.5
01 Dec 78 00Z	14.5
10 Dec 81 12Z	26.0
13 Dec 83 00Z	12.0
05 Feb 85 00Z	10.0
02 Dec 86 12Z	13.5

Atlantic Positive Cases:

Onset date and time	Duration (in days)
21 Jan 64 12Z	20.0
17 Dec 64 00Z	10.0
01 Feb 65 00Z	21.0
02 Jan 67 12Z	12.5
24 Dec 67 12Z	11.5
20 Jan 68 00Z	15.5
25 Dec 68 00Z	10.5
30 Jan 69 12Z	16.5
24 Feb 70 12Z	10.5
23 Jan 73 12Z	36.0
29 Dec 74 12Z	10.0
03 Dec 75 00Z	26.5
08 Jan 76 00Z	18.5
26 Dec 77 12Z	10.0
26 Dec 80 00Z	42.0
02 Feb 83 00Z	13.0
05 Feb 84 00Z	12.0
23 Jan 86 12Z	13.5

References

Anderson, J.R., and J.R. Gyakum, 1989: A diagnostic study of Pacific basin circulation regimes as determined from extratropical cyclone tracks. *Mon. Wea. Rev.*, **117**, 2672-2686.

Barnston, A.G., and R.E. Livezey, 1987: Classification, seasonality and persistence of low-frequency circulation patterns. *Mon. Wea. Rev.*, **115**, 1083-1126.

Berggren, R., B. Bolin and C.G. Rossby, 1949: An aerological study of zonal motion, its perturbation and breakdown. *Tellus*, **1**, 14-37.

Blackmon, M.L., 1976: A climatological spectral study of the geopotential height of the Northern Hemisphere. *J. Atmos. Sci.*, **33**, 1607-1623.

_____, J.M. Wallace, N.C. Lau and S.L. Mullen, 1977: An observational study of the Northern Hemisphere wintertime circulation. *J. Atmos. Sci.*, **34**, 1040-1053.

_____, R.A. Madden, J.M. Wallace and D.S. Gutzler, 1979: Geographical variations in the vertical structure of geopotential height fluctuations. *J. Atmos. Sci.*, **36**, 2450-2466.

_____, J.E. Geisler and E.J. Pitcher, 1983: A general circulation model study of January climate anomaly patterns associated with interannual variations of equatorial Pacific sea surface temperatures. *J. Atmos. Sci.*, **40**, 1410-1425.

_____, Y.-H. Lee and J.M. Wallace, 1984a: Horizontal structure of 500mb height fluctuations with long, intermediate and short time scales. *J. Atmos. Sci.*, **41**, 961-979.

_____, Y.-H. Lee, J.M. Wallace and H.-H. Hsu, 1984b: Time variations of 500mb height fluctuations with long, intermediate and short time scales as deduced from lag-correlation statistics. *J. Atmos. Sci.*, **41**, 981-991.

_____, S.L. Mullen, and G.T. Bates, 1986: The climatology of blocking events in a perpetual January simulation of a spectral general circulation model. *J. Atmos. Sci.*, **43**, 1379-1405.

Branstator, G., 1985: Analysis of general circulation model sea surface temperature anomaly simulations using a linear model. Part I: Forced solutions. *J. Atmos. Sci.*, **42**, 2225-2241.

Charney, J.G., 1947: The dynamics of long waves in a baroclinic westerly current. *J. Meteor.*, **4**, 135-162.

_____, and A. Eliassen, 1949: A numerical method for predicting the perturbations of the mid-latitude westerlies. *Tellus*, **1**, 38-54.

Colucci, S.J., 1987: Comparative diagnosis of blocking versus nonblocking planetary-scale circulation changes during synoptic-scale cyclogenesis. *J. Atmos. Sci.*, **44**, 125-139.

DaSilva, A.M., 1989: The role of temporal changes of the zonal wind on the excitation of large-scale transients. M.I.T. Dept. of Earth, Atmospheric and Planetary Sciences, Ph.D. thesis.

_____, and R.S. Lindzen, 1987: A mechanism for excitation of ultra-long Rossby waves. *J. Atmos. Sci.*, **44,** 3625-3639.

Dole, R.M., 1982: Persistent anomalies of the extratropical Northern Hemisphere wintertime circulation. M.I.T. Dept. of Meteorology and Physical Oceanography, Ph.D. thesis.

_____, 1986a: Persistent anomalies of the extratropical Northern Hemisphere wintertime circulation: Structure. *Mon. Wea. Rev.*, **114,** 178-207.

_____, 1986b: The life cycles of persistent anomalies and blocking over the North Pacific. *Adv. in Geophysics*, **29**, 31-69.

_____, 1989: Life cycles of persistent anomalies. Part I: Evolution of the 500mb height anomalies. *Mon. Wea. Rev.*, **117,** 177-211.

_____, and N.D. Gordon, 1983: Persistent anomalies of the extratropical Northern Hemisphere wintertime circulation: Geographical distribution and regional persistence characteristics. *Mon. Wea. Rev.*, **111,** 1567-1586.

_____, and R.X. Black, 1990: Life cycles of persistent anomalies. Part II: The development of persistent negative height anomalies over the North Pacific Ocean. *Mon. Wea. Rev.*, **118,** 824-826.

Eady, E.T., 1949: Long waves and cyclone waves. *Tellus*, **1,** 33-52.

Edmon, H.J., 1980: A study of the general circulation over the Northern Hemisphere during the winters 1976-77 and 1977-78. *Mon. Wea. Rev.*, **108,** 1538-1553.

_____, B.J. Hoskins and M.E. McIntyre, 1980: Eliassen-Palm cross sections for the troposphere. *J. Atmos. Sci.*, **37,** 2600-2616.

Farrell, B.F., 1982: The initial growth of disturbances in a baroclinic flow. *J. Atmos. Sci.*, **39,** 1663-1686.

_____, 1984: Modal and nonmodal baroclinic waves. *J. Atmos. Sci.*, **41**, 668-673.

_____, 1985: Transient growth of damped baroclinic waves. *J. Atmos. Sci.*, **42,** 2718-2727.

_____, 1989a: Optimal excitation of baroclinic waves. *J. Atmos. Sci.*, **46,** 1193-1206.

_____, 1989b: Transient development in confluent and diffluent flow. *J. Atmos. Sci.*, **46**, 3279-3288.

Frederiksen, J.S., 1978: Growth rates and phase speeds of baroclinic waves in multi-level models on a sphere. *J. Atmos. Sci.*, **35,** 1816-1826.

Frederiksen, J.S., 1982: A unified three-dimensional instability theory of the onset of blocking and cyclogenesis. *J. Atmos. Sci.*, **39,** 969-982.

_____, 1983a: Disturbances and eddy fluxes in Northern Hemipshere flows: Instability of three-dimensional January and July flows. *J. Atmos. Sci.*, **40,** 836-855.

_____, 1983b: A unified three-dimensional instability theory of the onset of blocking and cyclogenesis. II. Teleconnection patterns. *J. Atmos. Sci.*, **40,** 2593-2609.

_____, and K. Puri, 1985: Nonlinear instability and error growth in Northern Hemisphere three-dimensional flows: Cyclogenesis, onset-of-blocking and mature anomalies. *J. Atmos. Sci.*, **42,** 1374-1397.

_____, and R.C. Bell, 1987: Teleconnection patterns and the roles of baroclinic, barotropic and topographic instability. *J. Atmos. Sci.*, **44,** 2200-2218.

Geisler, J.E., M.L. Blackmon, G.T. Bates and S. Munoz, 1985: Sensitivity of January climatic response to the magnitude and position of equatorial Pacific sea surface temperature anomalies. *J. Atmos. Sci.*, **42,** 1037-1049.

Green, J.S.A., 1977: The weather during July 1976: Some dynamical considerations of the drought. *Weather*, **32**, 120-128.

Gruber, A., and A.F. Krueger, 1984: The status of the NOAA outgoing longwave radiation data set. *Bull. Amer. Meteor. Soc.*, **65,** 958-962.

Haines, K., and P. Malanotte-Rizzoli, 1990: Isolated anomalies in westerly jetstreams: A unified approach. Submitted to *J. Atmos. Sci.*.

Haltiner, G.J. and R.T. Williams, 1980: Numerical Prediction and Dynamic Meteorology. Wiley and Sons, 477 pp.

Hayashi, Y., and D.G. Golder, 1987: Effects of wave-wave and wave-mean flow interactions on the growth and maintenance of transient planetary waves in the presence of a mean thermal restoring force. *J. Atmos. Sci.*, **44,** 3392-3401.

Held, I.M., 1983: Stationary and quasi-stationary eddies in the extratropical troposphere: Theory. In: Large-scale Dynamical Processes in the Atmosphere, B.J. Hoskins and R. P. Pearce, eds., Academic Press, London, p. 127-168.

_____, 1986: Dissipative destabilization of external Rossby waves. *J. Atmos. Sci.*, **43,** 388-396.

Holopainen, E., and C. Fortelius, 1987a: High-frequency transient eddies and blocking. *J. Atmos. Sci.*, **44,** 1632-1645.

_____, and _____, 1987b: The damping of potential enstrophy in the large-scale transient eddies in the wintertime troposphere. *J. Atmos. Sci.*, **44,** 1973-1980.

Horel, J.D., 1981: A rotated principal component analysis of the interannual variability of the Northern Hemisphere 500 mb height field. *Mon. Wea. Rev.*, **109,** 2080-2092.

Hoskins, B.J., A.J. Simmons and D.G. Andrews, 1977: Energy dispersion in a barotropic atmosphere. *Quart. J. Roy. Meteor. Soc.*, **103,** 553-567.

_____, I. Draghici and H.C. Davies, 1978: A new look at the ω - equation. *Quart. J. Roy. Met. Soc.*, **104,** 31-38.

_____, and D. Karoly, 1981: The steady linear response of a spherical atmosphere to thermal and orographic forcing. *J. Atmos. Sci.*, **38,** 1179-1196.

_____, I.N. James, and G.H. White, 1983: The shape, propagation and mean-flow interaction of large-scale weather systems. *J. Atmos. Sci.*, **40,** 1595-1612.

_____, and M.A. Pedder, 1980: The diagnosis of mid-latitude synoptic development. *Quart. J. Roy. Meteor. Soc.*, **106,** 707-719.

_____, B.J., M.E. McIntyre and A.W. Robertson, 1985: On the use and significance of isentropic potential vorticity maps. *Quart. J. Roy. Meteor. Soc.*, **111,** 877-946.

Illari, L., and J.C. Marshall, 1983: On the interpretation of eddy fluxes during a blocking episode. *J. Atmos. Sci.*, **40,** 2232-2242.

Jacqmin, D., and R.S. Lindzen, 1985: The causation and sensitivity of the northern winter planetary waves. *J. Atmos. Sci.*, **42,** 724-745.

Kang, I.-S., 1990: Influence of zonal mean flow change on stationary wave fluctuations. *J. Atmos. Sci.*, **47,** 141-147.

Karoly, D.J., R.A. Plumb and M. Ting, 1989: Examples of the horizontal propagation of quasi-stationary waves. *J. Atmos. Sci.*, **46,** 2802-2811.

Knutson, T.R., and K.M. Weickmann, 1987: 30-60 day oscillations: Composite life cycles of convection and circulation anomalies. *Mon. Wea. Rev.*, **115,** 1407-1436.

Lau, N.C., 1979: The observed structure of tropospheric stationary waves and the local balances of vorticity and heat. *J. Atmos. Sci.*, **36,** 996-1016.

_____, 1988: Variability of the observed midlatitude storm tracks in relation to low-frequency changes in the circulation pattern. *J. Atmos. Sci.*, **45,** 2718-2743.

_____, and E.O. Holopainen, 1984: Transient eddy forcing of the time-mean flow as identified by geopotential tendencies. *J. Atmos. Sci.*, **41,** 313-328.

_____, and K.-M. Lau, 1984: The structure and energetics of midlatitude disturbances accompanying cold-air outbreaks over East Asia. *Mon. Wea. Rev.*, **112,** 1309-1327.

Lorenz, E.N., 1955: Available potential energy and the maintenance of the general circulation. *Tellus,* **7,** 157-167.

MacVean, M.K., 1985: Long-wave growth by baroclinic processes. *J. Atmos. Sci.,* **42,** 1089-1101.

Mo, K.C., J. Pfaendtner and E. Kalnay, 1987: A GCM study of the maintenance of the June 1982 blocking in the Southern Hemisphere. *J. Atmos. Sci.*, **44,** 1123-1142.

Mullen, S.L., 1987: Transient eddy forcing of blocking flows. *J. Atmos. Sci.*, **44,** 3-22.

Namias, J., 1978: Multiple causes of the North American abnormal winter 1976/77. *Mon. Wea. Rev.*, **106,** 279-295.

Navarra, A., 1990: Steady linear response to thermal forcing of an anomaly model with an asymmetric climatology. *J. Atmos. Sci.*, **47,** 148-169.

Neilley, P.P., 1990: Interactions between synoptic-scale eddies and the large-scale flow during the life cycles of persistent flow anomalies. M.I.T. Dept. of Earth, Atmospheric and Planetary Sciences, Ph.D. thesis.

Niehaus, M.C.W., 1980: Instability of non-zonal baroclinic flows. *J. Atmos. Sci.*, **37,** 1447-1463.

Nigam, S., I.M. Held and S.W. Lyons, 1986: Linear simulation of the stationary eddies in a GCM. Part I: The "no mountain" model. *J. Atmos. Sci.*, **43,** 2944-2961.

_____, and R.S. Lindzen, 1989: Sensitivity of stationary waves to variations in the basic state zonal flow. *J. Atmos. Sci.*, **46,** 1746-1768.

Palmer, T.N. and D.A. Owen, 1986: A possible relationship between some "severe" winters in North America and enhanced convective activity over the tropical West Pacific. *Mon. Wea. Rev.*, **114,** 648-651.

Plumb, R.A., 1983: A new look at the energy cycle. *J. Atmos. Sci.*, **40,** 1669-1688.

_____, 1985: On the three-dimensional propagation of stationary waves. *J. Atmos. Sci.*, **42,** 217-229.

_____, 1986: Three-dimensional propagation of transient quasi-geostrophic eddies and its relationship with the eddy forcing of the time-mean flow. *J. Atmos. Sci.*, **43,** 1657-1678.

Rex, D.F., 1950a: Blocking action in the middle atmosphere and its effects on regional climate. I: Aerological study of blocking. *Tellus*, **2,** 196-211.

_____, 1950b: Blocking action in the middle troposphere and its effect on regional climate. II: The climatology of blocking action. *Tellus*, **2,** 275-305.

_____, 1951: The effect of Atlantic blocking action upon European climate. *Tellus*, **3,** 1-16.

Sardeshmukh, P.D., and B.J. Hoskins, 1988: The generation of global rotational flow by idealized tropical divergence. *J. Atmos. Sci.*, **45,** 1228-1251.

Sawyer, J.S., 1970: Observational characteristics of atmospheric fluctuations with time scales of a month. *Quart. J. Roy. Meteor. Soc.,* **96,** 610-625.

Schubert, S.D., 1986: The structure, energetics and evolution of the dominant frequency-dependent three-dimensional atmospheric modes. *J. Atmos. Sci.,* **43,** 1210-1237.

Shukla, J., and K.C. Mo, 1983: Seasonal and geographical variation of blocking. *Mon. Wea. Rev.*, **111,** 388-402.

Shutts, G.J., 1986: A case study of eddy forcing during an Atlantic blocking episode. *Adv. in Geophysics*, **29,** 135-162.

Simmons, A.J., 1982: The forcing of stationary wave motion by tropical diabatic heating. *Quart. J. Roy. Meteor. Soc.,* **108,** 503-534.

_____, and B.J. Hoskins, 1977: Baroclinic instability on the sphere: Solutions with a more realistic tropopause. *J. Atmos. Sci.*, **34,** 581-588.

_____, J.M. Wallace and G. Branstator, 1983: Barotropic wave propagation and instability and atmospheric teleconnection patterns. *J. Atmos. Sci.*, **40,** 1363-1392.

Trenberth, K.E., and J.G. Olson, 1988a: Evaluation of NMC Global Analyses: 1979-1987. NCAR Technical Note, NCAR/TN-299+STR., Boulder, CO.

_____, and _____, 1988b: ECMWF Global Analyses 1979-1986: Circulation Statistics and Data Evaluation. NCAR Technical Note, NCAR/TN-300+STR., Boulder, CO.

_____, and _____, 1988c: Intercomparison of NMC and ECMWF Global Analyses: 1980-1986. NCAR Technical Note, NCAR/TN-301+STR., Boulder, CO.

Tsou, C.-H. and P.J. Smith, 1990: The role of synoptic/planetary-scale interactions during the development of a blocking anticyclone. *Tellus*, **42,** 174-193.

Valdes, P.J., and B.J. Hoskins, 1988: Baroclinic instability of the zonally averaged flow and boundary layer damping. *J. Atmos. Sci.*, **45,** 1584-1593.

_____, and _____, 1989: Linear stationary wave simulations of the time-mean climatological flow. *J. Atmos. Sci.*, **46,** 2509-2527.

Wallace, J.M., and D.S. Gutzler, 1981: Teleconnections in the geopotential height field during the Northern Hemisphere winter. *Mon. Wea. Rev.,* **109,** 784-812.

Weickmann, K. M., G. R. Lussky and J. E. Kutzbach, 1985: Intraseasonal (30-60 day) fluctuations of outgoing longwave radiation and 250 mb streamfunction during Northern winter. *Mon. Wea. Rev.,* **113,** 941-961.